Experimental and Computational Investigations of a Squeeze Film Damper Supported on Rotors

THESIS

Submitted to Delhi Technological University
For the award of the degree of

DOCTOR OF PHILOSOPHY

In

ENGINEERING

By

RATNESH KUMAR GUPTA
(2K17/PH.D/ME/22)

Under the Supervision of

Prof. Ramesh Chandra Singh

DELHI TECHNOLOGICAL UNIVERSITY
NEW DELHI-110042(INDIA)
2024

Experimental and Computational Investigations of a Squeeze Film Damper Supported on Rotors

THESIS

Submitted in Delhi Technological University

For the award of the degree of

DOCTOR OF PHILOSOPHY

In

ENGINEERING

By

RATNESH KUMAR GUPTA
(2K17/Ph.D/ME/22)

Under the Supervision of

Dr. Ramesh Chandra Singh
(Professor),
Department of Mechanical Engineering,
Delhi Technological University,
New Delhi-110042, India.

DELHI TECHNOLOGICAL UNIVERSITY
NEW DELHI-110042(INDIA)
2024

DELHI TECHNOLOGICAL UNIVERSITY
Shahabad Daulatpur, Main Bawana Road
Delhi-110042(India)

DECLARATION

I hereby declare that the thesis entitled **"Experimental and Computational Investigation of Squeeze Film Damper Supported on Rotors"** submitted by me for the award of the degree of ***Doctor of Philosophy*** to **Delhi Technological University (formerly Delhi College of Engineering)** is a record of *bonafide* work carried out by me under the guidance of Late. Prof. Vikas Rastogi, DTU and Prof. Ramesh Chandra Singh, DTU.

I further declare that the work reported in this thesis has not been submitted and will not be submitted, either in part or in full, for the award of any other degree or diploma in this Institute or any other Institute or University.

Ratnesh Kumar Gupta
Reg No: 2K17/Ph.D/ME/22
Department of Mechanical, Industrial,
Production, and Automobile Engineering
Place: New Delhi
Date:

DELHI TECHNOLOGICAL UNIVERSITY
Shahabad Daulatpur, Main Bawana Road
Delhi-110042(India)

CERTIFICATE

This is to certify that the thesis entitled **"Experimental and Computational Investigation of Squeeze Film Damper Supported on Rotors"** submitted by Mr. **Ratnesh Kumar Gupta** to Delhi **Technological University (formerly Delhi College of Engineering)**, for the award of the degree of "*Doctor of Philosophy*" in Mechanical Engineering is a record of the *bona fide* work carried out by him. He has worked under my supervision and has fulfilled the requirements for the submission of the thesis.

The results contained in this thesis are original and have not been submitted to any other university or institute for an award of any degree or diploma.

Prof. Ramesh Chandra Singh
Professor
Department of Mechanical, Industrial,
Production, and Automobile Engineering
Delhi Technological University (DTU)
Bawana, Delhi-110042

ACKNOWLEDGEMENTS

I would like to express my special appreciation and thanks to my advisors, Late. Prof. Vikas Rastogi and Prof. Ramesh Chandra Singh Department of Mechanical, Industrial Production and Automobile Engineering, Delhi Technological University. They have been tremendous mentors for me. Perseverance, exuberance, and positive approaches are just some of the traits they have imprinted on my personality. These lines are dedicated to my guides:

"गुरु ब्रह्मा गुरु विष्णु गुरु देवो महेश्वर
गुरू साक्षात परम ब्रह्म तस्मै श्री गुरुवे नमः"

"Guru Brahma Guru Vishnu Guru Devo Maheshwara
Guru sakshat Param Brahma tasmay Shri Guruve Namah"

They steered me through this journey with their invaluable advice, positive criticism, stimulating discussions, and consistent encouragement. If I would stand proud of my achievements, they are the main creditors undeniably. It is my privilege to be under their tutelage. Their advice on my research as well as on my career has been priceless. I would like to thank them for encouraging my research.

I would like to express My gratitude to Prof. Prateek Sharma, vice chancellor of Delhi Technological University Delhi for providing me this opportunity to carry out this work in this prestigious Institute.

I would like to thank Prof. R.S. Mishra DRC chairman, and Prof. S.K Garg head of the Department of Mechanical Engineering for their support in accomplishing this work. I wish to record my thanks and attitude to your all external and internal SRC experts, Prof. R.K Pandey (IIT Delhi), Prof. Mohammed Suhaib (Jamia University), Prof. D.S. Nagesh and Prof. Naokant Deo from Delhi Technological University for their valuable guidance, critical and constructive discussion during this work.

I would like to thank my followers, especially Mr. Gaurav Chaudhary, Abdul, Yamika, and Pooja for helping me and encouraging me throughout my research.

I also convey my sincere thanks to my staff colleagues Dr. Prabhakar Sharma and Dr. Dipankar Mishra and thanks to Mr. Phool Singh Ji who supported us in the development of this experimental test rig.

My sincere thanks to the anonymous reviewer were inside full and constructive comments and suggested revisions to improve the organization and clarity of the research

I am greatly inducted to my mother Smt. Shyama Devi and father late Atma Ram Gupta for their love and blessings to see me taking greater heights of life with immense pleasure and delight, I would like to thank my wife Mrs. Ratika Gupta for the emotional and moral support during this PhD journey. I appreciate my daughter Adrisha Gupta for abiding by the ignorance and patience she showed during my Ph.D. Words can never say how grateful I am to you. I truly appreciate the support that I got from my Institute Director and department without his motivation and arrangement pursuit of this PhD work would have never been possible.

Finally, I would like to express my thanks to the almighty lord Krishna and Shri Sairam for giving me patience and strength to overcome all types of hindrances These words of my inspiration during this journey.

Ratnesh Kumar Gupta

ABSTRACT

Squeeze film dampers (SFDs) are used to reduce the vibration amplitude of high-speed rotors. In this context, an SFD has been developed to meet the requirements of high-speed rotating shafts that are generally used in high-speed rotor application. In this study, the effect of SFD process parameters (rotation of shaft, oil pressure inside the damper, and oil blend sample) on the vibration amplitude of the shaft on the x-axis and vibration amplitude of shaft in the z-axis, is investigated, during the rotation of the flexible shaft up-to-speed 10000rpm. The oil sample used in the present work was mixed with 10%,20%,30%,40%, and 50% kerosene oil (Dynamic viscosity 1. 1287mPa.S), in independent experiment, with *5W30* crankcase oil (Dynamic viscosity 75.483 mPa.S) and used variable high-pressure oil supply system up to120bar.

The Taguchi approach (L25-orthogonal array) is utilized for experiment design, and the experimental findings are examined using analysis of variance (ANOVA). The table of response for an average value of the vibration amplitude of the shaft in the x-axis and z-axis, indicates that supply oil pressure is the most significant factor for shaft amplitude along the x- and z-axes, while blending Newtonian fluid is important for reducing the vibration amplitude. Analysis through ANOVA also supports similar results. It has also been discovered from SNR graph, that Pressure-100bar, Speed-4000rpm, Blend-40% (P5S2B4) in the x-axis and Pressure-100bar, Speed-4000rpm, Blend-50% (P5S2B5) in the z-axis are the optimal levels of process parameters for reducing vibration amplitude. The successful experimental validation confirms the accuracy and reliability of the optimized values for vibration control.

The experimental design used in this study uses the Box-Behnken design (BBD) method, which is a widely used approach in experimental design. The study also incorporates Response Surface Methodology (RSM) and Analysis of Variance (ANOVA) to optimize the input parameters and assess the statistical significance of the model.

Desirability-based optimization is used as a means to attain the intended objectives of vibration control.

The artificial neural network (ANN) model has shown somewhat reduced prediction errors and a greater coefficient of determination compared to the response surface methodology (RSM) for both the x and z axes of vibration amplitude.

During the fourth stage of our experiment, the position of the load was changed in intervals of 10 to 50 cm, in steps of 10 cm, from the end support. A distinct pattern in the amplitude of shaft vibrations in the x and z axes was observed. The amplitude noticeably increased as the load was closer to the support, and decreased correspondingly when the weight was moved farther away, especially beyond the midway of the shaft length.

In the second phase, we replaced the end support with a squeeze film damper (SFD) and directed our attention to assessing vibration amplitudes along the X and Z axes. This analysis included employing different oil samples with varying viscosities. Significantly, when a steady load was imposed, replicating the original configuration without the SFD, interesting results were noted. The findings demonstrated a constant reduction in vibration amplitude for both axis as the viscosity of the oil samples rose, ultimately reaching an ideal level. This finding highlights the substantial influence of oil thickness on determining the overall vibration properties in a system that employs a squeeze film damper. These findings provide valuable insights for developing and implementing Squeeze film dampers (SFD) in rotating shaft applications at high speeds, contributing to improved vibration control and enhanced performance.

Keywords: Vibration Amplitude; Taguchi approach; Optimization; Squeeze film damper (SFD); Box-Behnken design (BBD), analysis of variance (ANOVA), Response Surface Methodology (RSM); Root mean squared error (RMSE), Artificial Neural Network (ANN), mean absolute error (MAE), R-squared;

TABLE OF CONTENTS

Topics	*Page No.*
Candidate Declaration	i
Certificate	ii
Acknowledgments	iii-iv
Abstract	v-vi
Table of contents	vii-xi
List of Figures	xii-xv
List of Tables	xvi-xviii
List of Abbreviations	xix-xx
Nomenclatures	xxi-xxiii
Chapter 1: Introduction	**1-29**
1.1 Motivation	1
1.2 Overview of Squeeze Film Damper	5
1.3 Evolution of Squeeze Film Damper	5
1.3.1 The birth of squeeze film dampers (during the 1950s- 1960s)	6
1.3.2 Comparative and Experimental Research(1970 - 1980s)	7
1.3.3 Developments in Computational Methods in the 1990s	8
1.3.4 Modelling of squeeze film damper for rotor vibration with bond graph	10
1.3.5 Techniques of Optimization from the 2000s	12
1.3.6 Coupling with Innovative Materials (2010s)	13
1.3.7 Modelling of squeeze film damper to control the rotor vibration With FEM	13
1.3.8 Methods from a variety of disciplines and their applications in the business world (2020s)	16
1.3.9 Ongoing Research and Potential Future Developments	16
1.4 Classification of Squeeze Film Damper	17
1.4.1 Construction-based squeeze film damper	17

1.4.2 Squeeze Film Damper (SFD) Based on the Flow Direction of the Oil 18
1.4.3 Based on the operating Principal 20
1.4.4 Based on the SFD application 22
1.4.5 Based on the number of bearings used in SFD 21
1.5 Application of Squeeze Film Damper 22
1.6 Thesis Scope 24
1.7 Contribution of the Thesis 25
1.8 Organization of the Thesis 29
Chapter 2: Literature Review 32-61
2.1 Introduction 32
2.2 Literature study done using an analytical methodology 33
2.2.1 Investigation of type of oil use inside the SFD 33
2.2.2 Review of inertia force Analysis of the rotor for SFD. 37
2.2.3 Review Analysis of the oil feeding Grove in the SFD 41
2.3 Literature study was done using a computational approach 42
2.3.1 Review of SFD modelling with FEM, CFD 42
2.3.2 Review of SFD modeling with MatLab computation and optimization 42
2.3.3 Review of SFD modeling with ANN 45
2.3.4 Review of SFD modeling with Bond Graph 46
2.4 Literature study was done using an experimental approach 47
2.4.1 Review based on the geometry of squeeze film damper 47
2.4.2 Review based on damping effect of squeeze film damper 48
2.4.3 Review based on experimental of squeeze film damper with modelling 50
2.5 Concise Overview 51
2.5.1 Review summary of some most effective research 57
2.6 Outcome of Literature Review 59
Chapter 3: Experimental Investigations of Squeeze Film Damper Setup for High Rotational Speeds and Oil Pressure 62-96
3.1 Introduction 62

3.2	Materials and Methodology of Experiments	62
	3.2.1 Lubricant details	62
	3.2.2 Sample Preparation	65
3.3	Experimental Details	69
3.4	Methodology	75
	3.4.1 Taguchi analysis	75
	3.4.2 Design of Experiment	76
	3.4.3(a) Experimentation of rotor vibration without SFD	77
	3.4.3(b) Experimentation of rotor vibration with SFD	78
	3.4.4 Effect of Process Parameters on Vibration Amplitude	79
3.5	Experimental Results and Analysis	81
3.6	Experimental Confirmation	88
	3.6.1 Experimental validation of regression model for x-axis vibration amplitude	88
	3.6.2 Experimental Validation of regression model for z-axis vibration amplitude	88
	3.6.3 Experimental Validation of Optimized Value	89
3.7	Plot illustrating interactions and variables' effects on vibrational change at the x-axis	90
	3.7.1 Plot of interactions and the impact of various variables on the vibration's change at the z-axis	91
3.8	Response Surface and Contour plot showing parameter interaction	92
3.9	Summary of the Chapter	96
Chapter 4: Modelling of Squeeze Film Damper for Flexible Rotor utilizing RSM (Box-Behnken Design with Desirability Optimization		**97-125**
4.1	Introduction	97
4.2	Material and Method	97
4.3	Test Rig Detail and Experimentation	98
4.4	Methodology	101
	4.4.1 Flowchart of the proposed methodology	101
	4.4.2 Box-Behnken Design	102
4.5	Experiment Work	104
4.6	Experimental Results and Analysis	106
	4.6.1 RSM model for Vibration of the shaft at the ‘X’ axis	107

4.7 Variable operating parameters and x-axis vibration amplitude interaction 109
4.7.1 Interaction between supply oil pressure and shaft speed 109
4.7.2 Relationship between the blend ratio percentage and the flow of oil pressure. 111
4.7.3 Interaction between shaft speed and oil blend ratio percentage 112
4.8 RSM model for Vibration amplitude of the shaft at the 'Z' axis 113
4.9 Interaction between different operating parameters for Z-axis vibration amplitude 116
4.9.1 Interaction between speed of the shaft and supply oil pressure 116
4.9.2 Interaction between supply oil pressure and blend ratio percentage 117
4.9.3 Interaction between shaft speed and oil blend ratio percentage 119
4.10 Desirability-based optimization 120
4.10.1 Desirability criteria 121
4.10.2 Ramp diagrams of desirability 121
4.11 Experimental validation 123
4.12 Summary of the Chapter 125

Chapter 5: Experimental Investigation of Squeeze Film Dampers and a Comparative Analysis using Artificial Neural Networks (ANN) and Response Surface Methodology **126-171**

5.1 Introduction 126
5.2 Materials and Method 126
5.2.1 Preparation of oil samples 126
5.2.2 Experimentation 127
5.3 Methodology 129
5.3.1 Flowchart of the Methodology 129
5.3.2 Response Surface Methodology (RSM). 130
5.3.3 Box-Behnken Design 132
5.4 Experimental work 133
5.5 Results and Analysis 137
5.5.1 RSM(Box-Behnken) model for Vibration amplitude of the shaft at the 'X' and Z axes. 137
5.6 Analyses of the residual plot of the RSM predicted value at the x and z axes 146
5.7 Procedure of Artificial Neural Network (ANN) 149
5.8 Analysing the relative merits of RSM and ANN optimization methods 158
5.8.1 Methodology Comparison with respect to vibration amplitude of shaft in x-z axes of two methods RSM prediction, and ANN prediction with respect to experimental data 166

5.8.2 Methodology Comparison with respect to error term MAE, RMSE and R-squared 167
5.8.3 Analysis of the same presents the following facts 168
5.9 Summary of the Chapter 170

Chapter 6: Vibration Analysis of High-Speed Rotor Under Variable Point Load Condition with and without Squeeze Film Damper **172-186**

6.1 Introduction 172
6.2 Material and Method without SFD 173
6.3 Description of Experimental Test Rig without SFD 174
6.3.1 Description of Experimental Test Rig with SFD 175
6.4 Material and Method with squeeze film damper (SFD) 178
6.5 Experimentation without SFD 178
6.6 Experimental Finding with SFD 180
6.7 Experimental Findings and Discussion 184
6.8 Summary of the Chapter 185

Chapter 7: Conclusions and Future Directions **187-186**

7.1 Conclusions 187
7.2 Future Scopes 195

References 197-215
Publication from the present work 216

LIST OF FIGURES

Figure No.	*Title*	*Page No.*
Figure 1.1:	Details part of Squeeze film damper assembly with rolling element	4
Figure 1.2:	Development of squeeze film damper	5
Figure 1.3:	Classification of Squeeze Film Damper	17
Figure 3.1:	Different oil blend sample	68
Figure 3.2(a):	Schematic view of rotor bearing set-up without SFD	69
Figure 3.2(b):	Schematic view of squeeze film damper rotor set-up	70
Figure 3.3:	Actual test rig diagram along with pickup's location of the signal	70
Figure 3.4:	Sketch of squeeze film damper with assembly	71
Figure 3.5:	Actual Component of squeeze film damper after disassembly	71
Figure 3.6(a):	OROS 32-channel data analyser	72
Figure 3.6(b):	Vibro meter proximity sensor	72
Figure 3.6(c):	Proximity probe	72
Figure 3.7:	Flow chart of Taguchi procedure	76
Figure 3.8:	Effect of input process parameter at x-axis vibration	84
Figure 3.9:	Effect of process parameter at z-axis vibration	84
Figure 3.10(a):	Residual plot for vibration amplitude at x-axis	86
Figure 3.10(b):	S/N ratio residual plot for the x-axis vibration amplitude variation	86
Figure 3.11(a):	Residual plot for vibration amplitude at z-axis	87
Figure 3.11(b):	Residual plot for the S/N ratio for the change in vibration amplitude in the z-axis	87
Figure 3.12:	Interaction plot for a vibration amplitude of shaft in the x-axis	91
Figure 3.13:	Interaction plot for a vibration amplitude of the shaft in the z-axis	92
Figure 3.14:	Interaction for vibration at x and z axes between factors of speed and pressure	93
Figure 3.15:	Interaction for vibration at x and z axes between factors blend	94

	percentage and speed	
Figure 3.16:	Interaction for vibration at x and z axes between factors pressure and blend percentage	95
Figure 4.1:	Actual test rig diagram along with pickup's location of the signal	99
Figure 4.2:	Flowchart of the proposed methodology	102
Figure 4.3(a):	Normal probability plot of the residual	108
Figure 4.3(b):	Plot of the Predicted versus actual values.	108
Figure 4.4(a):	2D-contour depiction shows the shaft's vibration amplitude along the X axis in relation to the shaft's speed and supply oil pressure	110
Figure 4.4(b):	3D surface map within the damper pressure model displays the vibration amplitude of the shaft at the X-axis in response to shaft speed and supply oil pressure	110
Figure 4.5(a):	2D-Contour plot for vibration amplitude of shaft at X-axis with respect to supply oil pressure inside the damper and Y-axis oil blend ratio percentage	112
Figure 4.5(b):	3D-Surface plot for vibration amplitude of shaft at X-axis with respect supply oil pressure inside the damper and Y -axis to oil blend ratio percentage	112
Figure 4.6(a):	2D-Contour plot for vibration amplitude of shaft at X-axis with respect to speed of shaft and blend ratio percentage of oil	113
Figure 4.6(b):	3D-Surface plot for vibration amplitude of shaft at X-axis with respect to speed of the shaft and blend ratio percentage of oil.	113
Figure 4.7(a):	Normal probability plot of the residual at z axis	115
Figure 4.7(b):	Plot of the Predicted versus actual values at z axis	115
Figure 4.8(a):	2D-Contour plot for vibration amplitude of shaft at z-axis with respect to speed of shaft and supply oil pressure inside the damper	117
Figure 4.8(b):	3D-Surface plot for a vibration amplitude of shaft at z-axis with respect to the speed of the shaft and supply oil pressure inside the damper.	117
Figure 4.9(a):	2D-Contour plot for vibration amplitude of shaft at z-axis with respect to blend ratio percentage and supply oil pressure inside the damper	118

Figure 4.9(b):	3D-Surface plot for a vibration amplitude of shaft at z-axis with respect to oil blend ratio percentage and supply oil pressure inside the damper.	118
Figure 4.10(a):	2D-Contour plot for vibration amplitude of shaft at z-axis with respect to the speed of shaft and blend ratio percentage of oil	120
Figure 4.10(b):	3D-Surface plot for a vibration amplitude of shaft at z-axis with respect to the speed of the shaft and blend ratio percentage of oil	120
Figure 4.11:	Ramp diagrams of desirability	122
Figure 5.1:	Flowchart of the proposed methodology	130
Figure 5.2:	Residual plot of vibration at x-axis(experimental)	139
Figure 5.3:	Residual plot of vibration at z-axis(experimental)	140
Figure 5.4(a):	3D graphical representation of output data experimental and RSM (predicted)	145
Figure 5.4(b):	2D graphical representation of output data experimental and RSM (predicted).	145
Figure 5.5:	Error percentage graph of RSM x and z axes	146
Figure 5.6:	Residual plot of vibration amplitude at x- axis for RSM predicted data	148
Figure 5.7:	Residual plot of vibration amplitude at Z- axis for RSM predicted data	148
Figure 5.8:	Schematic illustration of ANN structure	149
Figure 5.9:	Neuron network training	151
Figure 5.10(a):	Training plots of neural network for vibration at x and z axes (a)Regression Performance for trained ANN	153
Figure 5.10(b):	Variation of error with epochs	153
Figure 5.10(c):	Error histogram plot	153
Figure 5.10(d):	Training state of ANN.	153
Figure 5.11(a):	3D Comparative graph of vibration amplitude at x and z axes of experimental data vs ANN data	156
Figure 5.11(b):	2D Comparative graph of vibration amplitude at x and z axes of experimental data vs ANN data.	156
Figure 5.12:	Percentage error plot between experimental and ANN-predicted data	157

Figure 5.13(a):	Comparative graph of vibration amplitude through Experiments, RSM and ANN for x-axis	167
Figure 5.13(b):	Comparative graph of vibration amplitude through Experiments, RSM and ANN for z-axis.	167
Figure 5.14:	Value of MAE, RMSE and R-Squared related to RSM and ANN modelling	168
Figure 6.1:	Rotor bearing system without squeeze film damper	175
Figure 6.2:	Rotor bearing system with squeeze film damper	177
Figure 6.3:	Actual Rotor bearing system with squeeze film damper	179
Figure 6.4:	Vibration amplitude of x-z axes without squeeze film damper	179
Figure 6.5:	Vibration amplitude of x-z axes with squeeze film damper oil1	181
Figure 6.6:	Vibration amplitude of x-z axes with squeeze film damper oil2	183
Figure 6.7:	Vibration amplitude of x-z axes with squeeze film damper oil 3	184

LIST OF TABLES

Table No.	*Titles*	*Page No.*
Table 2.1:	Shows the different types of SFDs and their input, and output process parameters, and the modeling technique	58
Table 3.1:	Dynamic & kinematic viscosity of crankcase oil and kerosene oil at 30ºC	68
Table 3.2:	Dynamic and Kinematic viscosities of the samples at 30ºC	68
Table 3.3:	Detail component of the squeeze film damper rotor setup	73
Table 3.4:	Process parameters and their levels	77
Table 3.4(a):	vibration amplitude at x and z axes without using SFD	78
Table 3.5:	Average value of experiment outcomes from three trials	78
Table 3.6:	Signal-to-Noise ratio (S/N ratios) of the shaft vibrations at X-axis and Z-axis.	80
Table 3.7:	Analysis of Variance (ANOVA) effect for S/N Ratios of vibration amplitude at X-axis.	82
Table 3.8:	ANOVA effect for S/N Ratios of vibration amplitude at the Z-axis	82
Table 3.9:	response table for the S/N ratio	83
Table 3.10:	Experimental validation of optimal solution process factors for x-axis	88
Table 3.11:	Experimental validation of optimal solution process factors for z-axis	89
Table 3.12:	Experimental validation of optimized value	90
Table 4.1:	Dynamic viscosity of crankcase oil and kerosene oil at 30 temps.	98
Table 4.2:	Dynamic viscosities of the samples at 30º C.	98
Table 4.3:	Detail component of the squeeze film damper rotor setup	100
Table 4.4:	Recommended an experimental run after optimizing the input parameters	105
Table 4.5:	Vibration amplitude of shaft at x-z axis on the recommended test run	106

Table 4.6:	Vibration amplitude at X-axis as determined by Analysis of Variance (ANOVA)	107
Table 4.7:	Vibration amplitude at Z-axis as determined by Analysis of Variance (ANOVA)	114
Table 4.8:	Parameters and their desirability	121
Table 4.9:	Details parameters and their optimized value	123
Table 4.10:	Conformation experiment	123
Table 4.11:	Experiment validation	124
Table 5.1:	Shows the details specifications of the experimental test rig	128
Table 5.2:	Displays the comprehensive collection of experimental Input process	133
Table 5.3:	Comprehensive collection of experimental setups and their responses	136
Table 5.4:	RSM predicted data along with percentage error of x and z axes.	142
Table 5.5:	ANN predicted data along with percentage error of x and z axes	154
Table 5.6(a):	RSM Predicted value at x axes and term related to MAE, RMSE and R-Squared	161
Table 5.6(b):	RSM Predicted value at z axes and term related to MAE, RMSE and R-Squared	162
Table 5.7:	RSM Predicted value at x and z axes and value of MAE, RMSE and R-Squared	163
Table 5.8(a):	ANN Predicted value at x axes and term related to MAE, RMSE and R-Squared	164
Table 5.8(b):	ANN Predicted value at z axes and term related to MAE, RMSE and R-Squared	165
Table 5.9:	ANN Predicted value at x and z axes and value of MAE, RMSE and R-Squared	166
Table 5.10:	Value of MAE, RMSE, and R-Squared for RSM and ANN modelling	168
Table 6.1:	Parameter detail for rotor vibration analysis with SFD	176
Table 6.2:	Vibration amplitude(μm) of the rotor shaft without SFD	179

Table 6.3: Vibration amplitude(μm) of the rotor shaft with SFD for oil 1 181
Table 6.4: Vibration amplitude(μm) of the rotor shaft with SFD for oil 2 182
Table 6.5: Vibration amplitude(μm) of the rotor shaft with SFD for oil 3 183

LIST OF ABBREVIATIONS

SFD	Squeeze Film Damper
FEA	Finite Element Analysis
CFD	Computational Fluid Dynamics
FEM	Finite Element Method
FSI	Fluid-Structure Interaction
RSM	Response Surface Methodology
ANN	Artificial Neural Networks
DOE	Design of Experiment
JFO	Jeffcott Rotor with Flexible Supports
ODE	Ordinary Differential Equations
MR	Magnetorheological
MODRO	Multi-Objective Discrete Robust Optimization
ISFD	Integrated Squeeze Film Damper
ERSFD	Elastic Ring Squeeze Film Damper
PR	Piston Ring
LPM	Liters Per Minute
RF-MEMS	Radio Frequency Microelectromechanical Systems
ANOVA	Analysis of Variance
GRA	Grey Correlation Analysis
NSGA	Non-Dominated Sorting Genetic Algorithm

ISFBD	Integral Squeeze Film Damper
HSFD	Hybrid Squeeze Film Damper
PAO	Poly Alpha Alafines
FFT	Fast Fourier Transform
SB	Smaller the Better
S/N	Signal to Noise
ME	Major Effect
SS	Sum of Squares
CI	Confidence Interval
DOF	Degrees of Freedom
RVFV	Residuals Versus Fatted Value
RVRP	Residuals Versus Order Plot
BBD	Frequency Versus Residual Plot
OLS	Ordinary Least Squares
MAE	Mean Absolute Error
RMSE	Root Mean Square Error
RPM	Revolutions Per Minute

NOMENCLATURES

P	Supply oil pressure in the damper
S	Speed of shaft
B	Type of blend of oil
L	Level
T	Trail one
n	Number of repetitions of the experiment
S/N	Signal to noise
k	Total number of elements
Y	Response
X_1, X_2, X_3	Input factors
β^0, β^1	Model coefficients
Va(x)	Average vibration amplitude of the x-axis
Va(z)	Average vibration amplitude of the z-axis
y_1, y_2	Vibration at x axis
h_1	Vibration at z-axis
b	Bias
y_i	Real-time experiment data
w_{ij}	Corresponding weights
J	Activation factors

c	Radial clearance
C_B, C_S	clearances for journal bearing and stabilizer, respectively
D/Dt	material derivative
e	journal eccentricity
EI	flexural rigidity of the rotor shaft
F_R,F_θ	fluid film forces
F	external static load per bearing
h	film thickness
I_b,I_r	rotor moment of inertia about the diametral axis for left or right span and middle span, respectively
J_b,J_r	polar moment of inertia of the rotor for left or right span and middle spa
k_1	catch spring stiffness
L	bearing length per land
L_B,L_S	land length for journal bearing and stabilizer, respectively
L_{st}	locations of the stabilizers and journal bearings
M	half rotor mass
M_b,M_r	rotor mass for left or right span and middle span, respectively
p	total pressure
δp_r,δp_s	small changes in force in r_e and s directions
R	journal radius

r_e,s	reference axes
(.)	d/dt
(,*m*)	d/dm
U	journal surface velocity
x,y,z	reference axes
α_t	stability parameter related to the rotor speed
βr, βs	angular displacements of rotor-axis about r_e and s directions
ω_{cr}	pin-pin critical speed of the flexible rotor
De	Deborah number

Greek symbols

ω	journal angular speed
℧	stress tensor component
λ	relaxation time
μ	fluid viscosity
ϵ	eccentricity ratio, e/c
ϕ	attitude angle
θ	angular coordinate
[ ]	element-arrays in multi bond graph
η	eccentricity of the rotor mass

CHAPTER-1

INTRODUCTION

1.1 Motivation

The crucial requirement to address and reduce the issues associated with vibrations in high-speed rotating shafts is the impetus for the research being conducted on squeezing film dampers. This need has been the driving force behind the study. [1] High-speed rotating equipment, such as compressors, turbines, and engines, often suffers harmful vibrations, which may lead to mechanical breakdowns, decreased efficiency, and higher expenses for maintenance. Squeeze film dampers provide a viable solution to the problem of these vibrations, as well as an improvement in both the overall performance and the dependability of rotating systems. The fundamental reason is the capability of squeezing film dampers to efficiently manage and dampen vibrations, hence enhancing the operational stability and longevity of high-speed rotating shafts.[2] These dampers function by generating a lubricating layer between the rotating components and the stationary components. This reduces the effect that vibrations have on the system while also allowing excess energy to be dissipated. The purpose of this study is to increase our knowledge of the complex dynamics involved in the application of squeeze film dampers by examining how different adjustments in factors such as speed, pressure, and oil mix might maximize their function. Furthermore, the motivation extends to the larger objective of offering important insights into engineering practices, where the deployment of appropriate vibration control methods is vital. This is because engineering practices are always striving to improve their efficiency. We hope that by conducting in-depth research on squeezing film dampers, they will be able to develop workable solutions for businesses that rely on high-speed rotating equipment, which would eventually lead to an improvement in such businesses' levels of productivity, dependability, and overall operational integrity.

The use of squeeze film dampers across a variety of different sectors has the potential to contribute to economic development in several different ways, including the following[3]**:**

- *Increased Machinery Efficiency*: Squeeze film dampers improve the overall efficiency and performance of important pieces of industrial equipment such as turbines, compressors, and engines by efficiently minimizing vibrations in high-speed rotating machinery. greater production, less downtime, and reduced maintenance costs are all direct results of greater machinery efficiency. These improvements have a favorable influence on the economic output of companies that depend on this equipment.
- *Extended Equipment Lifespan*:[4] Squeeze film dampers serve a critical function in decreasing wear and tear on rotating shafts by dampening vibrations. - Squeeze film dampers also play a role in extending the lifespan of equipment. A longer lifetime for equipment results in lower capital expenditures for replacements and upgrades, which in turn promotes cost savings for industries over the long run.
- *Enhanced dependability and Safety*: [5]The use of squeeze film dampers helps to improve the dependability and safety of high-speed rotating equipment. - Squeeze film dampers also help to reduce vibrations in machinery. A decrease in vibrations makes for a more steady functioning, which in turn reduces the likelihood of catastrophic occurrences and mechanical breakdowns. This greater dependability helps to create a working environment that is safer and safeguards important assets, which in turn helps to keep economic activity going.
- *Decreased Need for Frequent Maintenance Interventions*: [6] Squeeze film dampers aid in decreasing the need for frequent maintenance interventions by minimizing excessive vibrations that may contribute to component wear. This helps to reduce the overall cost of maintenance. The reduced need for maintenance translates into cheaper

operating expenses, which in turn frees up resources for additional investment possibilities and economic development projects.

- *Optimized Energy Consumption:*[7] Squeeze film dampers contribute to the optimization of energy consumption by decreasing the energy losses associated with excessive vibrations. This helps to make the system more efficient. Enhanced energy efficiency is essential for businesses that want to lower their operating expenses while also adhering to sustainable business practices, which will contribute favorably to the achievement of economic and environmental objectives.
- *Technological breakthroughs and Innovation*: [8] Research and development efforts focused on squeeze film dampers support technological breakthroughs and innovation in the area of rotating equipment. Continued advances in damper design, materials, and application procedures may lead to the creation of solutions that are more efficient and cost-effective, promoting a culture of innovation that promotes economic growth.
- *Competition in the Market*: Businesses that use innovative technology, such as squeeze film dampers, can acquire a competitive advantage in the market. - An increase in competitiveness may entice investments, propel the creation of new jobs, and contribute to the expansion of both the domestic and international economies.

In conclusion, the use of squeeze film dampers in industrial applications not only improves the performance of high-speed rotating machinery but also contributes to economic growth by increasing efficiency, extending the lifespan of equipment, lowering the cost of maintenance, and fostering innovation and competitiveness in the market.

1.2 Overview of Squeeze Film Damper

A squeeze film damper is a mechanical device that is meant to reduce vibrations in rotating equipment, especially in high-speed rotating shafts. It does this by compressing a film of oil

between two plates. It functions on the concept of producing a lubricating coating between the rotating and stationary components, which has the effect of efficiently reducing vibrations and dissipating excess energy. This particular kind of damper is often used in a variety of industrial applications, such as turbines, compressors, and engines, where it is essential to keep vibrations under control and improve system stability.[9] A squeeze film damper's essential construction normally consists of a hollow that is filled with lubricant and is situated between the rotor and the stator. Because of the rotation of the shaft, the lubricant layer undergoes compression, which results in the creation of a hydrodynamic pressure. This pressure works against and neutralizes the effects of the vibrational forces. This method results in the efficient reduction of vibrations, which contributes to the overall dependability and lifetime of the spinning equipment. sketch view is shown in Fig 1.1.

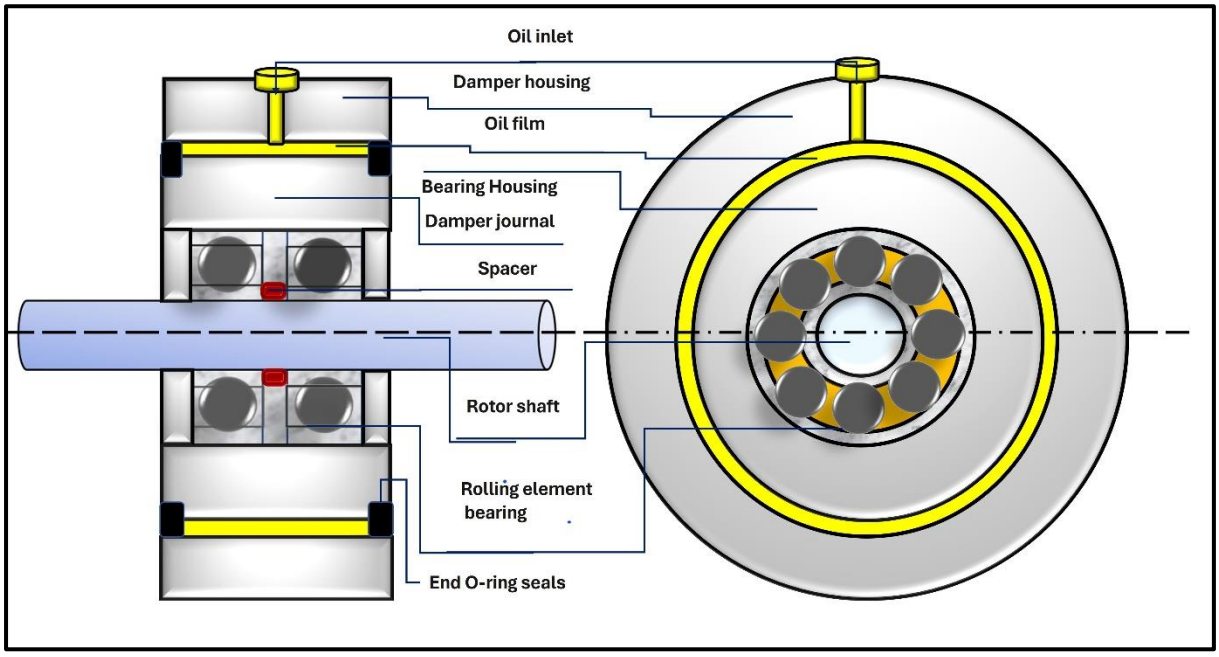

Figure1.1. Details part of Squeeze film damper assembly with rolling element.

The primary objective of research and development efforts in the area of squeeze film dampers is to improve the effectiveness of these devices by analyzing the effects of important factors such as rotating speed, oil pressure, and the make-up of the lubricating mix. The

objective is to arrive at the best possible design for high-speed rotating systems, one that will reduce vibrations as much as possible while maintaining effective functioning. Squeeze film dampers are an essential component of many manufacturing processes in sectors where accuracy, stability, and decreased mechanical wear are of the utmost importance. Ongoing research attempts continue to deepen our knowledge of the complicated dynamics of squeeze film dampers in order to provide practical solutions for enhancing the performance and reliability of high-speed rotating equipment across a variety of industrial sectors. The goal of these research activities is to provide solutions for improving the performance and reliability of high-speed rotating machinery.

1.3 Evolution of Squeeze Film Damper

In the 1950s and 1960s, as a solution to the problems that were caused by vibrations in high-speed rotating equipment, the idea of squeezing film dampers came into being as a reaction. This period was significant because it represented the beginning of the understanding of the need to address vibration-related concerns in order to increase the effectiveness and dependability of industrial equipment**.** Evolution shown in figure 1.2

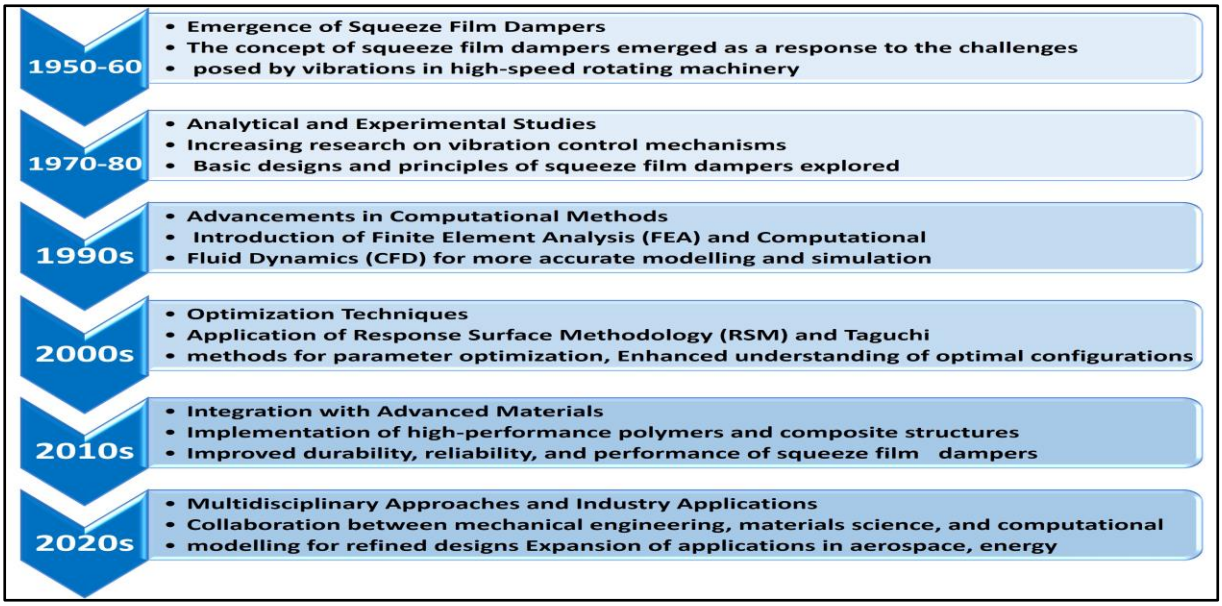

Figure 1.2 Development of squeeze film damper

Squeeze film dampers came into existence as a result of the awareness of vibration-related issues in high-speed rotating equipment. This realization was the driving force behind the development of the technology. Initial study paved the way for further breakthroughs in the discipline by laying the underlying concepts, laying the foundations for basic designs, and establishing foundational principles.

1.3.1 The birth of squeeze film dampers (during the 1950s- 1960s)

Initial realization of the need to solve vibration concerns in high-speed rotating equipment. The fundamental concepts that we presented focused on the use of a lubricating coating to reduce friction between the rotor and the stator[10].

- ***Recognizing the Problem:*** Scientists and engineers realized that vibrations negatively impacted high-speed rotating equipment, which resulted in mechanical breakdowns and decreased the machinery's overall efficiency. The existence of a system that could regulate and attenuate these vibrations became an obvious need.
- ***Fundamental Designs Developed***: The first designs of squeeze film dampers were distinguished by the incorporation of a lubricating film in the space between the components that rotated and those that remained fixed. These fundamental designs had the goals of reducing vibrations and increasing the machine's general stability while it rotated at high speeds.
- ***The fundamental Principles Are formed During this time period***,: the fundamental principles of squeezing film dampers were formed. These principles include the formation of a lubricating film as well as the influence that film has on the reduction of vibrations. Initial endeavours in the form of experimental studies and analytical approaches laid the groundwork for further endeavours in the form of exploration and development.

- ***The key Objective of the Preliminary Research***: When squeeze film dampers were first developed, the key objective of the preliminary research was to understand the underlying dynamics and principles that control their functioning. Early researchers were crucial in laying the framework for further investigations, both analytical and experimental, which would enhance the technology throughout the course of the next decades.

1.3.2 Comparative and Experimental Research (1970 - 1980s)

The decade of the 1970s and the decade of the 1980s saw a change in emphasis away from squeezing film dampers and toward a more in-depth investigation that included both comparative and experimental studies. This time period was significant because it represented the beginning of a greater knowledge of the mechanisms that are involved in dampening vibrations as well as a comprehensive analysis of the basic designs and operating ideas of squeeze film dampers. Principal Components of the Investigation[11]:

- ***A rise in Research effort:*** In the 1970s and 1980s, there was a large rise in the amount of research effort that was devoted to studying the behavior of squeeze film dampers. The researchers wanted to get a greater understanding of the complex dynamics involved in the process of dampening vibrations since they were aware of the important part that these dampers play in enhancing the stability of high-speed rotating gear.
- ***Comparative Studies:*** Researchers compared the performance of squeeze film dampers to that of a variety of different vibration control methods via the use of comparative research using this method, the goals were to determine the benefits and drawbacks of squeeze film dampers as well as evaluate how well they functioned under a variety of different operational settings.

- ***Experimental Investigations:*** [12]For the purpose of validating theoretical models and ideas, experimental investigations included the actual testing of squeeze film dampers in the real world. Experiments were carried out by the researchers in order to determine the amount by which vibration was reduced, examine response characteristics, and evaluate the influence of various operational factors, such as rotational speed, oil pressure, and materials.
- ***Basic Designs and Operating Principles:*** The researchers investigated the basic designs as well as the operating principles of squeeze film dampers. This phase involves the development and optimization of the first concepts presented during the birth of squeeze film dampers, with the goal of improving their performance and dependability.
- ***Validation of Analytical Models***: Experimental Evidence Used to Validate Analytical Models Experimental evidence was used to validate analytical models that were produced during this time period. The objective was to guarantee that theoretical models adequately portrayed the observable physical behavior of squeeze film dampers when used in actual-world scenarios.
- ***Experiments to study the Sensitivity of Squeeze Film Damper***: Performance to various Characteristics Researchers carried out experiments to study the sensitivity of squeeze film damper performance to a number of different characteristics, including film thickness, materials, and geometric configurations. The purpose of this was to determine the ideal settings for minimizing vibration while maintaining stability.
- ***Recent Developments in Analytical Instrumentation:*** The behaviour of the damper was able to be characterized in more depth and accuracy because of developments in measuring tools, such as sensors and data-collecting systems. An in-depth investigation of the dynamic response of squeezing film dampers was made possible

with the assistance of high-speed cameras, accelerometers, and other types of instruments.

1.3.3 Developments in Computational Methods in the 1990s

In the 1990s, a significant change occurred in the methodology used for investigating squeeze film dampers, as computational approaches were introduced and further developed. The use of these techniques facilitated the development of more advanced models, analysis, and simulations, hence enhancing the comprehension of the dynamic characteristics shown by squeeze film dampers.

The following are the key aspects of the developments[13]:

- ***The purpose of this section is to provide an overview of Finite Element Analysis (FEA).*** During the 1990s, there was a significant proliferation of Finite Element Analysis (FEA) as a widely used method in the examination of squeeze film dampers. Finite Element Analysis (FEA) has facilitated the development of comprehensive numerical models that depict the structure and behavior of dampers. This advancement has resulted in a more precise depiction of the intricate dynamics between the rotating and stationary components.
- ***Applications of Computational Fluid Dynamics (CFD):*** The use of Computational Fluid Dynamics (CFD) has seen a rise in its application for simulating the behavior of fluids inside the lubricating film of squeeze film dampers. Computational Fluid Dynamics (CFD) has facilitated the examination of flow patterns, pressure distributions, and temperature impacts inside the damper, hence offering valuable insights into the hydrodynamic attributes that contribute to the mitigation of vibrations.

- ***Multi-physics simulations have gained prominence due to the merging of structural mechanics and fluid dynamics***: The use of this methodology enabled the attainment of a thorough comprehension of the interconnected relationships between the mechanical configuration of the damper and the lubricating fluid, effectively capturing the complex dynamics at play.
- ***The use of computational approaches has facilitated the precise forecasting of the dynamic response shown by squeeze film dampers across diverse operational circumstances***. The efficacy of various designs, materials, and settings in vibration control may be evaluated by researchers, therefore reducing the need for expensive and time-consuming experimental testing.
- ***The use of computational tools has facilitated the efficient execution of parametric studies and sensitivity analysis:*** In order to comprehend the influence of damper performance and determine the most favorable design circumstances, researchers have the ability to methodically manipulate input parameters, including film thickness, oil viscosity, and geometric configurations.
- ***Validation against Empirical Evidence:*** The computational models underwent a thorough validation process using empirical data derived from physical experiments. The use of this validation procedure verified that the computational simulations effectively captured the real-world dynamics of squeeze film dampers, hence augmenting the dependability of numerical forecasts.
- ***Progress in computing Resources:*** Enhancements in computing resources, including accelerated processors and expanded memory capacities, facilitated the execution of more intricate and comprehensive simulations. The use of high-performance computers has played a significant role in facilitating the management of extensive

models, hence enhancing the accuracy and authenticity of the depiction of squeeze film damper behavior.

1.3.4 Modelling of squeeze film damper for rotor vibration with bond graph.

Squeeze film dampers are of exceptional importance in maintaining the stability of rotating machinery by attenuating vibrations. To comprehend and enhance the operation of these dampers, it is critical to employ an efficient modeling methodology. Bond graph modeling has become a highly effective and adaptable method for simulating the behavior of intricate mechanical systems, such as squeeze film dampers. The present introduction furnishes a comprehensive outline of bond graph modeling and its utilization in encapsulating the complex dynamics of squeeze film dampers[14].

1. Context regarding Squeeze Film Dampers: Solving vibrations and improving system stability are two common applications of squeeze film dampers in rotating machinery. In order to function, these dampers utilize the dynamic fluid film that forms between a stationary surface and a rotor. It is crucial to have precise models of these absorbers in order to optimize their design and forecast their performance.

***2. Bond Graph Modelling*:** A graphical and methodical approach to modelling multidomain engineering systems, bond graph modelling is a bond modelling technique. The framework facilitates the representation of mechanical, electrical, hydraulic, and thermodynamic components in a unified fashion, enabling a comprehensive comprehension of the dynamics of the system. When considering squeeze film dampers, the utilization of bond graph modeling is beneficial as it permits the seamless representation of both mechanical and fluidic aspects.

3. Constituents of Bond Graph Modelling: Bond graph models comprise fundamental constituents, including components, junctions, and bonds. Components symbolize the

tangible elements of the system, while junctions illustrate the connection locations and bonds represent the energy transfer between elements. Components of squeeze film dampers may consist of fluidic elements that represent the dynamic behavior of the lubricating film and mechanical elements that represent the rotor and stator.

4. *Positive Aspects of Bond Graph Modelling*:

Holistic Representation: By simulating mechanical and fluidic components concurrently, bond graph modeling provides a comprehensive representation of the squeeze film damper system.An energy-based approach is one that is fundamentally physical in nature and enables a more profound comprehension of energy exchanges occurring within the system.System Integration: By seamlessly integrating multiple domains, bond graphs enable a thorough examination of the fluidic and mechanical element interactions.

***5. Implementation in Squeeze Film Dampers*:** The utilization of bond graph modeling is especially advantageous when examining squeeze film dampers, owing to their multidomain characteristics by design. The model possesses the capability to depict the transient characteristics of the fluid film, the dynamics of the rotor, and the consequences of fluctuating operating conditions on the performance of the system.

6. *Importance of the Research*: Comprehending and optimizing the behavior of squeeze film dampers is critical for ensuring the dependable operation of rotating machinery. The versatility and comprehensiveness of bond graph modeling make a substantial contribution to the progress of research in this particular domain.

In conclusion, bond graph modelling is an essential instrument for gaining a thorough comprehension of the dynamics exhibited by squeeze film dampers. The method's capacity to incorporate both fluidic and mechanical components into a cohesive structure establishes it as

a fundamental approach for engineers and researchers aiming to improve the design and functionality of rotating machinery that incorporates squeeze film dampers.

1.3.5 Techniques of Optimization from the 2000s

The use of Taguchi techniques in conjunction with Response Surface Methodology (RSM) in order to optimize parameters. A deeper understanding of the setups that work best for squeeze film dampers. The introduction of optimization approaches, particularly the employment of Taguchi techniques in combination with Response Surface Methodology (RSM), was responsible for a huge leap forward in the research of squeezing film dampers throughout the 2000s. This was a significant step forward in the field. These methods were developed with the purpose of methodically optimizing various parameters and gaining a greater comprehension of the configurations that result in the most effective squeeze film dampers. During the 2000s, the optimization of squeeze film dampers made great progress thanks to the implementation of Taguchi methods in combination with the Response Surface Methodology. This strategy made it possible to efficiently construct experiments, optimize parameters in a systematic manner, and get a deeper knowledge of the configurations that, when combined, result in the best possible performance for the crucial components used in high-speed rotating equipment[15].

1.3.6 Coupling with Innovative Materials (2010s)

In the 2010s, there was a significant advancement in the domain of squeeze film dampers, which revolved on the incorporation of novel materials, notably high-performance polymers and composite construction materials.[16, 17] The objective of this transition was to improve the longevity, reliability, and overall effectiveness of squeeze film dampers, hence introducing a new age of sophisticated technical remedies. In brief, the integration of squeeze film dampers with novel materials in the 2010s represented a pivotal age, enhancing the

robustness, reliability, and overall efficacy of these essential constituents. The incorporation of high-performance polymers and composite construction materials has presented novel opportunities for use in a wide range of challenging operating settings.

1.3.7 Modelling of squeeze film damper to control the rotor vibration with FEM.

The Finite Element Method (FEM) is also used in the present study to model the Squeeze Film Damper (SFD) for rotor vibration.

Introduction: Squeeze film dampers (SFDs) are essential components in the mitigation of rotor vibrations, maintenance of system stability, and prevention of excessive wear in rotating equipment. [18]The Finite Element Method (FEM) offers a robust numerical technique for the modeling and analysis of intricate fluid-structure interactions occurring in squeezing film dampers. This introduction provides an overview of the importance of using Finite Element Method (FEM) to simulate squeezing film dampers in the context of rotor vibration applications[19].

This section provides an overview of the concept and significance of squeeze film dampers.

Squeeze film dampers are often used in the context of rotating equipment to effectively mitigate vibrations that arise during the operational process. The operational mechanism involves the generation of a lubricating film that separates the rotor from the stationary components. This film serves to mitigate vibrations and improve the overall stability of the system.The significance of modeling lies in its crucial role in comprehending the dynamic characteristics of squeeze film dampers and enhancing their design via accurate representation. [18]The Finite Element Method (FEM) provides a computational approach that allows for the modeling of complex interactions among the rotor, lubricating fluid, and other structural elements of the damper.The Finite Element Method (FEM) is a numerical approach used to address intricate engineering challenges by the subdivision of the system

into smaller, more manageable pieces. The interconnection of these parts at nodes facilitates the examination of the collective behaviour of the whole system. The Finite Element Method (FEM) has gained significant popularity because to its adaptable nature in modeling many physical phenomena. Consequently, it has become a suitable approach for investigating the dynamic features of squeezing film dampers.

The components used in Finite Element Method (FEM) modeling for squeeze film dampers are as follows[18]***:***

a. The Finite Element Method (FEM) enables precise depiction of the geometric aspects of a damper, including the rotor, stator, and fluid film.
b. The model incorporates material parameters, such as the stiffness and damping coefficients of the fluid layer and solid components.
c. Fluid-Structure Interaction (FSI) is a computational technique that utilizes the Finite Element Method (FEM) to simulate the dynamic interaction between a rotor and a lubricating fluid. This approach takes into account the deformations and motions of both entities.
d. There are many advantages associated with the use of the Finite Element Method (FEM) in the modeling of SFD.
e. The Finite Element Method (FEM) offers a complete framework for conducting a thorough analysis of the dynamic characteristics shown by squeezing film dampers across a range of operational scenarios.
f. Parameter sensitivity analysis enables the examination of the sensitivity of the damper's performance to various design parameters and operating circumstances.
g. The Finite Element Method (FEM) enables the accurate estimation of crucial dynamic properties, including natural frequencies, mode shapes, and transient responses.

Research Significance: The use of Finite Element Method (FEM) in the modeling of squeezing film dampers for rotor vibration has considerable importance for research and development in the field of rotating equipment. The use of dampers contributes to the enhancement of design efficacy, performance optimization, and overall assurance of equipment dependability throughout diverse industrial sectors. In conclusion, the use of the Finite Element Method to model squeezing film dampers in relation to rotor vibration serves as a crucial tool in furthering our comprehension of their dynamic characteristics. The Finite Element Method (FEM) enables researchers and engineers to effectively model intricate fluid-structure interactions, hence offering significant insights into the design and optimization of squeezing film dampers in rotating equipment[18].

1.3.8 Methods from a variety of disciplines and their applications in the business world (2020s)[20]:

Collaborative effort for developing enhanced designs using mechanical engineering, materials science, and computer modelling.[20] Increase in the number of applications in the aerospace, energy, and industrial industries The decade of the 2020s was a time of great advancement in squeeze film damper technology, spurred by joint work across a variety of disciplines. Increased dependability and application possibilities have been realized in the aerospace, energy, and industrial manufacturing sectors as a direct result of the combination of cutting-edge computational modeling techniques, intelligent materials, and industry-tailored solutions. Because of the persistent dedication to research and development, squeeze film damper technology is certain to continue its march toward more sophistication over the next several years.

1.3.9 Ongoing Research and Potential Future Developments:

The continued research of ideas and concepts related to Industry 4.0, including real-time adaptive control and smart materials. [21]Predictive maintenance and optimization are two areas that might potentially benefit from the combination of artificial intelligence and

machine learning. This overview provides a historical explanation of the significant advances that have taken place in the development of squeeze film dampers throughout the course of their history. The emphasis is made on the development from basic concepts to sophisticated multidisciplinary procedures, as well as on the present research that is being undertaken for future advancements. Additionally, the focus is placed on the progression from fundamental principles to sophisticated techniques.

1.4 Classification of Squeeze Film Damper

Different types of squeeze film dampers may be categorized according to a wide range of characteristics, such as their structural design, the operating principles they adhere to, and the characteristics that are unique to their particular applications. Within the field of squeeze film damper technology, this categorization offers a comprehensive grasp of the myriad configurations and functionalities that are available. The classification is shown in figure1.3.

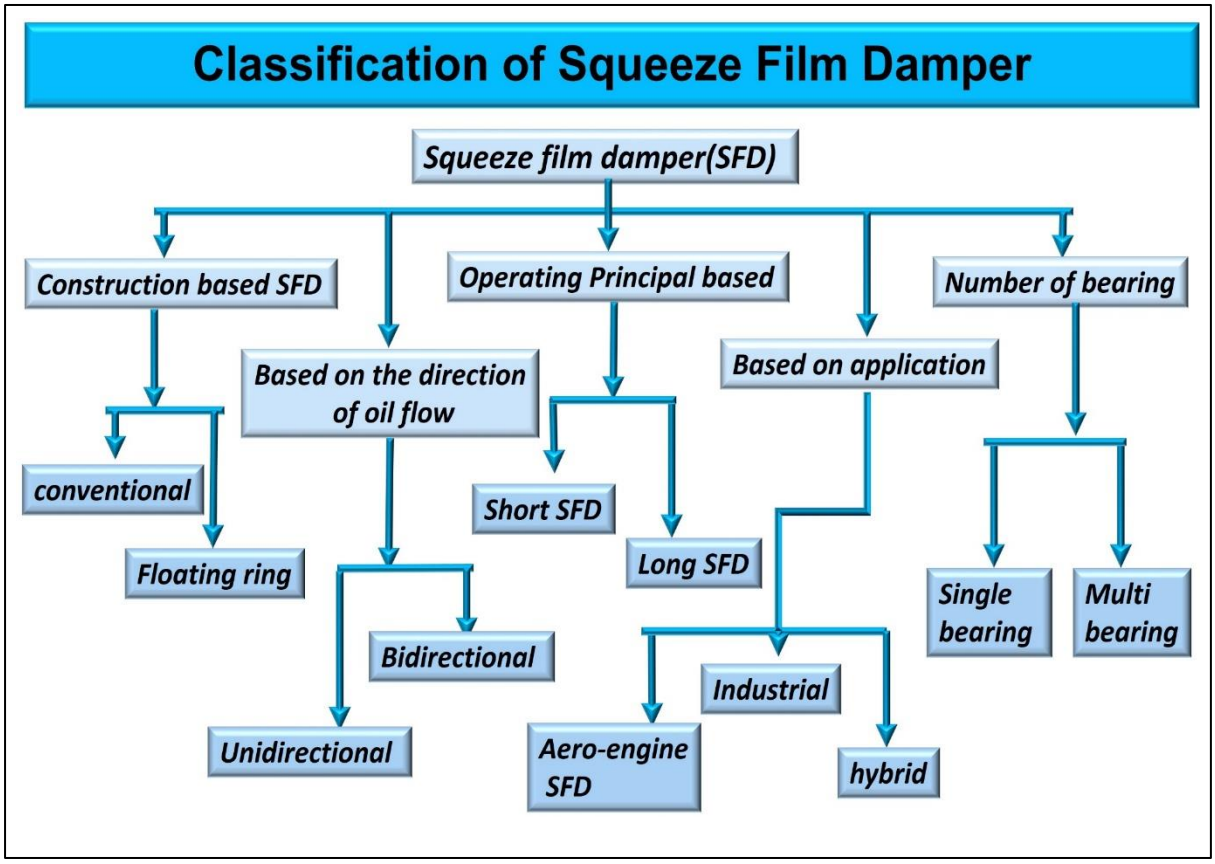

Figure 1.3 Classification of Squeeze Film Damper

1.4.1 Construction-based squeeze film damper

The construction of squeeze film dampers is a pivotal factor that significantly impacts their ability to regulate vibrations in rotating machinery. There are a multitude of construction-based designs, each possessing distinct characteristics and benefits. The following is a synopsis of squeeze film dampers utilized in construction:

(a) Conventional SFD:[22] The typical squeeze film damper (SFD) is a widely used design in diverse sectors to mitigate vibrations in spinning equipment. The fundamental design of this mechanism is the creation of a lubricating film between the shaft in rotational motion and the housing that remains stationary. This film serves the purpose of mitigating vibrations and augmenting the overall stability of the system. The design, characterized by a simplistic arrangement, exhibits a high degree of dependability and finds extensive use in the aerospace, power generation, and industrial production sectors. Ongoing research is now investigating developments in the field of conventional SFDs, with a focus on integrating modern materials and smart technologies to enhance their performance. These efforts aim to build upon the existing reputation of simplicity and dependability associated with conventional SFDs.

(b)Floating ring SFD: The purpose of the unique design known as the floating ring squeeze film damper (SFD) is to enhance the damping performance of spinning equipment. To further improve the damper's ability to suppress vibrations, this particular version incorporates a floating ring inside the device. Because the design enables more adaptation to various operating circumstances, it is especially useful in applications with dynamic and variable loads. This is because the design allows for greater versatility. Floating ring solid-state dampers (SFDs) provide an innovative answer to the problem of precise vibration control. In comparison to traditional damper designs, these SFDs provide enhanced adaptability and performance[23].

1.4.2 Squeeze Film Damper (SFD) Based on the Flow Direction of the Oil

There are different types of squeeze film dampers based on the direction of oil flow inside the damper.[24] These dampers are very important for reducing noise in spinning machines. This description helps us understand how the lubricating oil moves inside the damper and affects how well it dampens. Based on the way of oil flow, here is a list of SFDs:

(a) Radial Squeeze Film Damper for Flow: This type of SFD has rotational flow, which means that the rubbing oil moves from the center to the edges or the other way around. Construction: The damper is made to make it easier for the oil to move in a circle, making a thin film that reduces tremors. Performance: Radial flow dampers work well to stop vibrations that travel in a radial direction, which means they can be used in places where radial forces and vibrations are present[25].

(b) Squeeze film flow damper with circumferential flow: [26] Circumferential flow SFDs have oil flow that goes around the moving shaft, either along it or around it. Construction: The damper is set up to support the flow of rubbing oil around its edges, which makes it better at damping. In terms of performance, circumferential flow dampers work well in situations where shocks mostly happen around the moving parts themselves.

(c) Squeeze film damper for mixed flow:

Description: The oil flow pattern in mixed-flow SFDs has both circular and circumferential parts. The construction of these dampers lets oil move in both circular and circumferential directions, which gives you a lot of options for stopping shocks. Mixed-flow dampers work well in a wide range of situations with complicated shaking patterns because they can change them[26].

(d) Squeeze film damper for axial flow: As the name suggests, an axial flow squeeze film damper (SFD) lets lubricating oil move along the length of a spinning shaft. Construction:

The damper makes it easier for oil to move along the axis, which creates a lubricant film that stops motions along the axis. [26]Performance: Axial flow dampers work well to stop movements that happen mainly along the axis, which makes them good for uses where axial forces are present.

(e) Patterns of complex flow: [26]According to the needs of the application, some more advanced SFD designs may have flow patterns that are complicated and custom-made. Construction: These dampers are designed to get specific oil flow patterns that work best for reducing vibrations in complicated situations. Performance: Dampers with a complex flow pattern are made to precisely control certain sound qualities, making them a perfect fit for a wide range of uses.

1.4.3 Based on the operating Principle

(a) Short Squeeze Film Damper: [27] When it comes to controlling vibrations in rotating equipment, a short squeeze film damper is a design that is both small and straightforward. It generally comprises a condensed structure with a reduced axial length, which qualifies it for use in situations where space limitations or unique operating requirements need a damper that is more compact and uncomplicated. Short squeeze film dampers may have inherent limits in terms of their dampening capability; yet, the simplicity of these dampers and the ease with which they may be integrated make them useful in a variety of industrial situations.

(b) Long Squeeze Film Damper: An extended axial length is the defining characteristic of a long squeeze film damper. [27]This kind of damper offers higher dampening capacity in addition to greater stability. This type is often used in situations where increased vibration control is critical, and when it is possible for a longer extended damper to give higher performance. Long squeeze film dampers are well-suited for situations with greater rotational speeds or bigger vibrational amplitudes. This is because the longer length enables a more significant lubricating film, which contributes to efficient vibration abatement. In addition, long squeeze film dampers are more cost-effective than short-squeeze film dampers. While

the expanded design does provide improved dampening capabilities, it may need thorough engineering considerations in order to solve possible issues related with increasing complexity and the need for more space.

1.4.4 Based on the SFD application

Squeeze film dampers (SFDs) may be classified according to their specialized uses, allowing for the customization of their design and operation to accommodate the distinct demands of various sectors. This categorization offers valuable insights into the ways in which SFDs are tailored to suit certain purposes, hence enhancing their efficiency across diverse applications.

(a) Aerospace Squeeze Film Damper is a device used in the aerospace industry. [28] Aerospace SFDs are purposefully engineered for use in aircraft propulsion systems, gas turbines, and aerospace gear. The construction of these dampers places emphasis on the use of lightweight materials, the ability to withstand high temperatures and the precise management of vibrations. These features are crucial in order to fulfil the rigorous demands of the aviation and aerospace sectors. The performance of aviation engines is enhanced by the inclusion of Aerospace SFDs, which play a crucial role in maintaining stability and dependability. These devices effectively reduce vibrations, hence optimizing the overall performance of the engines.

(b) The Industrial Squeeze Film Damper (SFD) is specifically designed for use in demanding industrial environments, where it is used in conjunction with high-duty machinery.[29] These applications often include rotating equipment found in manufacturing facilities and other heavy machinery applications. The design of these dampers prioritizes sturdy construction, long-lasting performance, and convenient maintenance in order to meet the requirements of uninterrupted production operations. The use of Industrial SFDs has been shown to significantly boost the operating efficiency of equipment via the reduction of vibrations, mitigation of wear and tear, and improvement of overall dependability.

1.4.5 Based on the number of bearings used in SFD

The number of bearings that are integrated into the construction of squeeze film dampers (also known as SFDs) may be used to classify these dampers. This categorization sheds light on the structural complexity of SFDs as well as their capacity to adapt to a variety of various applications. The following is a rundown of several types of SFDs according to the number of bearings:

(a) Squeeze Film Damper with a Single Bearing: [30] Single-friction dampers that use a single bearing to support the spinning shaft inside the damper are referred to as single-bearing SFDs.The damper has a single bearing element in its construction, and this bearing is often positioned in the middle of the shaft. Application Single-bearing SFDs are used in applications where simplicity and convenience of design are important, and where a single point of support is adequate for vibration control. This kind of SFD is also used in situations where a single point of support is all that is required for support.

(b) Squeeze film damper with many bearings:[31] In order to provide support for the spinning shaft, multiple-bearing SFDs include more than one bearing element in their design. In terms of construction, these dampers include extra bearings that have been carefully placed along the length of the shaft to improve the damper's stability and disperse loads. Multiple-bearing SFDs are used in applications where a dispersed support system is required. This provides increased stability, which is particularly beneficial in situations with complicated loads.

1.5 Application of Squeeze Film Damper

Squeeze Film Dampers (SFDs) are used in many sectors where the exact management of vibrations and stability in rotating gear is of utmost importance. The following are few prevalent uses of Squeeze Film Dampers:

(a) Aerospace industry: [32]heavily relies on the use of SFDs in various components such as aircraft engines, gas turbines, and aerospace gear. The significance of SFDs in aerospace applications lies in their capacity to regulate vibrations, hence enhancing the stability and efficiency of aircraft engines. This is particularly crucial in such contexts where weight, dependability, and accuracy are of utmost importance.

(b) Power Generation: SFDs are used in the operation of turbines and generators found in power plants. Significance: Within power generating systems, the implementation of SFDs plays a crucial role in optimizing the efficiency and dependability of rotating equipment. This is achieved via the reduction of vibrations, promotion of seamless operation, and mitigation of potential damage caused by wear and tear[33].

(c) Industrial Manufacturing: Application:[34] SFDs find use in the operation of robust industrial gear, including compressors, pumps, and manufacturing equipment. Significance: Within industrial environments, the use of SFDs plays a crucial role in enhancing the durability and effectiveness of equipment.This is achieved via the mitigation of vibrations, minimization of mechanical deterioration, and enhancement of overall dependability.

(d) Automotive Engineering: Application: SFDs are used in the field of automotive engineering, namely in the context of high-performance and precise automobile Significance: Within the realm of automotive systems, the implementation of SFDs plays a crucial role in enhancing engine functionality by mitigating vibrations and optimizing the overall performance of the vehicle. [34] High-speed rotating equipment, such as spindles in machining centers and turbochargers in automobile engines, often use SFDs for their operations. Significance: Within high-speed applications, Self-Excited Forces SFDs have a pivotal position in the management of vibrations and the maintenance of stability in rotating

components. This, in turn, contributes significantly to the attainment of accuracy and dependability.

(e)The oil and gas industry use SFDs in several applications, [35]including their utilization in drilling equipment, compressors, and pumps. Significance: Within the oil and gas industry, squeeze film damper (SFDs) plays a crucial role in enhancing the stability and dependability of equipment, especially in scenarios involving elevated pressure and rapid operation.

(f) Research and Development:[36] Application: SFDs find use in research and development environments, where they are employed to investigate the management of vibration and the dynamic characteristics of rotating equipment. Significance: Within research settings, SFDs play a crucial role as helpful instruments for examining the impacts of various operational parameters on vibration control. This, in turn, facilitates the development of more effective and dependable systems.

(g) Customized industrial applications:[37] refer to the tailored use of technological solutions within industrial settings to meet specific requirements and optimize operational processes. The use of SFDs is prevalent in many industrial contexts that need meticulous management of vibrations. Significance: Custom applications include the use of customized equipment within various sectors such as research, manufacturing, and other industries. These applications are designed to address particular needs and overcome unique obstacles, hence highlighting the importance of personalized solutions known as specialized functional devices (SFDs). The use of Squeeze Film Dampers exhibits a wide range of applications, including several sectors that heavily depend on the operation of spinning gear. The capacity to provide efficient vibration control plays a significant role in enhancing dependability, minimizing maintenance requirements, and enhancing overall performance across a diverse array of applications.

1.6 Thesis Scope

Upon identification of the research gaps, the focus will shift toward the development of a Squeeze Film Damper that incorporates various combinations of lubricants. This damper will be designed specifically for high-speed rotor shafts. Subsequently, a set of goals will be established to guide the whole of the research endeavor. The current research effort intends to thoroughly meet the following objectives:

- To develop the analytical framework for squeeze film damper and feasible study of mixing two lubricants (Newtonian / viscoelastic).
- To develop a computational framework for modelling the SFD through FEM and Bond graphs.
- To develop experimental setup for testing and validation.
- To optimize the various parameters obtained through experiment using the design of experiment.

1.7 Contribution of the Thesis

The primary objective of this thesis is to investigate the experimental and computational aspects related to the study of the design and operating parameters of a squeeze film damper. The purpose of this investigation is to effectively regulate the amplitude of high-speed rotor shaft vibrations. The thesis makes a valuable contribution to the examination of the design and operating parameters of squeeze film dampers by analyzing input and response parameters, as well as conducting optimization.

(a) Study the different types of lubricating oil used in squeeze film dampers and the preparation of a new sample: The research centers on a thorough investigation of

several categories of lubricating oils used in squeezing film dampers, to comprehend their wide-ranging uses and customize their formulations to meet specific damper needs. The study entails a comprehensive examination of the lubricating oils currently used in squeeze film dampers on a worldwide scale. The examination of parameters such as viscosity, thermal stability, and lubricating qualities is conducted in order to identify the particular attributes that contribute to the optimum functioning of dampers. Furthermore, the scope of the inquiry includes the development of several formulations of lubricating oils specifically designed to cater to certain damper applications. This involves conducting experiments to explore different oil compositions in order to get acceptable characteristics, taking into account issues like as load capacity, temperature resistance, and shear stability. The primary objective of this study is to present a comprehensive analysis of the customization of lubricating oils for squeeze film dampers. This research aims to provide a detailed knowledge of how personalized lubrication solutions may improve the effectiveness and durability of these crucial components in various operating contexts.

(b) Experimental investigation of squeeze film dampers for high rotor speed and oil pressure: The primary objective of this research is to conduct empirical investigations on the performance characteristics of squeeze film dampers under certain operating situations via practical experimentation. The present study focuses on examining the performance characteristics of squeeze film dampers under conditions of elevated rotor speeds and variable oil pressures. The experimental methodology enables a practical investigation of the operational mechanisms of these dampers under situations that closely resemble real-world scenarios. The objective of this research is to provide significant insights into the performance attributes of squeeze film dampers, especially in scenarios that include high rotor speeds and

fluctuating oil pressure levels. The results obtained from this experimental study have implications for enhancing the design and performance of squeeze film dampers in applications involving high-speed rotating equipment.

(c) **Modelling of squeeze film damper for flexible rotor using Box-Behnken design with desirability optimization:** The study entails the use of the Box-Behnken design with desirability optimization to develop a squeeze film damper for a flexible rotor. This work centres on the systematic design of the squeeze film damper using the Box-Behnken experimental design technique. This statistical approach enables the efficient exploration of the design space. The use of desirability optimization is performed in order to determine the most ideal combination of parameters that contribute to the desired performance characteristics of the damper. The objective of this study approach is to augment comprehension about the interplay between different design factors and their influence on the flexibility and efficiency of the squeeze film damper within the framework of a flexible rotor system. The results obtained from this research have the potential to enhance the development of more efficient and optimal squeeze film dampers specifically designed for flexible rotor applications.

(d) **Comparative analysis of Artificial Neural Networks and Response Surface Methodology with Experimental Results:** This study conducts a thorough comparative analysis of Artificial Neural Networks (ANN) and Response Surface Methodology (RSM), including experimental data to integrate both approaches. The accuracy, efficiency, and adaptability of Artificial Neural Networks, which draw inspiration from the functioning of the human brain, and Response Surface Methodology, a statistical approach used for experimental design, are assessed in terms of their ability to capture intricate correlations within experimental data. The

primary objective of this study is to provide a comprehensive analysis of the advantages and disadvantages associated with each strategy, therefore offering significant insights for both academics and practitioners who are interested in using predictive modeling approaches. The incorporation of empirical findings guarantees the pragmatic significance of the study, providing a solid viewpoint on the efficacy of the approaches. This study has important in providing guidance for the selection of an appropriate modeling approach, taking into consideration the characteristics of experimental data. Ultimately, this contributes to the progress of predictive modeling techniques in many scientific and industrial domains.

(e) Vibration Analysis of High-Speed Rotor Under Variable Point Load Condition with and without Squeeze Film Damper: This chapter provides a comprehensive analysis of shaft vibrations under various point load scenarios. Additionally, it evaluates situations both with and without the incorporation of a squeeze film damper (SFD). The experimental configuration involves meticulous modifications in load positioning at distances varying from 10 to 50 centimeters from the terminal support. Vibration amplitudes are carefully monitored along the x and z axes throughout the whole procedure. The vibration amplitudes exhibit a notable increase when the load is in closer proximity to the support. Nevertheless, as the load is displaced to a greater distance, the magnitudes of vibration diminish, especially beyond the primary extent of the shaft. In addition, the consistent loaded state is guaranteed by the deployment of a Structural Force Distribution (SFD). When comparing vibration amplitudes, it is seen that the conditions remain constant regardless of whether there is a variable point loading or a fixed oil supply pressure. These conditions are similar to those observed when the SFD is not present. Furthermore, this research examines the influence of oil viscosity on vibration amplitude, demonstrating a progressive

decline as viscosity approaches its ideal threshold. Ultimately, a comprehensive examination of vibration amplitudes was carried out to examine the impact of the presence or absence of the SFD. The findings unambiguously demonstrate that the implementation of the SFD resulted in reduced amplitudes of rotor vibration. This exemplifies the significant influence of oil viscosity and the SFD in mitigating vibrations in the rotor system. This research offers useful insights into the dynamic behavior of the shaft under various load conditions and emphasizes the influence of the SFD on the observed vibrational patterns.This study expands its range by exploring the examination and formulation of experiments used in the enhancement of squeeze film dampers, encompassing both the input and response variables.

Upon doing an extensive examination of the literature, it becomes apparent that previous research has not adequately used approaches such as the Taguchi methodology or Box-Behnken design in the context of optimizing squeeze film dampers. This study seeks to address the aforementioned research gap by introducing innovative experimental design techniques. Specifically, the Taguchi methodology and Box-Behnken design are used to increase the comprehension and optimization of input and response parameters within the domain of squeezing film dampers. The present creative technique aims to provide significant contributions to the area by uncovering new pathways for enhancing the performance and efficiency of rotating machinery components, therefore offering useful insights that were previously untapped.

1.8 Organization of the Thesis

This thesis is composed of seven chapters, with the ***first chapter***, acting as an introductory section. Within this first portion, the primary aims are clarified using factual information and visual representations, serving as the driving force for the author's undertaking of this

research project. Furthermore, the chapter provides a succinct summary of squeeze film dampers, exploring their historical evolution and many methods of implementation. The comprehensive presentation of dampers in this study encompasses their categorization, working principle, and many applications in the control of vibrations in high-speed rotating shafts. This serves as a foundation for future chapters, which provide a more in-depth analysis of the topic. ***Second chapter****,* this chapter provides an overview of the prior research undertaken on the subject of the Squeeze film damper (SFD) of a spinning shaft. This chapter provides a comprehensive assessment of the existing literature on design modification and use of squeeze film dampers (SFDs) as well as advancements in regulating shaft vibration via SFD operation. This chapter also addresses the existing gap in the literature and outlines the objectives of the current study.

Third chapter, Experimental investigation of squeeze film dampers for high rotor speed and oil pressure: This chapter discusses the methodology and experimentation details for achieving the thesis objectives. This chapter is divided into three parts. In the first part, explain the various types of lubricant and the details of various sample preparations by blending two fluids. In the second part, explain the experimental test rig details along with the data collection process design of the experiment (DOE) also applied for optimization. ***Fourth chapter,*** Modelling of Squeeze Film Damper for Flexible Rotor utilizing RSM (Box-Behnken Design with Desirability Optimization: The experimental design optimizes the input parameters and determines the statistical significance of the model by using a Box-Behnken design Experimentation and verification are carried. The desirability optimization was also carried out for the process parameter for vibration-controlling through a squeeze film damper.

Fifth chapter, Experimental Investigation of Squeeze Film Dampers and a Comparative Analysis using Artificial Neural Networks (ANN) and Response Surface Methodology

(RSM): In this chapter experimental results compare to the ANN modeling prediction value as well as RSM modeling prediction value concerning error analysis. ***Sixth Chapter,*** this chapter discusses shaft vibrations under point loads. Squeezing film damper vs. non-SFD. The experimental setup includes precision load placement 10–50 cm from the terminal support. The process thoroughly measures x and z axis vibration amplitudes. More vibrations occur when the load is closer to the support. As the load goes away, vibration amplitudes decrease, particularly beyond the shaft's main length. A SFD ensures continual loading. With shifting point loading, vibration amplitudes match those without the SFD under constant oil supply pressure. This study also reveals that optimal oil viscosity reduces vibration amplitude. Compare SFD with non-SFD vibration amplitudes to conclude. SFD clearly lowers rotor vibrations. These data suggest oil viscosity and SFD minimize rotor system vibrations. This research illustrates how SFDs alter shaft vibrational patterns and dynamic behavior under different loads**.**

Seventh chapter, the seventh chapter should consist of the thesis's conclusion. It provides a summary of the main findings of the entire thesis and outlines the potential avenues for further research.

CHAPTER-2

LITERATURE REVIEW

2.1 Introduction

The focus of this chapter is on the investigation and review of squeezing film dampers of experimental, computational analysis-related studies and also a review of the optimization-related design and process parameters to effectively control vibration amplitudes in high-speed rotor shafts. Several research has been conducted to investigate different elements of vibration reduction using squeeze film dampers. These studies have used numerous strategies, including the use of short-length designs with O-ring and piston ring seals, as well as the utilization of different lubricants and the manipulation of the pressure position of the seal. The next portion of the thesis largely focuses on doing a literature study about the examination of squeeze film dampers in the context of controlling high-speed rotor vibration. The literature review may be roughly classified into three primary categories: experimental research, computational investigations, and analytical studies. The present study conducts a thorough review of the current literature, which serves as a foundation for the original contributions made by this thesis. These contributions mostly include experimental, computational, and analytical evaluations aimed at enhancing the performance of squeeze film dampers in vibration control.

Introduction- The purpose of this thesis is to conduct a comprehensive and in-depth literature study within the field of squeeze film dampers (SFD), taking into account the many uses of these dampers in the turbines, aircraft, and industrial sectors. The extensive range of applications for SFD brings about the need for this study. In order to appreciate the subtle development of knowledge in this specialized sector, it is necessary to conduct a comprehensive analysis of research initiatives that have been conducted in the past as well as

those that are now being conducted. The review of the relevant literature has been painstakingly divided into three independent approaches: analytical, computational, and experimental. The objective of this categorization is to provide a thorough and systematic grasp of the existing state of knowledge. In doing so, it provides a solid basis for the subsequent studies that will be analytical, computational, and experimental in nature, which will comprise the heart of this thesis.

2.2 Literature study done using an analytical methodology:

Aims to thoroughly examine research papers and academic works that use analytical techniques to investigate squeeze film dampers (SFDs). Analytical techniques involve a diverse range of mathematical and theoretical approaches aimed at comprehending the dynamic behaviour, performance, and optimization of SFDs. The review presents a comprehensive analysis of both current and past literature that explores the analytical elements of SFDs. This includes research on their structural design, dynamic modeling, and the impact of different factors on their performance. This section provides a comprehensive evaluation of the strengths and limitations of various analytical techniques used in the context of SFDs. It aims to develop a nuanced comprehension of the theoretical principles that form the basis for analyzing and optimizing these essential components in diverse engineering applications.

2.2.1 Investigation of type of oil use inside the SFD.

Še Dominik et al. (1989), [38]The author examines the force effects on the squeeze film damper's rotor using Newtonian and magnetorheological fluid. In Newtonian oil, which has a constant viscosity, the research examines how high velocities and narrow gap widths affect damper force effects. The experiment also uses variable-viscosity Magnetorheological fluid. The research found that force effects strongly rely on coil electric current. The study examines how viscosity, gap width, and electric current affect force effects in squeeze film

dampers using constant and changing viscosity lubricants. ***Olivier Bonneau et al. (1997)***, [39]The research presents several bearing dynamic behavior models that account for shaft flexibility and a nonlinear dampening feature. The research also uses a variable viscosity squeeze film damper to examine rotor behavior. Key criteria include shaft rotation speed, bearing properties, and radial clearance. Significantly, damper clearance increases damping, especially near the critical speed. A greater clearance increases squeeze film damper displacement and energy dissipation. This study improves our knowledge of bearing systems with nonlinear damping and variable viscosity dampers, which are useful for rotor dynamics and vibration control**.** ***Fulei Chu et al. (1998),*** [40]The research compares the simple iteration, quick integration, and H-B numerical approaches for fluid squeeze film dampers. The research examines annular clearance bearing, eccentricity ratio, and oil film forces. The study thoroughly evaluates each method's pros and cons and applies them to a nonlinear rotor system issue. The Runge-Kutta and rapid integration methods can handle varied situations, including oil film extent, and give steady-state and transient insights. This work explains computational methods for investigating the complicated dynamics of fluid squeeze film dampers in rotor systems. **J.I.** ***Inayat-Hussain et al. (2003)***,[41]The research analyzes the nonlinear relationship between dynamic forces from large rotor imbalance and fluid-film forces from cavitated squeeze film dampers, which may restrict their ability to reduce rotating equipment vibrations. These complex interactions cause rotor responses to bifurcate, which the research examines. The natural frequency, rotor angular speed, dynamic viscosity of the lubricant, spring parameter, and centering spring stiffness are important. The gravity parameter (W) is calculated by the rotor's weight before choosing the spring parameter (S) for squeeze-film dampers in spinning equipment. To demonstrate damper-facilitated rotor response bifurcations, the article only studies vibration response amplitudes. We can better build and use squeeze film dampers by understanding the complicated dynamics of rotor

systems thanks to this study. ***J. I. Inayat-Hussain ett al.(2005),***[42]This research examines how design and operating characteristics (bearing, gravity, and mass ratio) affect the response of a flexible rotor supported by a Squeeze Film Damper (SFD) without centering springs. The impacts of rotor stiffness, damper length, journal mass, bearing parameter, dynamic lubricant viscosity, and imbalance parameter are analyzed using direct numerical integration. In particular, the bearing parameter (B) affects bifurcation onset speed and speed parameter (X) non-synchronous response. Design parameters include the damper's length, radius, radial clearance, journal mass, rotor pin-pin critical speed, and lubricant viscosity, which affect the bearing parameter (B). The article also stresses the importance of lubricant temperature, which may greatly affect squeeze-film dampers. This study is useful for improving the design and operation of flexible rotors supported by SFDs and understanding their complex dynamic. ***J I. Inayat-Hussain et al.(2006),*** [43]A stiff rotor's imbalance response is studied numerically using dampers without centering springs and eccentrically controlled dampers with centering springs. The investigation examines a rotor with Squeeze Film Dampers (SFDs) without centering springs, including its half-mass (m), damper radius, length, radial clearance, the dynamic viscosity of the lubricant, rotor angular speed (x), and centering spring stiffness (k). In the first regime, period-doubling bifurcations of the period-1 rotor response cause chaos, according to the research. The period-3 rotor response exhibits chaotic vibrations from a saddle-node bifurcation through a succession of period-doubling bifurcations. In the third regime, a saddle-node bifurcation causes the period-3 orbit to evaporate, causing chaos and a possible boundary crisis. This study illuminates the intricate dynamics that cause chaos in rotor systems with varied dampers. ***D. susan-Resiga et al.(2009)*** [44] A stiff rotor's imbalance response is studied numerically using dampers without centering springs and eccentrically controlled dampers with centering springs. The investigation examines a rotor with Squeeze Film Dampers (SFDs) without centering springs,

including its half-mass (m), damper radius, length, radial clearance, dynamic viscosity of lubricant, rotor angular speed (x), and centering spring stiffness (k). In the first regime, period-doubling bifurcations of the period-1 rotor response cause chaos, according to the research. The period-3 rotor response exhibits chaotic vibrations from a saddle-node bifurcation through a succession of period-doubling bifurcations. In the third regime, a saddle-node bifurcation causes the period-3 orbit to evaporate, causing chaos and a possible boundary crisis. This study illuminates the intricate dynamics that cause chaos in rotor systems with varied dampers. ***Amir a. Younan et al.(2011),*** [35]As the mass ratio of air bubbles inside the oil grows, there is a corresponding drop in the pressure that is created. Notably, a reduction of 36% is found between pure oil and a mass ratio of 0.003. Furthermore, the impact of nonlinear forces decreases as the mass ratio of bubbles in the lubricant increases. The presence of air bubbles in the oil of a squeeze film damper results in a decrease in its load capacity. This highlights the fact that the more air bubbles are entrained in the oil, the lower the damper's ability to bear loads. ***Cai-Wan Chang-Jian et al.(2012)***[45] This work aims to examine the influence of the imbalance parameter on the vibrational properties of a gear-bearing system via theoretical analysis. The analysis explores the non-linear dynamic behaviour of the system, taking into account common assumptions for imbalance and different rotational speed scenarios. The objective of this study is to provide valuable insights into the impact of the imbalance parameter on the vibrational characteristics of gear-bearing systems. This will contribute to a more comprehensive comprehension of the dynamic reactions shown by these systems under various operational circumstances. ***Wei Chun Hsu et al.(2014)*** [46]**,** The present study presents a theoretical framework that serves as a basis for the development of efficient designs for Squeeze Film Dampers (SFDs). The equations of motion for the system are derived, taking into consideration a thorough pie oil film model that incorporates fluid inertia. The presented theoretical framework enhances

comprehension and possible enhancement of SFD design, providing useful insights for researchers and practitioners engaged in the domain of rotor dynamics and vibration control. ***Jaroslav Zapoměl et al.(2017)***[47],The study models magnetorheological (MR) dampers in rotor systems mathematically. Force couplings provide extremely non-linear equations that accurately describe the rotor system's behavior. Stability of computational methods for lateral vibration analysis is the main goal. This research improves the computational analysis of rotor systems using MR dampers, concentrating on non-linear dynamics and stability. ***Petr Ferfecki et al.(2017)*** [11],This article develops a mathematical model for a flexible rotor with magnetorheological squeeze film dampers. It describes how to get semi-analytical relations for damper gap magnetic induction. The essay describes these linkages' validity and application and highlights their main contributions. The research examines how magnetorheological damping devices reduce lateral vibrations in flexible rotors, revealing its effectiveness and usefulness in rotor dynamics. ***Jawaid I. Inayat-Hussain et al. (2009)*** [48]A flexible rotor supported by magnetorheological squeeze film dampers is mathematically modelled in this article. The damper gap's magnetic induction may be calculated using semi-analytical relations. These connections' validity and application are described throughout the paper, along with their main contributions. The paper investigates how magnetorheological damping devices reduce lateral vibrations in flexible rotors, revealing their performance and scope in rotor dynamics.

2.2.2 Review of inertia force Analysis of the rotor for SFD.

J. Zhang et al.(1993),[49]This research presents different methods of deriving the short cylindrical Squeeze Film Damper (SFD) by using a reduced two-dimensional Navier-Stokes equation as the fundamental basis. The study places particular emphasis on the importance of convective inertia factors throughout the derivation procedure. The main contributions of the paper are to the investigation of nonlinear inertia force components, which arise from both

temporal and convective sources. Through illuminating these complex facets, the study enriches our comprehension of the dynamic mechanisms operating within short cylindrical SFDs, providing vital perspectives for future progress in the realm of rotor dynamics and vibration mitigation. ***M.A.Rezvani et al.(2000)***[16],This study examines how damper ring rigidity, mass, and damping affect squeeze film damper frequency response. These factors greatly affect SFD performance and frequency response variations. Individual analyses of stiffness, mass, and damping explore their interplay and provide engineering insights. Challenges and limits guide future research. SFD design optimization improves the efficiency and performance of crucial components in varied engineering systems. ***J.Iqbal Inayat-Hussainet al.(2001)*** [50]To locate bifurcation sites and assess periodic solution stability, this study uses numerical continuation. This approach is shown to find crucial spots and understand solution stability from them. The numerical continuation technique is useful for identifying bifurcations and testing periodic solution stability in complex, dynamical systems. This work advances numerical methods for investigating nonlinear systems and illuminates bifurcation analysis and stability assessments. ***M.M.Altug et al.(2010)*** [51]**,**The Green's function technique is used to develop compact analytical models for compressible squeeze film dampers (SFDs). Distribution to the Reynolds equation captures coupling effects in the models. An analytical knowledge of compressible SFD behavior is simplified by Green's function. The models' compact but comprehensive framework for measuring compressibility's impacts on squeeze film dampers applies Reynolds equation distribution to coupling. This work advances analytical techniques for analyzing complicated dynamics in compressible SFDs. ***Cai-Wan C-Jian et al. (2010)*** [45]This study shows complex rotor system dynamics with periodic, subharmonic, and aperiodic responses. Adding a pair stress fluid improves system dynamics and reduces unwanted movements. A High-Speed SFD (HSFD) design with active control addresses squeeze film damper (SFD) system non-

synchronous vibrations. Two pairs of Proportional-Derivative (PD) controllers in static chambers with electro-hydraulic controlled orifices and actuators eliminate non-synchronous vibrations. This research helps improve rotor system dynamic responses for active control and dampening tactics. ***C.Wang et al.(2011)***[52]**,**The study designs a squeeze film air journal bearing using CFX and FEA simulations. The research examines the air layer between two flat plates with one vibrating sinusoidally. The squeeze film air journal-bearing design principles are derived from CFX and FEA simulations. The study uses computer analysis to optimize the bearing's design for better performance. This research provides bearing design expertise that might improve efficiency and functionality. ***Cheng Bai et al.(2014)***, [53]This research solves the nonlinear Reynolds equation with inhomogeneous boundary conditions to study analytical model border effects. The research analyzes system behaviour using Green's function technique. This analytical technique allows detailed border effect research, improving model correctness. The work makes the nonlinear Reynolds equation more realistic by including inhomogeneous boundary conditions. Through an analytical approach, this study illuminates squeezing film dynamics, notably border effects. ***Huizheng Chen et all.(2014)***[54]**,**This research examines three bifurcation modes in a rotor system, distinguished by transition sets like bifurcation and hysteresis in the system parameter plane. Dynamically varying Reynolds number reveals fluid inertia's effect on squeezing film dampers. The study illuminates rotor system bifurcation events and fluid inertia's impact on system dynamics by designating areas based on these sets. It advances rotor dynamics and squeeze film damper fluid inertia understanding. ***Giovanni Adiletta (2015)***[55] , study analyzes a two-lobe rotor extensively, including system description and parameter selection. Important system characteristics such wave amplitude, orientation angles, and gravity residuals are examined. Research reveals rotor system dynamics via careful discussion. Explaining system parameters and how they affect the two-lobe rotor is the focus. Rotor

dynamics are better understood by knowing how system parameters affect system behavior. ***Rajesh C. Shah (2015)***[56],This work provides a ferrofluid-lubricated bearing design system with an upper spherical surface and a flat porous plate that accounts for a changeable magnetic field. Self-lubricating porous plates are beneficial. Research determines and quantitatively calculates squeezing film properties to understand ferrofluid-lubricated bearing behaviour. The research helps explain how magnetic impacts affect the lubricating system by considering a fluctuating magnetic field. This research is important for ferrofluid and porous plate bearing design and optimization. ***H.R. Heidari (2016)***[57], This research examines system response and bifurcation occurrence when spring stiffness asymmetry increases in the y direction. It is interesting that such an increase does not affect system reaction or bifurcation. In the x direction, greater stiffness causes instability and period-doubling bifurcation in the system response. Note that gravity in the y direction causes these events. This study illuminates the system's complex dynamics and how stiffness factors and external forces affect bifurcation behavior. ***J Zapoměla et al.(2017)***[58], Based on current operating circumstances, the magnetorheological damper adjusts damping force magnitude. With this adaptive function, rotor vibration amplitudes may be reduced while rotor frame force is minimized. The damper dynamically adjusts damping forces to provide excellent vibration suppression and minimum force transfer to the rotor frame. To improve rotor system performance under various operating situations, this technology is flexible and responsive. ***Hamidreza Heidari et al.(2016)***[59], Stiff rotor supported by a squeeze film damper (SFD) with asymmetric centralizing springs is examined in this work. The shooting technique is used to examine the imbalanced rotor response, and the Floquet Theorem is used to verify the stability of the findings. Asymmetry in centralizing springs is examined in this thorough rotor-SFD system dynamic research. The Floquet Theorem is used to study the system's stability at imbalance by using sophisticated mathematical methods. ***Changhu Xing et***

al.(2010)[60],The research emphasizes that the nonlinearity of the inertia coefficients is mostly influenced by the modified Reynolds number, Re. In some instances, it is possible for them to demonstrate a limited reliance on this parameter. The aforementioned discovery highlights the significance of taking into account the modified Reynolds number while examining the nonlinear characteristics of inertia coefficients. This approach offers valuable insights into the complexities of fluid dynamics inside systems that are influenced by these coefficients.

2.2.3 Review Analysis of the oil feeding Grove in the SFD.

T.Qingchang et al. (1997)[61],The spinning rotor's orbit radius increases with a feeding groove. Increases diminish the squeeze film damper's (SFD) vibration isolation. Orbit radius rises with feeding groove size. A stiff rotor's imbalance reactions are affected by the feeding groove, which alters jump-down phenomena. The effects of feeding grooves on vibration isolation and imbalance responses in a rotor-SFD system are examined in this research. ***Qingchang Tan et al.(1999)***[62]**,**The objective of this research is to examine the influence of a feeding groove on the imbalance response of a flexible rotating squeeze film damper (SFD). This study presents novel film force modes that explicitly include the effects of the feeding groove and fluid inertia on the dynamic features of the system. The objective of this study is to investigate the impact of a feeding groove on the imbalance response in a flexible rotation SFD. This investigation considers the complex interaction among the feeding groove, fluid dynamics, and the dynamic characteristics of the system. ***Keir HarveyGroves et al.(2010)***, [63]The main objective of this work is to investigate the adjustment of the Reynolds equation in order to improve efficiency and mitigate cavitation in squeezing film dampers (SFDs). This research investigates a range of factors including feed grooves, feed ports, end plate seals, and supply pressure. The objective of this study is to enhance the performance of SFDs by analyzing the design and operational parameters specified via the manipulation of the

Reynolds equation. The comprehensive examination examines the influence of these factors on the behavior of the system, providing insights into approaches for enhancing effectiveness and addressing cavitation problems in squeeze film dampers. ***Gi AdilettaI et al.(2017)***[30],This study presents a thorough examination of a rotor with a two-lobe structure. It explores several elements, including the specification of the system and the careful selection of crucial parameters such as wave amplitude, orientation angles, and gravity residuals. By conducting a comprehensive analysis, this study provides valuable insights into the behavior and properties of a rotor with a two-lobe construction. The discourse contains crucial deliberations in delineating the system and selecting parameters, furnishing significant insights for comprehending the dynamics and efficacy of such rotor topologies.

2.3 Literature study was done using a computational approach

This research used computational methods to review the literature. This required computationally analyzing existing literature. To acquire, synthesize, and critically assess relevant computational works in the specified study topic. This method allowed methodical investigation of computational data, deepening comprehension and enabling informed research ideas.

2.3.1 Review of SFD modelling with FEM, CFD.

T. Veijola et al.(2009)[64],The research used Finite Element Method (FEM) simulations to evaluate the precision of basic and precise models in estimating gas-induced damping and spring forces. The findings suggest that both models exhibit effective performance by accurately representing the forces, particularly at frequencies that exceed the resonance frequency of the system's initial gap. ***M. Fischer et al.(1998)***[65]**,**The first verification of the Finite Element Method (FEM) model was conducted by examining the behavior of a plate capacitor. Subsequently, the model was expanded and used in the analysis of a polysilicon

torsional micromirror. The present model integrates the interplay between electrical and mechanical components in order to accurately represent the mechanical displacement resulting from an externally applied electrostatic force. The acquired findings are subject to the effect of internal material tensions that arise during the construction process of the mirror. The Finite Element Method (FEM) model has a high degree of adaptability in comprehensively representing the intricate interaction between electrical and mechanical variables, hence offering significant elucidation on the characteristics of polysilicon torsional micromirrors. ***John A. Tich(1990)***[66],This work presents a simplified model that closely matches JFO (Jeffcott rotor with flexible supports) circumstances and performs supporting tests. The integral technique derives the Ordinary Differential Equations (ODE) for the cavity boundary distance from the bearing centerline and the pressure profile at the centerline. This reduced model reduces numerical effort and maintains accuracy compared to the modified Elrod method. The investigation included testing with an open-ended submerged circular-centered orbit squeeze film damper bearing. ***Chiao-Ping Ku et al.(1990)***[66] ,This research evaluated three different methods: (1) a technique based on short bearing theory; (2) the modified Elrod algorithm using the finite element approach, which is believed to be an accurate solution of the Reynolds equation; and (3) a newly suggested way. The concise bearing model is very simple, although it necessitates enhancements in accuracy for certain scenarios, possibly resulting in overestimations of pressure peaks by as much as 100%. The objective of the assessment was to assess and evaluate the applicability and precision of different approaches, providing insights into their respective advantages and disadvantages in addressing the Reynolds equation. ***P.Y.P.Chen et al.(2000)***[67]**,**This research used Computational Fluid Dynamics (CFD) to examine how the performance of a circular orbiting squeezing film damper with a central circumferential feed groove is affected by the clearance between the end seal and the flow path length. The investigation sought to comprehend the

impact of differences in end seal clearance and flow route length on the operation of the damper. Computational Fluid Dynamics (CFD) methods were used to model and examine the fluid flow dynamics within the damper, yielding valuable information on its functionality in various scenarios.

2.3.2 Review of SFD modeling with MatLab computation and optimization.

Weiyang Qin et al.(2009) [68],The research investigates the analysis of non-linear response and bifurcation events of a rotor that is supported by a Squeeze Film Damper (SFD) and installed on an elastic basis. The research examines the complex interactions within the system, taking into account the non-linear characteristics and possible bifurcations. The research provides vital insights into the intricate behavior of mechanical systems by examining the interaction between the rotor and the SFD in the presence of an elastic basis. ***Jawaid I. Inayat-Hussain et al.(2009)***[48]**,**The work included performing numerical integration of equations using the MATLAB software program. A variable-step continuous solver, based on the explicit Runge-Kutta formula known as the Dormand-Prince pair, was used. The main emphasis was placed on an imbalance parameter (U) with a precise value of 0.1, which signifies the maximum allowable limit within the acceptable balance quality criteria for real-life rotor systems. The acquired numerical findings provide valuable insights into the behavior of the system under the defined parameters, contributing to the comprehension of rotor dynamics with practical applications. ***M.Sadegh et al.(2014)***[69] ,This research examined the effects of design and manufacturing characteristics using a finite element model. Comparison with experimental data from a bulk resonator that operated at its first two Lamé modes and the fundamental extensional mode verified the model's correctness. The system damping study showed that high-order resonators had a greater quality factor at higher frequencies than devices operating at their fundamental modes.

Xiuli Zhang et al.(2015) [70] ,The research emphasizes that the stiffness coefficients generally rise as the loads increase, however there are few cases where this trend does not apply for small eccentricity ratios. When dealing with scenarios where the eccentricity ratios are minor, the stiffness coefficients stay at a low level. Hence, the study indicates that while designing, engineers must meticulously choose the bearing's diameter, length, and radial clearance according to the operational circumstances to guarantee an adequately substantial eccentricity ratio for best efficiency. ***Novikov D.K et al.(2015)***[71] ,This work provides a complete study of parametric damper stage optimization in a "rotor-damper" system. Structural optimization of the damper aims to understand the best parameter selection procedure. The research considers material qualities, geometric requirements, and structural dynamics while configuring and designing damper stages. Through parametric and structural optimization, the thorough study helps optimize the rotor-damper system for maximum performance and efficiency. ***John a. Tichy (1984)***[72],This research shows that fluid inertia affects damping forces even at modest Reynolds numbers. The research shows that relative inertia forces are high throughout eccentricity ratios, underlining the relevance of fluid inertia in squeeze-film damper design. The results show that squeeze-film damper design and technology should account for fluid inertia. This information improves damper performance understanding and guides design. ***Jose J. Granda(2002)***[73],The study explores the use of the Bond graph approach as a modeling tool, specifically for creating state space models and non-linear models. The authors provide CAMP-G (Computer Aided Modeling Program with Graphical input), an advanced software program designed to automate the creation of computer models. Integrating these models with MATLAB-SIMULINK improves simulation capability. This method enables an efficient and automated procedure for developing and using intricate models, demonstrating the capabilities of Bond graph approaches in system modeling and simulation. ***Jose J. Granda & Jim Reus(1997)***[74],The research applies Bond

Graph Modeling to matrix state variable formulation and control system design utilizing MATLAB and its toolboxes. To provide the groundwork for logic, it covers causation and equation creation. The research demonstrates Bond Graph Modeling's potential for system modeling and control system design in MATLAB. Engineers and researchers in dynamic system analysis and control should comprehend the theoretical foundations and practical application of this technique.

2.3.3 Review of SFD modeling with ANN.

Giovanni Adiletta (2008)[75]**,**The study utilizes neural network methodologies to monitor the lubrication conditions in squeeze film dampers that provide support to rotors. The primary objective is to detect and examine pressure waves occurring inside the oil film. Neural networks are used in this application to effectively monitor the condition and analyze the dynamic behavior of lubrication in squeeze film dampers. This work makes significant contributions to the progress of predictive maintenance and real-time monitoring of rotor-bearing systems. It offers valuable insights into the lubrication process and assists in optimizing the operation of squeezing film dampers. ***K.H.Groves et al.(2013)***[76] ,Experimentally trained neural networks successfully recreate the input-output function over the squeeze film damper (SFD) clearance range. Neural networks are used to simulate and comprehend the intricate interaction between SFD performance factors. This method helps create more effective and adaptive squeeze film damper systems by predicting SFD behavior under different situations. Neural networks assist in SFD dynamics prediction and design and performance improvement.

2.3.4 Review of SFD modeling with Bond Graph.

A.Mukherjee &A.K.Samantaray(2000)[77]**,**The program 'SYMBOLS 2000' incorporates the concept of Encapsulation, which is a notable improvement in modeling capabilities. This

functionality allows modelers to generate and incorporate sub-system models, known as capsules, into larger plant or system models. Within a general capsule, there are many related capsules that occur in different causal positions. When a modeler incorporates a generic capsule, the program automatically loads the suitable concealed internal capsule according to the stated boundary constraints. The transparent and dynamic encapsulation of the 'SYMBOLS 2000' program improves the flexibility and effectiveness of system modeling. ***Liming YU& Xiaoye Qi(2012)***[78],Three main components make up this study. Section 1 introduces causal bond graphs. Section 2 discusses system inversion simulation using bicausal bond graphs. The final portion concludes with bond graph formulas for system control synthesis. The strategy in this study helps identify instances where simplifying assumptions may be harmful. In system engineering, the bond-graph approach is especially useful for characterizing physical systems, according to the authors. They say it helps engineers evaluate and solve systemic issues. ***A.K.Samantaray et al.(2010)***[79]The work presents the development of a bond graph model for a spinning shaft system that is powered by a nonideal source. The model clearly demonstrates the connection between the driving force and the sideways vibrations, taking into consideration gyroscopic effects, internal damping caused by rotation, and the impact of rotational imbalance. This modeling technique offers a thorough comprehension of the energy exchanges inside the system, illuminating the intricate dynamics that result from different forms of coupling.

2.4 Literature study was done using an experimental approach.

A comprehensive literature study was undertaken using an experimental technique to acquire a deeper understanding of the subject topic. This included a thorough analysis of empirical observations, research approaches, and results from other investigations, which contributed to a holistic comprehension of the subject field. Exploring experimental literature provides a basis for well-informed analysis and interpretation in the ongoing research project.

2.4.1 Review based on the geometry of squeeze film damper.

J. F. Walton et al.(1987)[80],The article presents the results of an experimental investigation that aimed to detect cavitation in squeeze-film bearing dampers, which are similar in design to the dampers commonly found in aircraft gas turbine engines. The inquiry utilized two discrete damper geometries, and observations were captured via high-speed motion images and stroboscopic video recordings at 20,000 revolutions per minute (r/min) of speed. ***M C Levesley et al.(1996)***[81] ,This paper presents a comparative analysis of the impact that three different variations have on the damping capacity of a squeeze-film damper. These variations are as follows: (a) changing the number of oil-feed holes in the central circumferential oil supply groove; (b) switching from end-seals to piston-ring seals for the sealing arrangement; and (c) adjusting the position of the circumferential supply groove. ***Rosana A. Dias et al.(2011)***[82], The research presents a novel damping design that incorporates air passages to increase the damping performance. The novel shape of this design has considerable promise for enhancing the performance of inertial sensors by providing more sensitivity and stronger noise reduction capabilities compared to current devices. ***P. Bonello et al. (2013)***[83]**,** Based on a twin-shaft test rig, the study presents the results of an exhaustive examination that combines theoretical analysis with practical observations. The configuration of the system is similar to that of actual aircraft engines, since it consists of two rotors that are not balanced and are connected in a nonlinear manner via a housing that may be installed in a flexible manner. When it comes to the dynamics and interactions that occur inside such complex systems, the study offers very helpful insights. ***Ajay Kumar H.N et al.(2016)***[84],The investigation entails the planning and construction of a standard Squeeze Film Damper (SFD) that makes use of Magnetorheological (MR) fluid. Through the use of experiments, it has been discovered that the damping that is produced by the MR fluid grows in a manner that is proportional to the intensity of the magnetic field. The research reveals that there is a

considerable decrease in the amplitude of vibration, which may reach up to 70 percent at the critical speed. In light of this, it seems that MR fluid-based SFDs have the potential to be an effective vibration control mechanism for rotating equipment.

2.4.2 Review based on damping effect of squeeze film damper.

M.J. Adams et al.(1994)[85],the purpose of analysing the squeeze film flow of plastic fluids under a no-slip wall boundary condition, the study makes use of lubrication theory. The fact that there are solutions for both Bingham and Herschel-Bulkley fluids is shown by this occurrence. It has been determined via measurements that the energy associated with extensional viscous flow is insignificant in comparison to the energy that is derived from plastic deformation in lubricated samples of Plasticine. The flow consistency that has been achieved is a combined value of shear and extension**. *Asad A. Khalida etal.(2006)***[86],This research provides a thorough examination of the complicated vibration characteristics shown by Teflon and steel squeeze film dampers. They conduct a thorough investigation to evaluate the magnitude of vibration and the frequency at which resonance occurs across different ranges of frequencies. An important component of their work is calculating the eccentricity ratio precisely at the speed of resonance. This comprehensive analysis offers unique insights into the dynamic characteristics of squeeze film dampers composed of diverse materials, providing a nuanced comprehension of their function under varied circumstances**. *Luis San Andreset al.(2014)***[87],The study presents a robust Squeeze Film Damper (SFD) test equipment specifically built to accommodate high loads. The researchers carefully studied the circular orbits caused by the dynamic load in a large clearance, centrally grooved SFD with open ends. The paper offers an in-depth investigation of the experimental force coefficients of the SFD, specifically defining their properties while operating with three distinct static eccentricities. This study provides vital insights into the dynamic behavior and performance of SFDs, specifically in relation to the fluctuating static eccentricities that occur throughout

operation. ***Fulei Chu et al.(2000)***[88],This study examines the behavior of a flexible shaft that has an overhung disc, which is supported by a Squeeze Film Damper (SFD). The investigation is conducted using both experimental and theoretical methods. Theoretical analysis utilizes the transfer matrix computation to analyze a system consisting of three masses. The research demonstrates that as the level of effective damping grows, the system's resonance moves towards a lower range of speeds. Moreover, the study emphasizes that while high damping is successful in decreasing vibration, it may not completely eradicate subharmonic and superharmonic resonances. This suggests that the connection between damping and resonance events in these systems is intricate and requires careful consideration.

2.4.3 Review based on experimental of squeeze film damper with modelling

C.C. Siew et al.(2002)[89]**,**Squeeze Film Dampers (SFDs) with four varied central groove depths and two different lubricants are the topic of this experimental investigation, which focuses on the vibration response of SFDs at varying degrees of imbalance. The focus of this investigation is on a damper that has a shallow groove. Based on the findings of the research, it can be concluded that the nonlinear vibration response of this particular kind of damper is in good agreement with the recommendations made by Tan et al. in their model 3. Through the use of a simplified Navier–Stokes equation, this model takes into consideration the effects of tiny inertia as well as flow interactions that occur between the groove and the thin film land. ***B. Haider et al.(1990)***[90] ,This research investigates the stability of a system by using both a Squeeze Film Damper (SFD) and a simple journal bearing. The journal bearing functions using Newtonian lubricants, while the stabilizer utilizes a combination of Newtonian and viscoelastic lubricants. The objective of the research is to evaluate and compare the stabilizing properties of various lubricants, offering valuable insights into the performance and efficacy of the combined SFD and journal bearing system. ***Grigory L. Arauz et al.(1997)***[91],The purpose of this work is to determine, via the use of experimental

research, the effect that a circumferential feeding groove has on the dynamic force response of a squeeze film damper. The research investigates a number of alternative designs, such as open-end and sealed dampers, taking into account a variety of groove depths, journal orbit radii, whirl frequencies, and fluid viscosity conditions. Within the context of squeezing film dampers, the outcomes of the experiment provide useful insights into the ways in which the circumferential feeding groove effects the dynamic force response.

2.5 Concise Overview

Squeeze film dampers (SFDs) have been effectively employed to increase damping, expand the range of rotating speed, and decrease vibration levels in numerous applications, including aircraft jet engines, turbo machinery, and commercial compressors. The improvement in operating speed and power-to-weight ratio in turbo-machinery design has led to a lighter and more efficient system of flexible rotor bearings. SFDs are frequently used in high-speed turbomachinery because of their capacity to lessen the forces transmitted to the structure and minimize the amplitude of rotor vibrations. Finding a practical way to reduce machine vibration is essential since rotor vibration is an increasingly common issue. Internal excitation is the most common rotor excitation source. A few examples of internal excitations are imbalance, misalignment, friction, and other elements. Thermal creep, for example, as well as fluid shock are examples of external excitations. As long as the stimulation frequency is somewhat near to the natural frequency, resonance will happen. Along with shortening the rotor's life, this will increase the likelihood of mishaps and costs [92, 93]. The extremely nonlinear behavior of SFDs, which is affected by the rotor's motion and directly affects the rotor's dynamics in the system, plays a role in this. Generally, adding SFDs to rotors significantly improves the system's vibration characteristics; nevertheless, due to their nonlinear properties [13, 94, 95]. It is important to ensure the correct SFDs' architecture and functionality, a rotor dynamic model must be constructed in order to analyze high-speed

turbomachinery vibration characteristics and the dampening effect of SFDs. The operating speed, rotor imbalance magnitude and dampening, and damper design parameters are typically linked to the satisfactory performance of SFDs [8]. By tangentially raising and radially lowering the fluid film response forces, the influence of fluid friction increases the ability of SFDs to dampen. In various research, both theoretically and physically, it has been explored how lubricant inertia affects SFD damping capacity [96–98]. Theoretically, the mass distribution near the midpoint and supports of the model of a basic elastic rotor focusing on elements with SFDs has been researched [99]. In order to determine how design and operational parameters affect, the bifurcation of the unbalance response of a squeeze film damped flexible rotor was studied using direct numerical integration. Speed of onset and improper behavior spectrum the steady-state response of a basic flexible rotor with and without stabilizing springs. The equation of motion created using the straightforward flexible rotor model is unsuitable for the majority of rotodynamic applications, which demand an accurate calculation of shifts in the rotor. Models of multiple-mass elastic rotors, on the other hand, accurately portray rotor behavior. The multiple mass shaft model breaks down the ongoing rotor into a limited number of parts having a limited number of degrees of freedom. Many theoretical investigations on multi-mass, multi-degrees-of-freedom rotors using SFDs have been done [100, 101]. The constant and transient reactions of a Jeffcott rotor supported by SFD with retainer springs were studied while fluid-film cavitation was taken into account. The results showed that the static eccentricity ratio of the journal should be less than 0.4 to produce a low transmission force [102].Zhol et al. [14] investigated journal static eccentricity under short bearing and cavitated-film approximations, as well as steady responses via Poincare map, whirl orbit, bifurcation diagram, and power spectrum analysis. Oscar et al.[105] conducted rotor imbalance response tests and impact tests, used to calculate the damping coefficients of a sealed integral SFD. End plates with known clearance seal both

ends of the SFD. The damping coefficients' finite element predictions agree well with the identified coefficients. The results of the experiments showed that the rotor synchronous response amplitudes at the first and second critical speeds are proportional to the imbalance displacement. Diaz et al. [106] described two methods for determining damping coefficients in a squeeze film damper. The first method involves fitting the damping forces in the time domain with a least-squares curve, while the second involves approximating the rotor orbit with its synchronous components. (Filtered Orbit Method) proposed a principle based on sealing control at the squeeze film damper ends. The axial direction of oil flow affects the pressure distribution inside the damper gap and thus the damping force. In this paper [107], the author used two sets of ball bearings as stabilizers and a journal bearing to control the vibration of a high-speed rotating shaft, and SFD data has been collected using different samples of lubricants. The lubricants sample was prepared with some Newtonian fluid and combined with some viscoelastic lubricants. During a whirl period [108] the thickness of the oil layer fluctuates during vibration, altering the pedestal contact status. Stiffness is provided by both the inner and outer oil films, whereas damping is mostly provided by the inner oil film. Different pedestal contact states were used to study the bearing capacity and oil film properties. Moreover, oil film coefficients in earlier research were usually described as linear functions, which do not accurately represent the characteristics of oil films. Chen et al.[109]utilizing the combined support test rig, a replica of the genuine dual rotor was constructed. Using the finite element approach and component mode synthesis methodology, the vibration characteristics and vibration response of natural bending were examined and integrated with the findings of experiments in both the time and frequency domains. [110–112] The basic flexible rotor model makes the assumption in which the rotor turns complete mass is either dispersed between the bearing centers and in the middle plane or the center of the shaft, or it focused there. The steady-state orbit whirls of a simple flexible rotor supported

by SFDs were examined in this work.[113] For the design of engineering structures with uncertainties, a novel multi-objective discrete robust optimization (MODRO) technique has been presented. The outcomes showed that the algorithm can provide an ideal design in a practical way. [114] To reduce rotor vibration, a squirrel-cage squeeze film damper was used, however it was large, had high nonlinearity, and was prone to nonlinear response. The rotor may experience bistable and locking events when it reaches a critical speed. Xu at al. [115] developed a method that gathers information about rotor vibration in real time. As opposed to this, the monitoring system merely offered fault alerts. Blade vibration must be addressed. [116] The notion of frictional energy dissipation was used to construct a friction damper. The friction damper, however, exhibits a substantial nonlinearity. According to the San et al. [117] an ISFD that is securely sealed has a somewhat greater damper than one that is loosely sealed. It was caused by a lower level of oil leakage in the lubricant furthermore, high supply pressure prevents air from entering the damper film region, according to experimental findings with piston ring sealed ends SFDs. Because of the dynamic pressure field distortion caused by the feed holes, the two identification techniques provide different force coefficients. Jeung et al. [118] work by reporting squeeze film pressure measurements and force coefficient identification in a piston ring-sealed, short-length (L/D=0.2, c/R=0.002) SFD end that is fed with a thin lubricant. The study offers a thorough dynamic force evaluation of a damper fitted with two sets of piston ring that appear to be identical in size but have different leakage flow resistances. This study's [119] objective is to identify and quantify the impacts of squeeze film dampers on dynamical structures in the linear and nonlinear regimes. SFD performance is also determined following substantial analytical research on SFDs. In this research [19], a calculation method is used to explore the dynamic properties and responsiveness of a rotor system supported by an elastic ring squeeze film damper (ERSFD). This article [120] calculated the force parameters in a piston ring

(PR)sealed short-length SFD, which is provided with a low-viscosity lubricant and tested at two different feed pressures: low and high. The 0.89 liters per minute per bar (LPM/bar) test SFD comprises two sets of PRs, with the second set having a larger slit gap, resulting in a higher leakage rate.[121] The study is to assess the advantage of the rotor backing in preventing total oil deprivation in the squeeze film damper. A scholarly rotor dynamic assessment platform has been established and concisely introduced. Trials were conducted for two stationary radial loading scenarios that mimic the complete and inactive states of a particular turbo engine.[86]Teflon and steel squeeze film dampers were used as the subject of vibration analysis, which was conducted using a rotor bearing system that was designed and constructed. In various frequency ranges, the vibration amplitude and resonance frequency are evaluated. The results show that the steel damper has a 10% lower resonant vibration amplitude than the Teflon damper. On the other hand, using the Teflon damper led to a 36% weight decrease.[122] The study looks at how squeeze film dampening affects the Radio Frequency Microelectromechanical Systems (RF-MEMS) switches' ability to respond dynamically. The finite element method is used to study the impact of squeeze film damping on switching time, both with and without perforations.[123] Squeeze film dampers (SFD) effectively suppress the magnitude of transient responses. Flight maneuvers can certainly enhance the dampening impact on the aircraft. During some maneuvers, the forces of aerodynamics impacting on the aircraft vary fast, causing fluctuations in the aircraft's velocity and attitude. These alterations can have an impact on the aircraft's aerodynamic stability and reaction to disturbances. The stiffness of the central spring structure is discovered to play an essential impact in the damping behavior of SFD. Sub- and super-harmonic resonances can occur during flying maneuvers for linear damping supports.[124]This article created a finite element model of the cantilever coupled support rotor with two discs to forecast and explain the nonlinear vibration phenomena. In this research [19] using a computational approach

(ERSFD-rotor). First, the ERSFD oil film pressure and force are calculated using the Reynolds equations. The elastic ring's deformation is then estimated using the finite element method (FEM) based on the Kirchhoff assumption.[125] The rotor dynamic model is created by discretizing the rotor components, including the rotor shaft and disk, into local elements with mass, stiffness, and gyroscopic matrices using the techniques of finite element analysis. [124] The model took into consideration the coupling effects between the rotor and combined support as well as the local nonlinear support force. The study sought to precisely anticipate the behavior and stability of the system by taking these elements into account. The inclusion of these intricate relationships yielded insightful knowledge about the system's operation. [109] The dynamic properties of a rotor system supported by a squeeze film damper (SFD) under aircraft maneuvering can be anticipated, providing theoretical and technological support for the dynamic design of an engine's rotor system mounted on a high maneuverability and agility aircraft.[4] ANOVA is used to investigate the sensitivity of various structural properties like stiffness and stress. For the purpose of multi-objective stiffness and stress optimization, grey correlation analysis (GRA) and the non-dominated sorting genetic algorithm (NSGA-II) are linked.[126]Using Taguchi's method, an optimum dataset of input parameters is created, which is then fed into the two prediction algorithms, artificial neural network (ANN) and multiple regression. [127]In order to analyze and enhance the process' performance, this study suggests using an artificial neural network and genetic algorithm (ANN-GA), a powerful modelling and optimization technique (applicable to any sort of data collection, whether orthogonal or non-orthogonal array design). [128]The Taguchi approach (L9-orthogonal array) is utilized for experiment design, and the experimental findings are examined using analysis of variance (ANOVA).[4] In this article, to develop a unique integral squeeze film-bearing damper(ISFBD), the multi-objective optimization problem is applied. The technique aims to decrease stiffness and stress

convergence. The analysis of variance (ANOVA) is used to investigate the sensitivity of various structural variables such as stiffness and stress. [129] This case study describes the findings of a planned experiment that used a 16-trial design experiment to investigate 14 design factors and one interaction. Conventional mathematical procedures, which are based on specific assumptions, are incapable of providing correct and practical answers to such complicated situations [130–132]. However, during the last several decades, analysis tools and techniques based on artificial intelligence (AI) have shown they have the ability to be consistently used for the modelling and optimization of complicated industrial processes [133–136] . A rise in AI applications has been caused by the ever-increasing processing power of computer systems, better data storage capabilities, and accessibility of current computing platforms [137–140] . This is why cutting-edge AI modelling tools like the artificial neural network (ANN) are ideal for simulating the non-linear vibration characteristics of steam turbine shaft bearings [141] . An example of the large-scale data used for its creation is ANN, which has a greater computational performance and a low memory storage demand. This exceptional quality of ANN allows for effective modelling and simulation of the system's components [142]. In a different study on a gas turbine rotor, ANN and continuous wavelet approach were used to detect vibration in a gas turbine rotor [143] .Using ANN or hybrid ANN-based modelling methodologies, several research investigations with a focus on the vibration reduction and defect detection of bearings have been carried out. A thermal power plant's steam turbine unit has a Neural network installed as a data-driven problem identification and diagnostic tool [139]. Similar to this, artificial neural networks (ANNs) were created for analysing and diagnosing the vibrations of wind turbine bearings [144, 145]. Power plant operational characteristics have been included in the steam turbine shaft bearing's vibration reduction operating strategy through ANN [146] . It is essentially composed of arrays of highly interconnected process elements, otherwise called neurons,

working harmoniously to model specific problems [147]. Its characteristic optimization intelligent structure and design have paved the way for its application in all fields of human endeavors, especially in engineering [148].A comparative study using RSM and ANN modelling for performance prediction[149–152] .A Comparative Study between Regression and Neural Networks for Modeling of different performance parameters test [146].

2.5.1 Review summery of some most effective research

Table 2.1 summarizes some important squeeze film damper research publications on enhancing high-speed rotating shaft vibration control. The research articles examine input and output parameters, rotor features, and vibration control methods. From rotating speed and film thickness to damper shape and external load conditions, input factors vary. System stability, vibration amplitudes, and energy dissipation are output parameters. Each research carefully considers rotor material and geometrical parameters. The optimization methods used include Artificial Neural Networks (ANN), Response Surface Methodology (RSM), and maybe hybrid approaches. In addition, the articles cover squeeze film dampers, including radial, circumferential, and hybrid arrangements. This brief highlights the abundant research on squeezing film dampers for high-speed rotating shaft vibration control and its multimodal approach.

Table 2.1 shows the different types of SFDs and their input, and output process parameters, and the modelling technique.

Authors	SFD type	Rotor details	Input parameters	Response parameters analysis	Type of Research	Technique used	Feature extract
[107] B.Halder et al. [1990]	SFD with stabilizer	Flexible rotor	Speed up to 6000rpm oil- 5 samples	Amplitude of whirl unbalanced responses	analytical experimental	Bond graph modelling	Role of Newtonian and viscoelastic lubricant oil
[153] A.EI.Shafei et al. [2000]	Adaptive hybrid SFD	Flexible rotor	speed up to 15000 rpm	uncertainty analyses, critical speed testing, Vibration amplitude	experimental	HSFD (Hybrid squeeze film damper)	Possible signal design through adaptive control
[112] P.Bonello et al. [2002]	SFD with unbalanced self-alignment ball bearing	Flexible rotor shaft	Speed frequency 500 Hz	Magnitude 10^{-2}m/N Eccentricity at x, y-axis	Modelling and experimental	Floquet stability test RHB, IVF	Versatile and tractable for large order system

[86] Asad.A.Khalid et al. [2006]	Teflon SFD Steel SFD	Flexible rotor two support	Speed of rotor 6000 rpm Oil pressure 3 bar	Vibration amplitude Resonance frequency Eccentricity ratio	experimental	Experimental analysis	Compression of steel and Teflon damper
[106] Sergio E et al. [2008]	SFD with bubbly lubricant	Conical mode of shaft of the rotor	Speed 6000pm, air volume friction 1, frequency 60Hz	Inertia Stiffness Damping	experimental modelling	Experimental analysis	Air damping inside SFD greatly affected by air entrainnet
[117] L.San Andress et al. [2018]	Sealed ends SFD	Variable rotor	Piston ring O -ring Oil pr. 2. Bar	Damping inertia	experimental	Analytical analysis	O- ring produces 20 more stiffness than a piston ring
[123] Bingbing et al. (2018)	SFD with central spring	Flexible rotor with multidisc	Speed, stiffness of spring	Maneuvers pitching, hovering rolling displacement time	Analytical, modelling	FEM, Hybrid Numerical method	Stiffness of the central spring structure is found important role in damping behaviour
[19] Z.Han et al. (2019) 35	Elastic ring SFD	Rigid rotor supported on two ERSFDS	Oil pressure, the thickness of oil film	Eccentricity, offset angle, journal whirl, oil coefficients	Modelling of the elastic ring	FEM Kirchhoff Assumption	ERSFD has better performance than elastic SFD, Oil film Characterise are discussed
[124] Z.Luo et al. (2019)	SFD with squirrel cage	Rotor elastic support	Dynamic viscosity, damper radius, speed shaft diameter, shaft length	Vibration orbit radius, displacement of the shaft at x, y-axis	Modelling, analytical	FEM, Newmark Range-kutta method	Non-synchronous response of the disc at different locations speed range
[125] Sina Hamzen et al. (2020)	Short-length cavitated SFD	Multimass flexible rotor	Squeeze Reynolds number Angular velocity 15000 rpm	Displacement magnitude, Vibration at x, and y-axis, transient orbit radius	Analytical Computational modelling	FEM MATLAB Simulink	Inertia effects of SFD for high-speed jet engines & turbines
[109] Xichen et al. (2020)	Elastic support SFD	Aero Engine rotor system	Shaft diameter, length Speed Oil film	Flight parameters typical maneuver, turning, diving, climbing	Modelling of high-speed shaft	FEM Newmark HHT integration method	The whirl orbit of the journal is limited to a certain range
[4] Yipeng et al. (2021)	Integral SFD, bearing damper	Flexible rotor	Stress, stiffness length, angle Height of oil film	System energy Transmitted force	Modeling & Optimization	FEM, ANOVA, NSG-ii, GRA	ISFED distance26.6% rotor system energy reduces 59.3% transmitted force
[154] Haobo.wang et al. (2022)	SFD for bistable vibration	High pr. & low pr. rotor system	Shaft size, fulcrum stiffness speed, distance disk (HPC, HPT)	Whirl speed critical speed Vibration at the x-z axis Stiffness damping	Analytical Computational modelling	FEM 3D Modelling	Demonstrate the effect of imbalanced mass on rotor vibration.

2.6 Outcome of Literature Review

The literature research conducted on squeeze film dampers (SFDs) has provided valuable insights into several facets of their design, performance, and applications. Below are eleven crucial elements that summarize the results:

- Dynamic Response: Extensive studies have examined the dynamic response of SFDs, focusing on non-linear vibrations, the impact of imbalance, and the complex behavior of the rotor-SFD system.
- The combined lubrication strategy is a new method that combines using SFDs and plain journal bearings together. In this technique, Newtonian lubricants are used in the journal bearing, while both Newtonian and viscoelastic lubricants are used in the stabilizer to improve stability.
- Impact of Feeding Grooves: Experimental studies examined how circumferential feeding grooves affect dynamic force responses. Various damper setups, groove depths, and fluid viscosity conditions were taken into account.
- Bond Graph Modeling: The combination of Bond Graph Modeling with MATLAB has become a potent tool that enables the automated creation of computer models for precise simulations and analysis of intricate SFD systems.
- Optimization Strategies: The research is focused on enhancing the performance of SFDs by tailoring the lubricating fluids. Several formulations were examined, taking into account load capacity, temperature resistance, and shear stability for certain damper applications.
- Comparative Lubricant Analysis: This study examined several lubricating oils used in SFDs to assess their viscosity, thermal stability, and lubricating properties. The goal was to find the characteristics that contribute to the best performance of the damper.

- Development of Experimental Rig: The studies aided in the construction of experimental rigs specifically used for testing SFDs. These configurations enabled precise measurements of dynamic forces, circular trajectories, and force coefficients, yielding significant empirical data for validation purposes.
- Vibration investigation: The investigation of vibrations in SFDs, specifically focusing on Teflon and steel dampers, was carried out. Various frequency ranges were examined, and the eccentricity ratios at the speed of resonance were calculated.
- Investigations on the impact of dual lubrication in SFDs shown that increasing the magnetic field strength resulted in enhanced damping, leading to a significant decrease in vibration amplitudes at critical speeds.
- The ideal depth of grooves for SFDs was determined by studies that took into account elements such as the radii of the journal orbit, whirl frequencies, and lubrication conditions. The objective of this adjustment is to improve the performance and stability of the damper.
- The investigation of optimizing attractiveness and conducting trials in the field of squeeze film dampers (SFDs) exposes a deficiency in the current body of knowledge. Although there has been a significant amount of study conducted on SFDs, the focused use of desirability optimization approaches and systematic design of trials seems to have been insufficiently explored. Desirability optimization is identifying the most favorable combination of input parameters to get desired output responses. Likewise, the design of experiments refers to a methodical methodology for examining and enhancing processes by deliberately altering input components in a controlled manner.

These studies together enhance our knowledge of SFDs by covering many elements of their behavior, lubricating tactics, modeling tools, and experimental procedures.

CHAPTER-3

EXPERIMENTAL INVESTIGATIONS OF SQUEEZE FILM DAMPER SETUP FOR HIGH ROTATIONAL SPEEDS AND OIL PRESSURE

3.1 Introduction

In this chapter, the context of rotating equipment, the management, and mitigation of vibration has emerged as a crucial concern, given the presence of high-speed rotors and their associated vibration. In this intricate environment, Squeeze Film Dampers (SFDs) emerge as essential mechanisms engineered to address and mitigate the intrinsic magnitudes of vibrations linked to high-velocity rotors. This study aims to provide a comprehensive comprehension of SFDs, with a particular focus on their suitability for use in high-speed rotating shafts, which have special and rigorous performance criteria. The complex dynamics of this research are revealed when we explore the interaction of key factors in the SFD process, such as the rotational velocity of the shaft, the internal hydraulic pressure inside the damper, and the specific composition of the oil mixture used. In the context of a flexible shaft reaching a significant rotational speed of 10,000 revolutions per minute (rpm), the objective of this study is to shed light on the intricate aspects of SFD design. This research aims to provide valuable insights beyond the customary limits of vibration control in equipment operating at high speeds.

3.2 Materials and Methodology of Experiments

3.2.1 Lubricant details

In the beginning Squeeze film dampers (also known as SFDs) are essential components in high-speed rotating equipment because they provide dampening and stability. [24]The purpose of oil is to serve as the principal working fluid in SFDs, where it is responsible for

forming a thin coating between the rotor and the damper to minimize friction and dampen vibrations. Lubrication and viscous damping are two of the roles that oil plays in squeeze film dampers. The main purpose of the oil is to act as a lubricant between the rotor and the damper surface, with the end goal of lowering the amount of wear and friction that occurs. In addition to this, the oil coating creates viscous damping forces, which are very necessary for the regulation of vibrations.

1. Mineral oils and vegetable oils are the two primary types of used oil.

Composition: Result of refining operations applied to crude oil as the starting material. Features: It lubricates well and is affordable. Characteristics: Offers excellent lubricity. Applications: SFDs are a common use for this material in a variety of general-purpose industrial applications.

2***. Artificial or Synthetic Oils:***

Composition: Compounds that are the result of a chemical synthesis, such as polyalphaolefins (PAO) or esters. Having superior thermal stability, oxidation resistance, and a broad temperature range are all characteristics of this material. Applications: favored use in SFDs that must function in harsh environments or at very high temperatures.

3***. Oils derived from Vegetables:***

Composition: Produced from plant sources, non-toxic to the surrounding ecosystem. Biodegradable, renewable, and lubricant are some of the characteristics of this material. Emerging as an environmentally acceptable option in a number of SFD applications.

4. Oils that are biodegradable:

Composition: May have a mineral, synthetic, or vegetable foundation, with an emphasis on environmental deterioration as the primary concern. Biodegradable, less hazardous, and

acceptable for use in environmentally sensitive locations are some of its defining characteristics. Applications: Used in applications that are ecologically sensitive, taking into consideration issues about disposal and leakage.

Impact of Oil Characteristics on the Efficiency of the SFD:

Viscosity is an important feature that determines how well something dampens movement. The correct viscosity is essential for achieving the desired layer thickness and damping forces. Temperature Stability is of utmost importance in high-speed applications because of the considerable spike in temperature that might occur in these situations. Synthetic oils often do very well in terms of keeping their stability at extremely high temperatures. Experiments with a Variety of Oil Mixes to Improve the Damping Performance of SFDs The purpose of this research is to improve the damping performance of SFDs by experimenting with a variety of oil mixes. Example Research: Investigations on the effects of varying the proportions of kerosene oil to crankcase oil in order to produce Newtonian liquids. In order to assess the influence that dynamic and kinematic viscosities have on SFD performance, measurements of both types of viscosity were taken.

Concerns and Things to Take into Account:

Cavitation: In high-speed applications, it is necessary to take into consideration the possibility of cavitation as a result of low-pressure zones in the oil film. Leaking Oil: Having effective sealing mechanisms is very necessary in order to stop leaking oil, which may result in decreased performance as well as environmental problems [155]. The most important takeaway is that oil is an essential component of squeeze film dampers since it is responsible for supplying lubrication, viscous damping, and heat dissipation. Diversity of Oils: There are many various kinds of oils, such as mineral, synthetic, vegetable, and biodegradable oils, each of which has its own set of benefits and may be used to create custom solutions for a

variety of applications. Ongoing study: Reflecting the ever-evolving nature of the study in this sector, ongoing studies are investigating the optimum oil mixes to be used in squeeze film dampers, with the goal of improving their damping qualities.

3.2.2 Sample Preparation

As per the study of the various research papers regarding the use of Newtonian and viscoelastic oils for controlling the high vibration amplitude at a high swivel shaft rotational speed inside the damper,[107, 156]at high speeds, the vibration's amplitude can be enhanced by using a Newtonian liquid. Following a comprehensive analysis, different mixtures of kerosene oil and crankcase oil were prepared to create various samples of the Newtonian liquid. The choice of kerosene oil and crankcase oil as the Newtonian liquid in the study is based on several rationales:

a) **Physical Properties**: Kerosene oil and crankcase oil exhibit Newtonian behaviour, which means their viscosity remains constant regardless of the applied shear rate. This property simplifies the analysis and modelling of the fluid behaviour in the squeeze film damper system. Newtonian fluids are commonly used in vibration control studies due to their predictable and well-understood flow characteristics.
b) **Availability and Compatibility**: Kerosene oil and crankcase oil are widely available and commonly used in various industrial applications. Their availability ensures easy access for experimentation and enables practical implementation of the findings in real-world scenarios. Moreover, these oils are compatible with typical squeeze film damper materials, such as metal surfaces, minimizing the potential for adverse chemical reactions or compatibility issues.
c) **Similarity to Real-World Applications**: Kerosene oil and crankcase oil share similarities with other lubricants used in rotating machinery, such as engine oils.

These oils are often utilized in similar operating conditions where vibration control is critical, such as in automotive engines, turbines, or other high-speed rotating equipment. By studying the behavior of these oils in the squeeze film damper setup, the findings can be extrapolated and applied to similar applications.

d) **Previous Research and Established Standards**: The selection of kerosene oil and crankcase oil for vibration control studies in squeeze film dampers is supported by previous research and established standards in the field. These oils have been widely used in previous studies, providing a basis for comparison and facilitating the comparison of results across different research works.

These samples were subjected to pilot experiments to determine the appropriate proportions for five new test samples.

1. Pilot Experiments: The pilot experiments were designed to assess the performance of different oil blend ratios in controlling vibration amplitudes. We conducted a series of preliminary tests using various blend ratios of kerosene oil and crankcase oil. These experiments involved applying controlled vibration forces to the rotating shaft system and measuring the resulting vibration amplitudes at the X-axis and Z-axis.

2. Evaluation of Vibration Amplitudes: The vibration amplitudes obtained from the pilot experiments were carefully analysed and compared. we assessed the damping characteristics and effectiveness of each oil blend ratio in reducing vibration amplitudes. The objective was to identify blend ratios that demonstrated favourable damping properties and achieved significant reductions in vibration amplitudes.

3. Optimization Criteria: Two main factors formed the basis of the precise criteria that were utilized to choose the final blend ratios for the test samples.

a. Vibration Reduction: The primary criterion was to choose blend ratios that exhibited the maximum reduction in vibration amplitudes. We compared the performance of different blend ratios and selected those that consistently demonstrated the highest reduction in vibration amplitudes across multiple test runs.

b. Stability and Consistency: Another important criterion was the stability and consistency of the results. we looked for blend ratios that consistently provided effective vibration control without exhibiting significant fluctuations or variations in the measured vibration amplitudes. This criterion ensured the reliability and reproducibility of the results.

4. Iterative Refinement*:* The selection of final blend ratios involved an iterative process. Based on the results and analysis of the pilot experiments, we identified initial blend ratios that showed promising performance. These initial ratios were then further refined through subsequent pilot experiments to optimize the vibration control effectiveness. A magnetic stirrer was utilized to blend the two oils at a temperature of 30 °C for the new test samples. The five test samples were prepared using a blend of 10%, 20%, 30%, 40%, and 50% of kerosene oil with a kinematic viscosity of 1.263 mm2/s and crankcase oil with a kinematic viscosity of 89.496 mm2/s. The dynamic and kinematic viscosities of these samples were measured using an SVM3000 viscometer. The dynamic viscosity and kinematic viscosity values of 5W30 crankcase oil and kerosene oil at 30°C are shown in Table 3.1. The dynamic and kinematic viscosities of numerous samples are similarly shown in Table 3.2 at a temperature of 30 °C.

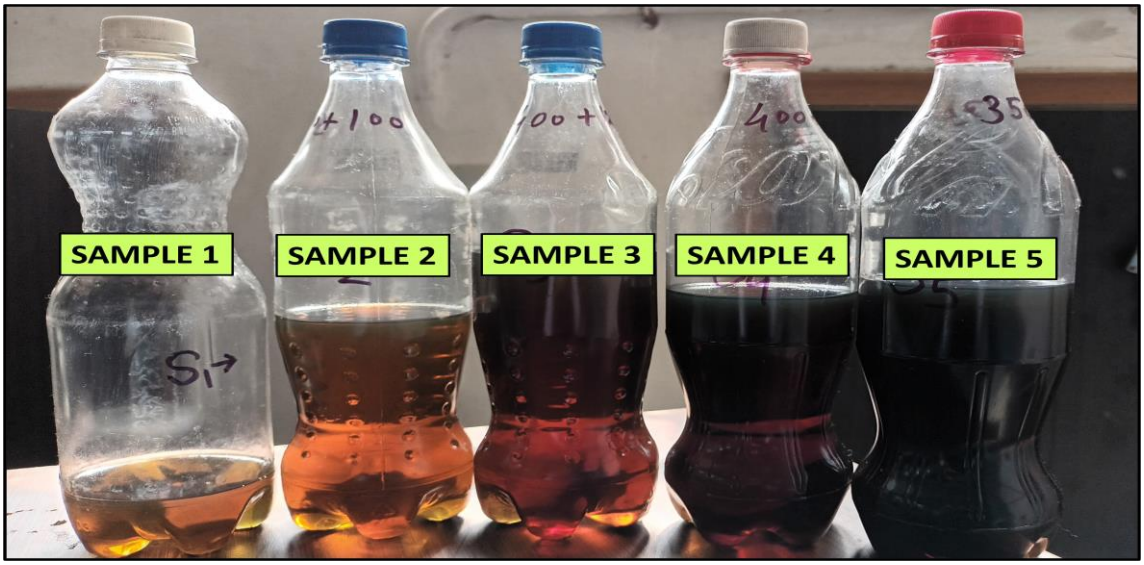

Figure 3.1 Different oil blend sample.

Table 3.1 Dynamic & kinematic viscosity of crankcase oil and kerosene oil at 30ºC

Sample oil name	Dynamic viscosity	Kinematic viscosity
5W30 crankcase oil	75.483 mPa.S	89.496 mm^2/s
Plain kerosene oil	1.1287mPa.S	1.263mm^2/s

Table 3.2 Dynamic and Kinematic viscosities of the samples at 30ºC

Name of sample	Blend Ratio	Dynamic viscosity	Kinematic viscosity
Sample 1	10%	15.786 mPa.S	18.449 mm2/s
Sample 2	20%	19.476 mPa.S	22.811 mm2/s
Sample 3	30%	23.695 mPa.S	27.807 mm2/s
Sample 4	40%	33.684 mPa.S	39.662 mm2/s
Sample 5	50%	46.271 mPa.S	54.666 mm2/s

The offered information is essential for comprehending the viscosity properties of the aforementioned oils and samples, which are important for vibration measurement and control, specifically for applications utilizing squeeze film dampers. The viscosity measurements at the required temperature help researchers in the field better understand the damping efficacy and vibration attenuation characteristics of the oils.

3.3 Experimental Details

A flexible rotor kit with three pinned supports was used in the experimental arrangement. One of the pinned supports that was far from the drive motor was taken out. A pedestal was built to replace the lost support that included a bearing unit and a SFD unit. the conceptual and real views of the test rig are shown in Figure 3.2(a), (b). & 3.3.

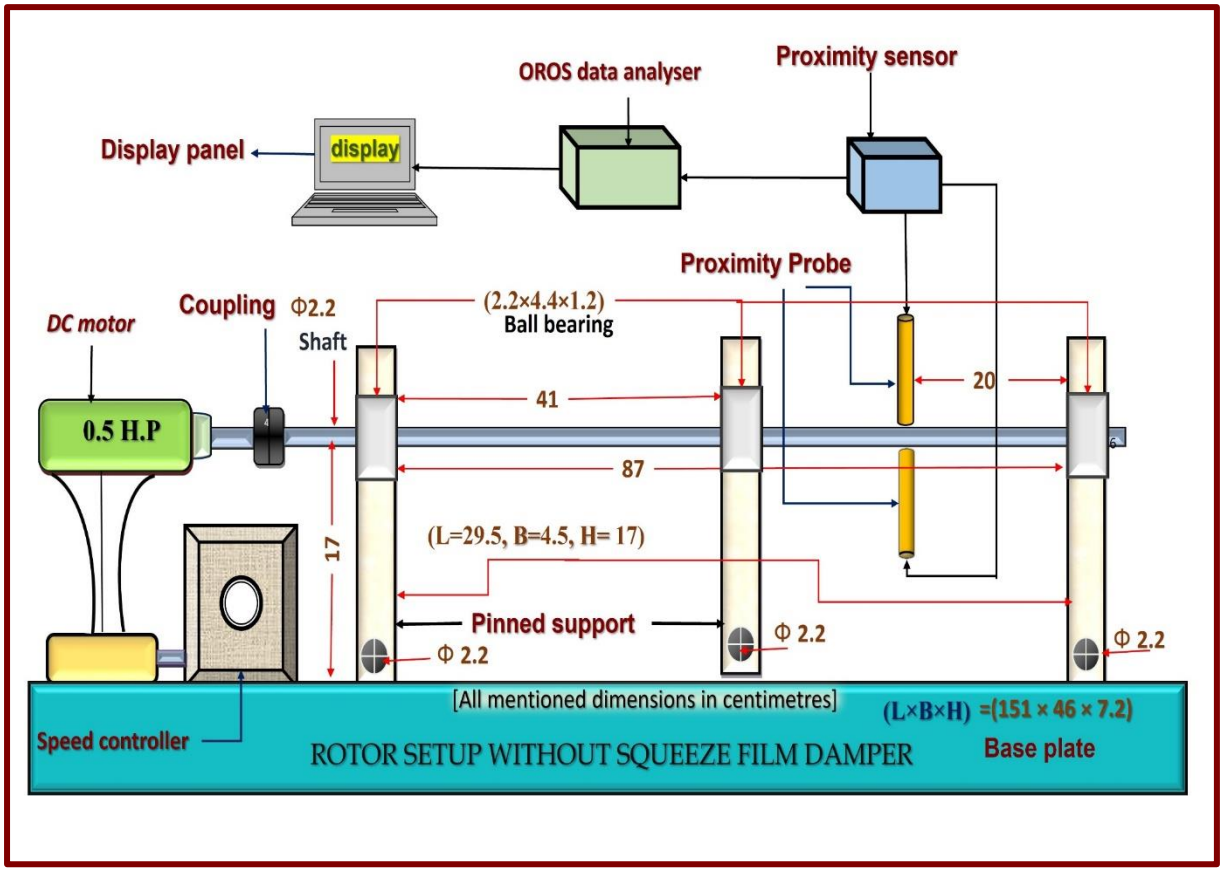

Figure 3.2 (a)Schematic view of rotor bearing set-up without SFD.

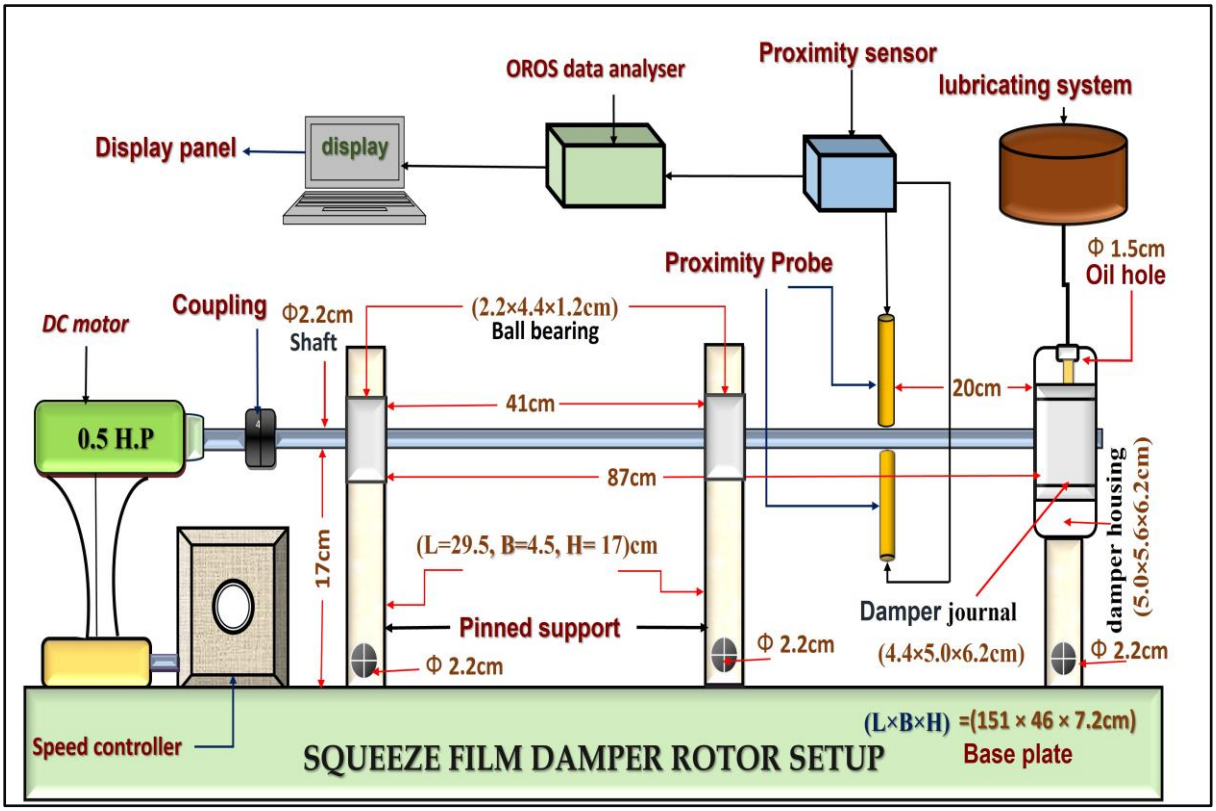

Figure 3.2 (b)Schematic view of squeeze film damper rotor set-up.

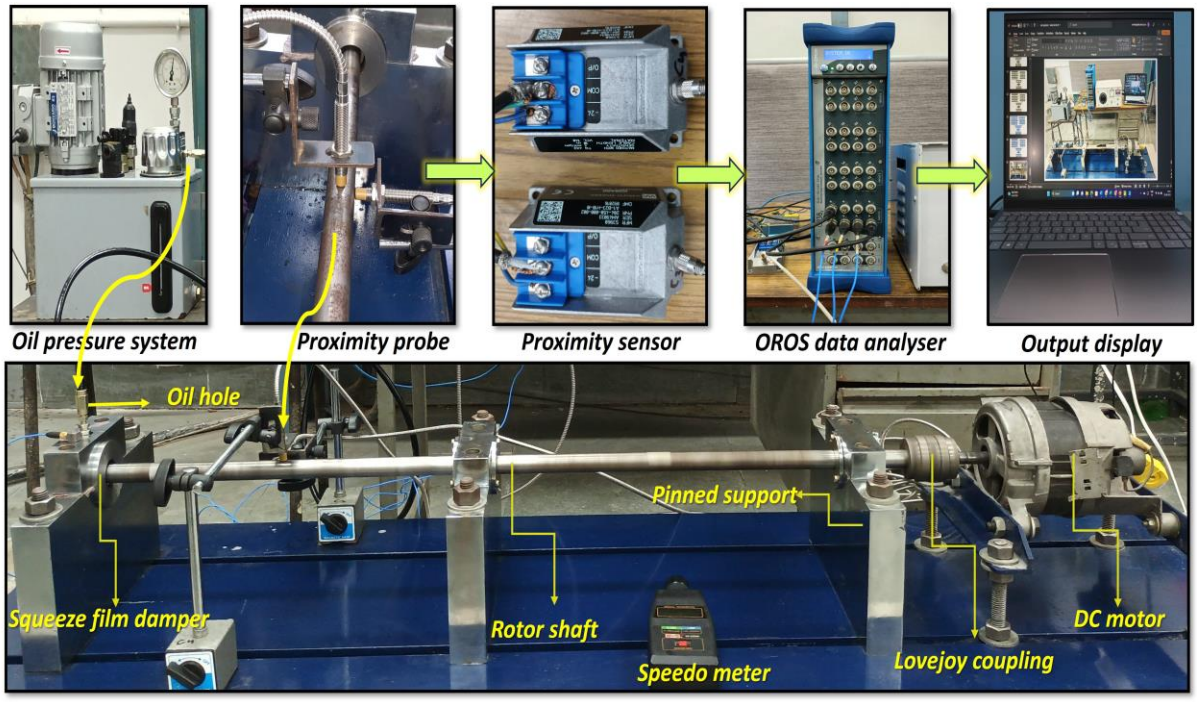

Figure 3.3 Actual test rig diagram along with pickup's location of the signal

Two sets of ball bearings are split by a spacer and make up the squeeze film damper mechanism. The ball bearings were fitted onto the shaft and secured firmly to prevent any radial movement. The lock screw prevented the outer races from rotating and was placed inside a hole with a bigger diameter in the spacer. The schematic and actual views are shown in Figure 3.4 and Figure 3.5.

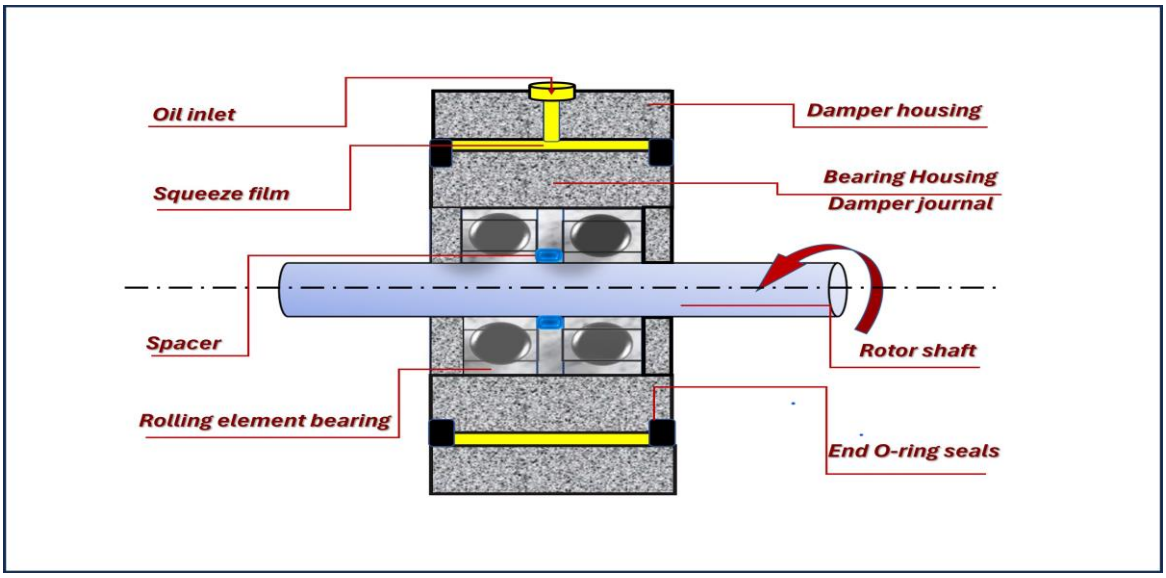

Figure 3.4 Sketch of squeeze film damper with assembly.

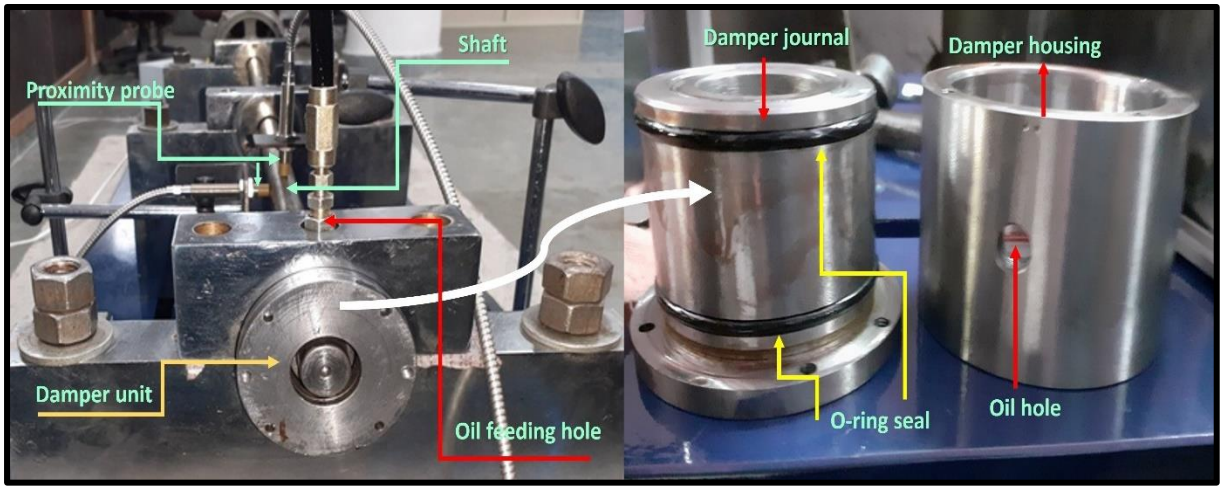

Figure 3.5. Actual Component of squeeze film damper after disassembly.

This design allowed for radial compression[157]. The squeezing film damper was lubricated by high pressure (up to 100 bar) provided by circumferential grooves at the vertical mid-

planes. The rotor was driven by a DC motor (up to 10,000 rpm) with an external speed regulator through a flexible connection.

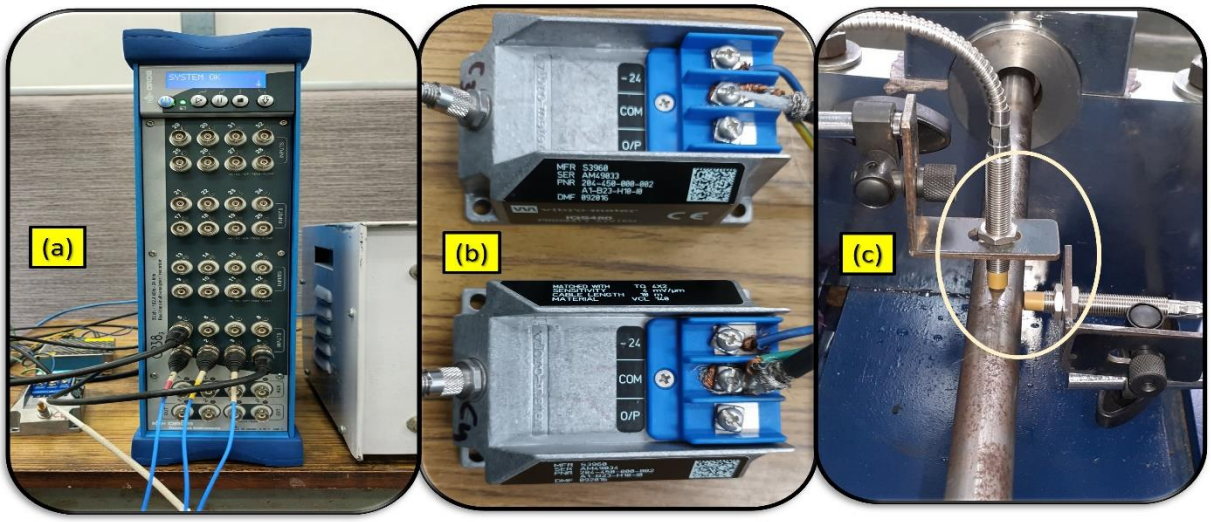

Figure 3.6 (a) OROS 32-channel data analyser, (b) Vibro meter proximity sensor, (c) Proximity probe.

OROS 32-channel data analyser The OROS 32 Channel acoustic data analyzer Figure 3.6(a) is a powerful tool for monitoring and analyzing acoustic waves. With its large channel capacity, it enables simultaneous monitoring of multiple channels in complex acoustic settings. The device offers real-time analysis capabilities and provides signal processing functions such as FFT, filtering, and correlation. Proximity vibrometer the proximity vibrometer, shown in Figure 3.6(b), is a non-contact device used to measure and monitor vibrations. It investigates a Doppler shift in the frequency range of the rebounded laser light using the laser Doppler vibrometry hypothesis. It uses a laser beam to indirectly measure the displacement and velocity of vibrating objects without actually touching them. Figure 3.6(c) depicts a proximity probe, a non-contact distance sensor. The electromagnetic induction method, which powers the probe, emits a field of alternating magnets from a coil. When a target object is nearby, eddy currents are created, creating a magnetic field that is in opposition to the probe's field. In order to evaluate the effectiveness of vibrations control in high-speed rotating shafts, an experimental setup is used that includes a squeeze film damper

(SFD). Table 3.3 provides an overview of the test rig's main parts and parameters. and the Test rig details provide crucial details about the components of the squeeze film damper rotor setup, which are essential for understanding the design and operation of the experimental setup. These details facilitate the replication of the experimental setup and aid in analysing the performance and effectiveness of the squeeze film damper in controlling vibration in high-speed rotating shafts.

Table 3.3 detail component of the squeeze film damper rotor setup.

Specifications of the Experimental Test Rig	
SFD and rotor shaft components' materials	*Mild steel*
Rotor shaft's length and diameter	*1000mm, 22mm*
Boundary dimension of damper journal	*44×50×64mm*
Boundary dimension of damper housing	*50×56×64mm*
Length of the damper	*50 mm*
length between one support and damper unit	*500mm*
Boundary dimension of ball bearings is utilized in squeeze film damper, type	*22×44×12mm, Koyo*
Spacer in between two ball bearings	*4mm*
DC motor 0.5 hp single phase rated speed	*12000rpm*
Type of coupling	*flexible Lovejoy*
O-ring seal material and diameter	*Rubber, 46mm*
Speed controller (Dimmer stat auto transformer single phase, 0-270V)	*2 amperes open type*
Vibrometer proximity probe (TQ402, range: 4mm API670, body thread M10, body length 50mm)	*flexible cable 10m with magnetic stand*

The vibration response was measured using two Vibrometer proximity probe which are placed perpendicular on the centre of two pinned support near the rotating shaft with a specification (TQ402, range: 4mm API670, body thread M10, body length 50mm, flexible cable 10m with magnetic stand) sensors connected to the spinning shaft on the X and Z axis.

The output signal data of the spinning shaft was acquired at a number of different steady-state input parameters using a sampling rate of 25.6 ks/sec (kilo sample/second). Recordings of the output signal varied in duration from seven to nine seconds. We took the measures three times to make sure they are accurate and eliminate any chance of making a mistake. The precision of the analysis is improved when a specialized 32 channels OROS data analyzer. Using the Hanning kernel function, the signals in the time domain have been transformed into signals in the frequency domain in preparation for future data processing. The Hanning kernel function is a window function that has distinguishing properties that make it appropriate for a variety of signal processing applications, particularly those that include spectral analysis. The tapering, symmetry, mainlobe width, amplitude scaling and sidelobe attenuation qualities of this element all contribute to a more precise and trustworthy frequency analysis of signals. In addition, the built-in statistical tools of Microsoft Excel enable for an even more in-depth investigation of the data. By allowing for a comprehensive analysis of the gathered data, the use of such a holistic approach not only assures the use of a reliable method of analysis but also boosts the credibility of the findings obtained from the study.

To reduce potential sources of error in the experiment setting, we followed the following steps:

a. All of the variables and parameters used in the experiment, including the independent variables (speed, oil pressure, blend %) and dependent variables (vibration at the x-axes and z-axes), were thoroughly listed.
b. Throughout the experiment, we employed properly calibrated equipment and thoroughly assessed the sensitivity and calibration of the proximity transducer to guarantee reliable data.
c. We repeated each experiment three times and used a reasonable sample size of 25.6 KS/s with a sampling frequency of 20 kHz in order to produce reliable findings.

d. To reduce human error, we were vigilant throughout data collection, making sure there were no errors in collecting data or misinterpretation of parameters (such as RPM or oil pressure).
e. In order to avoid any outside impacts on the experiment, we paid close attention to ambient conditions such temperature changes, humidity levels, air movement, and potential electromagnetic interference.
f. In order to confirm the consistency and dependability of our results, we compared the experimental results with those of earlier pertinent research.

3.4 Methodology

Taguchi, known as the "Father of Quality Engineering," was a pioneer in incorporating sophisticated applied statistical approaches into engineering processes to achieve higher stability and capability. Taguchi's parameter design has been shown to be the most potent step for process optimization among the three stages of the offline quality engineering system (system design, parameter design, and tolerance design). Taguchi's parameter design process is the topic of this research (also referred to as robust design methodology). Taguchi's parameter design, also known as the robust design technique, aims to maximize performance and quality while minimizing costs. This is primarily accomplished by establishing the ideal settings for those design or process characteristics that affect product performance variance and fine-tweaking those design or process parameters that impact average performance.

3.4.1. Taguchi analysis

The experiment in this study is designed using the Taguchi method, and the significance of the parameters is examined. A statistical technique for assessing the effect of process variables on trials is ANOVA. The F-test determines the parameters' influence on the process' reaction. The ANOVA table indicates the importance of variables and their interactions by prob 0.05 (for 95% certainty interval, CI). An L25 orthogonal array was employed for three parameters, each with five levels, requiring just 25 tests. The use of an L25 orthogonal array

allows for efficient experimentation with a minimal number of tests while still capturing the effects of multiple factors and their interactions. This systematic approach enables the identification of critical factors and helps optimize the performance of the squeeze film damper for high rotational speeds, oil blend percentage and oil pressure. Fig. 3.7 depicts the entire Taguchi procedure.

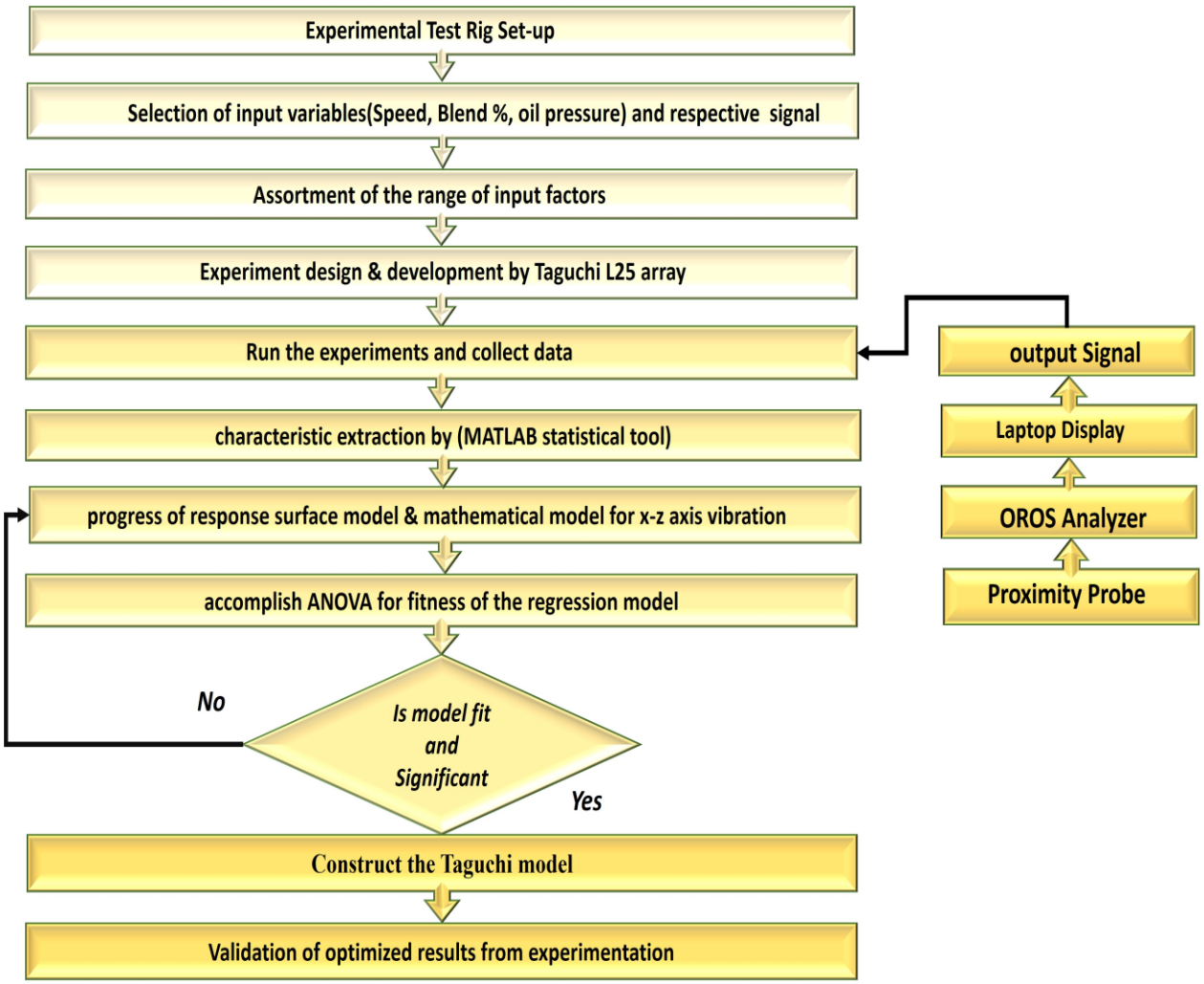

Figure 3.7 flow chart of Taguchi procedure

3.4.2 Design of Experiment

The design of experiments (DOE) method is a formal and systematic approach to solve engineering issues that employs a variety of ideas and procedures to assure the availability of coherent, sound, and substantiated findings. Randomization, Replication, Blocking, Orthogonality, and Factorial Experimentation are fun-elemental principles. This shift in the

independent variables is commonly assumed. The primary goal is to achieve optimum outcomes with the least quantity of data. However, this strategy necessitates significant work and important time. A variety of factors influence the processes. Similarly, the operating performance of a squeeze film damper is determined by design characteristics such as the size of the squeeze film damper, the kind of oil supply within the damper, the supply oil pressure, and the flexible shaft RPM type of seal provided for the damper. Operating characteristics such as rotating mass load, oil pressure applied inside the damper, shaft speed, and damper oil blending ratio, among others, affect squeezing film damper performance.

Factors and the DOE for five levels with three factors (speed of shaft, oil mix percentage, supply oil pressure) has been created using the Taguchi Technique. All variables are rated at the five levels (L1, L2, L3, L4, L5) in Table 3.4 as can be seen.

Table 3.4 process parameters and their levels

Input parameters	Supply oil pressure in Damper(bar)	Speed of the shaft(rpm)	Type of blends of oil (%)
Symbol	P	S	B
Level 1	20	2000	10
Level 2	40	4000	20
Level 3	60	6000	30
Level 4	80	8000	40
Level 5	100	10000	50

3.4.3 Experimentation

3.4.3(a)Experimentation of rotor vibration without SFD

In order to analyze the vibration amplitude of the rotor shaft along the X and Z axes, five experimental sets were carried out spanning a rotational speed range of 2000 RPM to 10000

RPM. This was done especially in the absence of a squeeze film damper (SFD) at the end support. The data that were obtained, which were provided in table 3.4(a), indisputably reveal that the vibration amplitudes are higher throughout all rotor shaft speeds when the SFD is not applied, and this hold true for both the X and Z axes. By seeing the influence of the SFD on lowering vibration amplitudes in rotor systems throughout a range of operating speeds, this observation offers useful insight into the subject matter.

Table 3.4(a) vibration amplitude at x and z axes without using SFD.

Speed(rpm)	2000	4000	6000	8000	10000
Vibration at x-axis(μm)	25.40	41.50	92.30	112.50	150.84
Vibration at z-axis(μm)	24.98	41.85	92.90	112.90	149.50

3.4.3(b) Experimentation of rotor vibration with SFD

The data presented in Table 3.5 displays the input parameters and corresponding values for twenty-five distinct experiments (accordance with the experimental design L_{25} orthogonal array). In order to guarantee precision and consistency, each experiment was conducted three times, denoted as T1, T2 and T3. The shaft's vibration along both the x-axis and z-axis was measured and recorded for each trial, and the resulting average values are included in the Table 3.5.

Table 3.5 average value of experiment outcomes from three trials

Exp. No	Levels of Process Parameters			Response Parameter Average Value	
	P	**S**	**B**	Vibration of shaft At X-Axis (µm)	Vibration of shaft At Z-Axis (µm)
1	20	2000	10	8.51	7.52
2	20	4000	20	7.27	7.06
3	20	6000	30	7	6.01
4	20	8000	40	6.4	5.4
5	20	10000	50	6.5	5.5
6	40	2000	20	7.05	6.05
7	40	4000	30	6.01	5.5
8	40	6000	40	5.5	5.2
9	40	8000	50	5.5	5.2
10	40	10000	10	6.32	6
11	60	2000	30	6	5.6
12	60	4000	40	4.45	4.44
13	60	6000	50	5.7	5.25
14	60	8000	10	6.11	5.01
15	60	10000	20	7	6.9
16	80	2000	40	4	4.01
17	80	4000	50	4.18	4.2
18	80	6000	10	5.01	5
19	80	8000	20	5	5.02
20	80	10000	30	4.83	4.9
21	100	2000	50	2.01	1.93
22	100	4000	10	2.22	2.01
23	100	6000	20	2.5	2.26
24	100	8000	30	2.8	2.82
25	100	10000	40	2.9	2.81

P, oil pressure; S, speed; B, blending percentage;

Using the proximity probe time domain data for displacement, average vibration amplitude values are obtained.

3.4.4 Effect of Process Parameters on Vibration Amplitude

The formula below determines the S/N ratios for shaft vibration along the X and Z axis. The Taguchi technique is used to examine the outcomes of vibration control parameter responsible for the smaller (SB) the better criterion.

$(S/N)_{SB}$= - 10log (mean of sum of squares of measured data) …… (3.1)

$$(S/N)_{SB} = -10\log(1/n \sum_{i}^{n} yi^2)$$

where n = number of repetitions.

A signal-to-noise (S/N) ratio for each observation's reaction using the Taguchi approach (Eq.3.1) is displayed in Table 3.6.

Table 3.6 Signal-to-Noise ratio (S/N ratios) of the shaft vibrations at X-axis and Z-axis.

Experiment. no	S/N ratio of vibration at x-axis	S/N ratio of vibration at z-axis
1	-18.5986	-17.5244
2	-17.2307	-16.9761
3	-16.902	-15.5775
4	-16.1236	-14.6479
5	-16.2583	-14.8073
6	-16.9638	-15.6351
7	-15.5775	-14.8073
8	-14.8073	-14.3201
9	-14.8073	-14.3201
10	-16.0143	-15.563
11	-15.563	-14.9638
12	-12.9672	-12.9477
13	-15.1175	-14.4032
14	-15.7208	-13.9968
15	-16.902	-16.777
16	-12.0412	-12.0629

17	-12.4235	-12.465
18	-13.9968	-13.9794
19	-13.9794	-14.0141
20	-13.6789	-13.8039
21	-6.06392	-5.71115
22	-6.92706	-6.06392
23	-7.9588	-7.08217
24	-8.94316	-9.00498
25	-9.24796	-8.97413

The vibration amplitude at x and z-axis values must be modest since the assessment is based on the "smaller is better" premise. To calculate the signal-to-noise ratio, control variables and the process reaction are taken into account. In order to forecast the "optimal combination," a combination of the regulating elements, to determine whether controlling trait was statistically significant, an ANOVA was also carried out [158, 159]. The S/N ratio is determined by the Taguchi technique and is given as follows [160].

3.5 Experimental Results and Analysis

The aim of the current research is to reduce shaft vibration along the x-axis and z-axis of a high-speed rotating shaft. To achieve lower vibration amplitude, it is always preferable, and the smaller the better alternative chosen. Eq. (3.1) calculates the signal-to-noise ratio (S/N) of the x-axis and z-axis vibration. In the research, L25 orthogonal array design was taken into consideration. In this, 25 separate experimental sets were done, and five levels of data were used for the experiment design for each process parameter. Runs have 24 degrees of freedom (DOF) over these 25 combinations. In order to investigate the process variables (S-speed, P-pressure, and B-blend percent), twelve of the twenty-four degrees of freedom (DOF) that are available are employed, four for each major effect (ME). Twelve more DOF are now

accessible to examine the statistical significance of the variables in an ANOVA,[161].In the event of modest effects, it could be essential to get a suitable DOE, sensitivity, and sample size. The precision and effectiveness of the trial will rise as there are more replications, which offer error terms more DOE. The linear polynomial sum of squares (SS) and mean of squares (MS) were calculated using an ANOVA using a 95% confidence interval (CI) at the 5% level of significance to test for "probability>(F")" (=0.05). For the vibration amplitude model at the x and z-axes, the value of F for each parameter (P, S, B) of the x-axis vibration 80.90,1.56 and 3.58, and z-axis 49.12,0.99 and 2.28 as shown in Table 3.7 and 3.8.

Table 3.7 Analysis of Variance (ANOVA) effect for S/N Ratios of vibration amplitude at X-axis.

Parameters	Degree of freedom	Adj SS	Adj MS	F-value	P-value	% contribution
P	4	259.288	64.8219	80.90	0.000	90.86
S	4	5.010	1.2525	1.56	0.247	1.76
B	4	11.484	2.8711	3.58	0.038	4.02
Residual Error	12	9.615	0.8013			3.36
Total	24	285.397				100

Table 3.8 ANOVA effect for S/N Ratios of vibration amplitude at the Z-axis

Parameter	Degree of freedom	Adj SS	Adj MS	F-value	P-value	% contribution
P	4	231.744	57.926	49.12	0.000	88.69
S	4	4.659	1.165	0.99	0.451	1.80
B	4	10.744	2.686	2.28	0.049	4.10
Residual Error	12	14.153	1.179			5.41
Total	24	261.30				

In the ANOVA Table, model terms with P-values less than 0.05 are considered significant. Here, pressure (P) and blend percentage (B) are two key model variables. When p-values are higher than 0.05, however, model terms are considered to be inconsequential. Tables 3.7 and 3.8 demonstrate how each input process parameter is involved. The oil pressure is rated 1 and displays the greatest delta value. i.e., pressure is the utmost momentous factor, oil blend percentage graded 2, which means it is a second effective parameter, and speed graded 3, means lower effective parameter for vibration reduction at the x-axis and z-axis as seen in Table 3.9.

Table 3.9 response table for the S/N ratio.

Response	level	Pressure of oil(P)	Speed of Shaft(S)	Type of Blend(B)
vibration at the X-axis (Smaller is better)	Delta	9.194	1.395	1.673
	Rank	1	3	2
vibration at the Z-axis (Smaller is better)	Delta	8.569	1.333	1.756
	Rank	1	3	2

[161] According to Tables 6 and 7, the analysis of variance (ANOVA) findings for vibration studies at the x and z axes similarly indicate that the supply oil pressure plays a major part in the vibration of the x and z axes, respectively, with a main role of roughly 90.86% and 88.69%. The effect of several factors, such as speed (S), pressure (P), and blend % (B), is depicted in Figs. 3.8(a) and 3.9(a) using means of means data for both the x- and z-axes. Fig. 3.8(a) this graph identifies the values of the input process factors that reduce vibration amplitude. At level 5 for pressure, level 2 for speed, and level 4 for blend percent, the x-axis experiences the least amount of vibration, the best value level across various parameters for

minimizing vibration amplitude of the shaft is P5 S2 B4, and the respective value is Pressure-100bar, Speed-4000rpm, Blend-40%.

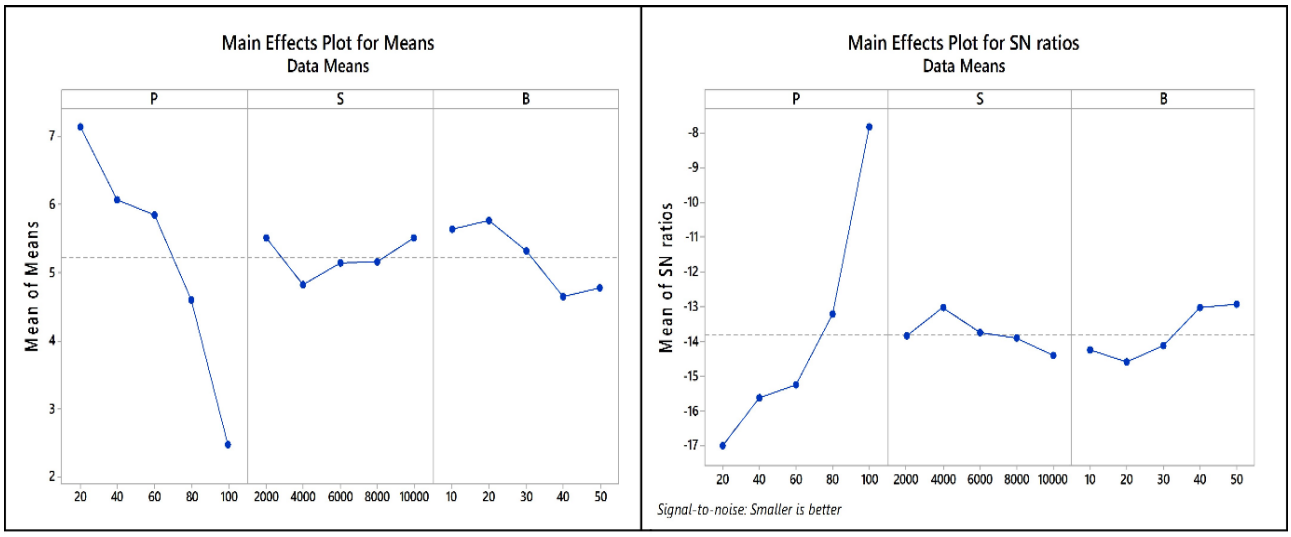

(a) Raw data **(b) S/N data**

Figure 3.8 Effect of input process parameter at x-axis vibration

In Fig.3.9(a) the minimum vibration is achieved for z-axis at level 5 for pressure, level 2 for speed, and level 5 for blend percentage. The best value level across various parameters for minimizing vibration amplitude of the shaft is P5 S2 B5, and the respective value is Pressure-100bar, Speed-4000rpm, Blend-50%.

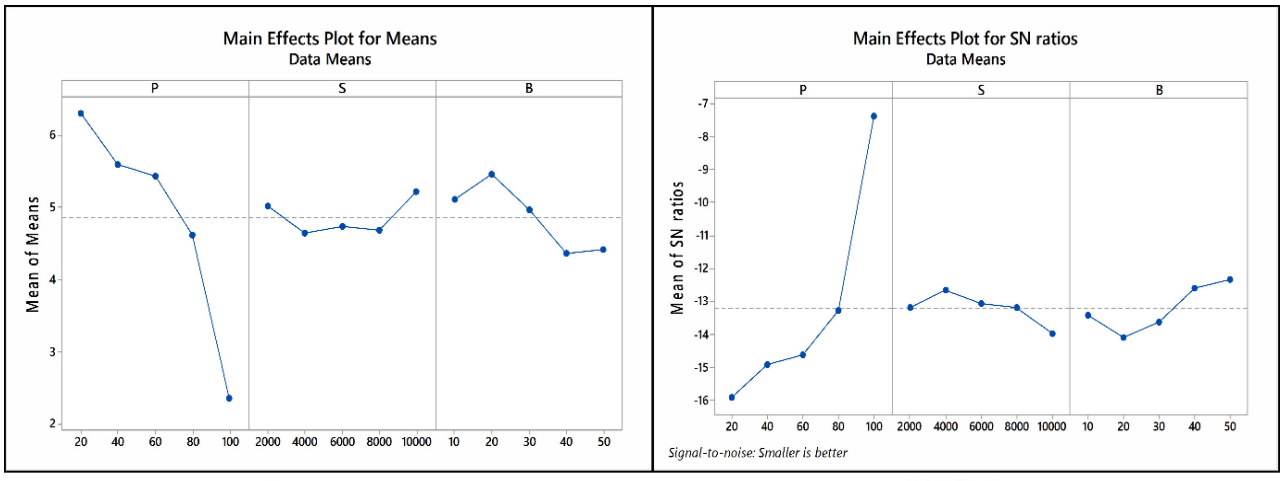

(a) Raw data **(b) S/N data**

Figure 3.9 Effect of process parameter at z-axis vibration

It is discovered that vibration and the value of the regulating parameters (pressure, speed, and mix percentage) are linearly related. A linear regression model is constructed to predict vibration using ANOVA with predetermined parameters for speed, pressure, and mix percentage. This model is displayed below. The developed model provides a regression among the variables that can't be measured and their parameters. Regression Equation of vibration amplitude of x-axis

$$Y_{x\text{-}axis}=9.549-0.0069*P-0.000568*S-0.02147*B-0.000561*P^2+0.000003*PS\ldots\ldots\ldots \quad (3.2)$$

Regression Equation of vibration amplitude of z-axis

$$Y_{z\text{-}axis}=8.215+0.0137*P-0.000564*S-0.01706*B-0.000673*P^2+0.000004*PS\ldots\ldots\ldots \quad (3.3)$$

Equations (3.2) and (3) state that the x-axis vibration amplitude at P5 S2 B4 is 1.339 and the z-axis vibration amplitude at P5 S2 B5 is 1.392. The points on Figs.3.10a, b and 3.11a, b's normal probability graph indicated that the tactic was successful. since they showed a fairly linear trend has a slightly deviated normal distribution, which is used to create a model for forecasting vibration, was successful [162, 163] .

Additionally, Figs. 3.10a, b and 3.11a, b demonstrate a random pattern on the Residuals (The differences between actual and expected outcomes in a statistical model are known as residuals versus fatted value (RVFV) graph, demonstrating the remaining variation is nearly constant. The collected data can be utilized to identify the non-random errors, as shown by the Residual versus Order Plot (RVOP). Additionally, the Frequency versus Residual Plot (FVRP) exhibits no outliers, showing that the information was more diversified. However, the bar graph has a different bias, showing that the early observations are far more significant to the final outcomes [127].

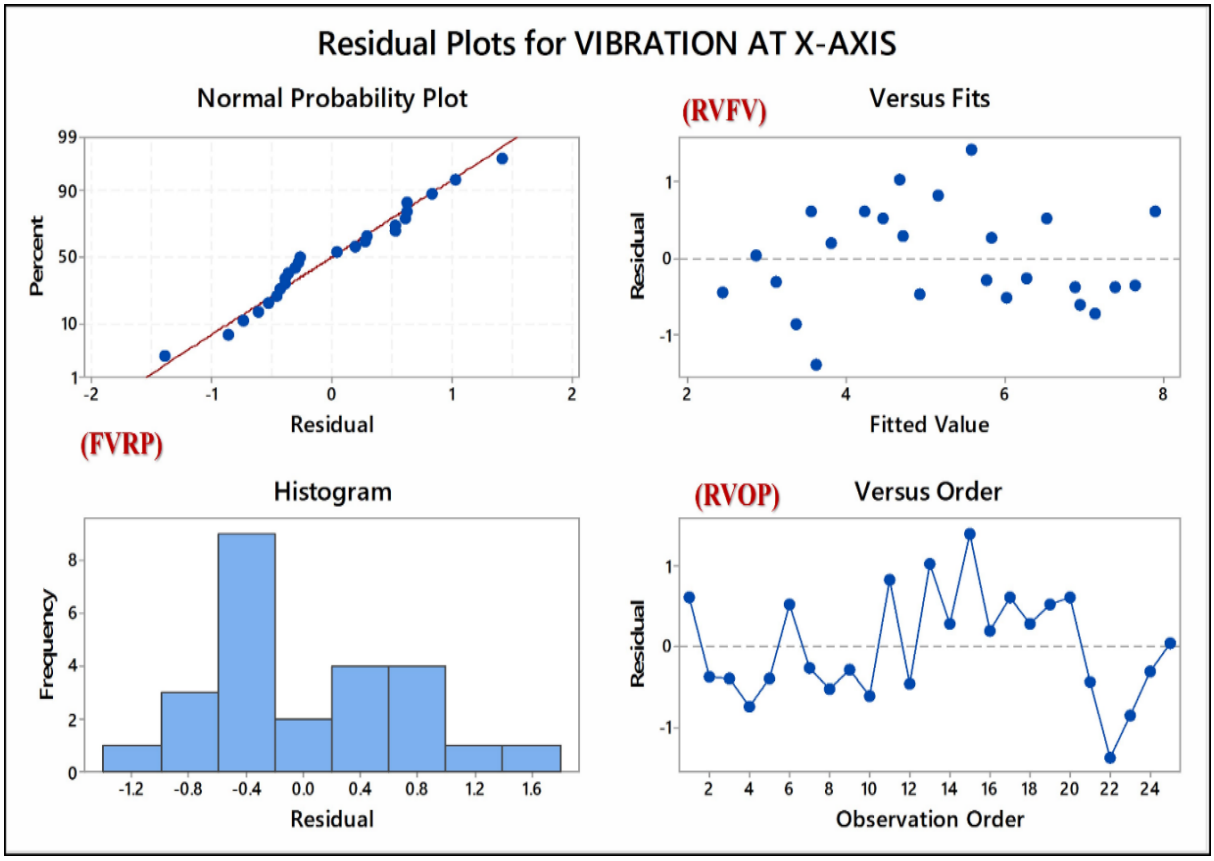

Figure 3.10a Residual plot for vibration amplitude at x-axis.

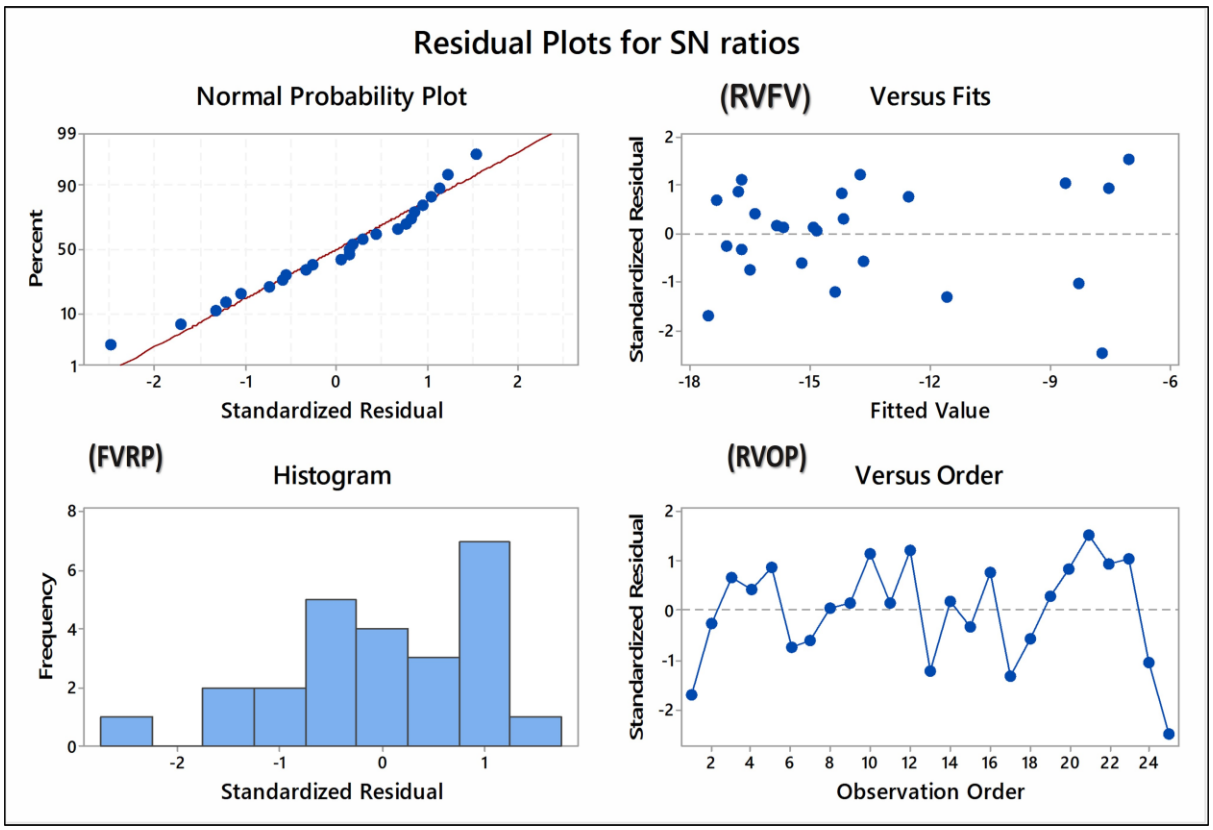

Figure 3.10b S/N ratio residual plot for the x-axis vibration amplitude variation.

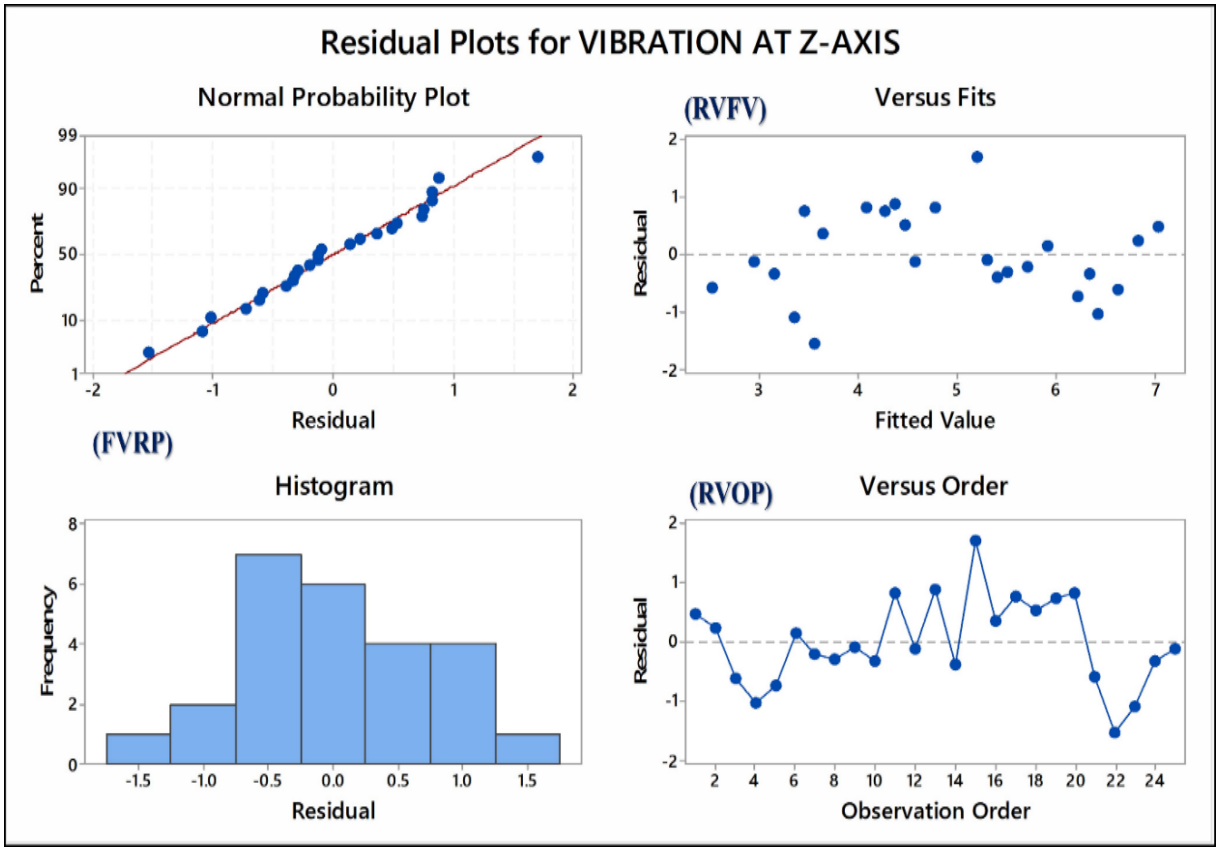

Figure 3.11a Residual plot for vibration amplitude at z-axis.

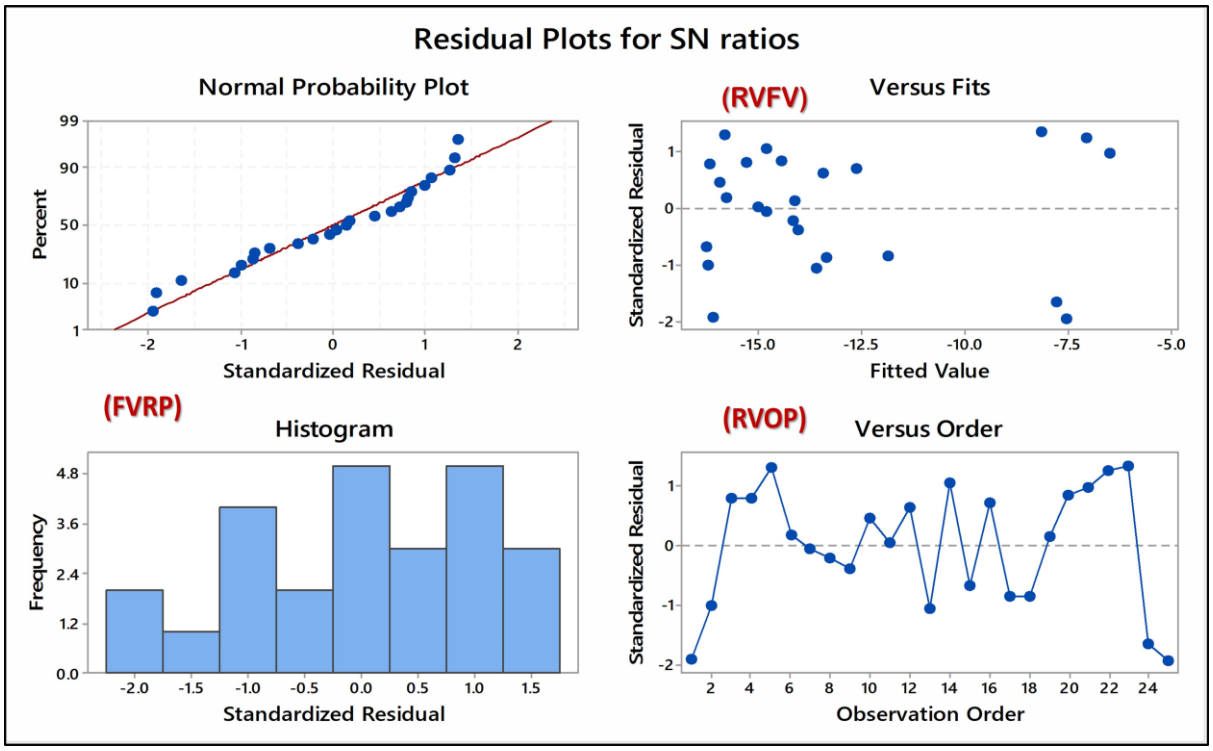

Figure 3.11b Residual plot for the S/N ratio for the change in vibration amplitude in the z-axis.

3.6 Experimental Confirmation

3.6.1 Experimental validation of regression model for x-axis vibration amplitude

The research study developed a regression model to predict vibration amplitudes at the x-axis based on specific input parameters. The optimized set of input parameters and their predicted vibration amplitudes are presented in Table 3.10. Experimental validation showed that all predicted values closely matched the experimental results within a ±10% error margin, demonstrating the model's accuracy. The regression equation proved effective for estimating vibration amplitudes at the x-axis, making it valuable for practical applications in engineering and industrial settings.

Table 3.10 Experimental validation of optimal solution process factors for x-axis

Process factors (closet to optimal solution)				**Vibration amplitude at the x-axis(µm)**	
Trial No.	**P**	**S**	**B**	**Predicted value**	**Experimental value**
1	10	3000	10	7.595±0.7595	6.845
2	30	6000	25	5.432±0.543	5.863
3	50	2000	35	6.214±0.621	6.004
4	90	7000	45	1.324±0.132	1.434
5	70	9000	50	2.022±0.202	2.162

P-pressure(bar), S-speed(rpm), B-oil blend (%)

Table 3.10, presents the results of experimental validation for the optimized predicted values. The actual vibration amplitudes obtained from experiments are compared with the predicted values from the regression model. The statement indicates that all predicted values have been validated with experimental data, and the results show that the predicted values closely match the experimental values, falling within an error margin of ±10%.

3.6.2 Experimental Validation of regression model for z-axis vibration amplitude

The actual experiment has been conducted for the closet optimum process parameter generated by regression model equation. The predicted value generated by regression

equation is compered to actual experimental data. The accuracy of validation Process parameter along with respective value under ±5% error data show in Table 3.11.

Table 3.11 Experimental validation of optimal solution process factors for z-axis

Process factors (closet to optimal solution)				**Vibration amplitude at the z-axis(µm)**	
Trial No.	**P**	**S**	**B**	**Predicted value**	**Experimental value**
1	10	3000	10	6.542±0.654	6.992
2	30	6000	25	4.930±0.493	5.291
3	50	2000	35	5.891±0.589	6.121
4	90	7000	45	1.790±0.179	1.681
5	70	9000	50	1.921±0.192	2.071

P-pressure(bar), S-speed(rpm), B-blend (%)

The experimental validation was then compared to the predicted values from the regression model. Remarkably, the comparison revealed that all the predicted process parameters, along with their respective values, fell within a small error margin of ±5% of the actual experimental data. This level of agreement demonstrates the high accuracy and reliability of the regression model in predicting the optimal process parameters. The successful validation process not only confirms the effectiveness of the regression model, but also provides valuable insights into the process optimization for the given application. The ability of the model to closely match experimental results within the ±5% tolerance, indicates that it can offer precise and reliable predictions for similar scenarios.

3.6.3 Experimental Validation of Optimized Value

The real experiment has been carried out for the confirmation of the optimal value, of the vibration amplitude at the x and z-axes, displayed in Table 3.12. Validating the optimal vibration amplitude values at the x- and z-axes required doing the real trials. The optimized

values, obtained from the optimization techniques, were compared with the results of the experiments and it is under the range of 5% accuracy.

Table 3.12 Experimental validation of optimized value

Process factors (optimal solution)						Vibration amplitude of shaft(μm)	
Trail No.	Axis	Optimized set	P	S	B	Predicted	Experiment
1	X	P5S2B4	100	4000	40	1.339±.0669	1.430
2	Z	P5S2B5	100	4000	50	1.392±.0696	1.461

P-pressure(bar), S-speed(rpm), B-oil blend (%)

3.7 Plot illustrating interactions and variables' effects on vibrational change at the x-axis.

Fig.3.12 depicts how different process parameters (Data means) affect the vibration amplitude of the shaft at the x-axis. Although factors related to the highest decreasing lines have the most impact, those related to the close to horizontal line have minimal impact. While variables corresponding to the highest decreased lines have the most substantial impact, factors relating to the near horizontal line have little influence. The pressure of oil inside the SFD had the greatest negative influence on the vibration amplitude of the shaft at the x-axis, whereas the other components had less of an effect. As oil pressure in the side damper and blending ratio are increased, the vibration amplitude of the shaft at the x-axis decreases. The magnitude of the shaft's x-axis vibration increases concurrently with a drop in oil pressure and blending ratio. With the maximum oil pressure inside the SFD and the highest blending ratio, the lowest shaft vibration amplitude at the x-axis was discovered Similar research was conducted by [86] and comparable patterns in the parameters were found.

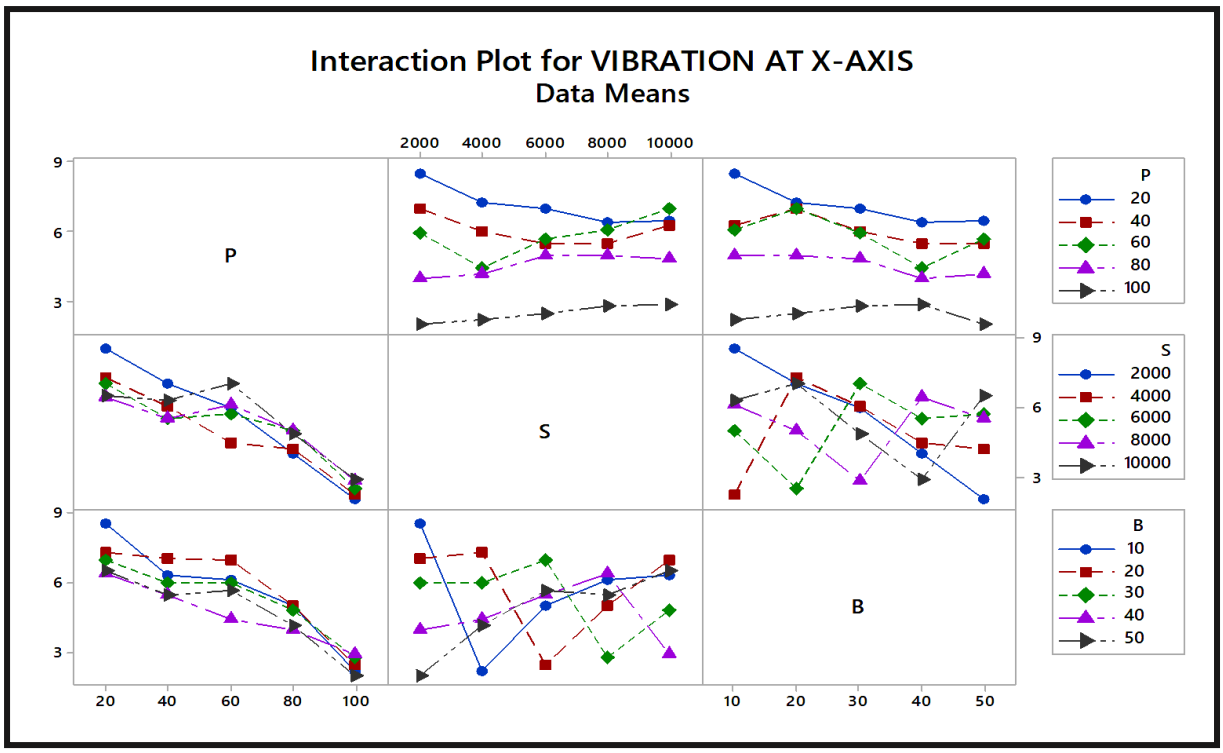

Figure 3.12 Interaction plot for a vibration amplitude of shaft in the x-axis

3.7.1 Plot of interactions and the impact of various variables on the vibration's change at the z-axis

Fig.3.13 depicts how the different process parameters (Data means) affect the shaft's vibration amplitude at the z-axis. Compared to variables corresponding to the highest decreased lines, those belonging to the near horizontal line have the least significant impact. The most significant negative impact on the shaft's vibration at the z-axis was caused by the oil pressure within the SFD, whereas the other components had less effect. When oil pressure in the side damper and blending ratio rises, the shaft's x-axis vibration becomes less pronounced. Together with the drop in oil pressure and blending ratio, the shaft's amplitude at the z-axis vibration increases concurrently. For the maximum oil pressure inside the SFD and the highest blending ratio, the shaft's z-axis vibration amplitude was determined to be the lowest. The same investigation was carried out by [86, 107] and comparable patterns in the parameters were found.

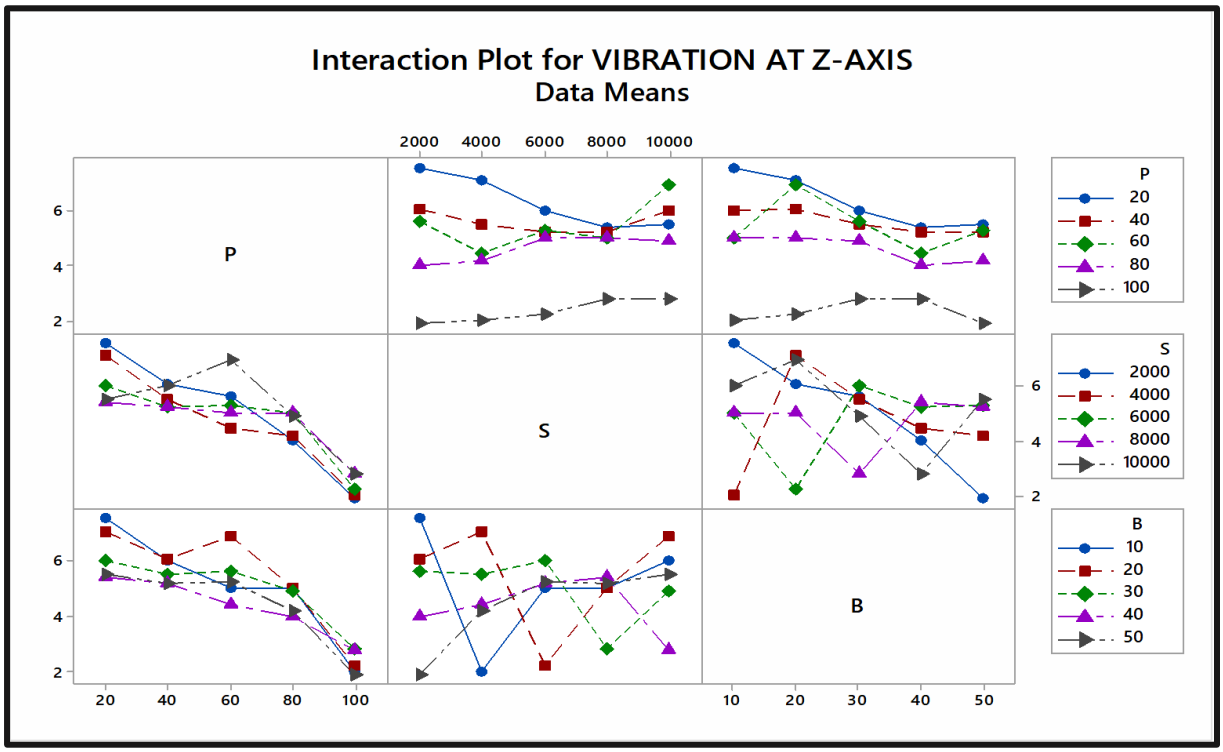

Figure 3.13 interaction plot for a vibration amplitude of the shaft in the z-axis

3.8 Response Surface and Contour plot showing parameter interaction

The results displayed in comparison to different variations in process parameters are represented in two dimensions (2D) by the contour plot. A three-dimension(3D) depiction of the actions ' behaviour as a function of different variety of process inputs is called a response surface plot. For the vibration amplitude of the shaft at the x- and z-axes, the interaction effect between the speed and pressure of the oil on the surface plots in three dimensions (3D) can provide a more accurate representation for the response surface over contour graphs. When speed and oil pressure interact to affect vibration amplitude at the x-axis, as shown in Fig. 3.14(a), At high speeds, the vibration amplitude decreases substantially. The amplitude increases after 8000 rpm at the lower oil pressure side but reduces when the oil pressure rises from 60 bar to 90 bar at 4000-5000 rpm. Additionally, Figure 3.14(a) shows dark blue areas with lower z-values (vibration at the x-axis). A low value at 8000 rpm and high oil pressure

are seen in the contour levels. In this area, vibration amplitude ratings range from 2 to 3. Examining Fig. 3.14(b), which depicts the interaction between speed and oil pressure for a shaft's vibration amplitude at the z-axis, reveals that all responses in terms of vibration value ranges are essentially the same as those in the x-axis. In the x-axis and z-axis of the vibration response contour plot, comparable but varied amplitude can be seen [164]. The linear regression equation results in curved contour lines being seen.

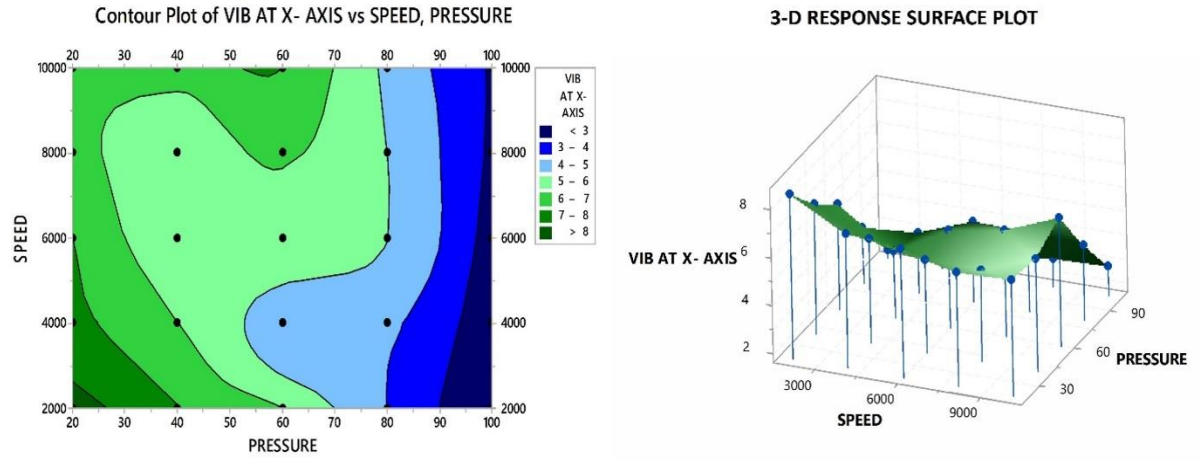

(a) Interaction for vibration at x-axis between factors speed and pressure.

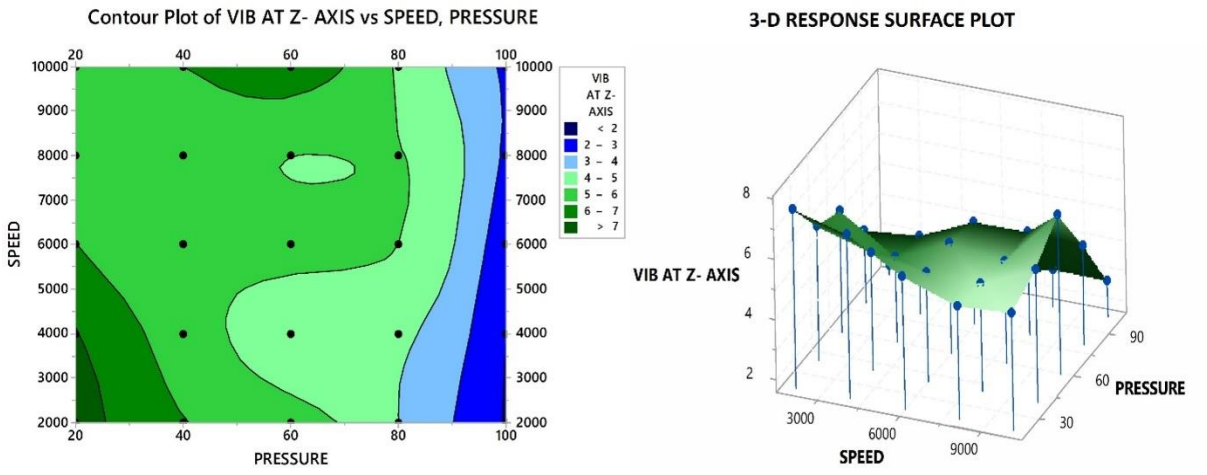

(b) Interaction for vibration at the z-axis between factors speed and pressure.

Figure 3.14 interaction for vibration at x and z axes between factors speed and pressure

The vibration amplitude of the shaft in the x-axis is shown as a contour plot in Figure 3.15(a), together with the influence of oil mix % and speed. When the oil is blended between 10% and

20%, the vibration amplitude is larger near the speed range of 6500–9000 rpm, and when the oil is blended between 40% and 50%, the vibration amplitude is lower. In Fig. 3.15(b) almost similar pattern is seen for the vibration amplitude of the shaft at the z-axis only magnitude may be slightly different.

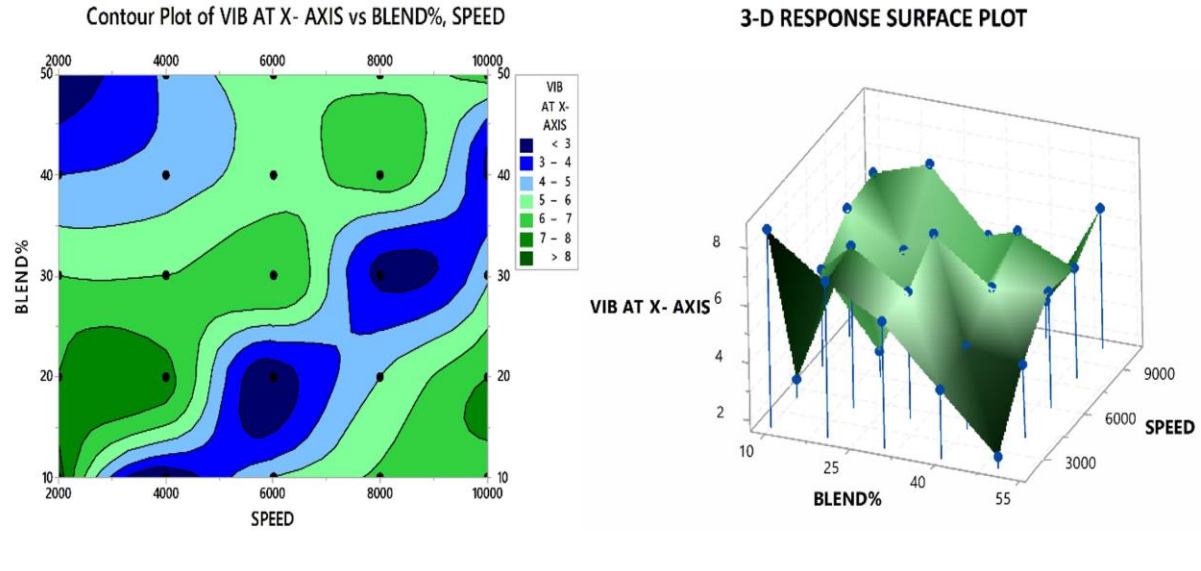

(a) Interaction for vibration at the x-axis between factors blend% and speed.

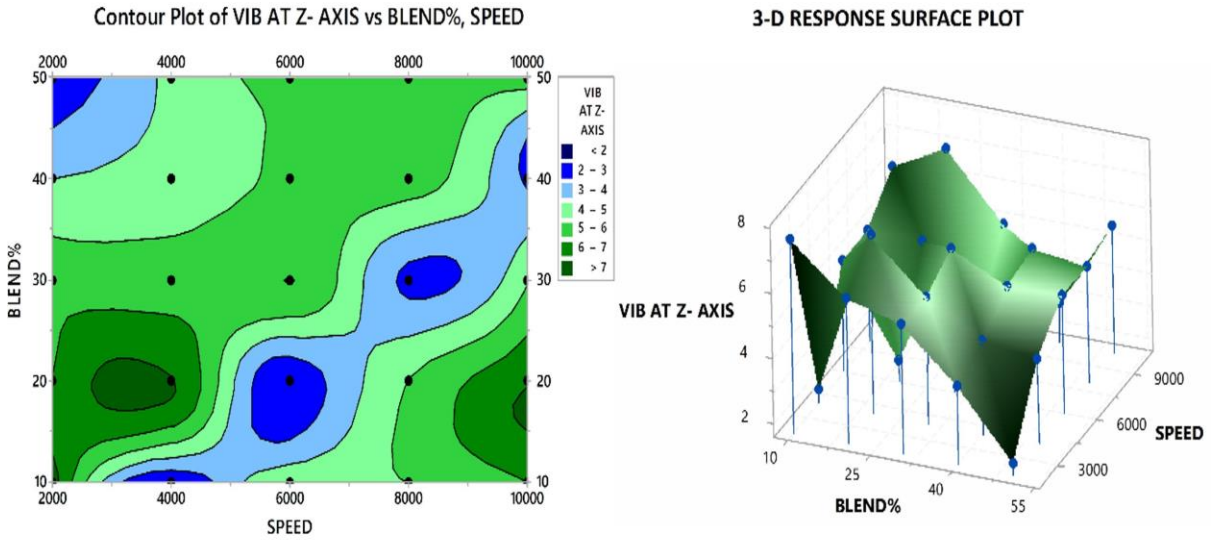

(b) Interaction for vibration at the z-axis between factors blend% and speed.

Figure 3.15 interaction for vibration at x and z axes between factors blend% and speed

The interaction between oil pressure and blend percentage for a vibration amplitude of the shaft at the x-axis and z-axis is plotted in Fig. 3.16(a)&(b). the vibration amplitude of the shaft for both the x-z axis is decreasing with increasing oil pressure, the most significant

reduction takes place when the oil pressure increases to 90 bar and above and the blending ratio increases from 40% to 50%.

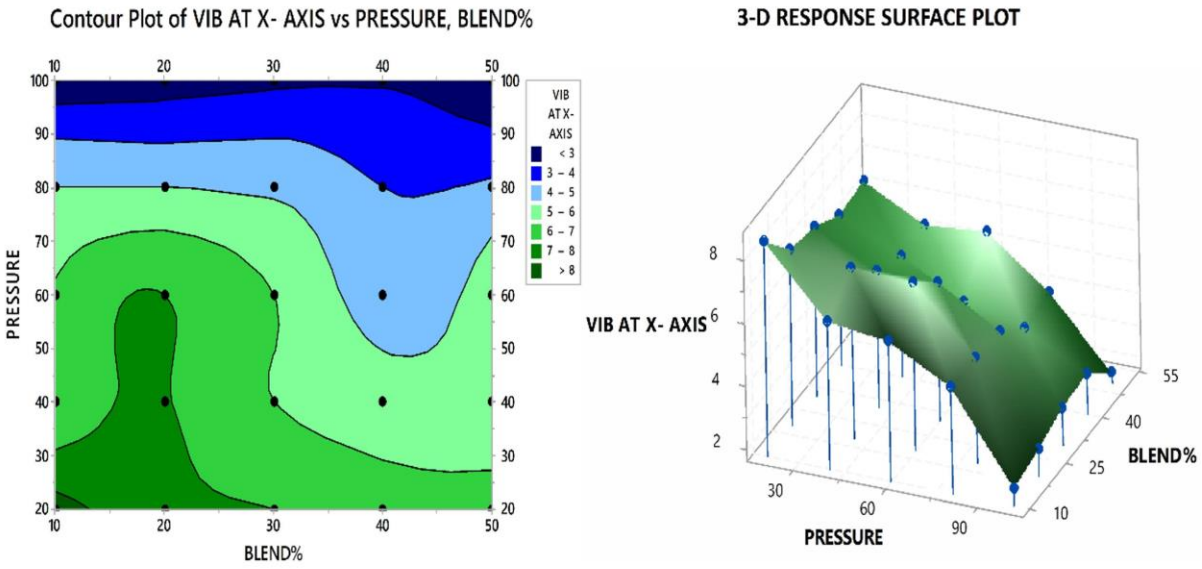

(a) Interaction for vibration at the x-axis between factors pressure and blend%.

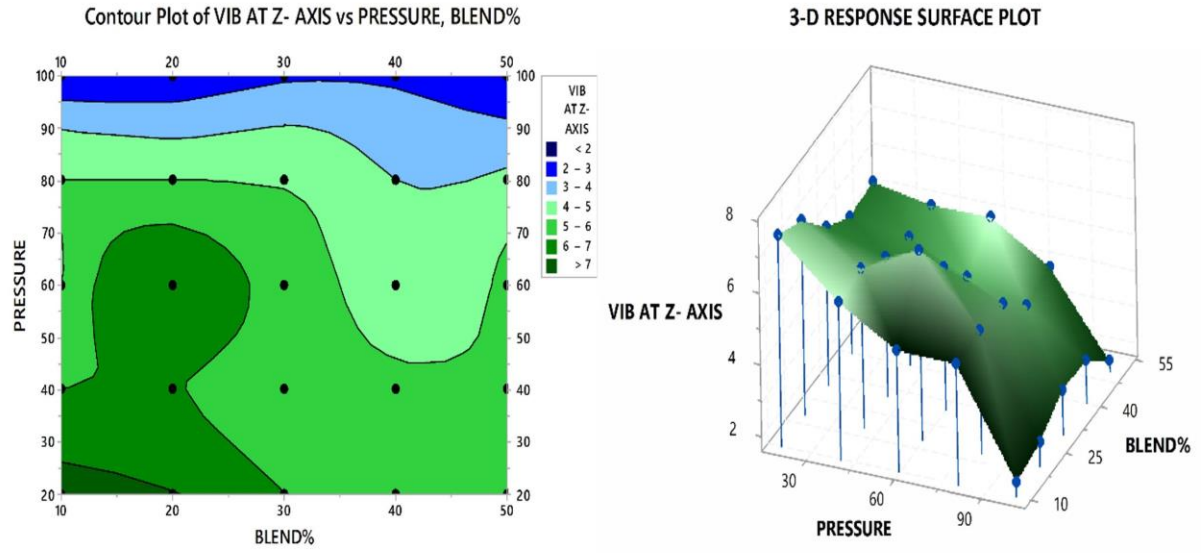

(b) Interaction for vibration at the z-axis between factors pressure and blend%.

Figure 3.16 interaction for vibration at x and z axes between factors pressure and blend percentage.

3.9 Summery of the Chapter

Squeeze Film Dampers (SFDs) play a crucial role in mitigating vibration amplitudes in high-speed rotors. This research included the development of a specifically designed SFD to

effectively address the complex requirements associated with high-speed rotating shafts. The study centered on examining the impact of several factors of the SFD (squeeze film Damper) process, namely shaft rotation, oil pressure inside the damper, and the composition of the oil mix, on the amplitudes of vibrations along the x-axis and z-axis. These vibrations were measured during the acceleration of a flexible shaft up to a speed of 10,000 revolutions per minute. The experimental oil sample consisted of a mixture of kerosene oil, with varying proportions ranging from 10% to 50%, and 5W30 crankcase oil. The oil blend was subjected to a high-pressure oil delivery system capable of reaching pressures up to 120 bar. The study used the Taguchi technique in its experimental design, especially using an L25-orthogonal array. The resulting data were then subjected to Analysis of Variance (ANOVA) for analysis. The findings underscore the importance of oil supply pressure as the primary determinant of shaft amplitude in both the x- and z-axes. Moreover, the incorporation of Newtonian fluid has been identified as a pivotal element in the reduction of vibration amplitudes. The results obtained were supported by the analysis of variance (ANOVA). The study determined that the most effective process parameters for minimizing vibration amplitude were as follows: a pressure of 100 bar, a speed of 4000 rpm, and a blend composition of 40% (P5S2B4) in the x-axis direction, and a pressure of 100 bar, a speed of 4000 rpm, and a blend composition of 50% (P5S2B5) in the z-axis direction. The significance of obtaining optimum performance and decreasing vibration amplitudes in high-speed rotating shafts is highlighted by this research, which emphasizes the necessity of certain pressure levels, rotational speed, and oil mix composition.

CHAPTER-4

MODELLING OF SQUEEZE FILM DAMPER FOR FLEXIBLE ROTOR UTILIZING RSM (BOX-BEHNKEN DESIGN WITH DESIRABILITY OPTIMIZATION

4.1 Introduction

In this chapter, the purpose of this research is to build a sophisticated Squeeze Film Damper (SFD), which has been precisely constructed to cut down on the vibration amplitudes that occur in high-speed rotating shafts. The inquiry digs into the subtle impacts of key SFD process factors as a flexible shaft accelerates to a challenging speed of 8,000 revolutions per minute. These essential SFD process parameters include shaft rotation, oil pressure inside the damper, and the amount of oil mix. The extensive investigation of vibration amplitudes along both the x and z axes give essential insights into the dynamic behavior of the SFD under a variety of different settings. This research endeavors to not only maximize the input parameters by using a Box-Behnken design (BBD) method, in conjunction with Response Surface Methodology (RSM) and Analysis of Variance (ANOVA), but it also tries to rigorously examine the statistical significance of the model. The goal of the study is to get the highest level of control possible over the results of vibration by using desirability-based optimization. The ensuing experimental validation acts as an important step, confirming the efficiency of the optimized values in effectively reducing vibrations in the high-speed rotating shaft. This is a critical phase in the process. This endeavor not only makes a contribution to the development of technology for vibration control, but it also shows promise for improving the efficiency and durability of high-speed rotating equipment.

4.2 Material and Method

A review of several research articles:

- High vibration amplitude with high shaft rotational speeds inside the squeeze film damper may be controlled by using viscoelastic and Newtonian oils[107].

- To establish the proper ratios for five new test samples, two oils were blended using a magnetic stirrer at a temperature of 30°C. the dynamic viscosities of these oils are shown in Table 4.1. The five test samples were made with a mixture of crankcase oil and kerosene oil with a blend of 10%, 20%, 30%, 40%, and 50%.
- An SVM3000 viscometer was used to test the dynamic viscosities of these samples. The values are shown in Table 4.2.

Table 4.1 Dynamic viscosity of crankcase oil and kerosene oil at 30 temps.

Sample oil name	***Dynamic viscosity***
5W30 crankcase oil	75.483 mPa.S
Plain kerosene oil	1.1287mPa.S

Table 4.2 Dynamic viscosities of the samples at 30º C.

Name of sample	***Blend Ratio***	***Dynamic viscosity***
Sample 1	10%	46.271 mPa.S
Sample 2	20%	33.684 mPa.S
Sample 3	30%	23.695 mPa.S
Sample 4	40%	19.476 mPa.S
Sample 5	50%	15.786 mPa.S

4.3 Test Rig detail and Experimentation

A flexible rotor kit with three pinned supports was used in the experimental arrangement. One of the pinned supports that was far from the drive motor was taken out. A pedestal was built to replace the lost support that included a bearing unit and a SFD unit. the conceptual and real views of the test rig are shown in Figure 4.1.

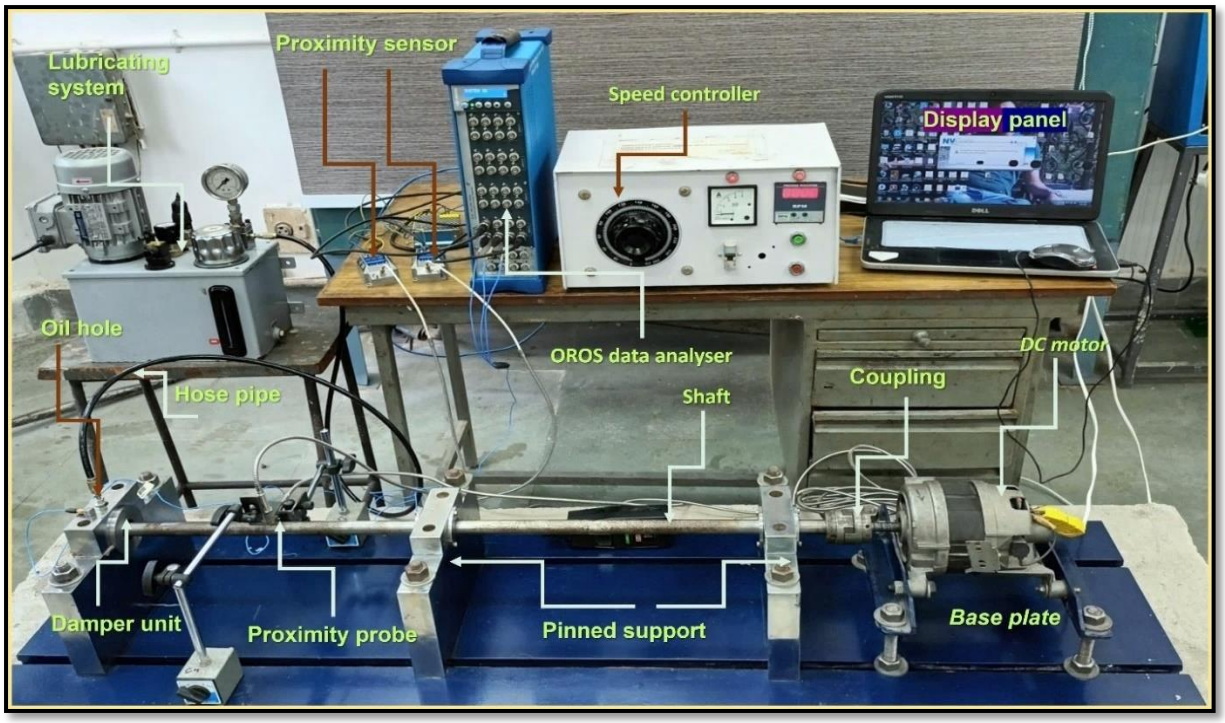

Figure 4.1 Actual test rig diagram along with pickup's location of the signal.

Two sets of ball bearings are split by a spacer and make up the squeeze film damper mechanism. The ball bearings were fitted onto the shaft and secured firmly to prevent any radial movement. The lock screw prevented the outer races from rotating and was placed inside a hole with a bigger diameter in the spacer. This design allowed for radial compression[157]. The squeezing film damper was lubricated by high pressure (up to 100 bar) provided by circumferential grooves at the vertical mid-planes. The rotor was driven by a DC motor (up to 10,000 rpm) with an external speed regulator through a flexible connection. Table 4.3 provides an overview of the test rig's main parts and parameters. and the Test rig details provide crucial details about the components of the squeeze film damper rotor setup, which are essential for understanding the design and operation of the experimental setup. These details facilitate the replication of the experimental setup and aid in analysing the performance and effectiveness of the squeeze film damper in controlling vibration in high-speed rotating shafts.

Table 4.3 detail component of the squeeze film damper rotor setup.

Details for the TEST -RIG components flexible Rotor-Bearing System	
SFD and rotor shaft components' materials	(Mild steel)
Rotor shaft's diameter and length of shaft	(22×1000mm)
Boundary dimension of damper housing	(50×56×64mm)
Boundary dimension of damper journal	(44×50×64mm)
Length of the damper	(50 mm)
length between one support and damper unit	(500 mm)
Boundary dimension of ball bearings is utilized in squeeze film damper	(22×44×12mm)
DC motor 0.5 hp single phase rated speed	(12000rpm)
Spacer in between two ball bearings	(4mm)
Speed controller (Dimmer stat auto transformer single phase, 0-270V, 2 amperes open type),	
Type of coupling	(flexible Lovejoy)
O-ring seal	(material-rubber and diameter 40mm)

The vibration response was measured using two Vibrometer proximity probe which are placed perpendicular on the centre of two pinned support near the rotating shaft with a specification (TQ402, range: 4mm API670, body thread M10, body length 50mm, flexible cable 10m with magnetic stand) sensors connected to the spinning shaft on the X and Z axis. The output signal data of the spinning shaft was acquired at a number of different steady-state input parameters using a sampling rate of 25.6 ks/sec (kilo sample/second). Recordings of the output signal varied in duration from seven to nine seconds. We took the measures three times to make sure they are accurate and eliminate any chance of making a mistake. The precision of the analysis is improved when a specialized 32 channels OROS data analyzer. Using the Hanning kernel function, the signals in the time domain have been transformed into signals in the frequency domain in preparation for future data processing. The Hanning kernel function is a window function that has distinguishing properties that make it appropriate for a variety of signal processing applications, particularly those that include spectral analysis. The tapering, symmetry, mainlobe width, amplitude scaling and sidelobe attenuation qualities of this element all contribute to a more precise and trustworthy frequency analysis of signals. In

addition, the built-in statistical tools of Microsoft Excel enable for an even more in-depth investigation of the data. By allowing for a comprehensive analysis of the gathered data, the use of such a holistic approach not only assures the use of a reliable method of analysis but also boosts the credibility of the findings obtained from the study.

4.4 Methodology

4.4.1 Flowchart of the proposed methodology

The proposed methodology for controlling the vibration amplitude of shaft high speed rotating shaft by the use of a squeeze film damper under different sets of conditions is shown in Figure 4.2. The flowchart depicts a research-oriented experimental optimization process. Setting up a test rig and selecting input variables for the study are the first steps. The range of values for these variables has been carefully selected. Experiments are efficiently organized using a Box-Behnken design (BBD) to investigate the impact of input factors influencing the response. studies gather data, and a response surface model is built to explain the link between the input factors and the response. The correctness of the model is evaluated using ANOVA to establish its importance in explaining response variance. If the model is substantial, desirability-based optimization is used to determine the optimum combination of input variable settings that maximizes the desired output. This enables researchers to acquire best findings in a timely manner. Additional experimentation is carried out to confirm the dependability of the adjusted settings. This validation process demonstrates the feasibility and efficacy of the adjusted circumstances in fulfilling the study objectives.

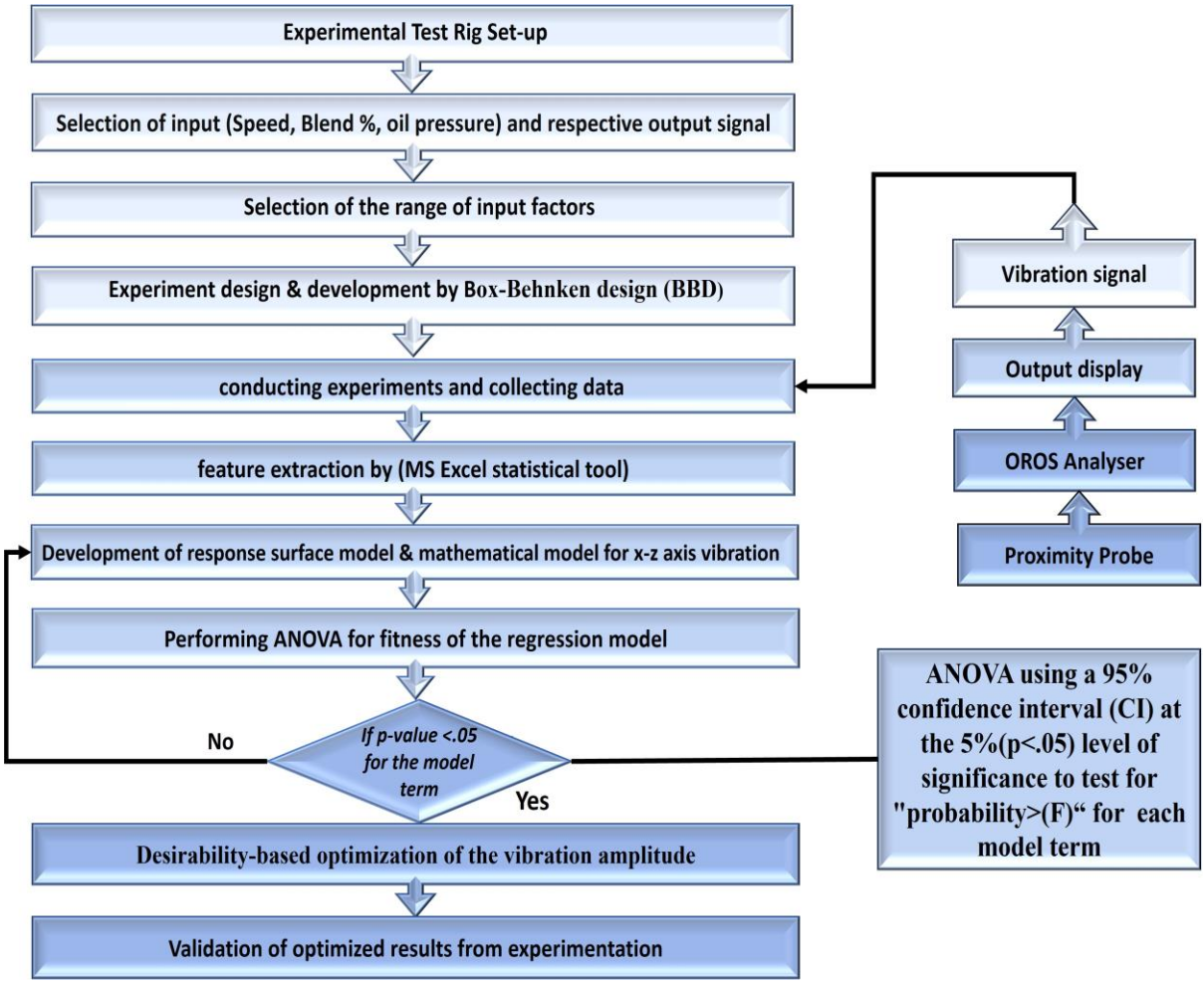

Figure 4.2 Flowchart of the proposed methodology.

4.4.2 Box-Behnken Design.

The Box-Behnken design (BBD) is a form of response surface approach used to determine the link between the input factors and the output responsiveness to maximize a system's or process's response. The variables are set at three levels (-1, 0, and 1) and the design points are selected to minimize the curvature of the response surface. This is a three-level design. Since each combination of the elements receives an equal amount of design points, the BBD is a symmetrical design. The formula n = k(k-1)/2, where k is the total number of elements, yields the total number of design points. The BBD, for instance, would contain 15 design points if there were three elements (n = 3(3-1)/2 = 3). Comparing the BBD to other response surface designs, there are various benefits. One of its main benefits is that it takes fewer runs than similar designs while still giving precise data on the response surface. The BBD is very

effective at detecting the curvature of the response surface, which is crucial for determining the best conditions for operation. The following assumptions of BBD are considered for modeling the vibration amplitude of rotor shaft with Squeeze film damper.

- **Linearity:** Assumes linear relationships between experimental factors and outcomes.
- **No Interactions Beyond the Second Order**: Does not consider interactions between factors beyond quadratic (second-order) interactions.
- **Independence of Errors**: The assumption that errors or residuals are unrelated.
- **Normality of Residuals**: Frequently implies residuals follow a normal distribution. The assumption is that factor levels are fixed and not subject to stochastic variation.
- **Constant Model Parameters:** Assumes that model coefficients are constant throughout the specified range.
- **Lack of Multicollinearity:** Assumes minimal correlation (multicollinearity) between the variables.
- **No anomalies:** Assumes no extreme anomalies exist in the data.
- **No Systematic Errors**: Assumes that data collection contains no systematic errors or biases.

A second-order polynomial model is frequently used to define the response surface of a BBD, which is subsequently applied to assess the results. The use of second-order polynomial models in designs is motivated by their ability to effectively capture intricate and non-linear interactions between inputs and responses. These models achieve an optimal balance between accuracy and complexity, facilitating the examination of interactions between factors, offering interpretability for gaining insights, and adhering to established scientific research methodologies. As a result, they serve as a helpful instrument for optimizing and comprehending intricate systems. Ordinary Least Squares (OLS) regression has been utilized

to change coefficients in second-order polynomial models in the Box-Behnken Design (BBD).

The model may be found in equation (1).

$$Y = \beta 0 + \beta 1X1 + \beta 2X2 + \beta 3X3 + \beta 12X1X2 + \beta 13X1X3 + \beta 23X2X3 + \beta 11X1^2 + \beta 22X2^2 + \beta 33X3^2 \qquad (4.1)$$

where Y is the response, X1, X2, and X3 are the factors, and β0, β1, β2, β3, β12, β13, β23, β11, β22, and β33 are the model coefficients.

Impact and influence of Ordinary Least Squares (OLS) regression choice on the results.

Effect on the Outcomes. Accuracy: OLS tries to find the best linear fit to the data, giving accurate predictions when the data is close to being linear.

Easy to understand: OLS values are easy to understand, which helps people understand how factors affect each other.

Assumptions: OLS assumes normality, constant variance, and independence of residuals, all of which should be true for safe results.

Sensitivity to Outliers: OLS can be sensitive to outliers, which means they need to be dealt with correctly.

Non-Linearity: OLS may not work well with highly non-linear data, so you may need to look at other regression methods.

A study of the experimental data using regression can be used to identify the coefficients. Following fitting, the model may be used to identify the optimal operational settings that maximize responsiveness. Depending on any factor limitations, this can be done by figuring out the values of the variables that optimize the expected response.

4.5 Experiment Work

Processes are influenced by a multitude of factors. Similarly, the operational performance of a squeeze film damper is governed by design features such as the damper's size, the variety of

oil supply within the damper, the supply oil pressure, and the flexible shaft RPM type of seal for the damper. Squeezing film damper performance is affected by operating variables such as oil pressure applied inside the damper, shaft speed, and damper oil blending ratio. For the experiment in the software, selection of the speed of the shaft is chosen between 2000 and 10000rpm. Supply oil pressure inside damper housing between 40 and 100 bar. Oil blends between 10% and 50%. Design-Expert program software output, after optimizing the test run, is provided in Table 4.4 below.

Table 4.4 recommended an experimental run after optimizing the input parameters.

Experimental Run No.	Supply oil Pr. (A)	RPM of the shaft (B)	Oil Blend % (C)
1	100	10000	30
2	100	2000	30
3	100	6000	50
4	70	6000	30
5	70	10000	10
6	40	2000	30
7	70	6000	30
8	70	10000	50
9	100	6000	10
10	70	6000	30
11	70	2000	50
12	70	6000	30
13	70	6000	30
14	70	2000	10
15	40	6000	10
16	40	6000	50
17	40	10000	30

The data presented in Table 4.5 displays the input parameters and corresponding values for seventeen distinct experiments that is design by Design-Expert program software. In order to guarantee precision and consistency, each experiment was conducted twice, denoted as T1 and T2. The shaft's vibration along both the x-axis and z-axis was measured and recorded for each trial, and the resulting average values are also included in the table(matrix).

Table 4.5 vibration amplitude of shaft at x-z axis on the recommended test run.

Experimental Run No.	Supply oil Pr. (A)	RPM of the shaft (B)	Oil Blend % (C)	Vibration at X	Vibration at Z
1	100	10000	30	3.91	3.92
2	100	2000	30	3.29	3.3
3	100	6000	50	3.79	3.81
4	70	6000	30	4.314	4.315
5	70	10000	10	3.8	3.79
6	40	2000	30	5.35	5.34
7	70	6000	30	4.313	4.314
8	70	10000	50	5.31	5.29
9	100	6000	10	3.811	3.812
10	70	6000	30	4.314	4.313
11	70	2000	50	3.32	3.34
12	70	6000	30	4.31	4.312
13	70	6000	30	4.305	4.31
14	70	2000	10	5.5	5.6
15	40	6000	10	5.15	5.14
16	40	6000	50	4.51	4.52
17	40	10000	30	4.89	4.9

4.6 Experimental Results and Analysis

The present study's goal is to minimize the vibration amplitude of high-speed rotating shaft along both the x and z axis. Table 4.4 displays recommended (software instructed) experimental run after optimizing the input parameters. Table 4.5 shows the vibration amplitude of the shaft at the x-z axis on the recommended(software-instructed) test run. After processing, the experimental findings were subjected to ANOVA for each output response, using response surface methodology modelling of box-Behnken design (BBD). The results of 17 distinct tests have been reported (table 4.5). These numerical calculations were carried out using the design expert software program. Table 4.6, displays the analysis of variance (ANOVA) results of the RSM model for the vibration amplitude of the shaft at the x-axis, and Table 4.7 shows the analysis of variance (ANOVA) results of the RSM model for the

vibration amplitude of the shaft along the z-axis, as well as a response table indicating the percentage role of each input operation parameter.

4.6.1 RSM model for Vibration of the shaft at the 'X' axis.

The RSM (Response Surface Methodology) model was employed to assess the vibration amplitude of the high-speed rotating shaft specifically in the 'X' axis. The model's performance and statistical significance were evaluated through various regression values and analysis of variance. Table 4.6 summarizes the comprehensive results.

Table 4.6 Vibration amplitude at X-axis as determined by Analysis of Variance (ANOVA).

Source	Sum of Squares	Degree of freedom	Mean Square	F Value	p-value Prob > F	
Model	7.288148	6	1.214691	60.08715	< 0.0001	significant
A-Pressure	3.249975	1	3.249975	160.7665	< 0.0001	
B-Speed	0.025313	1	0.025313	1.252134	0.2893	
C-Blend	0.221445	1	0.221445	10.95423	0.0079	
AB	0.2916	1	0.2916	14.42458	0.0035	
AC	0.09579	1	0.09579	4.738457	0.0545	
BC	3.404025	1	3.404025	168.3869	< 0.0001	
Residual	0.202155	10	0.020215			
Lack of Fit	0.202096	6	0.033683	2291.339	< 0.0001	significant
Pure Error	5.88E-05	4	1.47E-05			
Cor Total	7.490303	16				

The statistical metric known as the F-value contrasts the variance within and across groups. Given that a big F-value shows a substantial difference across groups, the model may be significant and account for data changes. In this instance, the Model F-value of 60.09 is significant and has a very low likelihood of being noise-induced (0.01%). This supports the model's relevance and its capacity for accurate forecasting. Additionally, the relevance of

some model terms is shown by the "Prob > F" values. The associated terms are significant and significantly affect the response variable if the values are less than 0.0500. Values higher than 0.1000, on the other hand, signify insignificance and imply that deleting such variables might improve the model's performance. When dealing with a large number of meaningless model words, it is crucial to take into account their possible contribution to sustaining hierarchy or other limitations within the model before eliminating them. The gap between actual data and predictions is gauged by the Lack of Fit F-value. There is a considerable mismatch between the model and the data in this instance, as shown by the significant Lack of Fit F-value of 2291.34. This indicates a poor match between the model and the data, underscoring the need to look into and fix the causes of the poor fit. Adding new terms to the model or changing the model's functional form are two potential fixes. The model's performance may be enhanced, resulting in more precise predictions, by carefully examining and correcting the origins of the Lack of Fit. Regression model equation:

$$X = 9.579 - 0.0425*A - 0.000489*B - 0.0956*C + 0.00000225*A*B + 0.000258*A*C + 0.0000115*B*C \quad (4.2)$$

Here, A denotes pressure, B is the speed in rpm, and C is the oil blending ratio.

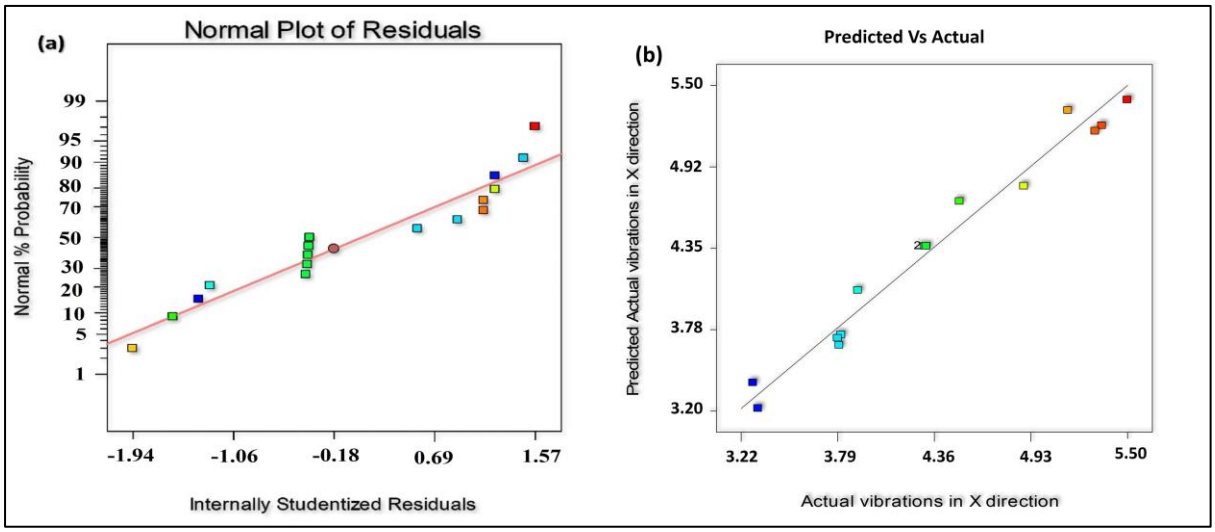

Figure 4.3. Evaluation of RSM correlation for minimizing the vibration amplitude of shaft at x-axis. (a) Normal probability plot of the residual (b) plot of the Predicted versus actual values.

Figure 4.3 (a)'s Normal Probability Plot of the Residual Graph displays: The residuals derived from the RSM analysis are shown in this subplot as a normal probability plot. The observed residuals are shown on the Y-axis, while the X-axis depicts the theoretical quantiles of the standard normal distribution. The residuals from the plot have a normal distribution and the data points closely follow a straight line the residuals are assumed to be normally distributed, and the RSM model is shown to be adequate. Figure 4.3(b) shows the plot of predicted vibration amplitude on the x-axis vs actual values. With the help of this subplot, we can compare the RSM model's predicted values to the actual measured vibration amplitude values. Actual values are shown on the X-axis, while forecasted values are shown on the Y-axis. Each data point represents an individual experimental situation. How closely the anticipated values match the actual values may be seen by looking at the graphic. The predictability and precision of the prediction model are easier to comprehend. The degree of agreement between expected and observed values may be determined by analysing the trends, patterns, and closeness of the plotted points. This information is crucial for assessing the success of the model. A sign that the RSM model is reliable is the data's tight alignment with a diagonal line at a 45-degree angle, which shows a high degree of agreement between the model's predictions and experimental findings.

4.7. Variable operating parameters and x-axis vibration amplitude interaction.

4.7.1 Interaction between supply oil pressure and shaft speed.

Figure 4.4(a), a 2D contour plot, displays the shaft's amplitude of vibration along the X-axis. The graph shows how the damper's vibration amplitude fluctuates with shaft speed and supply oil pressure. The contour lines on the plot connect points with equal vibration amplitudes. Usually, these lines are marked with the corresponding values of vibration amplitude. The minimum vibration amplitude is 3.702 at speeds below 6000 rpm and oil pressures above 90 bar, while the maximum vibration amplitude is 4.912 at speeds exceeding

8000 rpm and oil pressures below 50 bar. The graphic illustrates the correlation between shaft vibration amplitude and fluctuations in speed and oil pressure. However, it is important to note that this value does not encompass the cumulative impact of all parameters. The shaft's vibration amplitude along the X-axis is shown in a 3D surface plot in Figure 4.4(b). This graph displays the three-dimensional connection between the vibration amplitude, supply oil pressure inside the damper, and shaft speed. With the height of the surface corresponding to the amplitude magnitude, the surface plot shows the vibration amplitude as a function of the two input parameters. More specifically, this graph demonstrates the connection between variations in speed, oil pressure, and vibration amplitude.

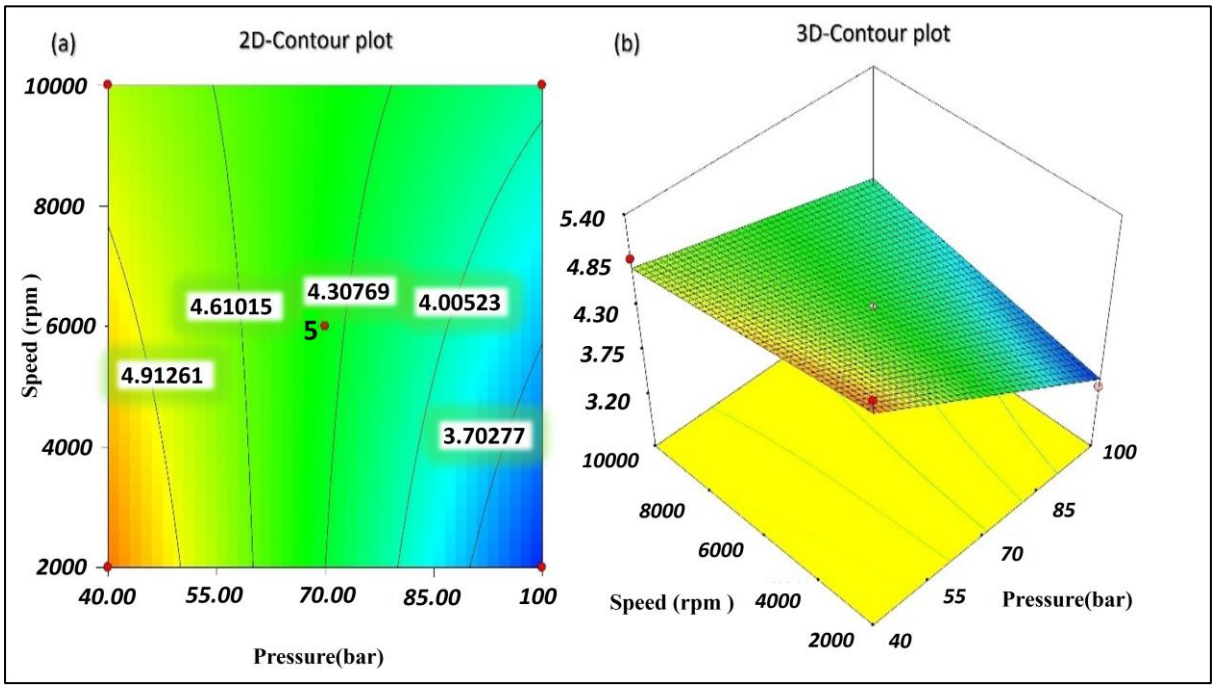

Figure 4.4. (a) 2D-contour depiction shows the shaft's vibration amplitude along the X-axis in relation to the shaft's speed and supply oil pressure. (b)3D surface map within the damper pressure model displays the vibration amplitude of the shaft at the X-axis in response to shaft speed and supply oil pressure.

Understanding how input variables for shaft vibrational amplitude, such as oil pressure and shaft speed, impact the vibration is critically dependent on the data presented in these graphs. The red colour zone represents the region with the highest amplitude of vibration, while the

blue colour zone indicates the region with the lowest amplitude of vibration in relation to both parameters.

4.7.2 Relationship between the blend ratio percentage and the flow of oil pressure.

Figure 4.5 (a) depicts the vibration amplitude of a shaft along the X-axis as a 2D-Contour plot. The graphic displays the relationship between the vibration amplitude and the supply oil pressure within the damper and the oil blend ratio percentage. The oil pressure that is delivered to the damper system is referred to as the supply oil pressure inside the damper. A damper is a tool for regulating vibrations and quelling oscillations. The percentage composition of two distinct oils combined together is referred to as the oil blend ratio percentage. It shows how much of each oil there is in the combination. The contour plot allows for the identification of regions where vibration amplitudes are minimized or maximized. The minimum vibration amplitude is 3.982 when the oil pressure exceeds 90 bar and the oil blend percentage is below 20%, indicated by a blue color. Conversely, the maximum amplitude is 5.05 when the oil pressure is below 40 bar and the oil blend ratio increases by more than 25% display the color red. The contour plot aids in identifying the optimal blend percentage and supply oil pressure for effectively controlling and minimizing vibration amplitudes. The x-axis of the 2D-Contour plot indicates the supply oil pressure within the damper, and the y-axis is the percentage of oil blends. The contour lines on the map show the shaft's vibration levels for various mixtures of supply oil pressure and oil blend ratio. In order to create a continuous curve, the contour lines join locations with the same vibration amplitude. The change in vibration amplitude increases steeply with the proximity of the contour lines to one another. In contrast, contour lines with greater spacing suggest a shift in vibration amplitude that occurs more gradually. The link between the vibration amplitude of the shaft at the X-axis, supply oil pressure inside the damper, and oil mix ratio percentage is further illustrated by Figure 4.5(b), a 3D-Surface map. The supply oil pressure

is represented by the x-axis, the oil mix percentage is shown on the y-axis, and the vibration intensity is shown on the z-axis. A more in-depth illustration of how the vibration amplitude fluctuates over the range of supply oil pressure and oil mix ratio values may be seen in the 3D-Surface map. When supply oil pressure and oil mix ratio are combined, the height or depth of the surface indicates the vibration amplitude.

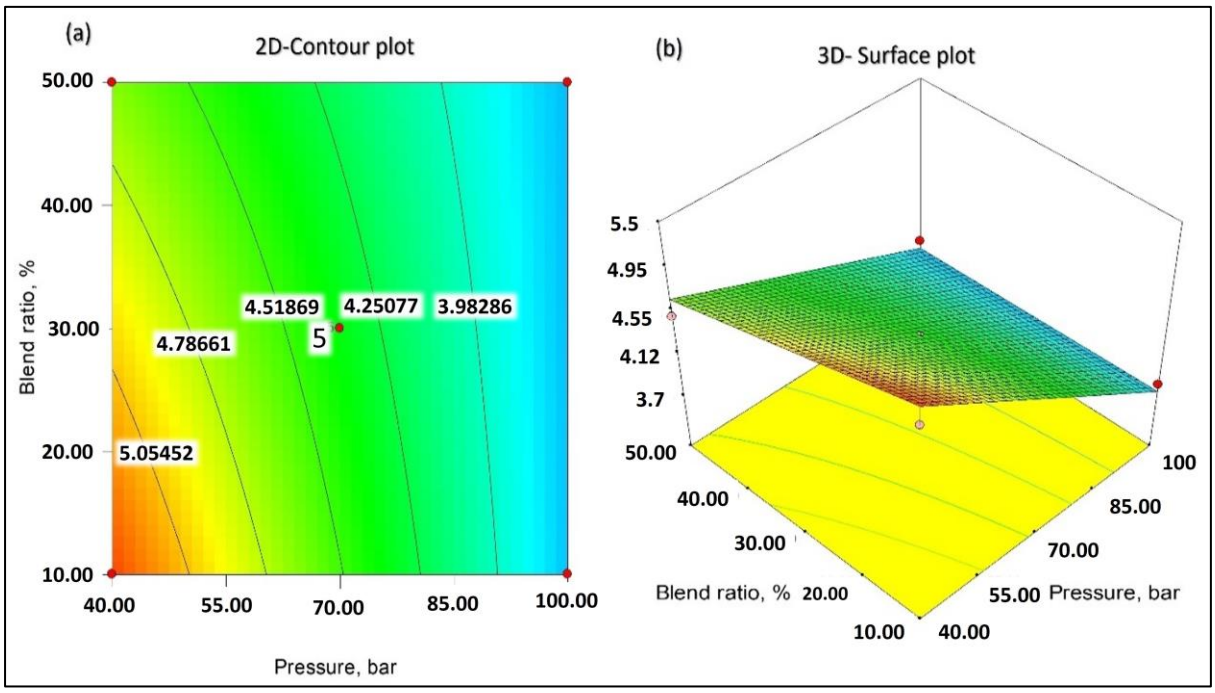

Figure 4.5 (a) 2D-Contour plot for vibration amplitude of shaft at X-axis with respect to supply oil pressure inside the damper and Y-axis oil blend ratio percentage, Figure 4.5 (b) 3D-Surface plot for vibration amplitude of shaft at X-axis with respect supply oil pressure inside the damper and Y -axis to oil blend ratio percentage.

4.7.3 Interaction between shaft speed and oil blend ratio percentage

The contour plot illustrates the relationship between the vibration amplitude of a shaft and two variables: the oil blend percentage and the speed of the shaft. The plot uses contour lines to connect points with the same vibration amplitude. Closely spaced contour lines indicate significant changes in vibration amplitude, while widely spaced lines suggest more gradual changes. The contour plot analysis reveals that vibration amplitude reaches its minimum value of 3.581 at speeds below 4000 rpm and blend ratios below 20%, which are represented

by the color blue. Conversely, the maximum vibration amplitude of 5.033 occurs at speeds exceeding 10000 rpm and oil blend percentages exceeding 40%, which are represented by the color red. The contour plot facilitates the visualization of the relationship between the oil blend percentage and shaft speed, and their impact on vibration amplitude. This visualization assists in identifying the optimal combination of these factors to effectively control and minimize vibrations. Figure 4.6(a) depicts a 2D-Contour plot of the vibration amplitude of a shaft at the X-axis as a function of shaft speed and oil blend percentage. The contour lines show varying degrees of vibration amplitude, illustrating how these factors affect the performance of the shaft, in Figure 4.6(b), which is a 3D-Surface plot. It offers a visual picture of how these factors' various combinations affect the vibrations amplitude.

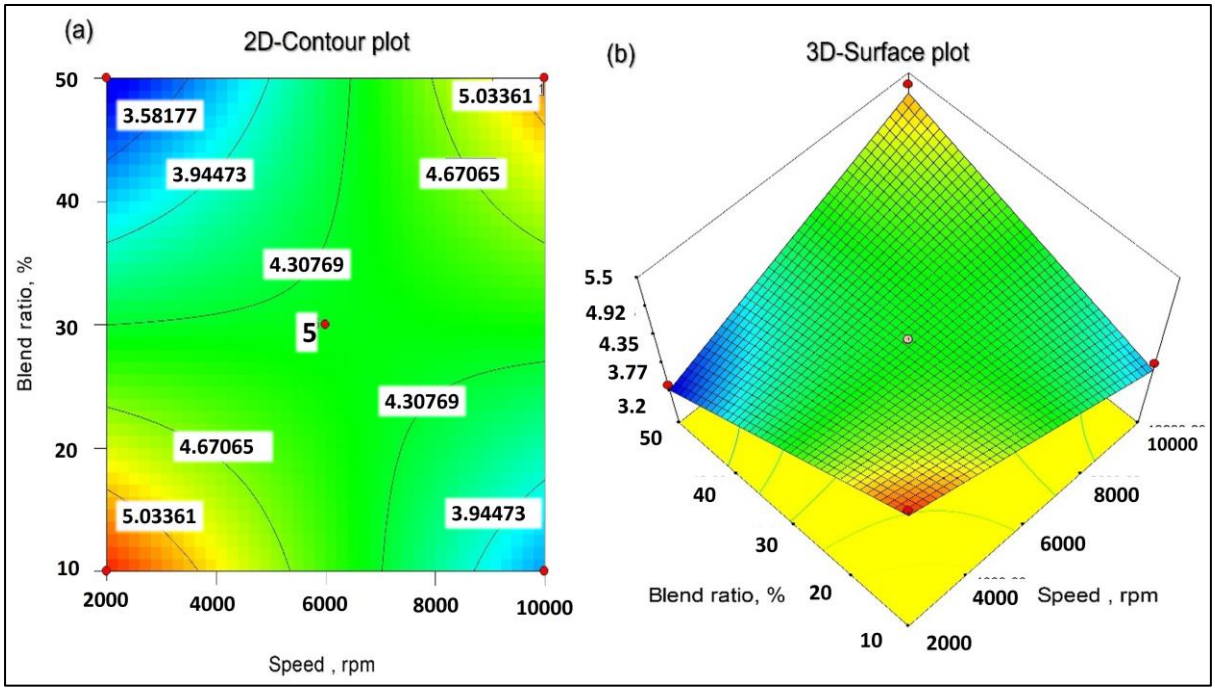

Figure 4.6 (a) 2D-Contour plot for vibration amplitude of shaft at X-axis with respect to speed of shaft and blend ratio percentage of oil, (b) 3D-Surface plot for vibration amplitude of shaft at X-axis with respect to speed of the shaft and blend ratio percentage of oil.

4.8 RSM model for Vibration amplitude of the shaft at the 'Z' axis.

The RSM model was applied for measuring the vibration amplitude of the high-speed rotating shaft at the z-axis. All the related regression values and analysis of variance results are shown in Table 4.7

Table 4.7. Vibration amplitude at Z-axis as determined by Analysis of Variance (A**NOVA).**

Source	Sum of Squares	Degree of freedom	Mean Square	F Value	p-value Prob > F	
Model	7.288148	6	1.214691	60.08715	< 0.0001	significant
Model	7.360242	6	1.226707	55.20243	< 0.0001	significant
A-Pressure	3.197921	1	3.197921	143.908	< 0.0001	
B-Speed	0.0128	1	0.0128	0.576006	0.4654	
C-Blend	0.238741	1	0.238741	10.74344	0.0083	
AB	0.2809	1	0.2809	12.64064	0.0052	
AC	0.095481	1	0.095481	4.296693	0.0650	
BC	3.5344	1	3.5344	159.0498	< 0.0001	
Residual	0.22222	10	0.022222			
Lack of Fit	0.222205	6	0.037034	10009.23	< 0.0001	significant
Pure Error	1.48E-05	4	3.7E-06			

A statistical model is a tool used to describe the relationship between one or more variables. The F-value is a measure of the goodness of fit of the model. A high F-value indicates a good match between the model and the data, whereas a low F-value indicates a poor fit. The model appears to be important in this instance and provides a good fit to the data, as indicated by the Model F-value of 55.20. Simply examining the Model F-value is insufficient, though. The relevance of each model term must also be taken into account. It is clear that some model terms A, C, AB, and BC—are important while others are not. It's important to note that if there are several irrelevant model terms, model reduction may enhance the model as a whole. Lack of Fit F-value is another crucial indicator to take into account. The degree to which the

model fails to adequately account for the data is gauged by this statistic. A low number indicates a good fit, whereas a large value indicates the model does not well fit the data. This situation shows a significant lack of fit, which is undesirable, as shown by the Lack of Fit F-value of 10009.23. The goal is for the model to closely match the data. In conclusion, when working with statistical models, it's important to consider various metrics to assess the model's performance. The Model F-value and individual model term significance can help us understand how well the model fits the data. The Lack of Fit F-value can indicate areas where the model needs improvement to fit the data better. By considering all these metrics, we can make better-informed decisions about the model and the data.

Regression model equation:

$$Z = 9.6297 - 0.04205*A - 0.000497*B - 0.09716*C + 0.0000022*A*B + 0.000257*A*C + 0.0000118*B*C \quad \ldots\ldots (4.3)$$

Here A denotes pressure, B is the speed in rpm, and C is the oil blending ratio

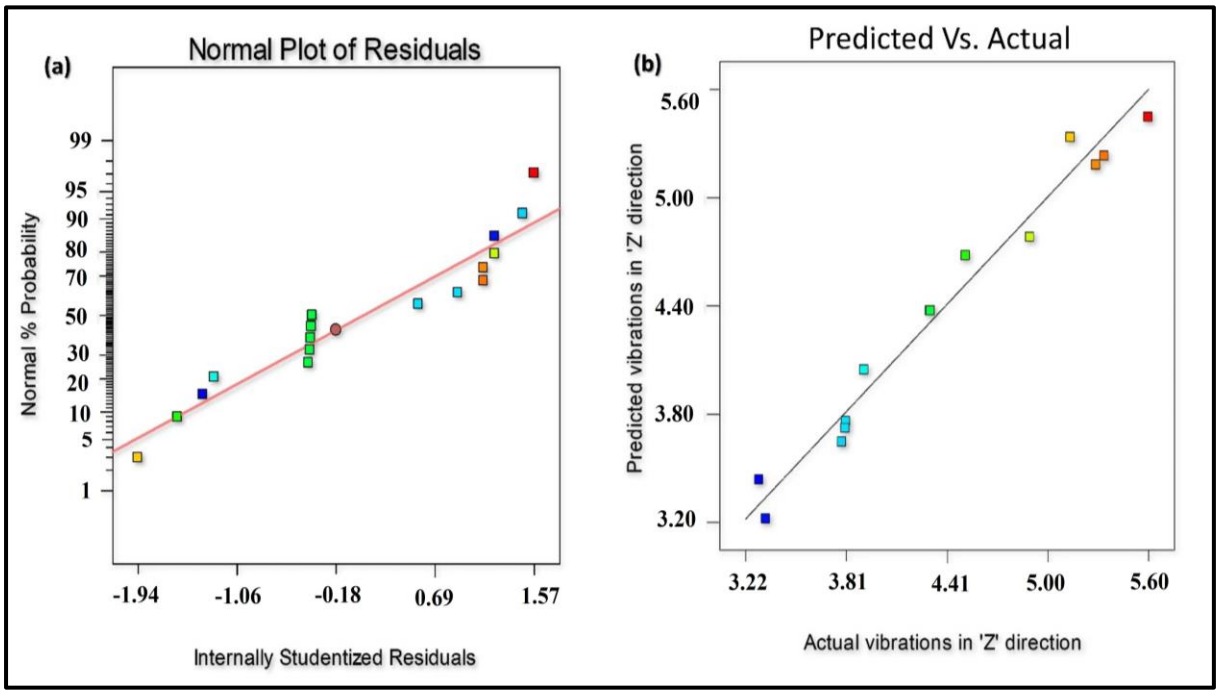

Figure 4.7 Evaluation of RSM correlation for minimizing the vibration amplitude of shaft at z-axis. (a) Normal probability plot of the residual (b) plot of the Predicted versus actual values.

The Residual Graph's Normal Probability Plot in Figure 4.7(a) shows: This subplot displays the residuals obtained from the RSM analysis as a normal probability plot. The Y-axis represents the actual residuals, while the X-axis represents the theoretical quantiles of the normal distribution. The plot's residuals follow a normal distribution. The RSM model is proven to be sufficient because the data points roughly resemble a straight line and the residuals are considered to be normally distributed. The plot of expected vibration amplitude on the z-axis vs. actual values is displayed in Figure 4.7(b). This subplot compares RSM model predictions to observed vibration amplitude values. The Y-axis shows forecasted values while the X-axis shows actual values. One experimental condition per data point. The chart shows the link between anticipated and actual figures. The RSM model's correctness may be assessed by aligning data points with a 45-degree diagonal line, which shows a high concordance between model predictions and experimental observations.

4.9 Interaction between different operating parameters for Z-axis vibration amplitude

4.9.1 Interaction between speed of the shaft and supply oil pressure

The contour plot helps visualize how adjusting oil pressure and speed of the shaft can affect the vibration amplitude, assisting in finding the optimal combination to control and minimize vibrations. In Figure 4.8(a) 2D-Contour Plot: This plot uses contour lines on a two-dimensional plane to depict the vibration amplitude. The shaft speed is shown by the Y-axis, while the X-axis indicates the supply oil pressure inside the damper. The contour lines on the plot connect points with equal vibration amplitudes. Usually, these lines are marked with the corresponding values of vibration amplitude. The minimum vibration amplitude is 3.733 at speeds below 6000 rpm and oil pressures above 90 bar, while the maximum vibration amplitude is 4.930 at speeds exceeding 8000 rpm and oil pressures below 50 bar. The graphic illustrates the correlation between shaft vibration amplitude and fluctuations in speed and oil pressure. However, it is important to note that this value does not encompass the cumulative

impact of all parameters. In Figure 4.8(b): The vibration amplitude is shown in three dimensions by this figure. The shaft's speed is represented by the Y axis, the supply oil pressure by the X axis, and the vibration intensity by the Z axis. A smooth, continuous surface is shown in the surface plot, and height variations represent the amplitude values.

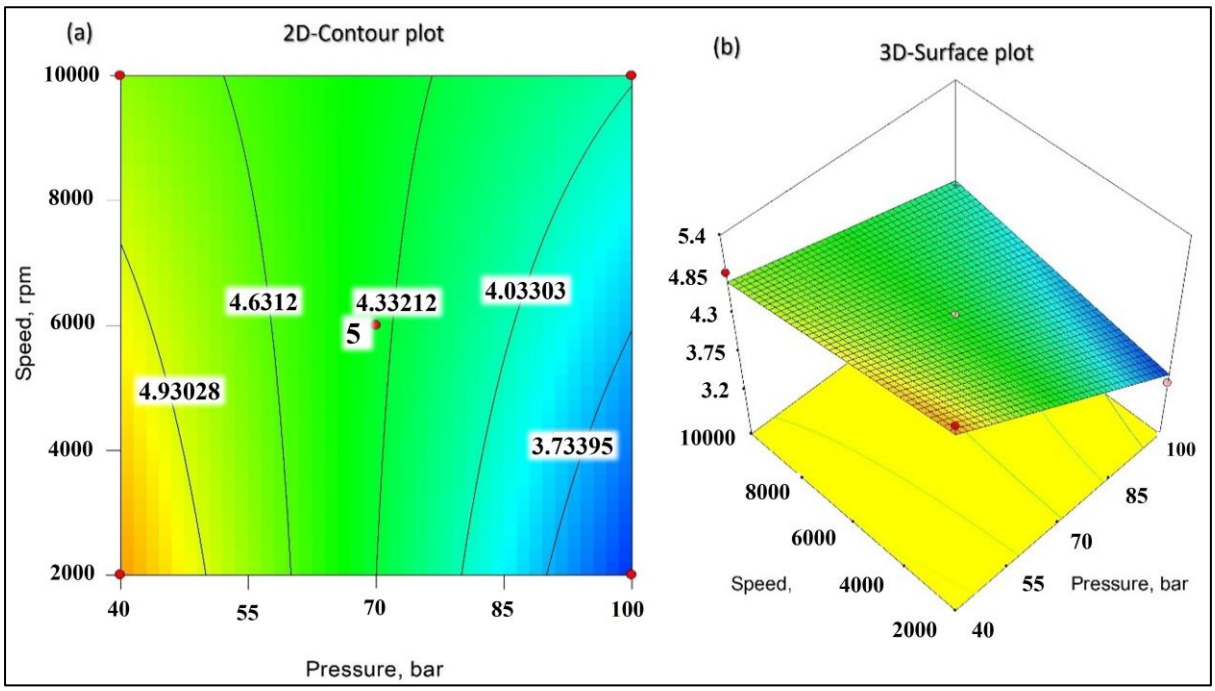

Figure 4.8 (a) 2D-Contour plot for vibration amplitude of shaft at z-axis with respect to speed of shaft and supply oil pressure inside the damper, (b) 3D-Surface plot for a vibration amplitude of shaft at z-axis with respect to the speed of the shaft and supply oil pressure inside the damper.

4.9.2 Interaction between supply oil pressure and blend ratio percentage.

The contour plot provides a visual tool to understand how adjustments in oil blend percentage, oil pressure, and speed impact the vibration amplitude, aiding in determining the optimal combination to control and minimize vibrations. As a 2D-Contour plot with regard to the mixture ratio percentage and the supply oil pressure within the damper, Figure 4.9 (a) displays the vibration magnitude of a shaft at the z-axis. The contour lines represent different levels of vibration amplitude, with closer lines denoting greater changes. Using a contour plot, one can see how two factors- shaft speed and oil pressure inside the damper housing—impact the shaft's vibration amplitude. A further factor affecting the vibration amplitude is

the proportion of the oil blend. The contour plot shows the vibration amplitude on the z-axis with contour lines linking locations of equal amplitude. Closely spaced lines indicate significant changes in amplitude, while widely spaced lines suggest more gradual changes. By analysing the plot, one can identify regions where the vibration amplitude is minimized or maximized. The contour plot allows for the identification of regions where vibration amplitudes are minimized or maximized. The minimum vibration amplitude is 3.989 when the oil pressure exceeds 90 bar and the oil blend percentage is below 20%, indicated by a blue color. Conversely, the maximum amplitude is 5.063 when the oil pressure is below 40 bar and the oil blend ratio increases by more than 25% display the color red. The contour plot aids in identifying the optimal blend percentage and supply oil pressure for effectively controlling and minimizing vibration amplitudes. A 3D-Surface plot of the relationship between the shaft's vibration amplitude at the z-axis, oil mix ratio, and supply oil pressure inside the damper is shown in Figure 4.9 (b). The graphic illustrates how the vibration amplitude changes for various combinations of these factors.

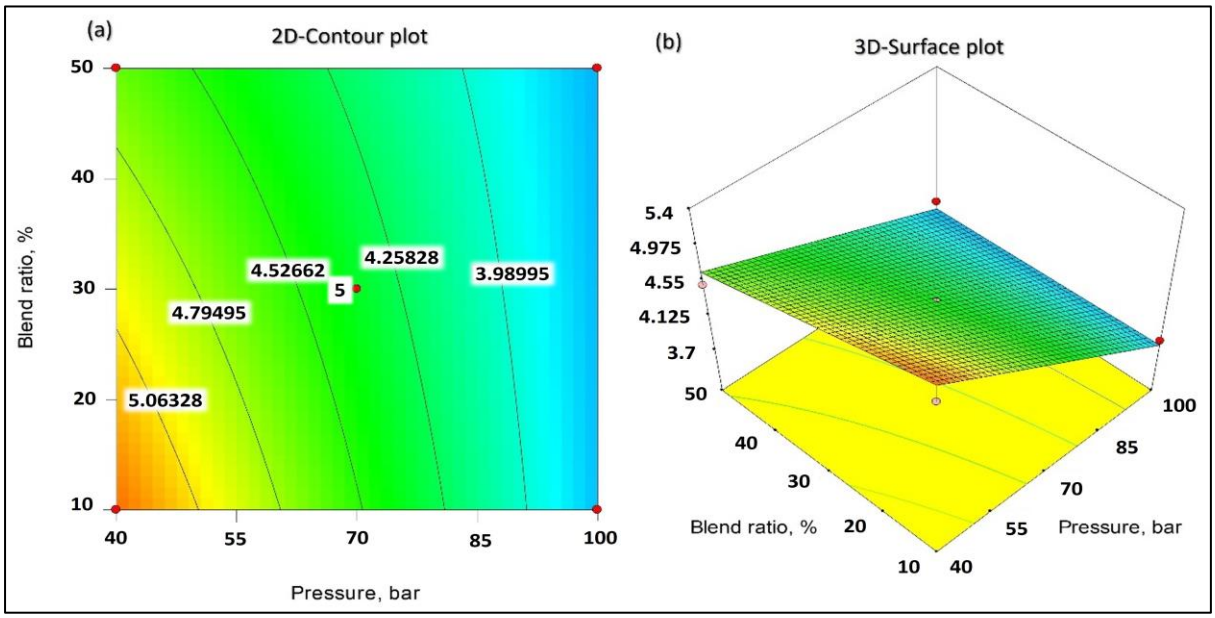

Figure 4.9 (a) 2D-Contour plot for vibration amplitude of shaft at z-axis with respect to blend ratio percentage and supply oil pressure inside the damper, (b) 3D-Surface plot for a vibration amplitude of shaft at z-axis with respect to oil blend ratio percentage and supply oil pressure inside the damper.

4.9.3 Interaction between shaft speed and oil blend ratio percentage.

The contour plot helps visualize how adjusting shaft speed and oil blend percentage can impact the vibration amplitude, aiding in finding the optimal combination to control and minimize vibrations. Figure 4.10 (a) displays a 2D-Contour plot that demonstrates how shaft speed and oil mix percentage affect the vibration amplitude of a shaft at the z-axis. The contour lines demonstrate the different levels of vibration amplitude and how these elements influence the shaft's vibration. To help the viewer grasp the relationship, the figure connects locations with the same vibration amplitude using contour lines. While widely separated contour lines show more gradual shifts, lines that are closely spaced indicate considerable changes in vibration amplitude. The map may be examined to determine the locations where the vibration amplitude is either decreased or maximized. The contour plot analysis reveals that vibration amplitude reaches its minimum value of 3.590 at speeds below 4000 rpm and blend ratios below 20%, which are represented by the color blue. Conversely, the maximum vibration amplitude of 5.073 occurs at speeds exceeding 10000 rpm and oil blend percentages exceeding 40%, which are represented by the color red. The contour plot facilitates the visualization of the relationship between the oil blend percentage and shaft speed, and their impact on vibration amplitude. This visualization assists in identifying the optimal combination of these factors to effectively control and minimize vibrations. Figure 4.10 (b), a 3D-Surface plot, shows the correlation with the shaft's vibration amplitude at the z-axis, speed, and oil mix percentage. It offers a visual picture of how the vibration amplitude changes when these factors are combined in various ways.

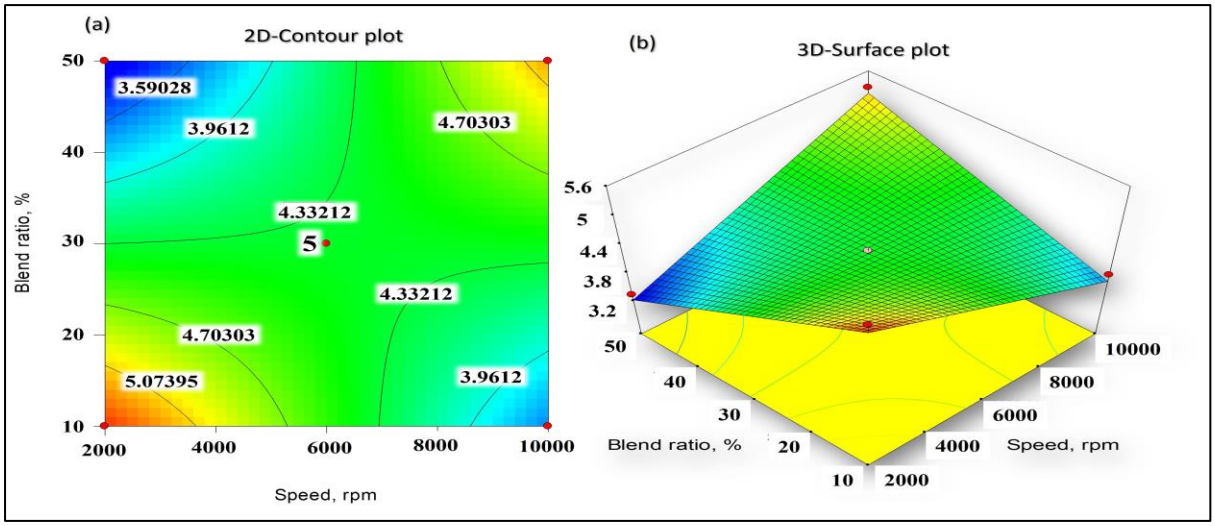

Figure 4.10 (a) 2D-Contour plot for vibration amplitude of shaft at z-axis with respect to the speed of shaft and blend ratio percentage of oil, (b) 3D-Surface plot for a vibration amplitude of shaft at z-axis with respect to the speed of the shaft and blend ratio percentage of oil.

4.10 Desirability-based optimization

Searching for the ideal set of input parameters that results in good output responses is an important strategy used in experimental design and analysis. It enables numerical optimization by combining many response variables into a single objective function, referred to as the desirability function. The desirability function assigns a desirability value to each input variable combination after taking into account the significance of each response variable and any limitations. This number goes from 0 to 1, with 0 denoting an undesirable result and 1 denoting the optimum result. The desirability function is used in experimental design, process optimization, and product development to find the ideal circumstances for producing desired attributes or results. A potent method called desirability-based optimization allows for the simultaneous optimization of several response variables while taking into account their relative significance. It is very helpful for non-linear function optimization and allows for varying uncertainty in input and output. This method determines the ideal mixture of input elements to produce desired output outcomes. The choice of ramp level within the context of optimization parameter or response characterization is pivotal, as it conveys the directional preference inherent in the optimization process. The selection of the

ramp level effectively dictates the prioritization of specific optimization outcomes, making it a crucial technical consideration. When defining the level of ramp, it establishes a gradient of **desirability** across the spectrum of potential parameters or response values. This gradient is representative of the engineering or scientific objectives, where higher ramp levels often signify a greater desire for higher parameter values or responses, while lower ramp levels indicate a preference for lower values. Applications for desire-based optimization include product development, process improvement, and experimental design. Compared to conventional optimization techniques, it delivers more precision and relevance.

4.10.1 Desirability criteria

Desirability-based optimization of the vibration amplitude of the shaft about the x and z axis was done. The details of the parameters used and their desirability are shown in Table 4.8.

Table 4.8 Parameters and their desirability.

Parameters	Desirability
Pressure	In range
Speed	Maximize
Blending ratio	In range
Vibration 'X'	Minimize
Vibration 'Z'	Minimize

4.10.2 Ramp diagrams of desirability

The graph obtains for the optimization from desirability criteria, the pressure of oil that's selected in range (40-100bar), the maximum value of the pressure of oil is 99.82 bar recommended by the software for controlling the vibration amplitude of both the x-z axis at a maximum speed of shaft that about 10000 rpm shown figure 4.11(a)&4.11(b). the blending of oil recommended is 13.08 % for minimizing the vibration amplitude of the shaft which appears in Figure 4.11(c).

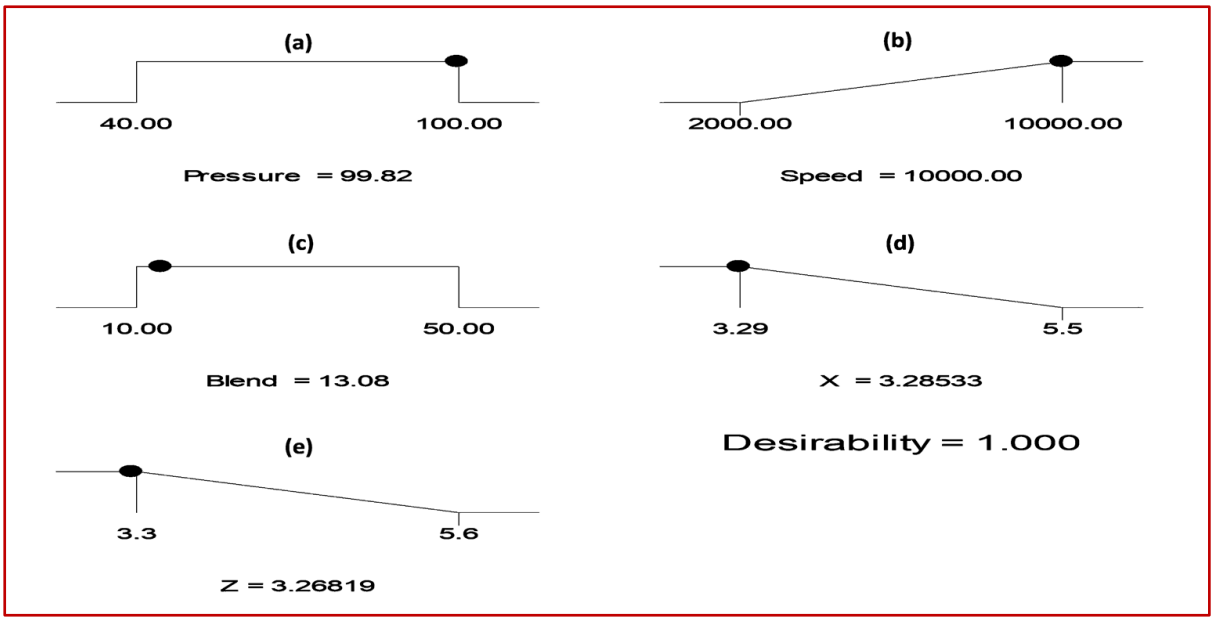

Figure 4.11 Ramp diagrams of desirability.

The optimization was completed according to desirability criteria as shown in table 8. The respective graphs are shown in Figure16 and the respective parameters and their values are given in Table 4.9. The ramp level serves as a quantifiable representation of the optimization target, guiding the optimization algorithm to explore and potentially converge towards regions of the parameter space that align with the desired outcomes.

- In this case, it is desirable to maintain any value oil pressure and blending percentage within a specific range for optimization. The graph exhibits a flat pattern when the parameters fall within this specific range. This suggests that our experiment or application should stay within this range ramp.
- Speed: In our graph, we selected the maximum speed, which places the maximum speed point at the upper side of the ramp. This indicates that a higher speed is desirable for our experiment, while lower speeds are less desirable.
- Vibration Amplitude (X and Z Axes): Our goal is to minimize the vibration amplitude. In the graph, the upper side of the ramp represents the minimum value of vibration, while the lower side represents the maximum vibration amplitude. This

implies that lower vibration amplitudes are preferred for our experiment, whereas higher amplitudes are not desirable.

Table 4.9 Details parameters and their optimized value.

Parameters	**Optimized values**
Pressure	99.82 (bar)
Speed	10000(rpm)
Blending ratio	13.08 (%)
Vibration at 'X' axis	3.285 (µm)
Vibration at 'Z' axis	3.268 (µm)

4.11 Experimental validation.

The conformation experiment examined how process factors (A, B, and C) affected the shaft's vibration amplitudes at the x-axis and z-axis. Table 4.10 summarizes the results of the experiment. Three trials of the experiment were run, with experimental and anticipated values recorded for each trial. The outcomes of the trial nearly matched the values anticipated, demonstrating the model's success in forecasting vibration amplitudes. This displays the model's capacity to examine how process variables affect shaft vibration and offers helpful information for enhancing the system's performance.

Table 4.10 Conformation experiment

Process factors				Vibration amplitude of shaft at the x-axis(µm)		Vibration amplitude of shaft at the z-axis(µm)	
Trail no.	A	B	C	Predicted	Experiment	Predicted	Experiment
1	20	10000	50	5.18±0.24	5.24	4.25±.23	4.08
2	60	4000	20	3.52±.024	3.41	3.57±.23	3.41
3	80	8000	40	3.18±0.24	3.30	3.16±.23	3.08

A-oil pressure, B-speed of the shaft, C-oil blend percentage.

The experimental validation was conducted to verify the effectiveness of the optimized values obtained for the parameters in controlling the vibration of the high-speed rotating shaft. The optimized values for Pressure, Speed, Blending ratio, Vibration 'X', and Vibration 'Z' were determined to be 99.82, 10000, 13.08, 3.285, and 3.268 respectively (as stated in Table 4.9). Under controlled test conditions, the experimental measurements were performed, and the obtained values were compared with the optimized values. Statistical analysis techniques were employed to quantify the discrepancies between the experimental and optimized values.The findings of the experimental validation showed that the experimental measurements and the optimized values were in good agreement. All the findings provided in Table 4.11 demonstrate that the measured values for Pressure, Speed, Blending ratio, Vibration 'X', and Vibration 'Z' were found to be very near to the optimum values, with deviations well within the acceptable range of less than 5%.

Table 4.11 Experiment validation

Process factors			Vibration amplitude of shaft at the x-axis(µm)		Vibration amplitude of shaft at the z-axis(µm)	
A	B	C	Predicted	Experiment	Predicted	Experiment
99.82	10000	13.08	3.285±0.164	3.391	3.268±0.163	3.401

A-oil pressure, B- shaft speed, C-oil blend percentage.

This successful experimental validation demonstrates the accuracy and dependability of the optimum values achieved for the parameters in managing the vibration of the high-speed rotating shaft. The validation method increases trust in the optimization approach's performance and strengthens the optimized values' appropriateness for practical deployment in vibration control systems. Overall, the validation study validates the applicability and efficacy of the optimized values in obtaining the intended vibration control results for the high-speed rotating shaft.

4.12 Summery of the Chapter

The primary focus of this investigation is on the creation of a Squeeze Film Damper (SFD), which is intended to reduce the vibration amplitudes experienced in high-speed rotating shafts. The purpose of this research is to investigate the impacts of SFD process factors during the rotation of a flexible shaft up to 10,000 rpm by examining vibration amplitudes along the x and z axes. These parameters include shaft rotation, oil pressure inside the damper, and oil mix %. The experimental design optimizes the input parameters and determines the statistical significance of the model by using a Box-Behnken design (BBD), Response Surface Methodology (RSM), and Analysis of Variance (ANOVA). The goal of desirability-based optimization is to accomplish the vibration control goals that are important to the user. The resultant x and z axis vibration amplitudes are 3.285 micrometres and 3.268 micrometres, respectively, when the input parameters are tuned to be 10,000 revolutions per minute, 13.08% blend ratio, and 99.82 bar oil pressure. Experimentation and verification are carried out in order to ascertain whether or not these optimum settings for vibration control of high-speed rotating shafts are effective. The empirical assessment demonstrates that there were shifts of 3.125% along the x-axis and 3.91% along the z-axis, which is evidence that the optimization strategy was successful. The values that were measured are very near to the values that were optimized, and the errors that were found are well below the permitted range, coming in at less than 5%. The fact that the experimental validation was successful lends credence to the precision and dependability of the values that were tuned for efficient vibration control. These results not only give useful insights for the development and implementation of SFDs in high-speed rotating shafts, but they also show promise for improving vibration control and overall performance in rotating equipment applications.

CHAPTER-5

EXPERIMENTAL INVESTIGATION OF SQUEEZE FILM DAMPERS AND A COMPARATIVE ANALYSIS USING ARTIFICIAL NEURAL NETWORKS (ANN) AND RESPONSE SURFACE METHODOLOGY (RSM)

5.1 Introduction

This study utilizes a combination of rigorous approaches, integrating the accuracy of Response Surface Methodology (RSM) with the efficiency of a Box-Behnken design, in order to conduct a thorough analysis. This study utilizes Artificial Neural Network (ANN) optimization approaches to explore the complexities of key aspects that impact a system. The factors that are subject to careful examination include important characteristics such as the rotational speed of the shaft, which may reach up to 8000 rpm, the oil pressure that ranges up to 100 bar, and the various oil mix ratios ranging from 10% to 50%. The research seeks to assess the errors and coefficients of determination present in the projected models by using different statistical techniques. The artificial neural network (ANN) model has emerged as a prominent competitor, demonstrating lower prediction errors and a higher coefficient of determination compared to the response surface methodology (RSM), specifically in respect to the x and z axes of vibration amplitude. In addition, the analysis rigorously scrutinizes important metrics such mean absolute error (MAE), root mean squared error (RMSE), and coefficient of determination (R-squared). The use of the Artificial Neural Network (ANN) approach not only demonstrates improved predicted accuracy but also highlights significant advantages in terms of efficiency and time conservation, hence strengthening its effectiveness in this complex investigation.

5.2 Materials and Method

5.2.1 Preparation of oil samples

On the basis of the analysis of several studies [107, 156] examining the use of viscoelastic and Newtonian fluids to control high vibration amplitudes at high swivel shaft rotational speeds within a damper, it has been found that using a Newtonian liquid can actually increase vibration amplitudes at high speeds. A thorough inquiry was done to address this. In order to create unique samples of the Newtonian liquid for this experiment, several mixtures of kerosene oil and crankcase oil were prepared. Preliminary studies on these produced samples were carried out in order to establish optimal proportions for five new test samples. The new test samples were created by carefully mixing the two types of oils at a constant temperature of 30°C using a magnetic stirrer. Blending kerosene oil with crankcase oil in quantities ranging from 10% to 50% yielded these test samples. The dynamic viscosity of kerosene oil is 1.1287 mPaS, whereas the dynamic viscosity of crankcase oil is 75.483 mPaS. The viscosity measurements at the required temperature help researchers in the field better understand the damping efficacy and vibration attenuation characteristics of the oils. An SVM3000 viscometer was used to accurately determine the dynamic viscosities of these various samples (referred to as Samples 1 through Sample 5). Each of these samples' dynamic viscosities were recorded as follows: 15.786 mPaS, 19.476 mPaS, 23.695 mPaS, 33.684 mPaS, and 46.271 mPaS for the first and fifth samples, at 30^0**C** respectively. The viscosity measurements at the required temperature help researchers in the field better understand the damping efficacy and vibration attenuation characteristics of the oils.

5.2.2 Experimentation

A specific test rig, shown in Fig. 3.3 and 3.4, was used in the experimental setting. This arrangement included three pinned supports, each of which held a flexible rotor. One of the pins supports far from the drive motor was removed to make room for the installation of the

squeeze film damper (SFD) unit. The squeeze film damper device was securely housed on a pedestal that was made to order in its place.

A high-pressure oil feeding pump was used to make lubricating the squeeze film damper easier. The vertical mid-planes of the bearings' circumferential grooves were where this pump delivered oil. A flexible coupling, more precisely a Lovejoy coupling, was used to build the power transmission mechanism concurrently. This experimental setup's primary objective was to precisely reproduce the rotor-bearing system's operation under controlled circumstances. The system's dynamic behavior may be measured precisely and in-depth analyzed to this method. It should be noted that in this configuration, two VIBROMETER proximity probes were carefully positioned perpendicular to one another, and they were positioned in the centers of the two pinned supports close to the rotating shaft. The purpose of these probes was to track and gather information on the movements and vibrations of the system.

Table 5.1 shows the details specifications of the experimental test rig.

Specifications of the Experimental Test Rig	
SFD and rotor shaft components' materials	*Mild steel*
Rotor shaft's length and diameter	*1000mm, 22mm*
Boundary dimension of damper journal	*44×50×64mm*
Boundary dimension of damper housing	*50×56×64mm*
Length of the damper	*50 mm*
length between one support and damper unit	*500mm*
Boundary dimension of ball bearings is utilized in squeeze film damper, type	*22×44×12mm, Koyo*
Spacer in between two ball bearings	*4mm*
DC motor 0.5 hp single phase rated speed	*12000rpm*
Type of coupling	*flexible Lovejoy*
O-ring seal material and diameter	*Rubber, 46mm*
Speed controller (Dimmer stat auto transformer single phase, 0-270V)	*2 amperes open type*
Vibrometer proximity probe (TQ402, range: 4mm API670, body thread M10, body length 50mm)	*flexible cable 10m with magnetic stand*

The shaft's output signal data was collected at various constant speeds using a sampling frequency of 20 kHz and a sampling rate of 25.6 ks/s. The measured output signal lasted between 7 and 9 seconds. Data collecting and analysis were conducted using a 32-channel OROS vibration analyzer, which has a frequency range of 20 kHz. This analyzer supports data in both the time domain and the Fast Fourier Transform (FFT). MATLAB code was used to perform additional analysis on the time domain signal data.

5.3. Methodology

5.3.1 Flowchart of the Methodology

The approach used to fulfill the research's specific aims is displayed and described through the illustration offered in the Fig 5.1. The methodology describes the step-by-step approach, tactics, and procedures used in the study to achieve the research goal. A technique for experimental optimization that is focused on research is shown in the flowchart. The initial steps in the investigation involve setting up a test rig and choosing the input variables. These variables' range of possible values has been chosen with care. In order to effectively explore the influence of input parameters impacting the response, experiments are structured using the Response Surface Methodology (RSM) and Box-Behnken design (BBD). In order to understand the relationship between the input variables and the response, studies collect data and create a response surface model. ANOVA and the regression model equation are used to assess the model's accuracy. Analysing the residuals and the regression equation are stepped in the process. This aids in the collection of projected response data based on the equation of the regression model. The actual data gathered from experiments is then contrasted with these expected values. We can assess how well our model matches the real data using metrics like Mean Absolute Error (MAE), Root Mean Square Error (RMSE), and R-squared, thanks to this comparison. Concurrently, we train an Artificial Neural Network (ANN) tool using the experimental dataset.

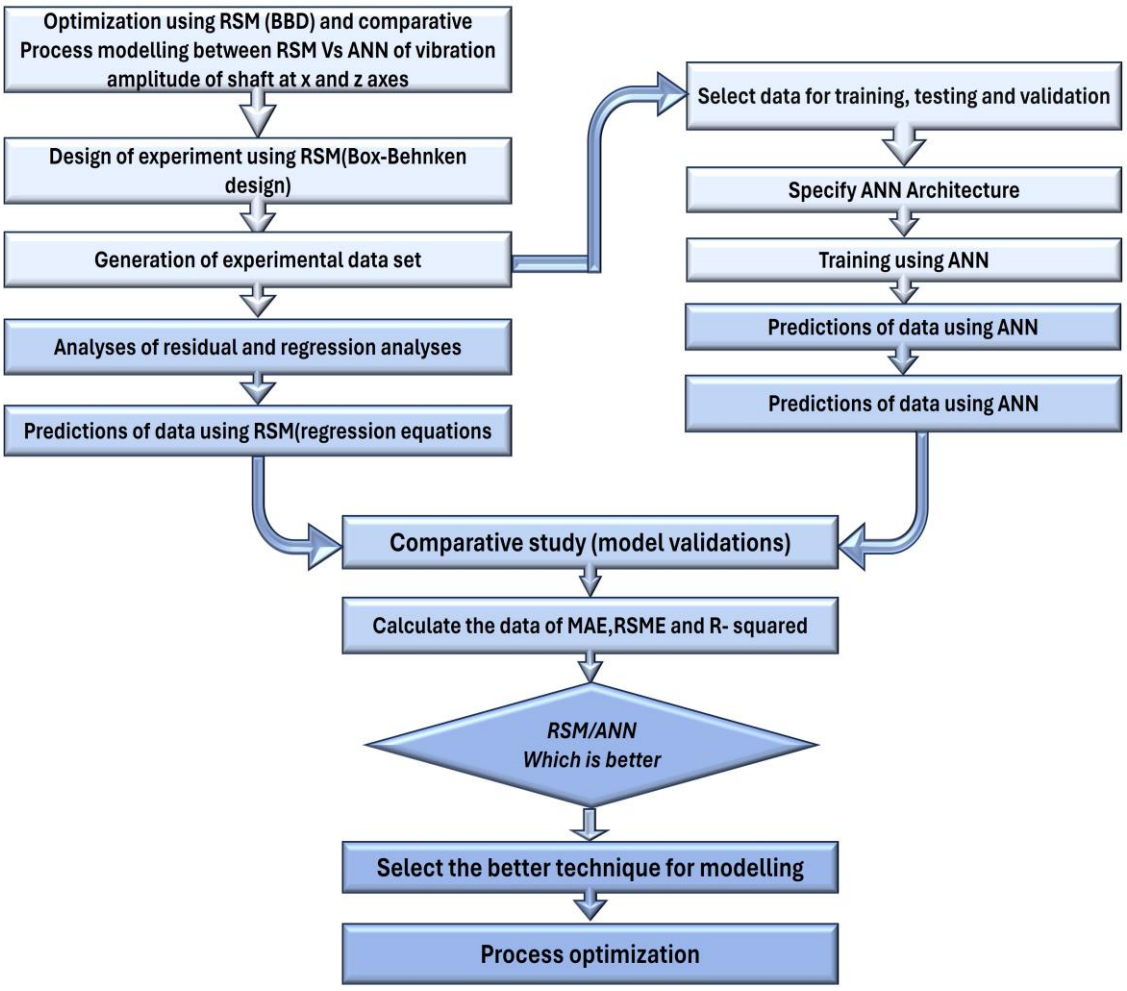

Figure 5.1Flowchart of the proposed methodology.

To enable the tool to learn from the experiment, this entails giving experimental data. The ANN is tested using data that we already have after it has been trained. This stage enables us to gauge the ANN's propensity for accurate result prediction. A design dataset's values are predicted using the trained ANN, as well. We determine the MAE, RMSE, and R-squared by contrasting these projected values with the experimental dataset. We may learn from these numbers how well the ANN's predictions correspond to the real data. Finally, we compare the outcomes of both approaches: RSM (Residual and Regression Equation) and the ANN technique. This comparison allows us to determine which strategy is most suited for forecasting designs. We can evaluate the most effective way for attaining accurate design predictions by assessing parameters such as MAE, RMSE, and R-squared.

5.3.2 Response Surface Methodology (RSM).

The response surface methodology (RSM), a mix of mathematical and statistical methodologies, is useful for planning experiments, developing empirical models, and assessing the models that are developed. RSM is based on fitting a polynomial equation to experimental data in order to describe the relationship between the response of interest and various variables, with the goal of evaluating the effects of independent variables, their interaction impacts, and obtaining the best conditions for the desired responses [165] .

Working of the RSM is as follows [166, 167]:

- A series of tests created with the Minitab -17 program software produces consistent results of interest.
- A second-order RSM model is constructed using the best experimental results.
- The most efficient experimental conditions were discovered to provide either the greatest or lowest response value.
- A visualizer application uses residual plots of x and z axes visualizations to show the interactive effects of process parameters. In order to analyze the linear relationship between numerous components and the response data, a multifunctional quadratic equation was constructed.
- The study factors were the shaft speed (S), the oil blend present (B), and the supply oil pressure (P), and the response values were the vibration amplitudes at the x and z-axes Va(x) and Va(z). To obtain the optimal value of the input parameters, fitting equations were established between the three components and the response values. The sensitivity of each variable to the target was determined using variance analysis.

5.3.3 Box-Behnken Design.

The Box-Behnken design (BBD) is a type of response surface technique used to maximize the response of a system or process by determining the relationship between input parameters and output responsiveness[168]. The variables are set to three levels (-1, 0), and the design points are chosen to reduce the curvature of the response surface. There are three levels to this design. The BBD is symmetrical because each element combination earns an equal number of design points. The total number of design points is obtained using the formula n = k(k-1)/2, where k is the total number of components. Using three elements as an example, the BBD would have 15 design points (n = 3(3-1)/2 = 3). There are many advantages when the BBD is compared to other response surface designs. One of its key advantages is that it needs fewer runs than comparable systems while still providing exact information on the response surface. The BBD demonstrates a high level of proficiency in identifying the curvature of the response surface, hence facilitating the determination of optimal operating parameters. The construction of a reaction surface for a Box-Behnken design (BBD) is a routine practice, whereby a second-order linear model is used. Subsequently, an analysis is conducted using this response surface as a foundation. Equation (1) shows the mathematical representation.[169, 170].

$$Y = \beta 0 + \beta 1X1 + \beta 2X2 + \beta 3X3 + \beta 12X1X2 + \beta 13X1X3 + \beta 23X2X3 +$$

$$\beta 11X1\text{^}2 + \beta 22X2\text{^}2 + \beta 33X3\text{^}2 \text{ ……..(5.1)}$$

where Y is the response, X1, X2, and X3 are the factors, and β0, β1, β2, β3, β12, β13, β23, β11, β22, and β33 are the model coefficients.

One approach to attaining this goal involves doing a regression analysis on the experimental data, afterwards using the obtained findings to compute the coefficients. After fitting, the model may discover the ideal operating settings for maximum responsiveness. In order to make the most of the potential that the system has, this may be done. In order to optimize the

anticipated response, it is necessary to determine the optimal values for the variables. It is very necessary, while carrying out this activity, to take into mind any constraints that may be imposed by other conditions.

5.4 Experimental work

In order to streamline the procedure of designing the response surface design, the Box-Behnken (BBD) approach was combined with the Minitab17 software. This was done in order to simplify the process. In order to carry out the experiment, it was required to take a significant amount of information into account. The components mentioned include three variables that were sequentially followed, 15 preliminary experimental trials, one central point, one block, and two duplicates. This resulted in a total of 30 experimental trials. In addition to this, it was essential to take into consideration the fact that there had been 15 early experimental trials. This study examined many aspects, including the speed range (2000 to 8000 rpm), the supply oil pressure range (20 bar to 100 bar), and the oil mix percentage range (10% to 50%). Table 5.2 displays the comprehensive collection of experimental setups for the Response Surface Methodology (Box-Behnken Design) and Table 5.3 Displays the comprehensive collection of experimental setups for the Response Surface Methodology (Box-Behnken Design) and their experimental results Va(x) and Va(z)).

Table 5.2 Displays the comprehensive collection of experimental Input process Parameter.

Run. No	**Levels of Process Input Parameter**		
	Speed (rpm)	**Pressure (bar)**	**Blend (%)**
1.	8000	60	50
2.	2000	60	10
3.	8000	60	10
4.	5000	60	30

5.	2000	60	50
6.	5000	100	10
7.	8000	20	30
8.	8000	100	30
9.	2000	100	30
10.	8000	20	30
11.	8000	100	30
12.	8000	60	50
13.	2000	60	10
14.	5000	20	50
15.	5000	60	30
16.	8000	60	10
17.	5000	20	10
18.	5000	60	30
19.	2000	20	30
20.	5000	60	30
21.	5000	100	10
22.	5000	20	50
23.	5000	100	50
24.	2000	100	30
25.	2000	20	30
26.	5000	20	10
27.	2000	60	50
28.	5000	60	30
29.	5000	60	30
30.	5000	100	50

In order to minimize potential sources of error within the experimental context, we adhered to the subsequent procedures:

- A detailed listing was supplied for all of the variables and parameters that were used in the experiment. This listing included not only the independent variables (speed, oil pressure, mix %), but also the dependent variables (vibration along the x- and z-axes).

- All during the course of the experiment, we made sure to use equipment that had been suitably calibrated, and we also carried out an exhaustive analysis of the sensitivity and calibration of the proximity transducer. This was done in order to guarantee the accuracy of the data that was collected.
- We repeated each experiment three times, and then we used the average value of the replies that each experiment generated to determine how confident we are in the results. The sample size for the experimental data was 25.6 kilo samples per second (KS/s), and the sampling rate for the data was 20 kilohertz (kHz).
- In order to reduce the likelihood of human mistake, we maintained a high level of attention throughout the process of data collecting. This ensured that there were no errors in the data gathering process or misunderstandings of crucial factors, such as revolutions per minute (RPM) or oil pressure.
- In order to reduce the impact of any outside factors on the results of the experiment, we carefully monitored the environmental variables, which included variations in temperature and humidity levels, air movement, and the likelihood of electromagnetic interference.
- An exhaustive statistical analysis was carried out with the help of the MATLAB program. Appropriate statistical tests were applied in order to guarantee the validity of the findings and verify their robustness.

Table 5.3 Comprehensive collection of experimental setups and their responses.

Run. No	**Levels of Process Input Parameter**			**Average Value of Response Parameter**	
	Speed (rpm)	**Pressure (bar)**	**Blend (%)**	**Va(x)Exp. (µm)**	**Va(z) Exp. (µm)**
1.	8000	60	50	24.5	23.5
2.	2000	60	10	15.4	15.6

3.	8000	60	10	21.3	21.3
4.	5000	60	30	22.1	22.4
5.	2000	60	50	15.2	14.9
6.	5000	100	10	11.1	11.4
7.	8000	20	30	35.1	34.4
8.	8000	100	30	9.6	9.1
9.	2000	100	30	6.1	5.7
10.	8000	20	30	35.1	34.4
11.	8000	100	30	9.6	9.1
12.	8000	60	50	24.5	23.5
13.	2000	60	10	15.4	15.6
14.	5000	20	50	40.1	39.5
15.	5000	60	30	21.9	21.7
16.	8000	60	10	21.3	21.3
17.	5000	20	10	44.3	45.01
18.	5000	60	30	22.4	22.5
19.	2000	20	30	17.6	17.2
20.	5000	60	30	21.4	21.7
21.	5000	100	10	11.01	10.93
22.	5000	20	50	42.1	41.9
23.	5000	100	50	17.1	17.3
24.	2000	100	30	6.1	5.7
25.	2000	20	30	17.6	17.2
26.	5000	20	10	40	39.7
27.	2000	60	50	15.2	14.9
28.	5000	60	30	22.1	22.5
29.	5000	60	30	22.2	22.5
30.	5000	100	50	14.23	15.1

A forward selection technique was used throughout the design process. Potential terms Speed (S), Pressure (P), and Blend (B) were taken into consideration for Response Surface Modeling (RSM). A 95% confidence level was used for all intervals while doing regression

analysis, too. With changes for sum of squares tests (type 3), a two-sided confidence interval was utilized. The utilization of this systematic methodology facilitated a methodical examination of multiple factors and their interconnections. This ultimately led to the creation of predictive models and a deeper understanding of how different variables affect the research objective.

5.5 Results and Analysis

The objective of the current study is to reduce the amplitude of vibration in a high-speed rotating shaft in both the x and z directions as well as compare the two-modelling technique RSM and ANN. Table 5.2 presents the experimental run that is advised based on the optimization of the input parameters as directed by the program. Table 5.3 The vibration amplitude of the shaft across the x-z axes during the test run is presented according to the suggestions given by the RSM (BBD) program. Following the completion of the processing stage, the experimental results were analysed using analysis of variance (ANOVA) for each output response. This analysis was conducted utilizing the box-Behnken design (BBD) of response surface methodology (RSM) modelling. Table 5.3 presents the outcomes of 30 individual examinations. The numerical computations were performed with the MINITAB17 software application. A regression equation was derived for both the x and z axes of vibration in order to determine the predictive value of the RSM model and also analyses of residual plot for both x and z axis vibration amplitude.

5.5.1 RSM(Box-Behnken) model for Vibration amplitude of the shaft at the ‘X’ and Z axes.

In order to evaluate the vibration amplitude of the high-speed rotating shaft, especially along the 'X' axis, a model based on the Response Surface Methodology (RSM) was used. The performance of the model as well as the statistical significance of the findings were examined using a number of different regression values, equation and analysis of residual plot. Residual

plots shown in Figures 5.2 and 5.3 facilitate the assessment of the predictive accuracy of our statistical models in relation to vibration amplitudes along the x and z axes, drawing upon empirical data. The use of these plots is vital in evaluating the accuracy and reliability of our forecasts. Additionally, regression equations, including equations 5.2 and 5.3, have been formulated. The equations presented below serve as mathematical models that depict the established correlations between the input components and the amplitudes of vibration. The use of the Response Surface Methodology (RSM) with a Box-Behnken Design (BBD) enables the formulation of predictions pertaining to vibration amplitudes. From a practical standpoint, these equations play a crucial role as helpful instruments. By substituting certain values for the input variables, we may use these equations to compute anticipated vibration amplitudes. This methodology enables us to approximate the vibration characteristics of the shaft without the need for undertaking supplementary tests, hence enhancing the efficiency and knowledge base of our work. Utilizing the knowledge acquired from experimental data, this approach effectively leverages insights to provide pragmatic forecasts for practical applications in the real world. The data points on the normal probability graph of Figures 5.2 and 5.3 suggest that the tactic employed was effective. The data exhibited a mostly linear pattern with a small departure from a normal distribution. The aforementioned data was used in the formulation of a predictive model for vibration, leading to a favourable conclusion[162, 163]. Furthermore, it can be shown from Figures 5.2 and 5.3 that the data points on the residuals versus fitted value (RVFV) graph exhibit a random dispersion. This suggests that the residuals, which are the differences between the observed and expected outcomes in a statistical model, have a uniform amount of variability over the whole range of projected values. The acquired data may be used for the purpose of analysing and detecting any non-random mistakes. The examination of the residual versus order plot (RVOP) may facilitate the accomplishment of this task. In addition, the lack of outliers shown in the

Frequency versus Residual Plot (FVRP) suggests that the dataset has a uniform distribution and encompasses a wide array of data points. The presented bar graph demonstrates a clear inclination towards prioritizing the significance of initial observations in influencing the ultimate results.

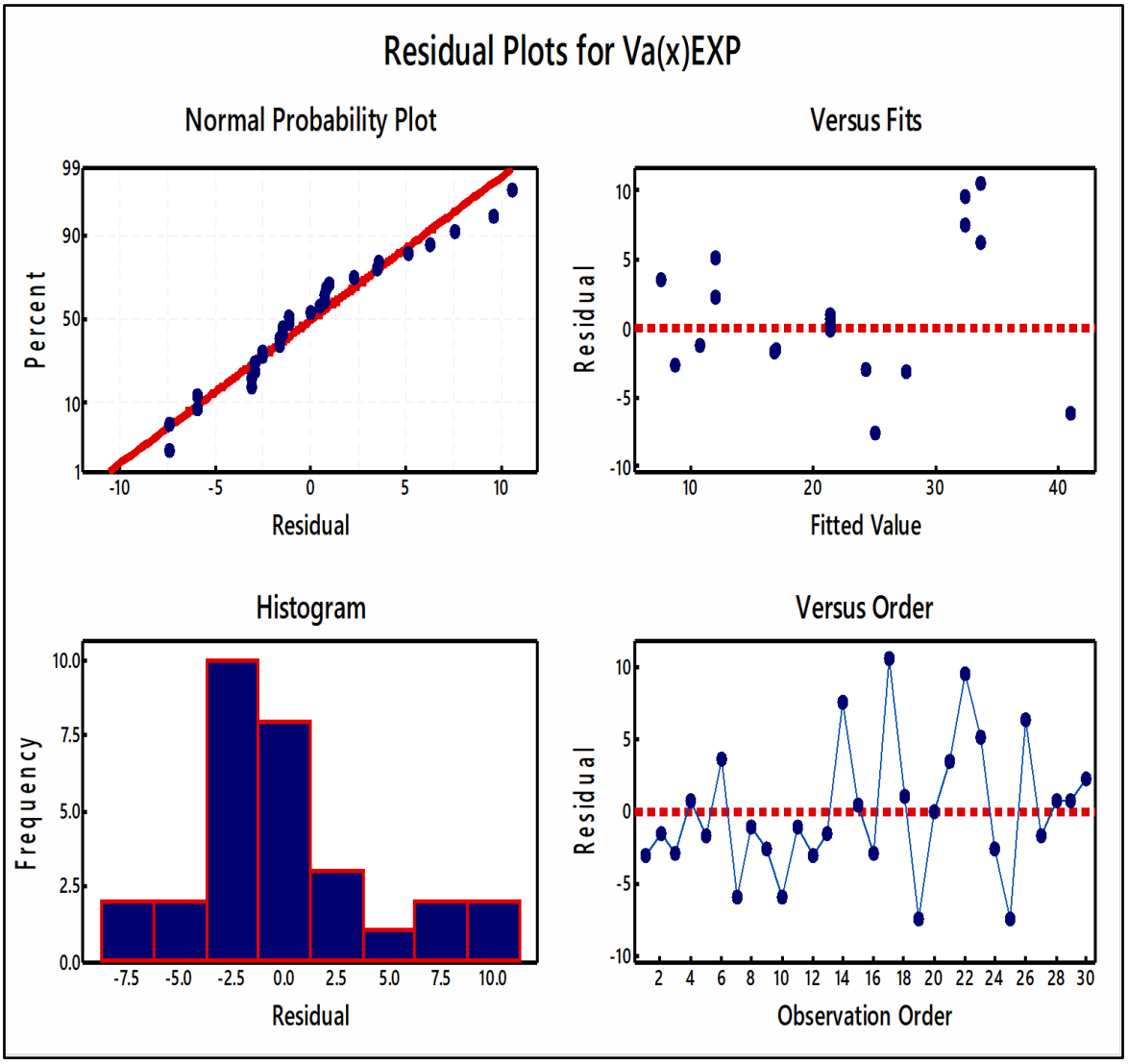

Figure 5.2 Residual plot of vibration at x-axis(experimental)

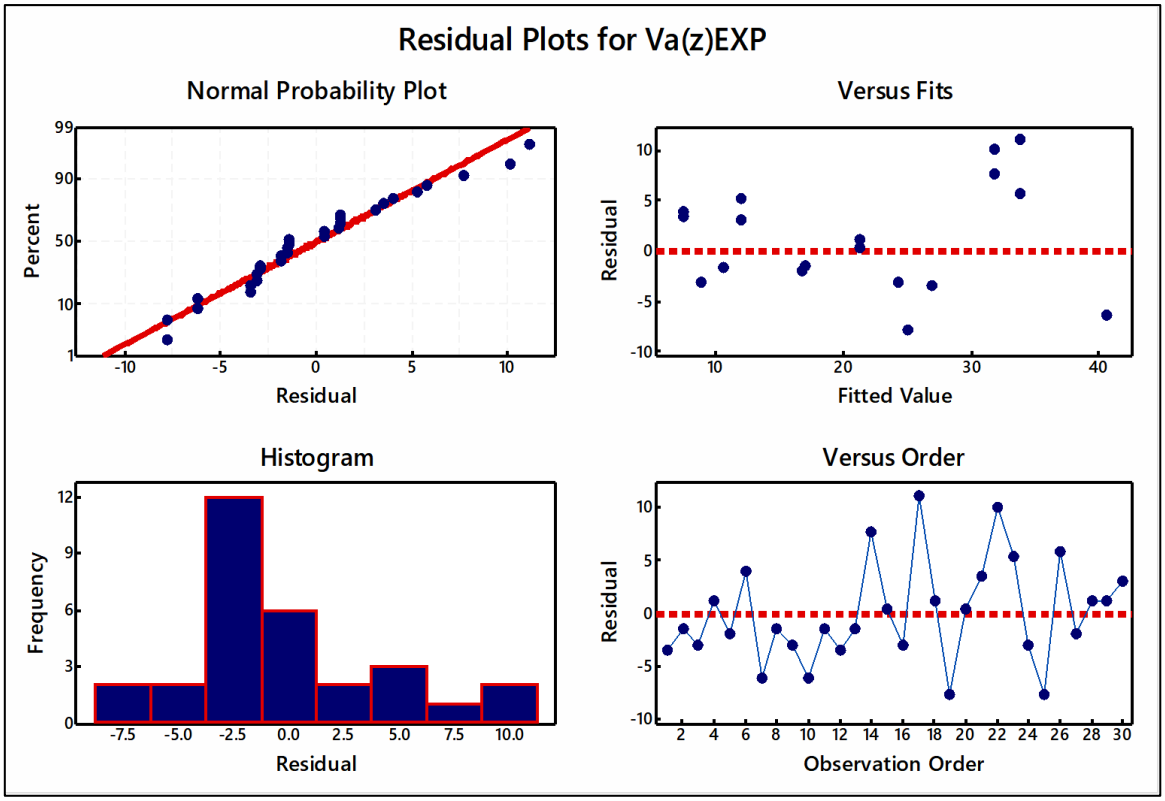

Figure 5.3 Residual plot of vibration at z-axis(experimental)

To predict shaft vibration amplitudes along the x and z axes, we built regression models. By using these equations, we are able to streamline our capacity to create precise predictions for applications that take place in the real world. For example, we may anticipate how the shaft would vibrate depending on certain input factors.

Regression Equation for vibration amplitude of shaft at x-axis.

$$Va(x)_{EXP.} = 26.71 + 0.00283\ S - 0.200\ P - 0.136\ B - 0.000029\ S*P + 0.000014\ S*B + 0.00177\ P*B \quad \ldots\ldots (5.2)$$

Regression equation for vibration amplitude of shaft at z-axis.

$$Va(z)_{EXP.} = 27.36 + 0.00282\ S - 0.208\ P - 0.155\ B - 0.000029\ S*P + 0.000012\ S*B + 0.00209\ P*B \quad \ldots\ldots (5.3)$$

Here, ***S****-speed of shaft(rpm),* ***P****- Pressure of Oil and* ***B****- oil blend used,*

In order to determine the values of Va(x)RSM and Va(z)RSM for each combination of S, P, and B values provided in the Table 4, it is necessary to insert the supplied values into the corresponding equations. It should be noted that the figures have been rounded to three decimal places. The aforementioned outcomes are derived by inserting the values of S, P, and B from the table into the provided regression equations (5.2) and (5.3) for Va(x)RSM and Va(z) RSM. Undoubtedly, I can provide you with a revised rendition of your statement that is more academically oriented. Table 5.4 presents significant findings regarding the precision of our forecasts for the vibration amplitudes of the shaft in relation to both the x-axis RSM and the z-axis RSM. The aforementioned forecasts have been created using our regression models. Furthermore, the table includes error percentages, which serve as indicators of the extent to which our forecasts diverge from the actual empirical data. The error percentages play a crucial role in evaluating the dependability and accuracy of our models. Table 5.5 provides a means of assessing the degree of alignment between our mathematical models and empirical measures, so facilitating an understanding of the accuracy of our predictions and identifying areas for future improvement in our models. Table 5.6 serves as a great tool for assessing the precision of the Response Surface Methodology (RSM) forecasts pertaining to the x and z axes. The table shown above offers a comprehensive understanding of the degree to which the RSM model corresponds with the empirical data, since it quantifies the percentage error. The percentage error quantifies the difference between the values predicted by the RSM and the actual values obtained from experimental data, and is shown as a percentage.

The calculation is expressed as= ([Predicted Value] - Experimental Value] / Experimental Value) × 100%.

A low percentage error signifies that the RSM model is generating predictions that exhibit a high level of accuracy, closely aligning with the experimental data. On the other hand, a substantial percentage error indicates that the RSM model exhibits lower accuracy and substantial deviations between its predictions and the observed experimental outcomes. The provided table functions as a succinct overview of the predictive accuracy of the RSM model for both the x and z dimensions. Through an analysis of the percentage error values, one may expeditiously discern the relative accuracy of forecasts and ascertain potential areas of reduced reliability inside the model.

A little percentage error seen in the table indicates that the RSM model is generating predictions of high accuracy, closely aligning with the experimental data. The reliability of these forecasts is noteworthy for their practical applicability.

Table 5.4 RSM predicted data along with percentage error of x and z axes.

Run No	Speed RPM	Pressure (bar)	Blend (%)	Va(x)Exp. (µm)	Va(x)RSM (µm)	% Error RSM for x axis vibration	Va(z) Exp. (µm)	Va(z)RSM (µm)	% Error RSM for Z axis vibration
1.	8000	60	50	24.5	27.54	12.408	23.5	26.84	14.212
2.	2000	60	10	15.4	16.872	9.5584	15.6	16.984	8.8717
3.	8000	60	10	21.3	24.252	13.859	21.3	24.184	13.539
4.	5000	60	30	22.1	21.366	3.3212	22.4	21.192	5.3928
5.	2000	60	50	15.2	16.8	10.526	14.9	16.76	12.483
6.	5000	100	10	11.1	7.47	32.702	11.4	7.3	35.964
7.	8000	20	30	35.1	41.052	16.957	34.4	40.604	18.034
8.	8000	100	30	9.6	10.74	11.875	9.1	10.42	14.505
9.	2000	100	30	6.1	8.64	41.639	5.7	8.74	53.333
10.	8000	20	30	35.1	41.052	16.957	34.4	40.604	18.034
11.	8000	100	30	9.6	10.74	11.875	9.1	10.42	14.505
12.	8000	60	50	24.5	27.54	12.408	23.5	26.84	14.212
13.	2000	60	10	15.4	16.872	9.5584	15.6	16.984	8.8717
14.	5000	20	50	40.1	32.43	19.127	39.5	31.74	19.645

15.	5000	60	30	21.9	21.366	2.4383	21.7	21.192	2.3410
16.	8000	60	10	21.3	24.252	13.859	21.3	24.184	13.539
17.	5000	20	10	44.3	33.654	24.031	45.01	33.868	24.754
18.	5000	60	30	22.4	21.366	4.6160	22.5	21.192	5.8133
19.	2000	20	30	17.6	25.032	42.227	17.2	25.004	45.372
20.	5000	60	30	21.4	21.366	0.1588	21.7	21.192	2.3410
21.	5000	100	10	11.01	7.47	32.152	10.93	7.3	33.211
22.	5000	20	50	42.1	32.43	22.969	41.9	31.74	24.248
23.	5000	100	50	17.1	11.91	30.350	17.3	11.86	31.445
24.	2000	100	30	6.1	8.64	41.639	5.7	8.74	53.333
25.	2000	20	30	17.6	25.032	42.227	17.2	25.004	45.372
26.	5000	20	10	40	33.654	15.865	39.7	33.868	14.690
27.	2000	60	50	15.2	16.8	10.526	14.9	16.76	12.483
28.	5000	60	30	22.1	21.366	3.3212	22.5	21.192	5.8133
29.	5000	60	30	22.2	21.366	3.7567	22.5	21.192	5.8133
30.	5000	100	50	14.2	11.91	16.303	15.1	11.86	21.456
				Total error % =		***545.513***	***Total error % =***		***615.083***

The purpose of images 5.4a and 5.4b is to visually represent and illustrate specific information. Figure 9a provides a clear depiction of a particular concept or data, while Figure 5.4b presents a sequential representation of a process or progression. These images serve to enhance the understanding and comprehension of the subject matter by providing visual aids that complement the accompanying text. The data exhibited a mostly linear pattern with a little deviation from a normal distribution. The aforementioned data was used in the formulation of a predictive model for vibration, leading to a favourable conclusion [162, 163]. Furthermore, it can be shown from Figures 5.2 and 5.3 that the data points on the residuals versus fitted value (RVFV) graph exhibit a random dispersion. This suggests that the residuals, which are the differences between the observed and expected outcomes in a statistical model, have a constant amount of variability over the whole range of projected values. The acquired data may be used for the purpose of analysing and identifying any

systematic mistakes. The examination of the residual versus order plot (RVOP) may facilitate the accomplishment of this task. Moreover, the lack of outliers shown in the Frequency versus Residual Plot (FVRP) suggests that the dataset has a uniform distribution and encompasses a wide array of information. The bar graph demonstrates a clear bias by placing emphasis on the significance of initial observations in influencing the ultimate results. The user's text is incomplete and does not provide any information. The vertical axis of the graph is used to depict the discrepancy between the values predicted by the RSM model and the actual experimental results.

When the value of the line is positive, it indicates that the Root Sum Square Method (RSM) has overestimated the amplitude of vibration. Conversely, when the value is negative, it signifies that the RSM has underestimated the amplitude of vibration. The horizontal axis in this context denotes various "run numbers," which effectively correspond to distinct scenarios or experimental situations. The following observations were made: The graph shown above exhibits many salient observations. Field of Study At run numbers 14, 17, and 22, notable disparities exist between the values predicted by the Response Surface Methodology (RSM) and the actual values obtained via experimentation.

The RSM model has limitations in accurately forecasting vibration amplitudes in the following areas. Negligible Discrepancies: Conversely, for run numbers 4, 11, 22, and 29, the disparities between the predictions generated by the Response Surface Methodology (RSM) and the results obtained via experimentation are quite insignificant. These observations suggest situations in which the RSM model exhibits stronger alignment with the empirical data.

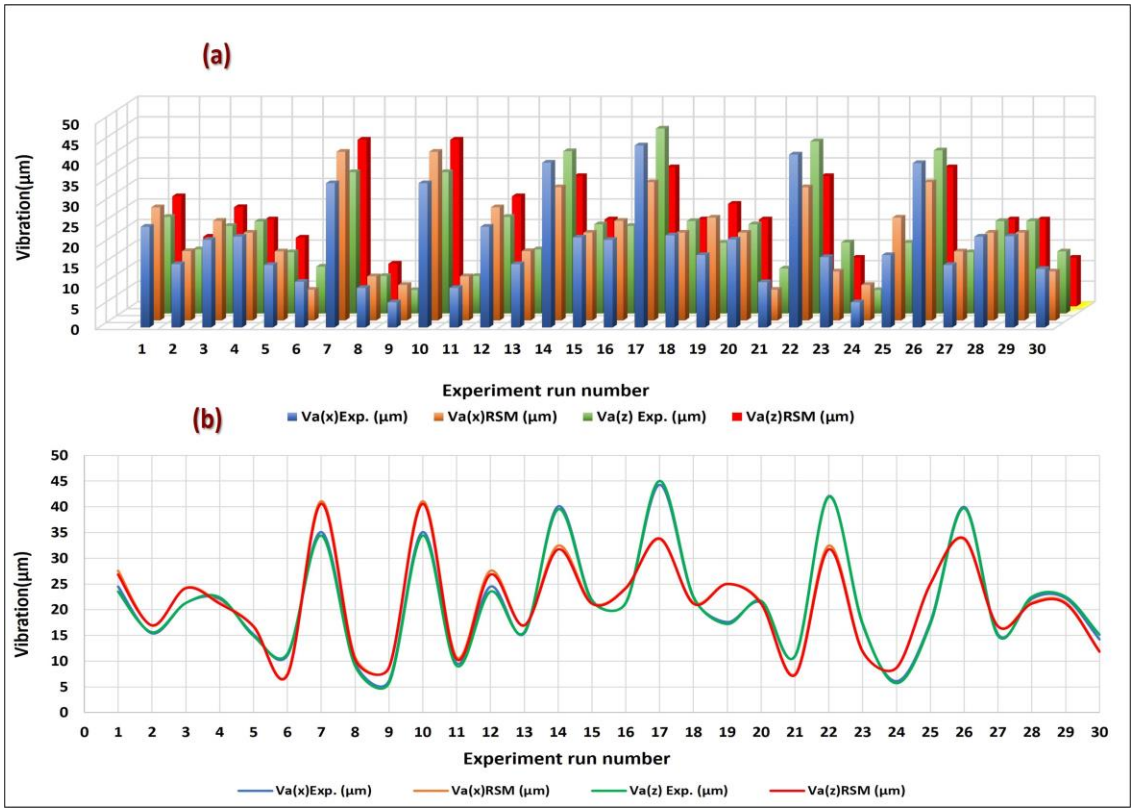

Figure 5.4 (a) 3D graphical representation of output data experimental and RSM (predicted),5.4(b)2D graphical representation of output data experimental and RSM (predicted).

Figure 5.4a illustrates the visual disparity between the predictions generated by the Response Surface Methodology (RSM) and the empirical data pertaining to vibration amplitudes. Conversely, Figure 5.4b offers a comprehensive examination of the specific locations and manner in which the RSM predictions diverge from the actual values across various experimental situations or run numbers. The provided information is of utmost importance in order to identify the specific areas where the model may need enhancements, as well as to determine the places where it demonstrates satisfactory performance. Figure 5.5 shows the deviation of the RSM predicted vibration amplitude values for the x and z axes. Compared to experimental values, this graph shows how accurate RSM forecasts are. The percentage inaccuracy in RSM forecasts varies between run numbers. Thus, RSM model accuracy changes during the trial. On the graph, runs 9 and 24 show a greater percentage disparity between RSM forecasts and experimental data. This means the RSM model predicted more

values than actual values at these run numbers due to more mistakes. But at runs 3, 10, 14, 15, 16, 17, and 23, the percentage error difference is substantially lower. These indicators indicate that the RSM model worked well, with predictions that matched experimental values.

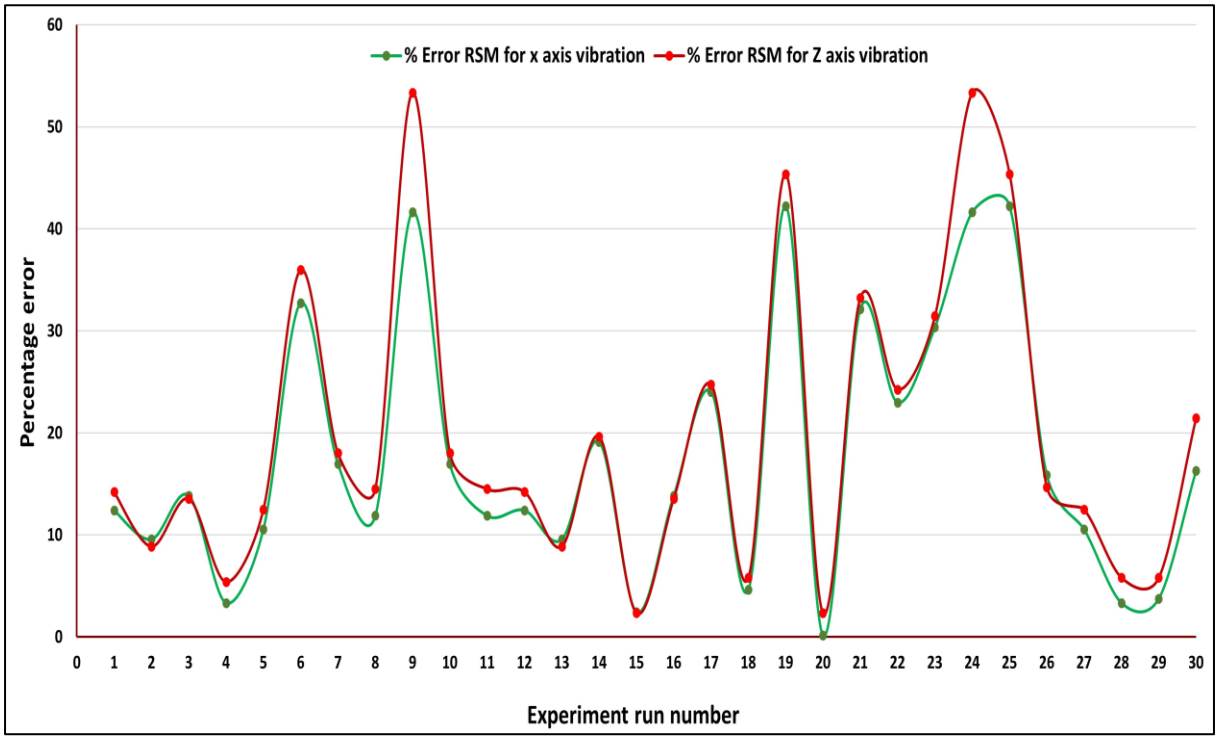

Figure 5.5 Error percentage graph of RSM x and z axes.

See Figure 5.5 for how the RSM model's x and z axis vibration amplitude predictions vary by experimental circumstance (run number). This shows areas where the model may require development and the relevance of considering this variability when using it to anticipate diverse situations.

5.6 Analyses of the residual plot of the RSM predicted value at the x and z axes.

Residual plots depicting the RSM-predicted values of the x and z axes are shown in Figures 5.6 and 5.7, respectively. These plots are used as important instruments for assessing the degree of alignment between the predictions made by the Response Surface Methodology (RSM) and the actual values obtained from experimental data. The analysis and interpretation

of Figures 5.6 and 5.7 involve various graphical representations, such as normal probability graphs, residuals versus fitted value (RVFV) graphs, residual versus order plot (RVOP), and frequency versus residual plot (FVRP). The concept of normal probability refers to the likelihood of an event occurring within a normal distribution. The normal probability graph is used to evaluate the conformity of data to a normal (Gaussian) distribution.

Figures 5.6 and 5.7 exhibit a relatively linear trend in the plotted data points. A predominantly linear pattern observed in a normal probability plot indicates that the data closely approximates a normal distribution. Nevertheless, real-world data often exhibits minor deviations from perfect linearity. This suggests that the modelling approach employed to forecast vibration amplitude has been effective, as it indicates that the data used for modelling closely approximates a normal distribution. The RVFV graph depicts the association between the predicted values and the residuals. A stochastic pattern observed in the RVFV graph indicates a positive indication. This suggests that the model's predictions exhibit both unbiasedness and consistency across various levels of predicted values.

The consistent variation of the model implies its accuracy remains relatively stable. The Residual versus Order Plot (RVOP) is a useful tool for detecting systematic errors or patterns in the residuals. The presence of specific patterns in the RVOP may suggest the absence of crucial factors or the presence of systematic errors in the data. Identifying these patterns is essential for the improvement of the model.

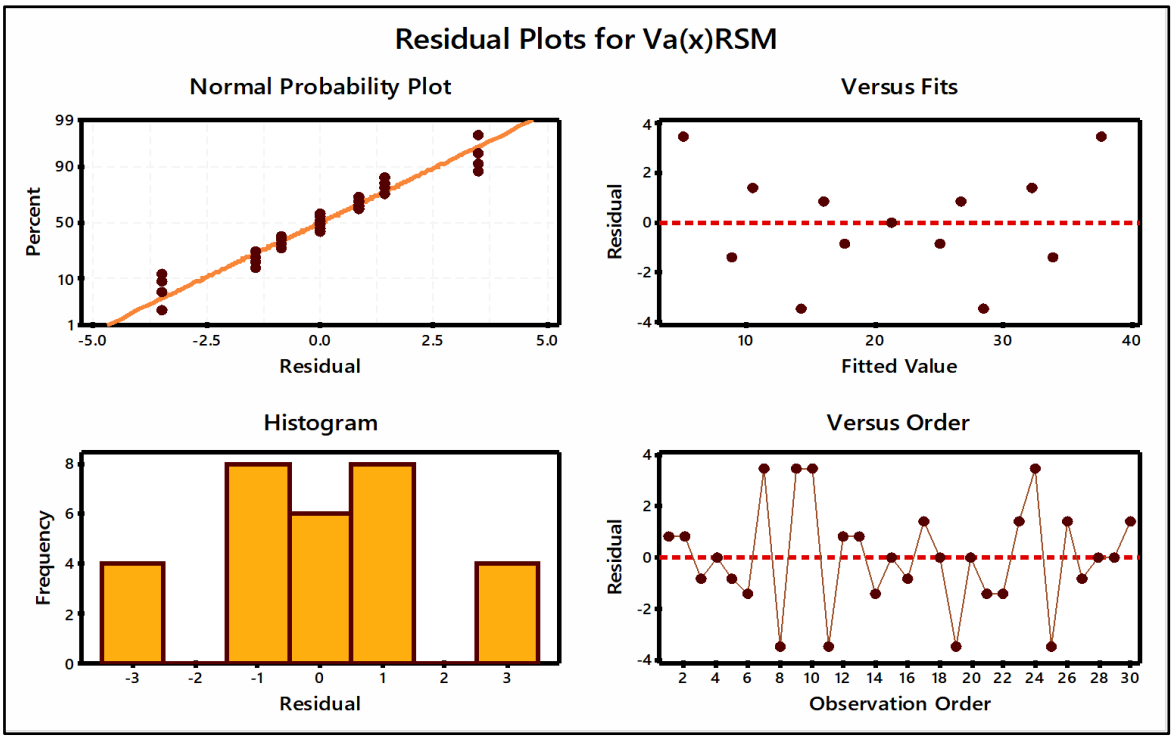

Figure 5.6 Residual plot of vibration amplitude at x- axis for RSM predicted data.

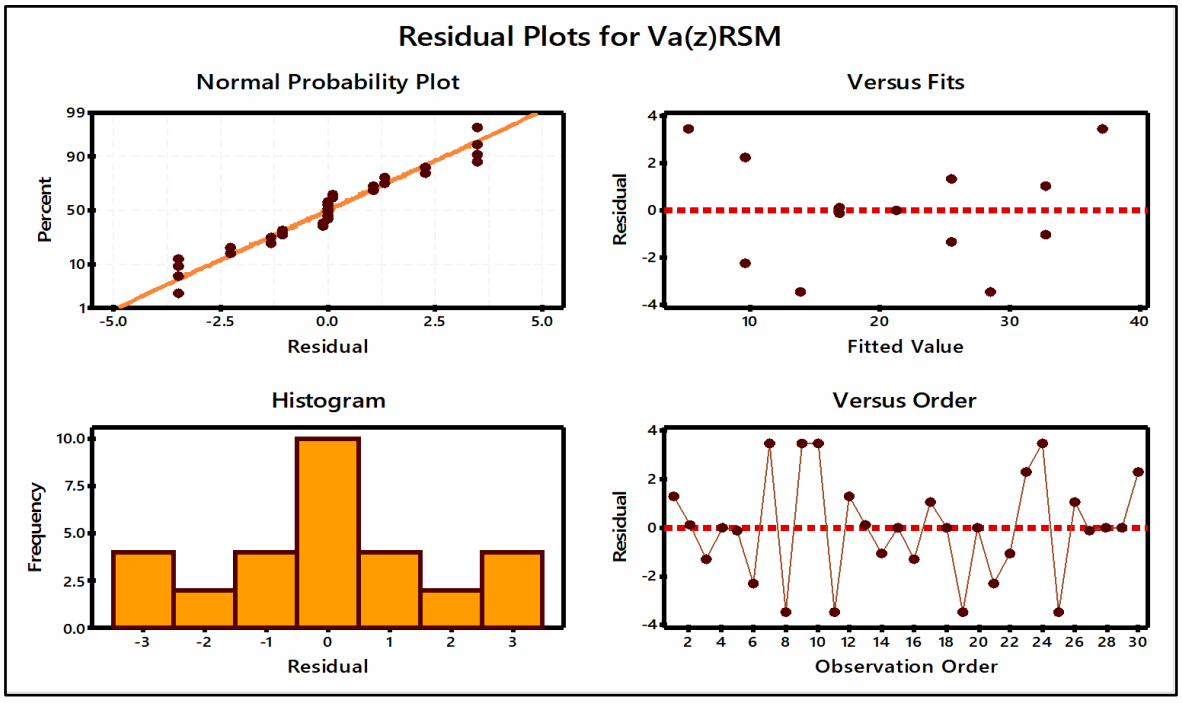

Figure 5.7 Residual plot of vibration amplitude at Z- axis for RSM predicted data.

The FVRP offers insights into residual distribution. The lack of outliers in the FVRP suggests that there are no extreme errors or unusual data points that have a substantial impact on the

model's performance. The increased diversity of information implies that the model incorporates a wide range of data points and is not unduly influenced by outliers. Bar graph bias refers to the possibility that the dataset, early data points, or observations could have a significant influence on the overall outcomes of the model. It is crucial to comprehend this bias's significance when making predictions using your model.

5.7 Procedure of Artificial Neural Network (ANN)

Artificial Neural Networks (ANN), which are more often known as neural networks, are comparable to biological neural networks. Artificial Neural Network (ANN) is one of the advanced deep learning techniques and is used for modelling and optimization purposes in various industrial sectors like manufacturing, energy, process industry and automobiles [171, 172]. These networks have been used to create an approximation of a function (in the form of a mathematical model) that is dependent on an extremely large number of inputs. Software is often employed since the computations that are involved in the process of developing the network are known for being very complicated.[127]The challenge of estimation with neural network models has three key components. Initially, Figure 5.8 depicts the neural network topology.

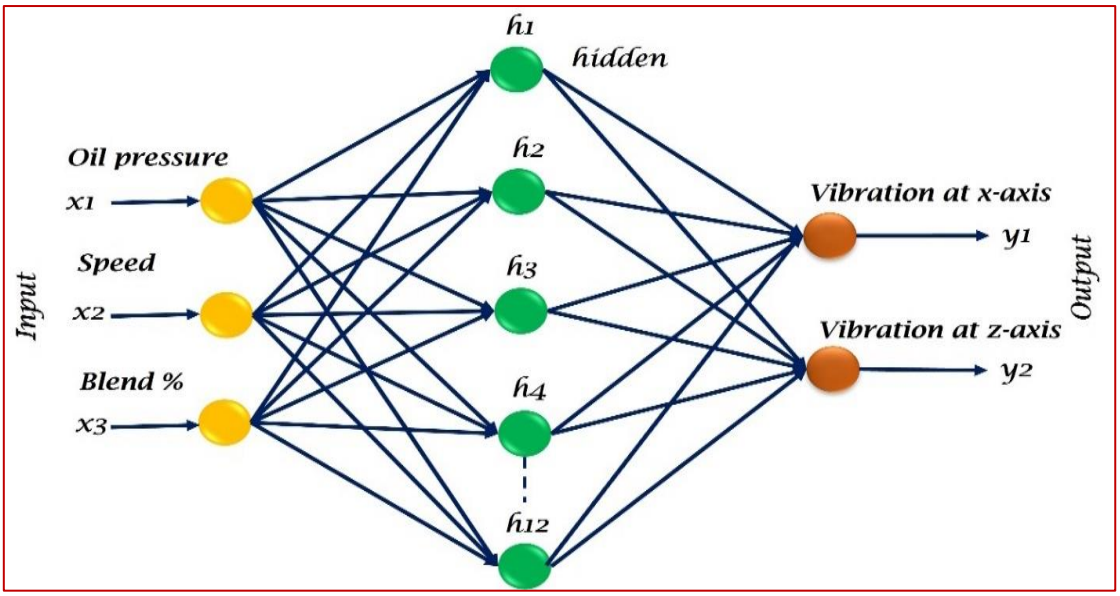

Figure 5.8 Schematic illustration of ANN structure.

Next, the selection of activation functions, initialization of process parameters, and determination of training algorithm parameters are carried out. Subsequently, the training algorithm is invoked. The efficacy of the neural network is evaluated by the process of simulating its output using measured input data, followed by a comparison with the corresponding measured outputs. This is juxtaposed with the quantified results. The execution of final validation necessitates the use of data that is separate from the original dataset [126]. In this study, the MATLAB R2021b program was used for the purposes of data training and testing. Neural networks consist of an input layer with neurons that correlate to different process parameters. The data pertaining to these parameters, whether experimental or obtained in real-time(y_i), is then inputted into the neurons of the input layer. The input data is sent to the hidden layer and output layer by the process of multiplying the weights (w_{ij}) between two neurons and then adding them using a summation function, as represented by Equation (5.4) [127]. The constructed feed-forward artificial neural network (ANN) model is used for the purpose of modelling the vibration amplitude of a shaft along the x and z axes, which serves as the response or output variable. The architecture used in this work consists of three input levels, whereby each layer is associated with a specific neuron representing speed, oil pressure, and oil blend percentage, respectively. The neural network architecture has 12 hidden layer neurons, together with two solitary output layer (3-12-2), as seen in Fig 5.8 and 5.9c.

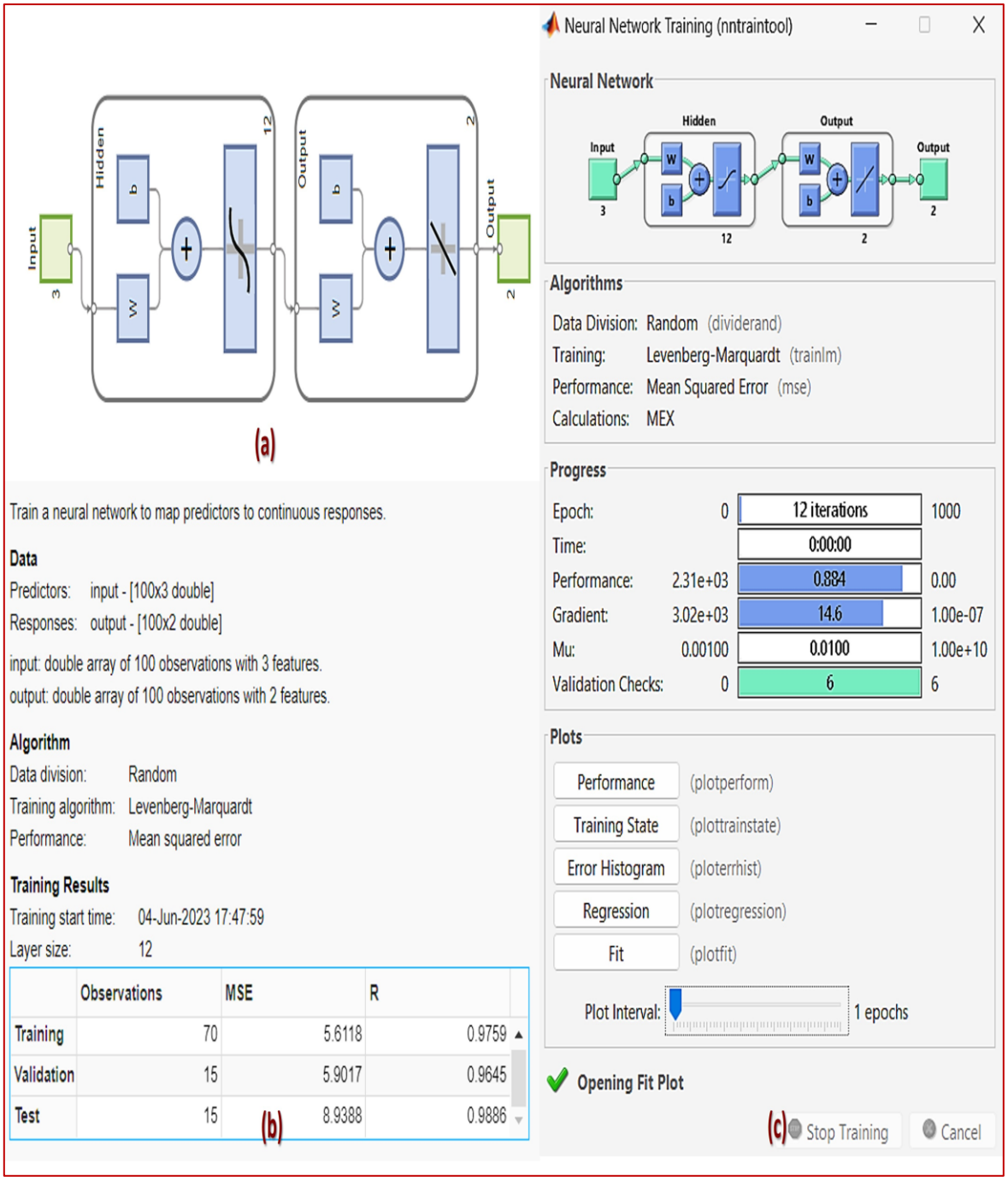

Figure 5.9 Neuron network training.

The artificial neural network design with a configuration of 3 input nodes, 12 hidden nodes, and 2 output nodes has been shown to be more suitable for data modelling in cases when the error approaches zero, as seen in Figure 5.9(c). The training technique used for the current dataset was 'trainlm', which is widely recognized as the quickest backpropagation algorithm available in the toolbox. The activation transfer functions, namely the 'logarithmic sigmoid

logsig' and the linear transfer function 'purelin', were selected because of their superior predictive capabilities. These functions are mathematical in nature and are responsible for converting and processing the input data of each layer to produce corresponding outputs. The training technique used in this context involves the iterative adjustment of weights and biases with the objective of optimizing the 'Levenberg-Marquardt' algorithm. This particular approach is often utilized for the resolution of non-linear least squares problems. In the process of training, testing, and validating an ANN, a distribution of 70%, 15%, and 15% of the available data is allocated for each corresponding purpose. Regression coefficients may be obtained for the training, validation, and testing sets after the implementation of an artificial neural network (ANN) training [173–175].

$$\text{Output}=f\left(\sum_{i=1}^{n} b + y_i\, w_i\right) \ldots\ldots\ldots\ldots\ldots\ldots\ldots (5.4)$$

Where, b is bias, Real-time or experimental data (y_i), corresponding weights (w_{ij}), f is activation function

The performance of the trained artificial neural network (ANN) is shown in Figure 5.10(a), demonstrating a satisfactory level of accuracy as evidenced by the proximity of the validation and test curves. The evidence provided by Figure 5.10c, depicting the error histogram , further substantiates this claim. The observation of the best validation performance, achieved at five (5) epochs, is a significant finding. This performance metric, denoted by a value of 5.9017, represents the culmination of the artificial neural network's training process, which involves multiple passes over the entire training dataset. Notably, the training process continues until the 11th epoch, as depicted in Figure 5.10 (b), where the best validation performance is visually represented. In Figure 5.10(d), the training state of the Artificial Neural Network (ANN) is shown. It can be seen that the final value of the gradient coefficient is around 1.9299, which approaches zero by the 11th epoch.

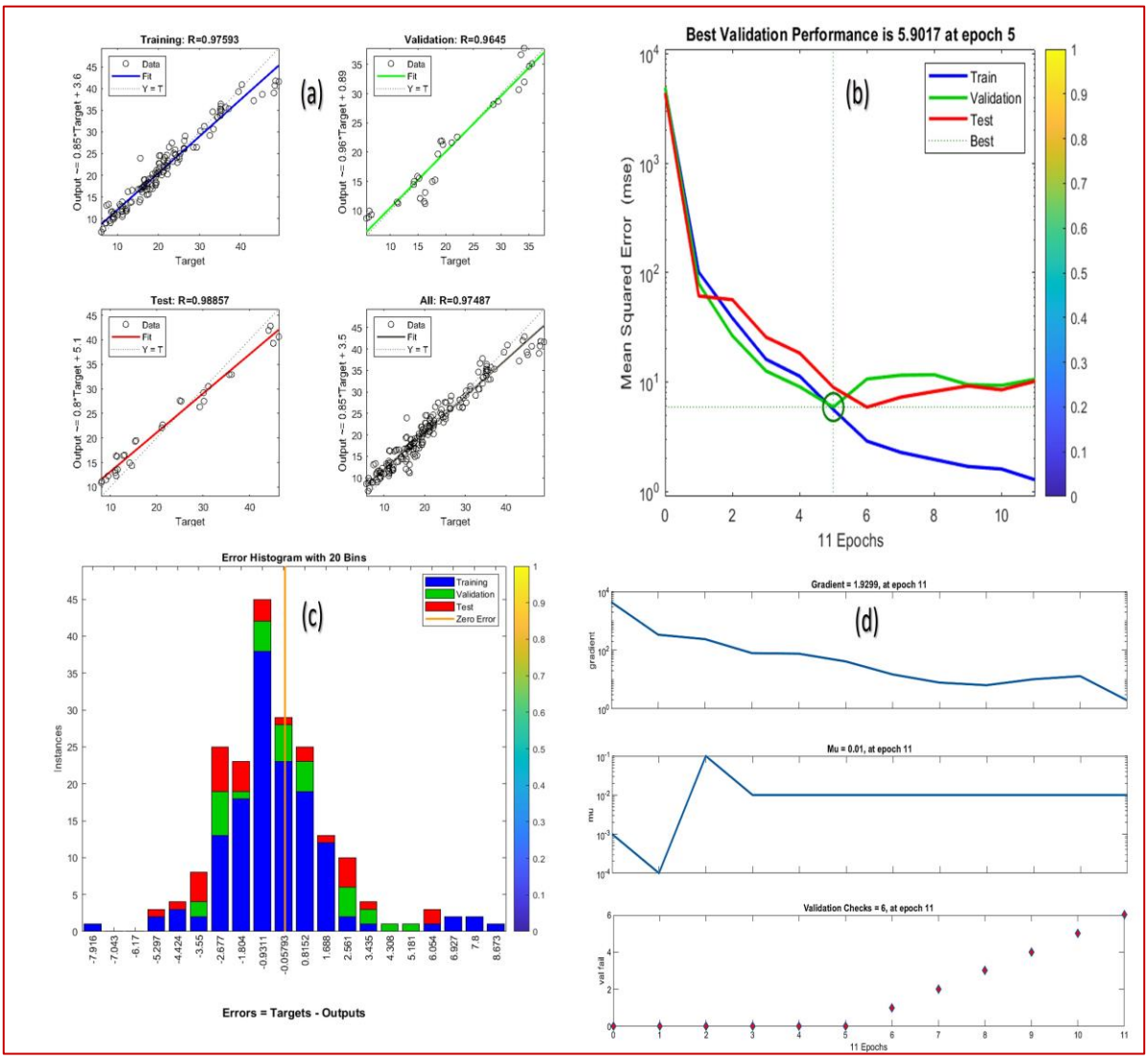

Figure 5.10 Training plots of neural network for vibration at x and z axes (a) regression Performance for trained ANN (b) variation of error with epochs (c) Error histogram plot (d) training state of ANN.

Table 6 serves as a great tool for assessing the precision of the artificial neural network (ANN) forecasts pertaining to the x and z axes. The table shown above offers a comprehensive understanding of the degree to which the ANN model corresponds with the empirical data, since it quantifies the percentage error.

The percentage error quantifies the difference between the values predicted by the ANN and the actual values obtained from experimental data, and is shown as a percentage.

The calculation is expressed as= ([Predicted Value] - Experimental Value] / Experimental Value) × 100%.

A low percentage error signifies that the ANN model is generating predictions that exhibit a high level of accuracy, closely aligning with the experimental data. On the other hand, a substantial percentage error indicates that the ANN model exhibits lower accuracy and substantial deviations between its predictions and the observed experimental outcomes. The provided table functions as a succinct overview of the predictive accuracy of the ANN model for both the x and z dimensions. Through an analysis of the percentage error values, one may expeditiously discern the relative accuracy of forecasts and ascertain potential areas of reduced reliability inside the model. A little percentage error seen in the table indicates that the ANN model is generating predictions of high accuracy, closely aligning with the experimental data. The reliability of these forecasts is noteworthy for their practical applicability.

Table 5.5 ANN predicted data along with percentage error of x and z axes.

Run. No	Speed (rpm)	Pressure (bar)	Blend (%)	Va(x)Exp. (µm)	Va(x)ANN (µm)	(%) Error ANN for x axis vibration	Va(z) Exp. (µm)	Va(z)ANN (µm)	(%) Error ANN for Z axis vibration
1.	8000	60	50	24.5	19.937	18.621	23.5	20.101	14.463
2.	2000	60	10	15.4	16.278	5.706	15.6	16.577	6.262
3.	8000	60	10	21.3	24.739	16.148	21.3	23.782	11.652
4.	5000	60	30	22.1	23.241	5.165	22.4	23.161	3.397
5.	2000	60	50	15.2	15.736	3.527	14.9	16.154	8.416
6.	5000	100	10	11.1	12.140	9.369	11.4	12.111	6.236
7.	8000	20	30	35.1	38.747	10.391	34.4	36.929	7.351
8.	8000	100	30	9.6	12.053	25.562	9.1	11.311	24.296
9.	2000	100	30	6.1	6.681	9.528	5.7	6.629	16.298

10.	8000	20	30	35.1	38.747	10.391	34.4	36.929	7.351
11.	8000	100	30	9.6	12.053	25.562	9.1	11.311	24.296
12.	8000	60	50	24.5	19.937	18.621	23.5	20.101	14.463
13.	2000	60	10	15.4	16.278	5.706	15.6	16.577	6.262
14.	5000	20	50	40.1	40.080	0.049	39.5	40.011	1.293
15.	5000	60	30	21.9	23.121	5.576	21.7	23.091	6.410
16.	8000	60	10	21.3	24.739	16.148	21.3	23.782	11.652
17.	5000	20	10	44.3	38.082	14.036	45.01	38.11	15.329
18.	5000	60	30	22.4	23.341	4.200	22.5	23.241	3.293
19.	2000	20	30	17.6	20.161	14.552	17.2	19.389	12.726
20.	5000	60	30	21.4	23.101	7.948	21.7	23.051	6.225
21.	5000	100	10	11.01	12.940	17.529	10.93	12.131	10.988
22.	5000	20	50	42.1	41.08	2.422	41.9	42.1	0.477
23.	5000	100	50	17.1	16.91	1.111	17.3	16.987	1.809
24.	2000	100	30	6.1	6.681	9.528	5.7	6.629	16.298
25.	2000	20	30	17.6	20.161	14.552	17.2	19.389	12.726
26.	5000	20	10	40	39.65	0.875	39.7	39.06	1.612
27.	2000	60	50	15.2	15.736	3.527	14.9	16.154	8.416
28.	5000	60	30	22.1	23.601	6.792	22.5	23.501	4.448
29.	5000	60	30	22.2	23.69	6.711	22.5	23.501	4.448
30.	5000	100	50	14.23	13.9	2.319	15.1	13.2	12.582
Total error percent of x-axis=						***292.186***	***Total error percent =***		***281.491***

Figures 5.11a and 5.11b provide a lucid representation of the methodology used to detect vibration amplitudes along the x and z axes, as well as the corresponding predictions made by an Artificial Neural Network (ANN). The aforementioned results provide valuable information into the precision and dependability of the ANN model's prognostications. Figure 5.11a presents a three-dimensional bar graph illustrating the vibration amplitudes observed for the x and z axes. The graph shown in this study integrates both the empirical data obtained from experiments and the predictions derived from the ANN model. The most

notable finding is the strong resemblance between the pattern of the anticipated values generated by the ANN and the experimental values. This observation suggests that the ANN model is successfully capturing the fundamental patterns and fluctuations present in the data. The strong correspondence between the predictions generated by the ANN and the experimental data indicates a notable degree of precision. From a practical standpoint, it may be inferred that the ANN model can be trusted to provide predictions that align with the observed experimental results.

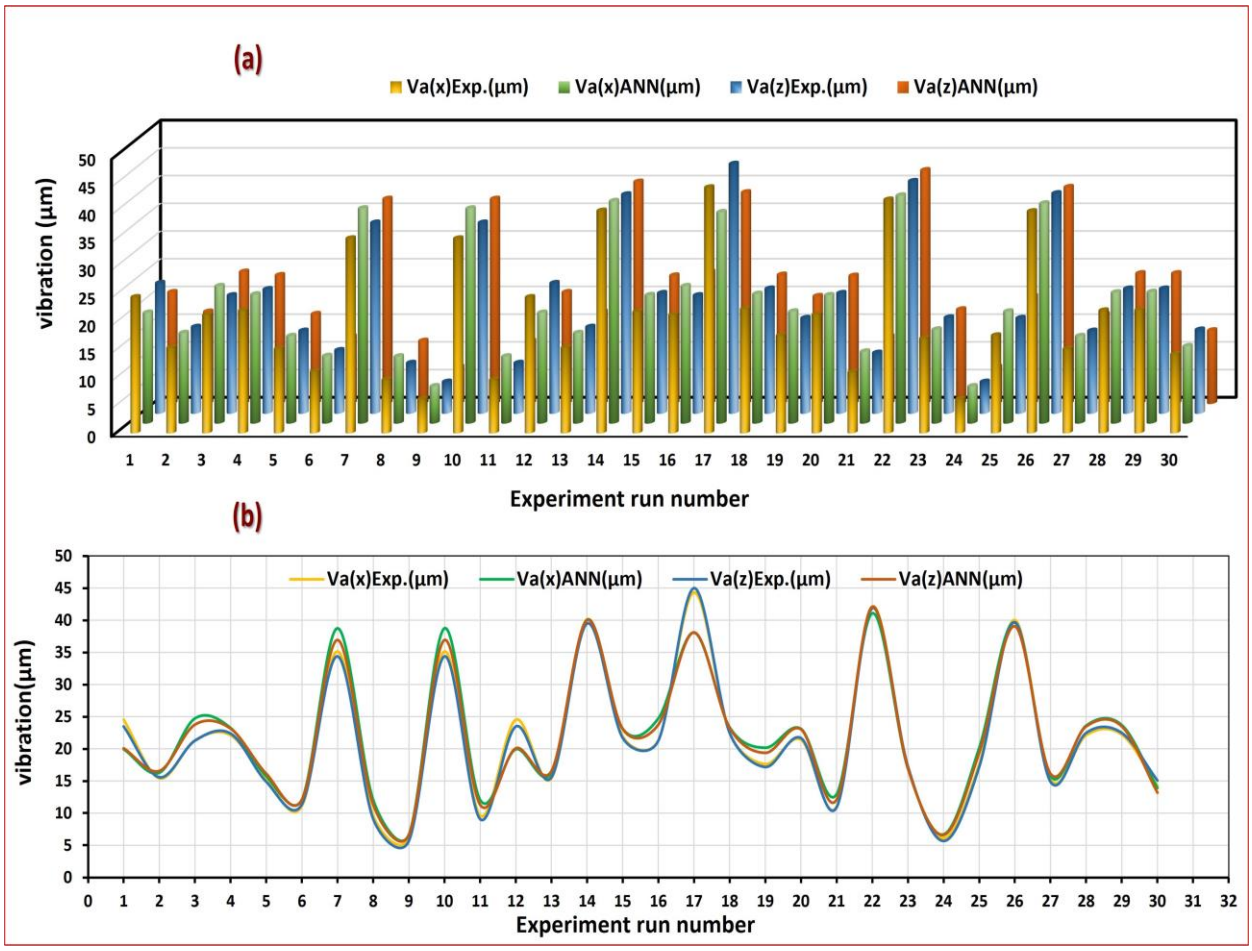

Figure 5.11a 3D Comparative graph of vibration amplitude at x and z axes of experimental data vs ANN data,5.11b- 2D Comparative graph of vibration amplitude at x and z axes of experimental data vs ANN data.

In contrast, Figure 5.11b depicts a two-dimensional line graph illustrating a comparison between the experimental values and the values predicted by the ANN for vibration amplitude. The graph shown above offers a comprehensive depiction of the disparities among

the aforementioned values, hence providing a more intricate and nuanced understanding of the subject matter. The most notable disparity between the values obtained from the experiment and those predicted by the ANN is seen at run number 17. This implies that the ANN model may face difficulties or ambiguities particularly within the context of this experimental situation. With the exception of run number 17, the line graph demonstrates generally negligible disparities between the ANN forecasts and the empirical measurements. This observation suggests that the predictions made by the ANN model align with the actual data for a majority of the experimental circumstances.

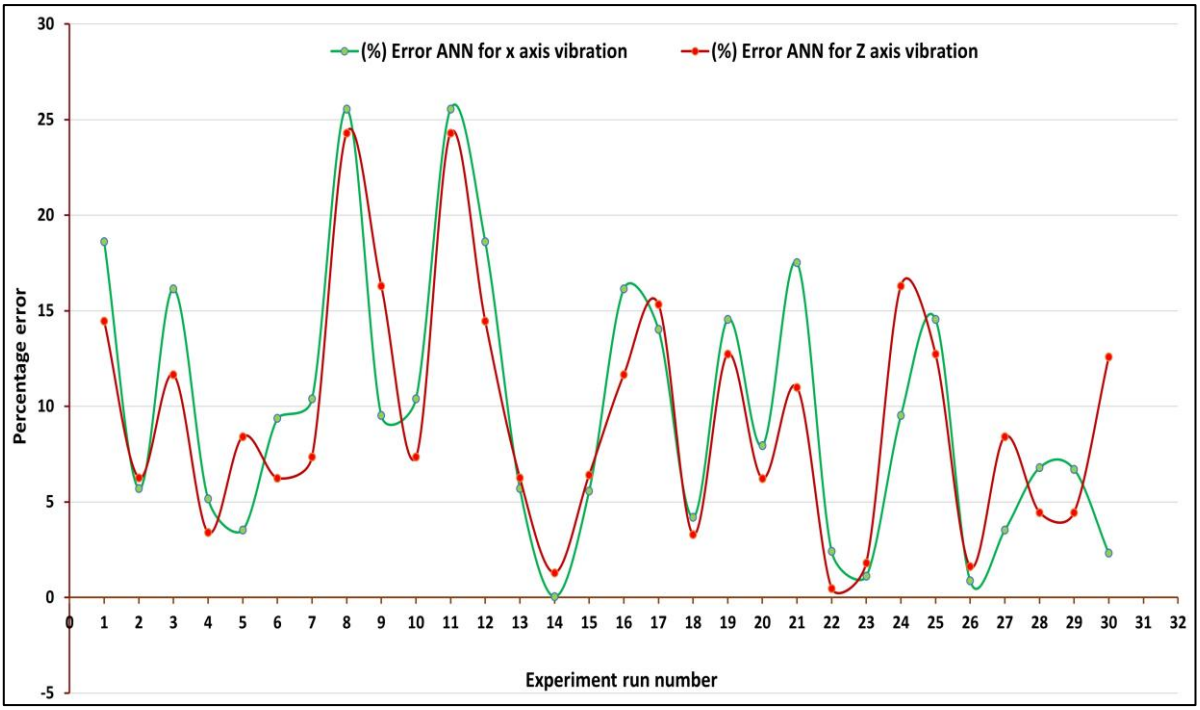

Figure 5.12 Percentage error plot between experimental and ANN predicted data.

Furthermore, an observable trend of decreasing gradient magnitude may be seen as the number of epochs increases. Based on the data shown in Figure 5.12, it is evident that the ANN accurately predicts the vibration values at the x and z axes, aligning closely with the actual measurements throughout the start and end states. The greatest discrepancy seen is 25.56% for Va(x) and 24.29% for Va(z), while the remaining errors are deemed very less. Figure 5.12 displays the plot depicting the percentage inaccuracy. Therefore, it can be concluded that the built ANN model has successfully acquired knowledge of the correlation

between the input variables and the Va(x) and Va(z) values. Consequently, this particular model has the potential to be used for the purpose of mitigating the magnitude of vibrations.

5.8 Analysing the relative merits of RSM and ANN optimization methods.

A research endeavour was conducted to assess and contrast the magnitude of vibration in the rotor shaft along the x and z axes by using two modelling systems: Response Surface Methodology (RSM) utilizing Box-Behnken Design (BBD), and Artificial Neural Network (ANN). We compared their performance using three different error metrics: mean absolute error (MAE), root mean squared error (RMSE), and correlation (R-squared) [176–178]. The following excerpt outlines a conceivable methodology for clarifying the topic, but with three errors. In quantitative research, the use of the statistical metric known as Mean Absolute Error (MAE) is one of the most prevalent uses for the measure. The purpose of this evaluation is to calculate the average absolute deviation that exists between the values that were predicted to be there and the actual values that were there. The software determines the arithmetic mean of the absolute differences between the values that were predicted and the values that were actually observed.

The Mean Absolute Error (MAE) is a statistical measure that provides a succinct assessment of the performance of a model. This metric is distinguished by its simplicity and ease of comprehension.

$$\mathbf{MAE = (1/n) * \Sigma |Actual - Predicted| \ldots\ldots\ldots\ldots\ldots\ldots\ldots\ldots (5.5)}$$

Throughout this discussion, we will refer to the total number of observations as "n." The letter Σ represents the summation operator in mathematical notation, whereas "||" represents the absolute value function. Both of these symbols are used interchangeably across the field.

1. The Root Mean Squared Error (RMSE) is a statistical measure that calculates the square root of the mean of the squared discrepancies between the predicted and observed values. Due to the fact that it has a propensity to give greater weight to more serious errors, RMSE has a higher level of sensitivity to the presence of outliers.

The assessment of error dispersion is used rather often in the solving of regression issues. The root mean square error (RMSE) formula is mathematically expressed as the square root of the average of the squared discrepancies between the observed and predicted values. In this formula, 'n' represents the total number of observations.

$$\textbf{RMSE} = \sqrt{[(1/n) * \Sigma (\text{actual} - \text{predicted})^2]} \quad \text{……..(5.6)}$$

2. The R-squared, sometimes called the coefficient of determination, measures the proportion of the variance in the dependent variable that the independent variables can account for in a regression model. The metric offers a numerical assessment of the level of agreement between the observed data points and the regression model. A statistical metric known as the coefficient of determination may take on values anywhere from 0 to 1 depending on the circumstances. R squared is another name for the coefficient of determination. It analyzes correlation to see how much one variable may illuminate another. The model integrates all dataset variables when the alignment is 1. This ideal alignment is "optimal." Zero means the model cannot handle any variability. This statement represents the coefficient of determination formula. This mathematical equation is commonly denoted "R squared."

$$\textbf{R-squared} = 1 - (\text{RSS} / \text{TSS}) \quad \text{…….(5.7)}$$

To get the TSS, we add up all the squared differences between the observed data and the mean. To do this, one may first get the average using arithmetic and then deduct the observed numbers from that value. To do this, first determine the arithmetic mean of a database, and then subtract each individual data point from that number. For the sake of giving a representative assessment of the whole dataset, we can calculate a numerical value that represents the "mean" of the dataset by adding up all of the data points and dividing by the total number of data points.

$$\textbf{TSS (Total Sum of Squares)} = \Sigma (\text{actual} - \text{mean})^2 \quad \text{……(5.8)}$$

The Residual Sum of Squares (RSS) is calculated by adding up all of the squared differences that exist between the observed values and the estimated values. The formula that was discussed before may be found in this location. The discovery of this gap necessitates conducting a comparison study between the values that were actually seen and those that were predicted.

$$\textbf{Residual Sum of Squares (RSS)} = \Sigma (\text{actual} - \text{predicted})^2 \ldots\ldots (5.9)$$

4. The Mean Absolute Percentage Error (MAPE) is a widely used technique for evaluating the precision of a forecast when generating numerical predictions, especially in the domain of time series analysis or demand forecasting. The Mean Absolute Percentage Error (MAPE) may be used for any of the aforementioned objectives. This phenomenon might be attributed to the fact that the Mean Absolute Percentage Error (MAPE) incorporates both relative errors and absolute mistakes in its calculation. The statistical indicator quantifies the extent to which the average actual values differ from the projected values. The formula for calculating the Mean Absolute Percentage Error (MAPE) is as follows.

$$\textbf{MAPE} = (\Sigma \mid (\text{Actual} - \text{Forecast}) / \text{Actual} \mid) * (100 / n) \ldots\ldots (5.10)$$

The number of observations, denoted by "n,".

The error term for Response Surface Methodology (RSM) modelling was determined by assessing the agreement between the predicted response from the model and the actual experimental outcomes. The study included using the data shown in Table 5.6a and b, which includes a variety of output characteristics used to calculate error terms for the x and z axes in the Response Surface Methodology (RSM) model.

Table 5.6a RSM Predicted value at x axes and term related to MAE, RMSE and R-Squared

Run. No	Speed (rpm)	Pressure (bar)	Blend (%)	Va(x) Exp. (µm) [A]	Va(x) RSM (µm) [B]	[A-B]	$[A-B]^2$	$[A-M]^2$
1.	8000	60	50	24.5	27.54	3.04	9.241	5.056
2.	2000	60	10	15.4	16.872	1.472	2.166	31.937
3.	8000	60	10	21.3	24.252	2.952	8.714	0.0023
4.	5000	60	30	22.1	21.366	0.734	0.538	1.319
5.	2000	60	50	15.2	16.8	1.6	2.56	40.339
6.	5000	100	10	11.1	7.47	3.63	13.176	97.048
7.	8000	20	30	35.1	41.052	5.952	35.426	172.887
8.	8000	100	30	9.6	10.74	1.14	1.299	147.654
9.	2000	100	30	6.1	8.64	2.54	6.451	241.843
10.	8000	20	30	35.1	41.052	5.952	35.426	172.887
11.	8000	100	30	9.6	10.74	1.14	1.2996	147.654
12.	8000	60	50	24.5	27.54	3.04	9.2416	5.056
13.	2000	60	10	15.4	16.872	1.472	2.166	31.937
14.	5000	20	50	40.1	32.43	7.67	58.828	333.013
15.	5000	60	30	21.9	21.366	0.534	0.285	0.201
16.	8000	60	10	21.3	24.252	2.952	8.714	0.0023
17.	5000	20	10	44.3	33.654	10.646	113.337	564.474
18.	5000	60	30	22.4	21.366	1.034	1.069	1.559
19.	2000	20	30	17.6	25.032	7.432	55.234	16.413
20.	5000	60	30	21.4	21.366	0.034	0.0011	0.201
21.	5000	100	10	11.01	7.47	3.54	12.531	106.529
22.	5000	20	50	42.1	32.43	9.67	93.508	426.367
23.	5000	100	50	17.1	11.91	5.19	26.936	15.613
24.	2000	100	30	6.1	8.64	2.54	6.451	241.843
25.	2000	20	30	17.6	25.032	7.432	55.234	16.413
26.	5000	20	10	40	33.654	6.346	40.271	340.353

27.	2000	60	50	15.2	16.8	1.6	2.56	40.339
28.	5000	60	30	22.1	21.366	0.734	0.538	1.559
29.	5000	60	30	22.2	21.366	0.834	0.695	1.559
30.	5000	100	50	14.23	11.91	2.32	5.382	37.838
M (mean value) =21.388(for x-axis)						**Σ[A-B] =105.172**	**Σ[A-B]^2 =609.292**	**Σ[A-M]^2 =3254.396**

Table 5.6b RSM Predicted value at z axes and term related to MAE, RMSE and R-Squared.

Run. No	**Speed (rpm)**	**Pressure (bar)**	**Blend (%)**	**Va(z) Exp. (µm) [C]**	**Va(z) RSM (µm) [D]**	**[C-D]**	**[C-D]^2**	**[C-M]^2**
1.	8000	60	50	23.5	27.54	3.34	11.155	5.056
2.	2000	60	10	15.6	16.872	1.384	1.915	31.937
3.	8000	60	10	21.3	24.252	2.884	8.317	0.002
4.	5000	60	30	22.4	21.366	1.208	1.459	1.319
5.	2000	60	50	14.9	16.8	1.86	3.459	40.339
6.	5000	100	10	11.4	7.47	4.1	16.81	97.048
7.	8000	20	30	34.4	41.052	6.204	38.489	172.887
8.	8000	100	30	9.1	10.74	1.32	1.742	147.654
9.	2000	100	30	5.7	8.64	3.04	9.241	241.843
10.	8000	20	30	34.4	41.052	6.204	38.489	172.887
11.	8000	100	30	9.1	10.74	1.32	1.742	147.654
12.	8000	60	50	23.5	27.54	3.34	11.155	5.056
13.	2000	60	10	15.6	16.872	1.384	1.915	31.937
14.	5000	20	50	39.5	32.43	7.76	60.217	333.013
15.	5000	60	30	21.7	21.366	0.508	0.258	0.201
16.	8000	60	10	21.3	24.252	2.884	8.317	0.002
17.	5000	20	10	45.01	33.654	11.142	124.14	564.474
18.	5000	60	30	22.5	21.366	1.308	1.710	1.559
19.	2000	20	30	17.2	25.032	7.804	60.902	16.413
20.	5000	60	30	21.7	21.366	0.508	0.258	0.201

21.	5000	100	10	10.93	7.47	3.63	13.176	106.529
22.	5000	20	50	41.9	32.43	10.16	103.22	426.367
23.	5000	100	50	17.3	11.91	5.44	29.593	15.613
24.	2000	100	30	5.7	8.64	3.04	9.241	241.843
25.	2000	20	30	17.2	25.032	7.804	60.902	16.413
26.	5000	20	10	39.7	33.654	5.832	34.012	340.353
27.	2000	60	50	14.9	16.8	1.86	3.459	40.339
28.	5000	60	30	22.5	21.366	1.308	1.710	1.559
29.	5000	60	30	22.5	21.366	1.308	1.710	1.559
30.	5000	100	50	15.1	11.91	3.24	10.497	37.838
M (mean value) =21.251(for z-axis)						**Σ[C-D] =113.124**	**Σ[C-D]^2 =669.233**	**Σ[C-M]^2 =3239.909**

After using the data from the table 7a, b and equations 5.5,5.6,5.7,5.8,5.9 we get the value of MAE, RMSE, and R^2 for the x and z axes, shown in Table 5.7.

Table 5.7 RSM Predicted value at x and z axes and value of MAE, RMSE and R-Squared.

OPTIMIZATION TECHNIQUE	RESPONSE	MAE	RMSE	R-SQUARED
Response Surface Methodology (RSM)	X-axis vibration, Va(x)	3.5057	4.5066	0.81277
Response Surface Methodology (RSM)	Z-axis vibration, Va(z)	3.77	4.7230	0.7934

The error term for artificial neural network (ANN) modelling was afterwards determined by comparing the output response of the model with the experimental response data. The calculation was based on the data presented in Table 5.8a and b, which provides an overview of the various output parameters necessary for calculating the error term in the ANN model, specifically with respect to the x and z axes.

Table 5.8a ANN Predicted value at x axes and term related to MAE, RMSE and R-Squared.

Run No	Speed (rpm)	Pressure (bar)	Blend (%)	Va(x) Exp. (µm) [A]	Va(x) ANN (µm) [B]	[A-B]	$[A-B]^2$	$[A-M]^2$
1.	8000	60	50	24.5	19.937	4.562	20.813	9.684
2.	2000	60	10	15.4	16.278	0.878	0.772	35.856
3.	8000	60	10	21.3	24.739	3.439	11.831	0.007
4.	5000	60	30	22.1	23.241	1.141	1.303	0.506
5.	2000	60	50	15.2	15.736	0.536	0.287	38.291
6.	5000	100	10	11.1	12.140	1.04	1.081	105.842
7.	8000	20	30	35.1	38.747	3.647	13.303	188.018
8.	8000	100	30	9.6	12.053	2.453	6.0219	138.956
9.	2000	100	30	6.1	6.681	0.581	0.337	233.722
10.	8000	20	30	35.1	38.747	3.647	13.303	188.018
11.	8000	100	30	9.6	12.053	2.453	6.021	138.956
12.	8000	60	50	24.5	19.937	4.562	20.813	9.684
13.	2000	60	10	15.4	16.278	0.878	0.772	35.856
14.	5000	20	50	40.1	40.080	0.02	0.0004	350.138
15.	5000	60	30	21.9	23.121	1.221	1.491	0.262144
16.	8000	60	10	21.3	24.739	3.439	11.831	0.007744
17.	5000	20	10	44.3	38.082	6.218	38.664	524.959
18.	5000	60	30	22.4	23.341	0.941	0.8854	1.0241
19.	2000	20	30	17.6	20.161	2.561	6.5601	14.34894
20.	5000	60	30	21.4	23.101	1.701	2.893	0.00014
21.	5000	100	10	11.01	12.940	1.93	3.724	107.702
22.	5000	20	50	42.1	41.08	1.02	1.040	428.986
23.	5000	100	50	17.1	16.91	0.19	0.036	18.386
24.	2000	100	30	6.1	6.681	0.581	0.337	233.722
25.	2000	20	30	17.6	20.161	2.561	6.560	14.3489

26.	5000	20	10	40	39.65	0.35	0.1225	346.4065
27.	2000	60	50	15.2	15.736	0.536	0.287	38.2913
28.	5000	60	30	22.1	23.601	1.501	2.253	0.506
29.	5000	60	30	22.2	23.69	1.49	2.220	0.659
30.	5000	100	50	14.23	13.9	0.33	0.108	51.236
Σ[A-B] =56.541				**Σ[A-B]^2=175.682**			**Σ[A-M]^2 =3254.396**	

Table 5.8b ANN Predicted value at z axes and term related to MAE, RMSE and R-Squared.

Run No	**Speed (rpm)**	**Pressure (bar)**	**Blend (%)**	**Va(z) Exp. (µm) [C]**	**Va(z) ANN (µm) [D]**	**[C-D]**	**[C-D]^2**	**[C-M]^2**
1.	8000	60	50	23.5	20.101	3.399	11.553	5.056
2.	2000	60	10	15.6	16.577	0.977	0.954	31.937
3.	8000	60	10	21.3	23.782	2.482	6.160	0.0023
4.	5000	60	30	22.4	23.161	0.761	0.579	1.319
5.	2000	60	50	14.9	16.154	1.254	1.572	40.339
6.	5000	100	10	11.4	12.111	0.711	0.505	97.048
7.	8000	20	30	34.4	36.929	2.529	6.395	172.887
8.	8000	100	30	9.1	11.311	2.211	4.888	147.654
9.	2000	100	30	5.7	6.629	0.929	0.863	241.843
10.	8000	20	30	34.4	36.929	2.529	6.395	172.887
11.	8000	100	30	9.1	11.311	2.211	4.888	147.654
12.	8000	60	50	23.5	20.101	3.399	11.553	5.0565
13.	2000	60	10	15.6	16.577	0.977	0.954	31.937
14.	5000	20	50	39.5	40.011	0.511	0.2611	333.013
15.	5000	60	30	21.7	23.091	1.391	1.934	0.2013
16.	8000	60	10	21.3	23.782	2.482	6.160	0.0023
17.	5000	20	10	45.01	38.11	6.9	47.61	564.474
18.	5000	60	30	22.5	23.241	0.741	0.549	1.559
19.	2000	20	30	17.2	19.389	2.189	4.791	16.413

20.	5000	60	30	21.7	23.051	1.351	1.825	0.201
21.	5000	100	10	10.93	12.131	1.201	1.442	106.529
22.	5000	20	50	41.9	42.1	0.2	0.04	426.367
23.	5000	100	50	17.3	16.987	0.313	0.0979	15.613
24.	2000	100	30	5.7	6.629	0.929	0.863	241.843
25.	2000	20	30	17.2	19.389	2.189	4.791	16.413
26.	5000	20	10	39.7	39.06	0.64	0.4096	340.353
27.	2000	60	50	14.9	16.154	1.254	1.572	40.339
28.	5000	60	30	22.5	23.501	1.001	1.002	1.559
29.	5000	60	30	22.5	23.501	1.001	1.002	1.559
30.	5000	100	50	15.1	13.2	1.9	3.61	37.838
Σ[C-D] =50.562			**Σ[C-D]2=135.228**			**Σ[C-M]2=3239.909**		

After using the data from the table 5.8a, 5.8b and equations 5.5,5.6,5.7,5.8 and 5.9 we get the value of MAE, RMSE, and R^2 for the x and z axes, shown in Table 5.9.

Table 5.9 ANN Predicted value at x and z axes and value of MAE, RMSE and R-Squared.

OPTIMIZATION TECHNIQUE	RESPONSE	MAE	RMSE	R-SQUARED
Artificial neural network (ANN)	X-axis vibration, Va(x)	1.8805	2.4190	0.9460
Artificial neural network (ANN)	X-axis vibration, Va(z)	1.7010	2.1230	0.9582

5.8.1 Methodology Comparison with respect to vibration amplitude of shaft in x-z axes of two methods RSM prediction, and ANN prediction with respect to experimental data.

Here, Graphs have been generated to illustrate the vibration amplitudes of a shaft in two specific directions, namely the x-axis and the z-axis. The analysis was conducted for three distinct scenarios: one involving actual experimental data, another involving data predicted using the RSM method, and a third involving data predicted using the ANN method of Tables 5.7a, b and 5.8a, b When you look at the graphs, for vibration amplitude in both the x and z axes in Fig. 5.13a and b. It's clear that the predictions made by the ANN method are much

closer to the actual experimental data than the predictions made by the RSM method. The ANN predictions exhibit a higher degree of accuracy in matching the actual experimental results compared to the RSM predictions. The results suggest that the ANN method outperforms other methods in predicting shaft vibration amplitudes. Using this method provides a higher level of accuracy in predicting the behaviour of vibrations in real-world scenarios. This is due to its enhanced ability to effectively analyse and interpret patterns and relationships within the data.

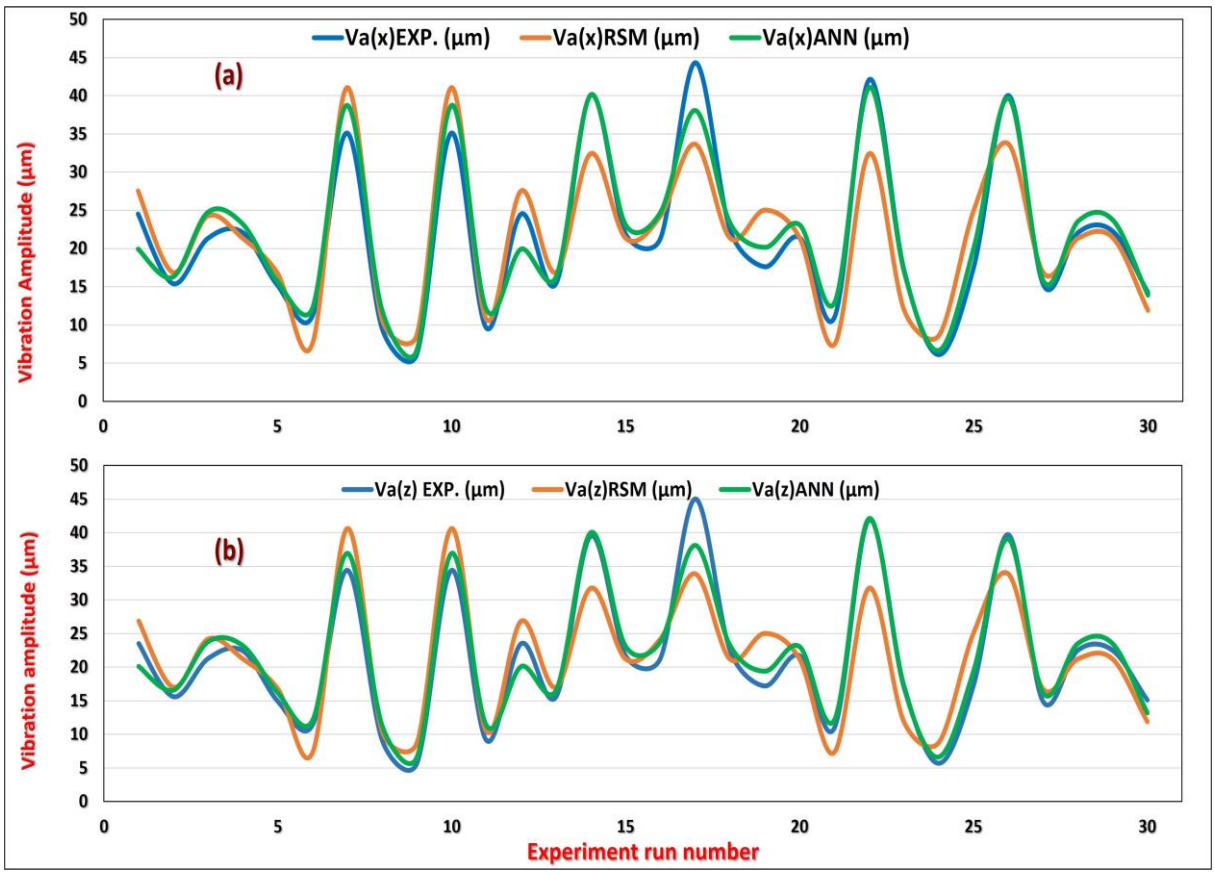

Figure 5.13(a)Comparative graph of vibration amplitude through Experiments, RSM and ANN for x-axis. (b) Comparative graph of vibration amplitude through Experiments, RSM and ANN for z-axis.

5.8.2 Methodology Comparison with respect to error term MAE, RMSE and R-squared.

value of error term for Response Surface Methodology (RSM) is obtained in Table 5.8 and Artificial Neural Network (ANN) in Table 5.10 summary of both the tables is presented in Table 5.11. A graphical representation of the summer is presented in Fig 5.14.

Table 5.10 Value of MAE, RMSE and R-Squared for RSM and ANN modelling.

OPTIMIZATION TECHNIQUE	RESPONSE	MAE	RMSE	R-SQUARED
Response Surface Methodology (RSM)	X-axis vibration, Va(x)	3.5057	4.5066	0.81277
Artificial neural network (ANN)		1.8805	2.4190	0.9460
Response Surface Methodology (RSM)	Z-axis vibration, Va(z)	3.77	4.7230	0.7934
Artificial neural network (ANN)		1.7010	2.1230	0.9582

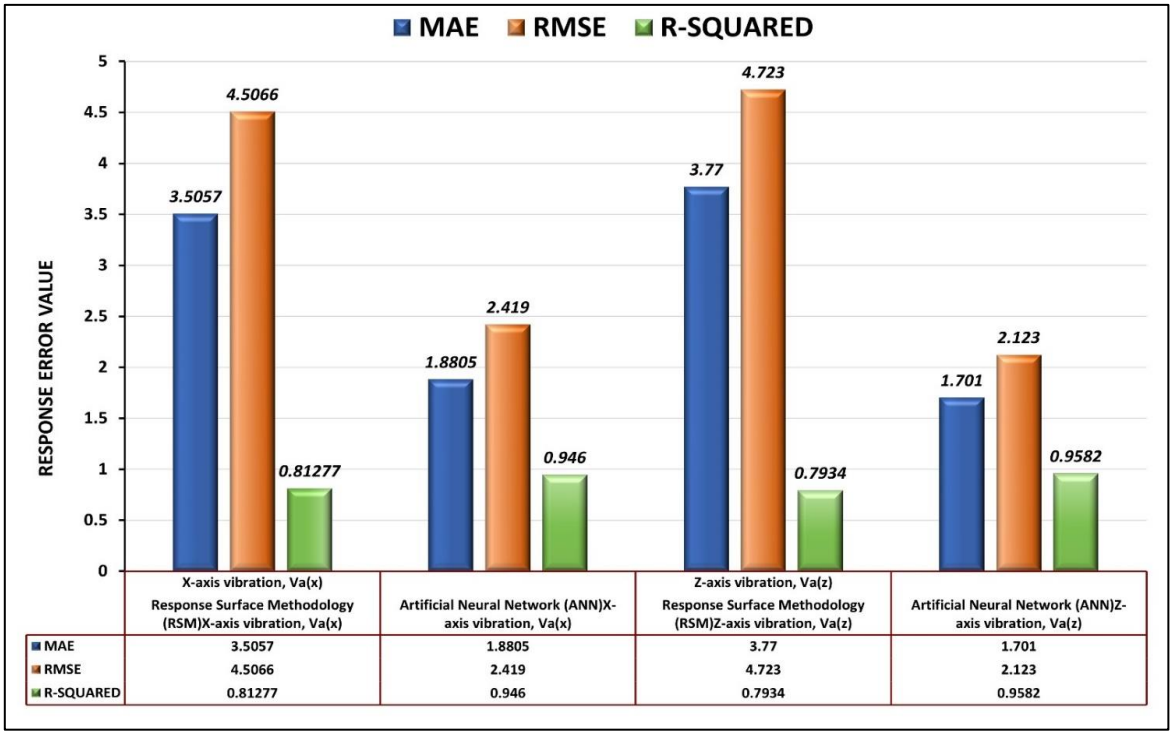

Figure 5.14 Value of MAE, RMSE and R-Squared related to RSM and ANN modelling.

5.8.3 Analysis of the same presents the following facts*:*

a. Mean Absolute Error (MAE):

The Mean Absolute Error (MAE) is a metric used to measure the average absolute difference between the predicted values and the actual values. The analysis quantifies the magnitude of prediction errors, regardless of their direction. Analysing the similarities and differences between two or more subjects. MAE values of the ANN method are noticeably lower than those of the RSM method for vibrations along both the x-axis and z-axis. The data suggests that, on average, the predictions made by the ANN model are significantly more accurate in estimating vibration amplitudes compared to the predictions made by the RSM model.

b. Root Mean Squared Error (RMSE):

The RMSE is a mathematical metric that quantifies the average difference between predicted values and actual values. It is calculated by taking the square root of the average of the squared differences between the predicted and actual values. The analysis takes into account both the size and orientation of errors.

The RMSE values for the ANN method show significant improvement in reducing both x-axis and z-axis vibrations compared to the traditional RSM method. The analysis suggests that the predictions made by the ANN method tend to have smaller errors in general.

c. R-squared (Coefficient of Determination):

The R-squared statistic quantifies the extent to which the independent variables (input factors) account for the variability in the dependent variable (vibration amplitudes). The range of values for this metric is from 0 to 1. Higher values within this range indicate a stronger fit or correlation.

The higher R-squared values observed in the ANN method for both x-axis and z-axis vibrations indicate that the ANN model is more effective in capturing the variability present in the data. The analysis reveals that a larger portion of the observed variation is accounted for, indicating a higher level of predictive capability.

Interpretation from a technical standpoint:

- The ANN technique consistently exhibits improved performance across all error measures on both axes. The consistent nature of these observations suggests that the observed patterns are not just fortuitous, but rather a reliable representation of the prediction ability of the methodologies used.
- Precision and Accuracy: The ANN technique exhibits notably lower MAE and RMSE values, suggesting that its predictions are not only more proximate to the actual values but also possess more precision. The level of accuracy shown here is suggestive of the ability to make correct forecasts.
- Model Fit and Variability: The elevated R-squared values observed in regard to the ANN approach suggest that it exhibits a greater capacity to accurately represent the inherent patterns and relationships within the dataset. The proposed model exhibits a high degree of conformity to the observed data points and has an enhanced capacity to capture the fluctuations in vibration amplitudes.

Based on an examination of error data and measurements using technological methods, a forecast may be made.

- The ANN technique clearly emerges as the preferred option in terms of predicted accuracy when it comes to reducing vibration amplitudes in both the x-axis and z-axis vibrations.
- The continually decreased MAE and RMSE numbers provide evidence of the ANN method's capacity to provide predictions that are more precise.
- The higher R-squared values provide further support for the assertion that an ANN model demonstrates a robust alignment with the observed distribution and patterns of the data.

5.9 Summery of the Chapter

The present study integrates the rigorous approaches of Response Surface Methodology (RSM) together with a Box-Behnken design, and utilizes the efficacy of Artificial Neural

Network (ANN) optimization procedures. The variables being examined include key aspects such as the rotational speed of the shaft, which may reach up to 8000 rpm, the oil pressure, which can range up to 100 bar, and the different oil mix ratios, ranging from 10% to 50%. A range of statistical measures are calculated in order to evaluate the errors and coefficients of determination of the projected models. The comparative analysis reveals that the ANN model exhibits a notable decrease in prediction errors and a higher coefficient of determination in comparison to the RSM when considering the vibration amplitude along both the x and z axes. The mean absolute error (MAE), root mean squared error (RMSE), and coefficient of determination (R-squared) values were computed for the x and z axes using the ANN model. The MAE and RMSE values for the x axis were found to be 3.50 and 3.77, respectively, while for the z axis, the values were 4.50 and 4.72. Additionally, the R-squared values for the x axis were 0.81, 0.79, and 1.88, and for the z axis, the values were 1.70, 2.41, and 2.12. The ANN model has a reduced overall mean absolute percentage error (MAPE) for both the x and z axes, with values of 9.73% and 9.38% respectively. In contrast, the RSM model exhibits a higher MAPE range of 18.18% to 20.50%. The conclusive research reveals that the ANN prediction model outperforms the regression model based on RSM, exhibiting superior accuracy in predicting vibration amplitudes. The ANN approach is a more advantageous option for calculating vibration amplitudes in high-speed rotating shafts. Additionally, it offers significant advantages in terms of efficiency and time savings. This study not only contributes significant new insights into optimal modeling techniques for effective vibration control, but also underscores the advantages of using ANN in predictive evaluations of this kind.

CHAPTER-6

VIBRATION ANALYSIS OF HIGH-SPEED ROTOR UNDER VARIABLE POINT LOAD CONDITION WITH AND WITHOUT SQUEEZE FILM DAMPER

6.1 Introduction

The major purpose of this chapter is to conduct an in-depth investigation of the amplitude of shaft vibrations under varying point load circumstances. As part of this investigation, we will compare and contrast situations in which a squeeze film damper is not present with those in which it is present. A systematic modification of load placement is included into the experimental setup. More specifically, the load placement is varied at distances of 10, 20, 30, 40, and 50 centimetres from the terminal support of the shaft. Measurements of the vibration amplitudes along the x and z axes are recorded after each placement. These measurements are taken with great care. When the load is positioned in close proximity to the support, there is a perceptible rise in vibration amplitudes along both axes. This is shown by the findings that were acquired from the various analysis of the vibrational signals. Alternatively, a corresponding decrease in vibration amplitudes is noticed when the load is moved farther away from the support. In addition, it is important to notice that the vibration amplitudes decrease at a faster rate when the loading point is greater than the main length of the shaft. This in-depth analysis not only provides useful insights into the dynamic behaviour of the shaft under varied load situations but also throws light on the influence that the application of squeeze film damper has on the vibrational patterns that have been observed.

- ***Implementation of a Squeeze Film Damper (SFD):*** During the subsequent stage of the investigation, the end support was substituted with a squeeze film damper (SFD), which ensured a steady loaded condition. The computation of vibration amplitudes along the X and Z axes was the primary objective. The

experiment entailed the utilization of distinct sets of oil samples, each of which possessed a unique viscosity and was maintained at a constant supply oil pressure of 5 bar.

- ***Variable Point Loading under Fixed Oil Supply Pressure:*** The loading condition exhibited no variation, mirroring the circumstances that were present in the absence of the SFD. The inquiry comprised an assortment of oil samples exhibiting diverse viscosities, all of which were subjected to an identical oil supply pressure of 5 bar. By employing this methodical approach, a comparative analysis of the vibration amplitudes along the X and Z axes was possible.
- ***The Influence of Oil Viscosity on Vibration Amplitude:*** The experimental findings unveiled a significant pattern. The vibration amplitude along both the X and Z axes decreased proportionally as the viscosity of the oil reached its optimal level. This indicates that the viscosity of the oil correlates physically with the amplitudes of the resulting vibrations.
- ***Vibration Amplitude Comparison Between the Omission and Presence of a Squeeze Film Damper***: Each oil sample underwent a comparative analysis of vibration amplitudes with and without the SFD. It was evident from the results that the rotor vibration amplitudes decreased as a result of the SFD's implementation. Additionally, the observed pattern suggested that a reduction in vibration amplitude occurred simultaneously with an increase in oil viscosity up to a certain threshold. This underscores the reciprocal impact of oil viscosity and the SFD in the reduction of vibration within the rotor system.

6.2 Material and Method without SFD

During the experimental examination, three different oil samples were used. These samples were carefully created by combining kerosene oil and crankcase oil in different amounts. The kinematic viscosities of the oil samples were measured as follows: oil sample 1 had a value of 18.449mm^2/sec, oil sample 2 had a value of 27.807 mm^2/sec, and oil sample 3 had a value of 54.666 mm^2/sec. The deliberate manipulation of oil composition and viscosity is a fundamental part of the experiments, to determine how lubricant qualities affect the dynamic behavior of the system.

A consistent oil pressure of 5 bar was maintained throughout the testing experiments. The dynamic forces on the system were represented by a rotating load. This load was varied routinely at five specific distances from the damper support. The distances were accurately positioned at 10, 20, 30, 40, and 50 cm from the end support. The vibration signals were measured using a proximity sensor placed strategically at a set distance of 5 cm from the end support. The careful positioning of the sensors guaranteed reliable data collection and enabled a detailed examination of the system's vibrational reactions to different loads. The testing also included a thorough examination of the system's reaction to various rotor speeds. More precisely, the rotor was exposed to five different speeds: 2500, 4500, 6500, 8500, and 10500 rpm. The incorporation of several speed settings was intended to comprehensively assess the system's performance across a wide range of operating circumstances. This sophisticated technique allows for a comprehensive examination of the interaction between oil properties, loading circumstances, and rotor velocities, providing an important understanding of the system's dynamics and the efficacy of the squeeze film damper in reducing vibrations.

6.3 Description of Experimental Test Rig without SFD

The experimental configuration consists of a rotor test rig equipped with a shaft measuring 2.2 cm in diameter and spanning a length of 87 cm between two fixed supports. A revolving mass, measuring 2.2 cm by 1.4 cm and weighing 550 grams, is strategically positioned at different locations along the rotor, as seen in Figure 6.1. Vibration amplitudes are precisely recorded on the X and Z axes using proximity probing, especially at a distance of 5 cm from the end support. Afterwards, the spinning mass is methodically moved to distances of 10, 20, 30, 40, and 50 cm from the endpoint support, and the resulting vibration amplitudes are recorded for thorough study.

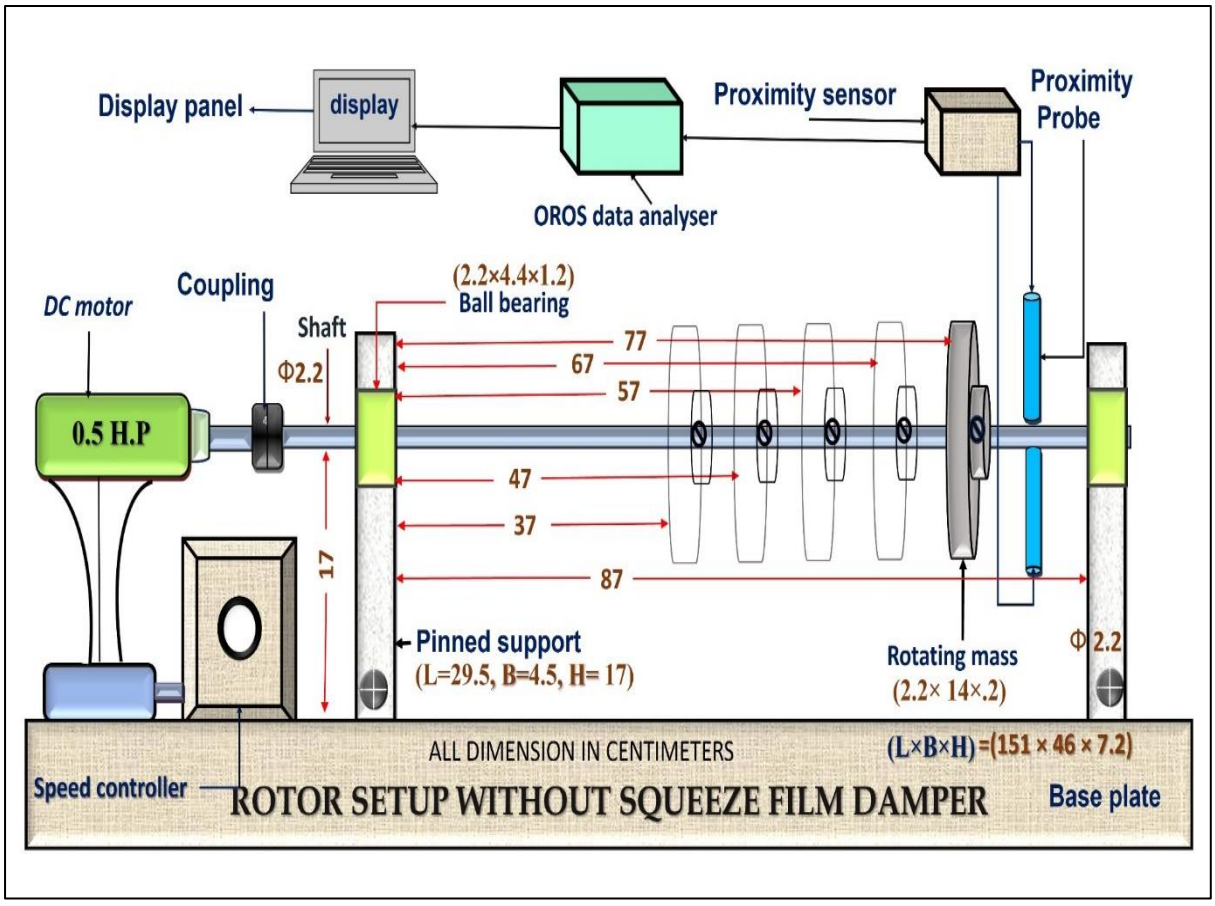

Figure 6.1 Rotor bearing system without squeeze film damper.

6.3.1 Description of Experimental Test Rig with SFD

The following Table.6.1 provides a comprehensive documentation of the particular characteristics that belong to the actual test rig, as well as the measurements of each individual component included inside it. By tabulating this information, the main parameters that are necessary for a thorough knowledge of the experimental setup are encapsulated. This allows for exact analysis and interpretation of the performance of the rig under a variety of scenarios.

Table 6.1 Parameter detail for rotor vibration analysis with SFD.

Specifications of the Experimental Test Rig	
SFD and rotor shaft components' materials	*Mild steel*
Rotor shaft's length and diameter	*1000mm, 22mm*
Distance between two supports of rotor	*870mm*
Boundary dimension of damper journal	*44×50×64mm*
Boundary dimension of damper housing	*50×56×64mm*
Length of the damper	*50 mm*
Boundary dimension of rotating mass	*22×140×20mm*
Mass of rotating disc	*550gm*
Boundary dimension of ball bearings is utilized in squeeze film damper, type	*22×44×12mm, Koyo, Japan*
Spacer in between two ball bearings	*4mm*
Mass of rotor shaft	*3.5kg*
Density of rotor shaft	*7800kg/m3*
O-ring seal material and diameter	*Rubber, 46mm*
DC motor 0.5 hp single phase rated speed	*12000rpm*
Type of coupling	*flexible Lovejoy*

Figures 6.2 and 6.3 provide a visual depiction of the experimental setup, which includes the squeeze film damper (SFD). These figures also provide a schematic model of the experimental arrangement. The experimental documentation is comprised of these figures,

which act as vital components and provide a thorough description of the setup of the test rig. A theoretical overview of the system is included in the schematic, which is displayed in Figure 28. The schematic also illustrates the desired arrangement of components. Figure 29, on the other hand, provides a picture that is accurate and incorporates the actual implementation of the test rig in the real world, complete with the squeeze film damper that is included in it.

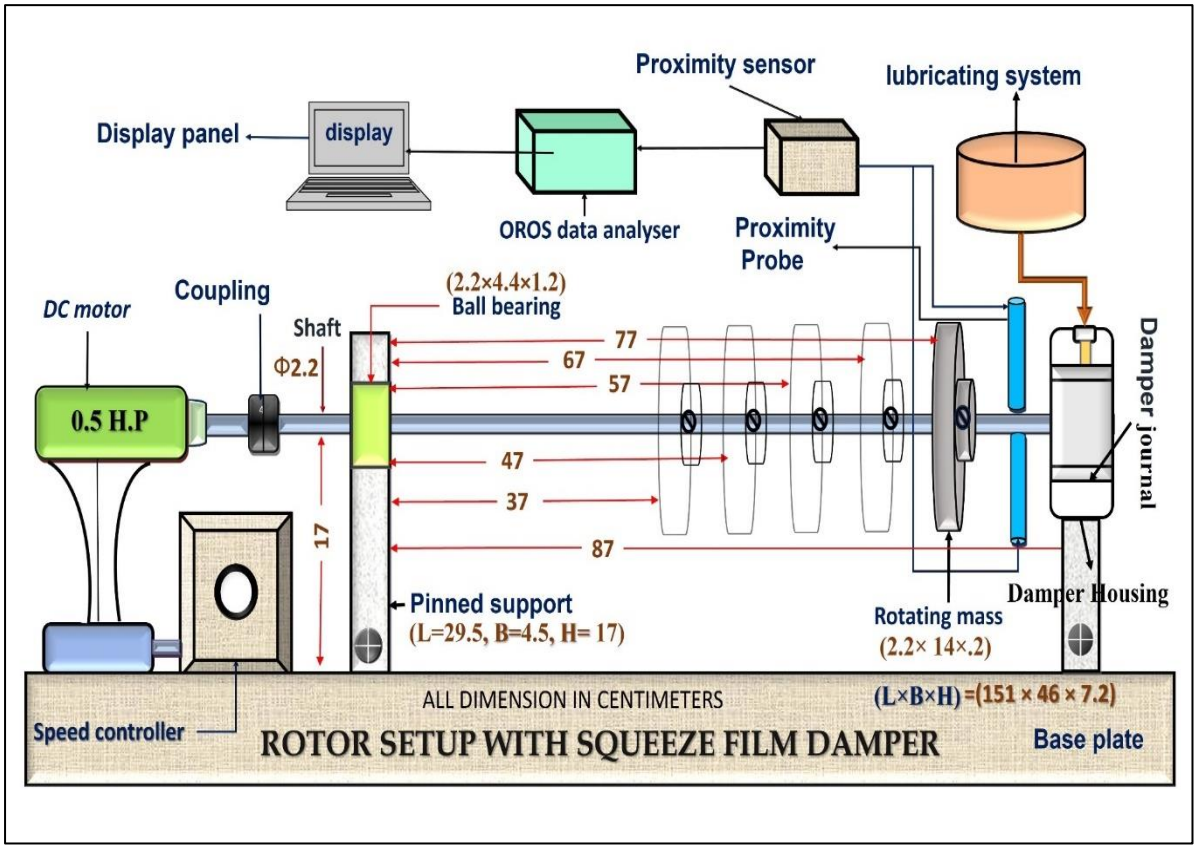

Figure 6.2 Rotor bearing system with squeeze film damper

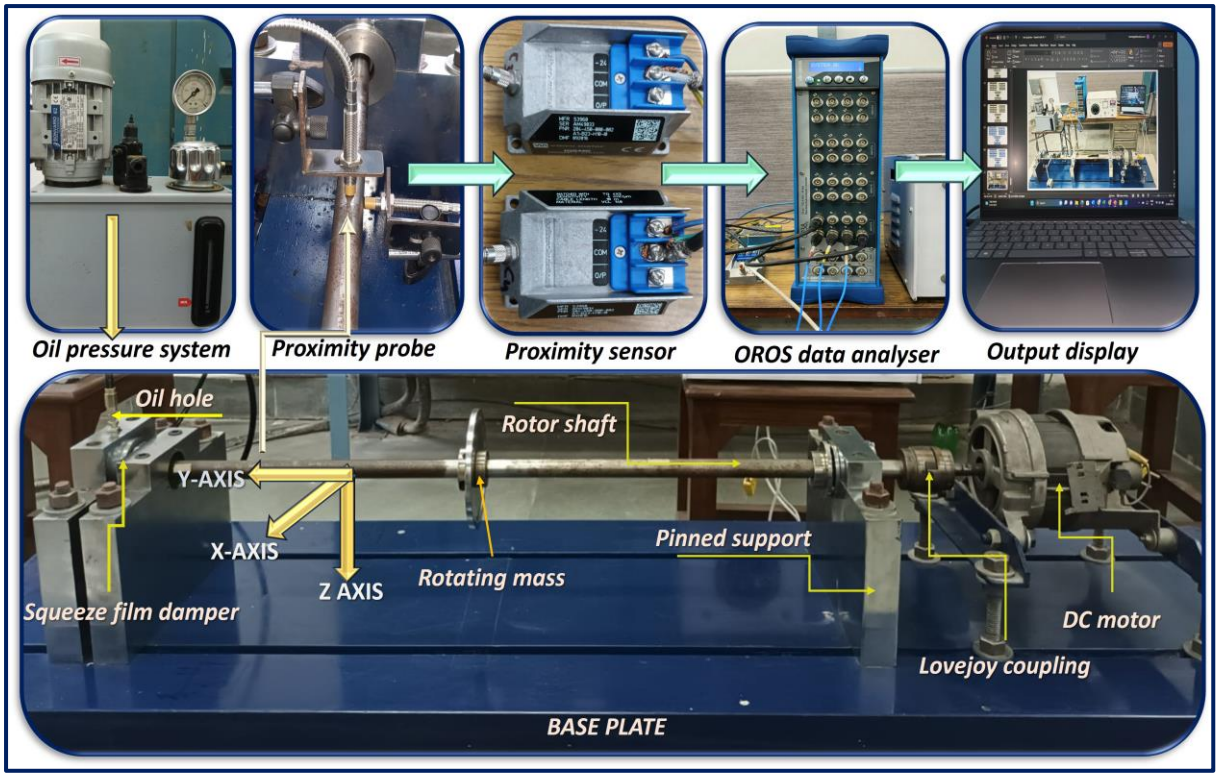

Figure 6.3 Actual Rotor bearing system with squeeze film damper

6.4 Material and Method with SFD

During the experimental examination, three different oil samples were used. These samples were carefully created by combining kerosene oil and crankcase oil in different amounts. The kinematic viscosities of the oil samples were measured as follows: oil sample 1 had a value of 18.449mm^2/sec, oil sample 2 had a value of 27.807 mm^2/sec, and oil sample 3 had a value of 54.666 mm^2/sec. The deliberate manipulation of oil composition and viscosity is a fundamental part of the experiments, to determine how lubricant qualities affect the dynamic behavior of the system.A consistent oil pressure of 5 bar was maintained throughout the testing experiments. The dynamic forces on the system were represented by a rotating load. This load was varied routinely at five specific distances from the damper support. The distances were accurately positioned at 10, 20, 30, 40, and 50 cm from the end support. The vibration signals were measured using a proximity sensor placed strategically at a set distance of 5 cm from the end support. The careful positioning of the sensors guaranteed reliable data

collection and enabled a detailed examination of the system's vibrational reactions to different loads. The testing also included a thorough examination of the system's reaction to various rotor speeds. More precisely, the rotor was exposed to five different speeds: 2500, 4500, 6500, 8500, and 10500 rpm. The incorporation of several speed settings was intended to comprehensively assess the system's performance across a wide range of operating circumstances. This sophisticated technique allows for a comprehensive examination of the interaction between oil properties, loading circumstances, and rotor velocities, providing an important understanding of the system's dynamics and the efficacy of the squeeze film damper in reducing vibrations.

6.5 Experimentation without SFD

A variety of speeds, ranging from 2500 to 10500 revolutions per minute (RPM), are applied to the rotor to be tested throughout the experimental process. Several loading points, ranging from 10 to 50 centimetres out from the end support, are carefully positioned to accommodate a rotating mass of 550 grams. The data of vibrations is shown in the table 6.2 that can be found below, and the accompanying graphical representation can be seen displayed in Figure 6.4.

Table 6.2 vibration amplitude(μm) of the rotor shaft without SFD

Speed (rpm)	**2500**		**4500**		**6500**		**8500**		**10500**	
Load Distance (c.m)	x-axis	z-axis	x-axis	z-axis	x-axis	z-axis	x-axis	z-axis	x-axis	z-axis
10	65.2	66.3	84.9	85.2	120.2	121.2	135.2	134.2	165.7	164.2
20	60.5	60.9	77.6	78.1	102.5	103.4	111.6	110.5	141.3	140.4
30	50.4	51.4	69.4	68.8	89.7	88.8	92.7	93.5	112.5	111.6
40	46.2	47.2	57.6	56.9	73.9	74.7	81.8	82.5	94.6	95.4
50	30.4	31.4	35.7	36.1	52.6	53.9	60.7	61.4	71.5	72.8

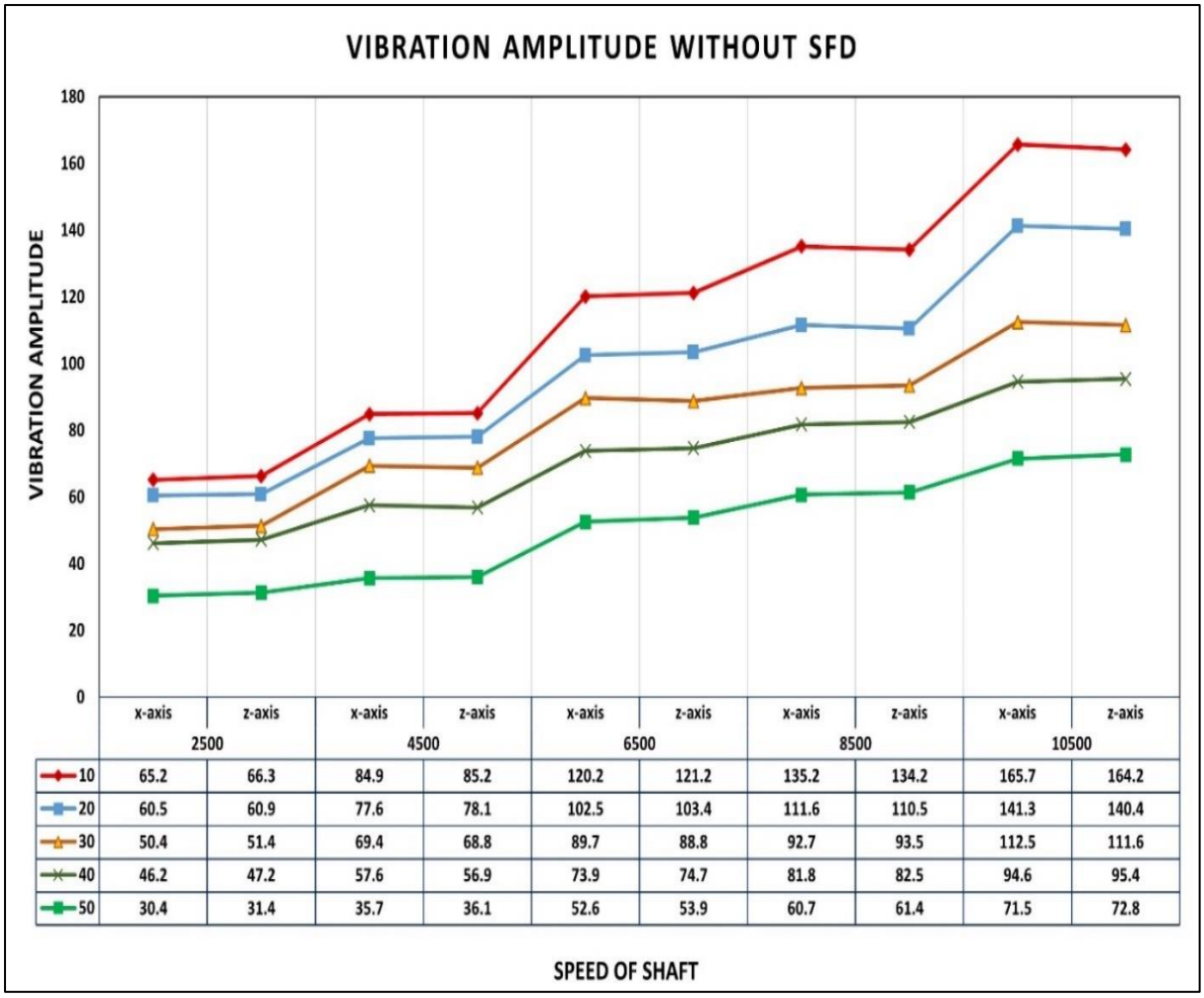

	2500		4500		6500		8500		10500	
	x-axis	z-axis	x-axis	z-axis	x-axis	z-axis	x-axis	z-axis	x-axis	z-axis
10	65.2	66.3	84.9	85.2	120.2	121.2	135.2	134.2	165.7	164.2
20	60.5	60.9	77.6	78.1	102.5	103.4	111.6	110.5	141.3	140.4
30	50.4	51.4	69.4	68.8	89.7	88.8	92.7	93.5	112.5	111.6
40	46.2	47.2	57.6	56.9	73.9	74.7	81.8	82.5	94.6	95.4
50	30.4	31.4	35.7	36.1	52.6	53.9	60.7	61.4	71.5	72.8

Figure 6.4 Vibration amplitude of x-z axes without squeeze film damper

Through a thorough analysis of the experimental results, it is clear that placing the load near the support led to a significant increase in vibration amplitude in both directions. This behaviour indicates an increased sensitivity of the system to loading circumstances near the support. On the other hand, when the load was moved farther away from the support in a systematic manner, there was a constant decrease in the amplitude of vibration. The complex connection between the load location and the resulting vibratory response is shown by this intricate relationship.

Remarkably, a very important finding arose when the loading point surpassed the midpoint of the shaft's length. Currently, there was a noticeable and swift decrease in the magnitude of vibration. This event indicates a crucial limit in the system's behavior, indicating that once a

particular distance from the support is reached, the system undergoes a stronger stabilization, perhaps because of a redistribution of forces and moments acting on the rotor. These discoveries have significant significance for the comprehension and improvement of rotor dynamics. The discovered patterns highlight the significance of load location as a determining element in the vibrational properties of the system. Additional examination of these dynamics has the potential to enhance the accuracy of prediction models and facilitate the creation of techniques for reducing vibrations in rotating equipment. This might have practical implications in several engineering disciplines.

6.6 Experimental Finding with SFD

Table 6.3 presents a detailed summary of the vibration amplitudes observed in the rotating shaft when the subject is systematically conditioned at different speeds. This dataset has been carefully compiled for a fixed oil supply pressure of 5 bar in the squeeze film damper. The observations provide a thorough analysis of oil sample 1, which has a kinematic viscosity of 18.449 mm^2/sec. The table contains information about different load points, speed ranges, and vibration amplitudes. This allows for a detailed analysis of the system's dynamic behavior based on the specified experimental parameters.

Table 6.3 Vibration amplitude(μm) of the rotor shaft with SFD for oil 1 sample

Speed (rpm)	**2500**		**4500**		**6500**		**8500**		**10500**	
Load Distance (c.m)	x-axis	z-axis	x-axis	z-axis	x-axis	z-axis	x-axis	z-axis	x-axis	z-axis
10	52.3	51.5	74.3	75.2	110.3	109.2	117.2	118.1	135.3	136.2
20	46.1	45.2	62.5	63.4	91.2	92.4	99.5	98.7	118.5	119.4
30	39.2	38.6	51.8	52.2	78.5	77.6	82.3	83.5	94.5	95.7
40	35.2	36.4	42.6	43.1	65.3	66.2	71.5	72.6	82.6	83.4
50	27.3	28.2	31.2	32.3	41.5	42.1	50.1	49.5	58.2	59.3

Figure 6.5 provides essential information that helps us identify trends, patterns, and relationships between important variables. This, in turn, improves our understanding of how load positioning, rotor speed, and oil viscosity affect the vibrational responses in the squeeze film damper setup.

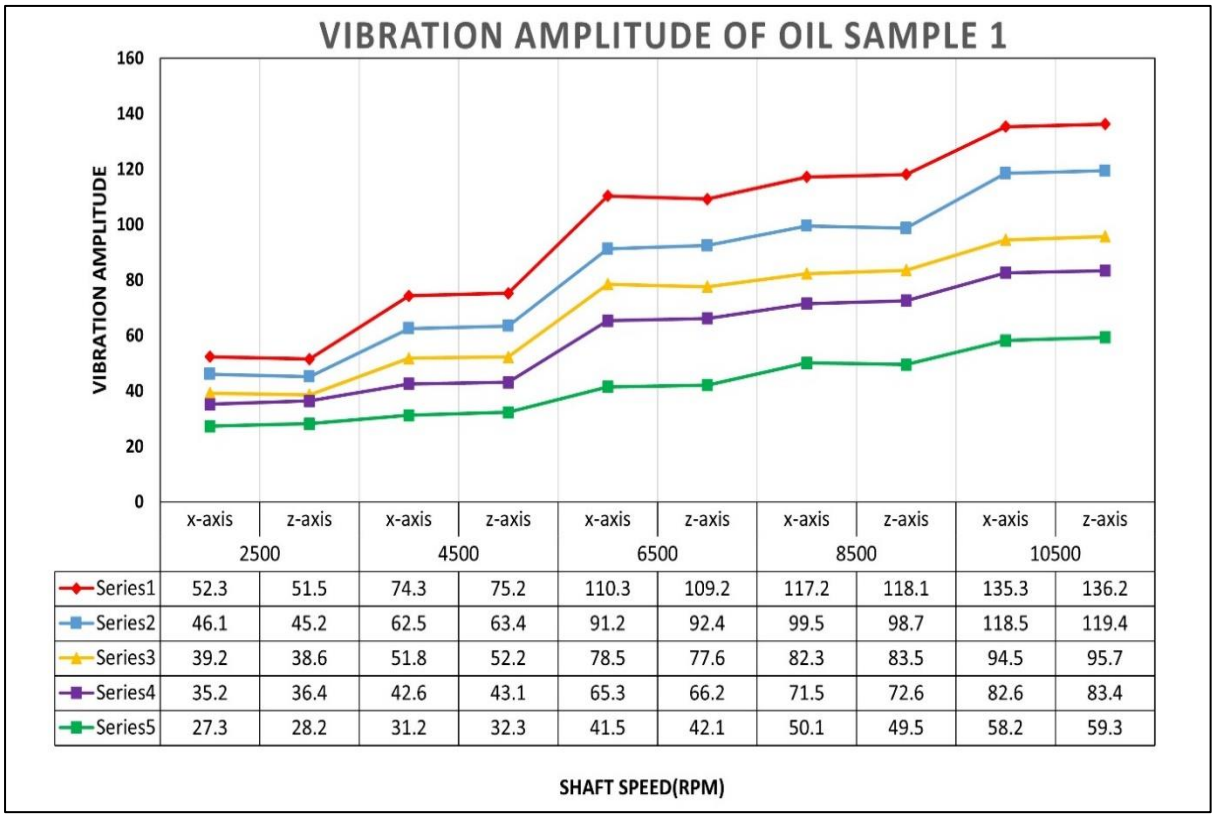

	x-axis	z-axis	x-axis	z-axis	x-axis	z-axis	x-axis	z-axis	x-axis	z-axis
	2500		4500		6500		8500		10500	
Series1	52.3	51.5	74.3	75.2	110.3	109.2	117.2	118.1	135.3	136.2
Series2	46.1	45.2	62.5	63.4	91.2	92.4	99.5	98.7	118.5	119.4
Series3	39.2	38.6	51.8	52.2	78.5	77.6	82.3	83.5	94.5	95.7
Series4	35.2	36.4	42.6	43.1	65.3	66.2	71.5	72.6	82.6	83.4
Series5	27.3	28.2	31.2	32.3	41.5	42.1	50.1	49.5	58.2	59.3

Figure 6.5 Vibration amplitude of x-z axes without squeeze film damper oil1

Table 6.4 presents a detailed summary of the vibration amplitudes shown by the spinning shaft under various loading circumstances across different speed ranges. The information is meticulously compiled for a constant oil supply pressure of 5 bar in the squeeze film damper. The observations provide a comprehensive analysis of oil sample 2, which is distinguished by a kinematic viscosity of 27.807 mm^2/sec. Every row in the table represents a distinct combination of load point, speed range, and resulting vibration amplitude. This allows for a detailed investigation of the system's dynamic behaviour based on the supplied experimental conditions.

Table 6.4 Vibration amplitude(μm) of the rotor shaft with SFD for oil sample 2

Speed (rpm)	**2500**		**4500**		**6500**		**8500**		**10500**	
Load Distance (c.m)	x-axis	z-axis	x-axis	z-axis	x-axis	z-axis	x-axis	z-axis	x-axis	z-axis
10	42.3	41.4	64.3	65.2	99.9	99.1	109.2	110.1	124.3	125.8
20	36.2	35.3	52.5	53.4	81.2	82.4	89.5	88.7	108.6	109.5
30	29.2	28.6	41.8	42.2	68.5	67.6	72.3	73.5	84.5	85.7
40	25.2	26.4	32.6	33.1	55.3	56.2	61.8	62.7	82.6	83.4
50	20.3	21.2	24.2	25.3	33.5	34.1	40.1	41.5	54.7	55.3

Figure 6.6 provides essential information that helps us identify trends, patterns, and relationships between important variables. This, in turn, improves our understanding of how load positioning, rotor speed, and oil viscosity affect the vibrational responses in the squeeze film damper setup.

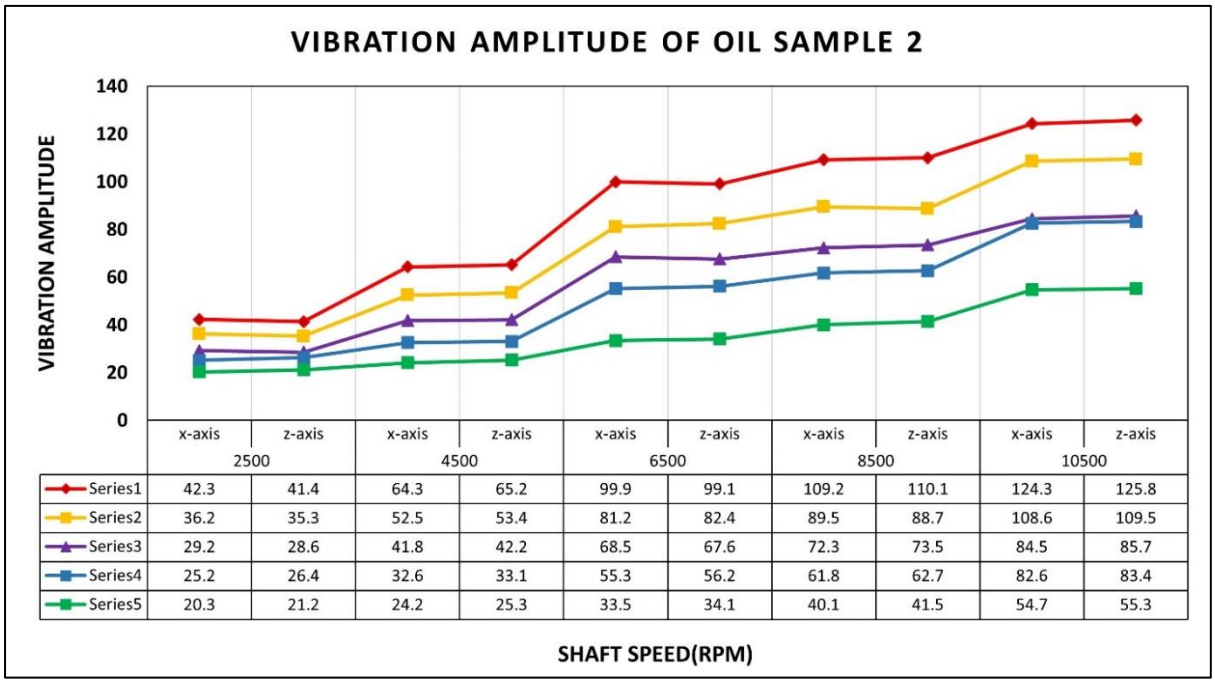

Figure 6.6 Vibration amplitude of x-z axes without squeeze film damper oil2

Table 6.5 presents a detailed summary of the vibration amplitudes shown by the spinning shaft under various loading circumstances across different speed ranges. The dataset provided is meticulously selected for a constant oil supply pressure of 5 bar in the squeeze film damper. The observations provide a comprehensive analysis of oil sample 3, which is distinguished by a kinematic viscosity of 54.666 mm^2/sec. Each row in the table represents a distinct combination of load point, speed range, and resulting vibration amplitude, allowing for a detailed examination of the system's dynamic behavior under the stated experimental conditions.

Table 6.5 Vibration amplitude(μm) of the rotor shaft with SFD for the oil sample3

Speed (rpm)	**2500**		**4500**		**6500**		**8500**		**10500**	
Load Distance (c.m)	x-axis	z-axis	x-axis	z-axis	x-axis	z-axis	x-axis	z-axis	x-axis	z-axis
10	32.4	31.7	54.3	55.2	87.3	88.2	97.2	98.1	115.3	116.2
20	27.1	26.2	42.5	43.4	71.3	72.7	79.5	78.7	98.9	99.8
30	20.2	21.6	34.8	35.2	58.4	57.6	62.3	63.5	74.5	75.7
40	15.2	16.4	22.6	23.1	35.5	36.8	51.5	52.6	64.6	63.4
50	11.3	10.5	15.2	16.5	21.5	22.7	30.1	29.5	38.4	37.5

Figure 6.7 provides us with vital information that assists us in recognizing patterns, trends, and correlations between significant factors. Our comprehension of how load location, rotor speed, and oil viscosity influence the vibrational responses in the squeeze film damper setup is advanced as a result of this.

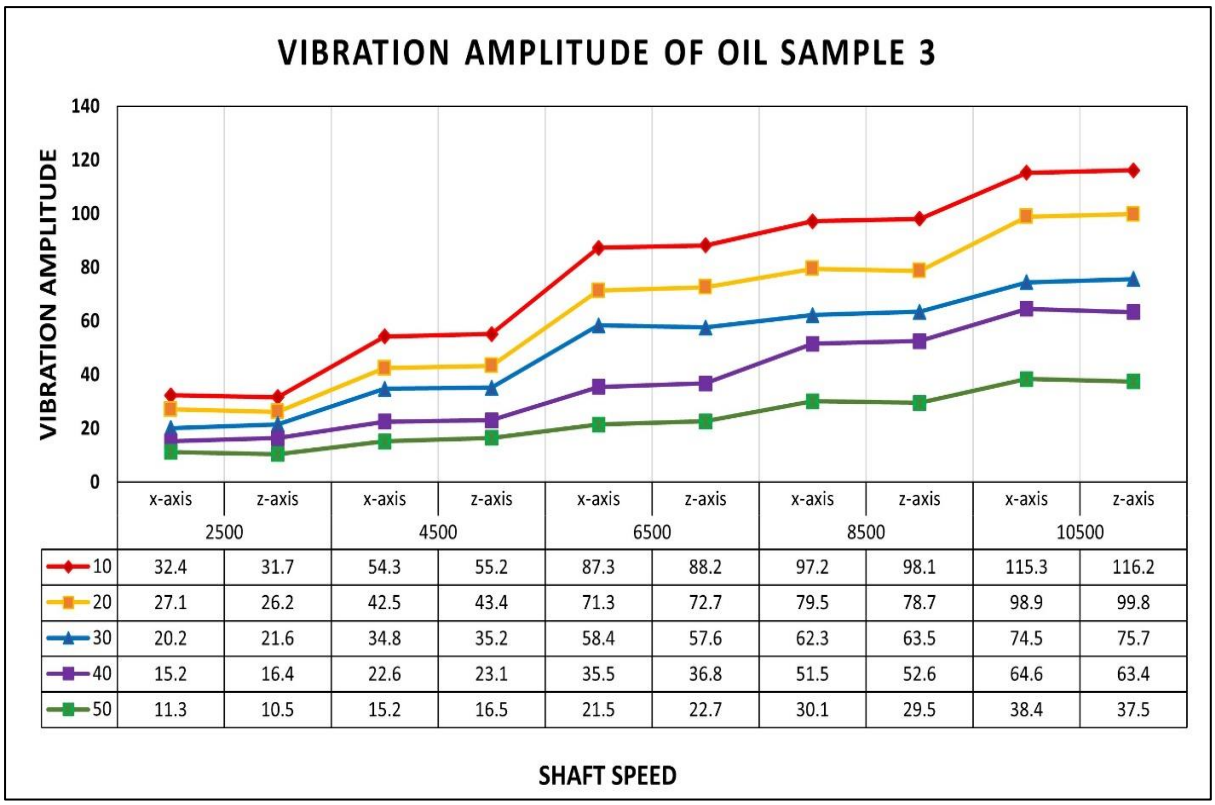

	2500		4500		6500		8500		10500	
	x-axis	z-axis	x-axis	z-axis	x-axis	z-axis	x-axis	z-axis	x-axis	z-axis
10	32.4	31.7	54.3	55.2	87.3	88.2	97.2	98.1	115.3	116.2
20	27.1	26.2	42.5	43.4	71.3	72.7	79.5	78.7	98.9	99.8
30	20.2	21.6	34.8	35.2	58.4	57.6	62.3	63.5	74.5	75.7
40	15.2	16.4	22.6	23.1	35.5	36.8	51.5	52.6	64.6	63.4
50	11.3	10.5	15.2	16.5	21.5	22.7	30.1	29.5	38.4	37.5

Figure 6.7 Vibration amplitude of x-z axes without squeeze film damper oil3

6.7 Experimental Findings and Discussion

A. Initial Phase of the Investigation:

During the preliminary stage of our inquiry, we deliberately positioned the load at intervals of 10, 20, 30, 40, and 50 cm from the end support. As a result, we saw discernible patterns in the vibration amplitudes of the shaft along the x and z axes. Significantly, placing the load near the support resulted in a noticeable rise in vibration amplitude in both axes. On the other hand, when the load was shifted farther from the support, there was a corresponding decrease in the amplitude of vibration. An outstanding finding was the rapid decrease in vibration amplitude as the loading point beyond the midpoint of the shaft length.

B. Second Phase of the Investigation

After replacing the end support with the squeeze film damper (SFD) in the second stage of our research, we redirected our attention towards determining the vibration amplitudes along the X and Z axes. This was done by analyzing several oil samples with differing viscosities. When the experiment was conducted with a consistent load, replicating the first setup but excluding the SFD, it yielded fascinating observations.

Different Oil Study Samples and Viscosity Levels:

The results demonstrated a distinct link between the viscosity of oil and the amplitude of vibration. Observations revealed a constant decrease in vibration amplitude for both the X and Z axes as the viscosity of the oil samples rose, reaching an optimal level. This discovery implies that the selection of oil viscosity has a vital impact on defining the overall vibration characteristics in a system that uses a squeeze film damper.

Comparative study was conducted to compare the effects of implementing the squeeze film damper (SFD) on rotor vibration amplitudes.

The research showed that the presence of the SFD led to a significant decrease in rotor vibration amplitudes. The decrease was consistently found in many oil samples and their diverse viscosities. The research highlights the efficacy of the squeeze film damper in reducing vibrations and offers significant information for enhancing the damper's performance in real-world scenarios.

6.8 Summary of the Chapter

This chapter delves into a thorough examination of shaft vibrations when subjected to different point load conditions. It also compares scenarios with and without the inclusion of a squeeze film damper (SFD). The experimental setup includes precise adjustments in load

placement at distances ranging from 10 to 50 centimeters from the terminal support. Vibration amplitudes along the x and z axes are meticulously measured throughout the process. The vibration amplitudes are significantly higher when the load is closer to the support. However, as the load is moved farther away, the vibration amplitudes decrease, particularly beyond the main length of the shaft. Furthermore, the steady loaded condition is ensured by the implementation of an SFD. A comparison of vibration amplitudes with variable point loading under fixed oil supply pressure shows consistent conditions that mirror those without the SFD. In addition, this study delves into the impact of oil viscosity on vibration amplitude, revealing a gradual decrease as viscosity reaches its optimal level. Finally, a thorough analysis of vibration amplitudes was conducted to compare the effects of having or not having the SFD. The results clearly show that implementing the SFD leads to lower rotor vibration amplitudes. This demonstrates the important role of oil viscosity and the SFD in reducing vibrations within the rotor system. This analysis provides valuable insights into the dynamic behavior of the shaft under different load situations and highlights the impact of the SFD on observed vibrational patterns.

CHAPTER-7

CONCLUSIONS AND FUTURE SCOPE

7.1 Conclusions

This research offers the results of an empirical inquiry into the ways in which squeeze film dampers may be used to regulate vibrations in high-speed rotating shafts in a variety of operating settings. In particular, the research investigated the influence of various operating circumstances or parameters. These include high oil supply pressure and the usage of a wide variety of oil mixes. A modelling method was used to determine which process parameters for the squeeze film damper would provide the greatest results. This was accomplished by using a Box-Behnken design in conjunction with Response Surface Methodology (RSM), and then optimized for effectiveness. This experimental investigation was systematically constructed, and it continued further to incorporate a comparison examination of the predictive powers of Response Surface Methodology and Artificial Neural Networks (ANN) in data prediction. In addition, the research carried out an in-depth investigation of the comparison study, throwing light on the intricate differences that exist between the two research approaches via the use of error analysis. In general, the findings of this research contributes to the ongoing discussion in the academic community on the suppression of vibrations in high-speed rotating shafts. In order to do this, it employed real-world experiments, statistical approaches, and artificial intelligence to provide a comprehensive picture of how things function.

In the first chapter of this thesis, The Groundwork was done by elaborating on the motive that drove the research attempt. We examined the history of squeeze film dampers as well as their categorization. An in-depth look at the operational concepts behind these dampers was done. In addition, investigation of variety of technologies that are now being used to improve

equipment for squeezing film dampers was also done. This was done in particular about the regulation of vibration in high-speed rotating shafts.

The purpose of the second chapter, A forum for addressing the significance of the thesis's breadth and contribution was set up. An overview of research initiatives linked to the control of vibration in high-speed rotating shafts utilizing squeeze film dampers was undertaken a presentation of a synthesis of the accumulated data and insights obtained from a variety of researchers working in this field was obtained. It sheds light on the numerous elements of managing vibrations under a variety of different operating situations. The literature research that was carried out , was able to identify important results and provide a summary of the information that was gathered about the efficiency of squeeze film dampers in reducing vibrations caused by high-speed rotating shafts. This preliminary study laid the foundations for future chapters, providing a context in which the unique contributions and insights that are provided in the thesis may.

- The precise selection of process parameters has a considerable impact on the vibration behavior of rotating shafts when squeeze film dampers are being used, and this influence may be substantial.
- The research that has been published so far demonstrates that the majority of emphasis has been paid to investigating vibration management in rotating shafts, while other areas, such as modeling using response surface approach and experimental design, have received relatively little attention.
- The research indicates that using an O-ring seal in the squeeze film damper is superior to using other piston rings that do not have a centralizing spring. The greater prices of the materials and the need for more in-depth analytical investigations, on the other hand, make this option less attractive.

- Although researchers have focused their attention on analyzing the seal and using finite element modeling (FEM) for squeezing film dampers, there has been a striking lack of investigation into other significant components of the management of high-speed rotating shaft vibrations. This is a significant problem.
- Historically, the majority of researchers have concentrated their efforts on single-response factor studies. On the other hand, it has been shown that the optimal process parameters alter depending on the response factor. When trying to optimize numerous replies at the same time, it is recommended that you make use of an optimization strategy that considers multiple objectives.
- Squeeze film dampers with extended rotating shafts are becoming more in demand, especially in applications such as compressors, and turbine engines.
- Although some researchers have engaged in analytical modeling of squeeze film dampers to gain a better understanding, there is a need to incorporate experimental design and other modeling techniques to acquire an all-encompassing understanding of the process parameters influencing the vibration amplitude of high-speed rotating shafts.

***Chapter 3*;** The first phase of development was completed, and further preliminary research was conducted. To determine the appropriate sample size and assess the results of the experiments, the Taguchi approach was used. The use of the ANOVA technique serves to reinforce the validity of the results. The use of S/N plots facilitated the identification of optimal process parameters and their corresponding values. Conversely, the main effect plots for means are employed to assess the influence of input process parameters on vibration amplitude responses. The empirical investigation yields the following important inference.

- Carried out 25 distinct experimental runs, each with five levels for the respective process parameter (speed, pressure, and blend%), using the L25 orthogonal array design for a total of 75 trials.
- Used the analysis of variance (ANOVA) to determine whether or not the process parameters are statistically significant. According to the findings, the contribution of oil pressure to the decrease of vibration along the x and z axes was about 90.86 percent and 88.69 percent, respectively. The proportion of blended substance also displayed a substantial influence on the decrease of vibration.
- Using the Taguchi method, it was discovered that the amplitude of the vibration rises when the oil pressure within the damper is lowered, and that it reduces when the oil pressure is raised. In addition, when the oil pressure increases, the vibration amplitude first reduces but then begins to increase after 6000 revolutions per minute. Using a mixture of oil that was 50% of the total, we were able to get the best possible decrease in vibration amplitude.
- ANOVA indicates that oil pressure and mix significantly impact shaft vibration amplitude in the Z-axis. According to the Taguchi technique, the shaft's vibration amplitude at the z-axis decreases as oil pressure rises, first increasing but then decreasing. Shaft vibration amplitude decreases with oil pressure up to 5000rpm. It rises again from 5000 to 8000 rpm, then stays steady until 10000. The shaft vibration amplitude is lowest at 50% oil mix and 100 bar oil pressure.
- Based on particular input process factors, an effective model to forecast vibration amplitudes at the x-axis and z-axis was built using the regression equations (Equations 2 and 3). The regression model's correctness and dependability were confirmed throughout the validation phase, which revealed that the projected values nearly matched the experimental findings. As the objective of the present study is to

minimize the vibration amplitude of the shaft so, that the shaft may rotate without excessive whirl effect.

- The S/N plots in the Taguchi technique are used to decide the optimal setting of process parameters to get the best response. It is observed that the optimum level of process parameters for the vibration amplitude of the shaft in the x-axis for the squeeze film damper (SFD) is Pressure-100bar, Speed-4000rpm, Blend-40% (P5S2B4) and Pressure-100bar, Speed-4000rpm, Blend-50% (P5S2B5) in the z-axis, show that by carefully choosing and optimizing the parameters, it is possible to get reduced vibration amplitudes.
- The regression model's ability to be used in actual engineering and industrial applications is further supported by the experimental validation of these improved values.

Chapter 4; this part elucidated the modelling of squeeze film damper along with , the validation experiments carried out to confirm the efficiency of the optimized values in regulating the vibration of the high-speed shaft that rotates has provided solid proof of their application and usefulness. With errors well below the permitted range of less than 5%, the experimental results nearly matched the optimum values for Pressure, Speed, Blending ratio, for Vibration 'X', and Vibration 'Z'.

- The findings of the experimental validation show good agreement between the optimized values and the experimental data. This shows that under the evaluated conditions, the optimized values precisely regulate the high-speed rotating shaft's vibration. The insignificant deviations in parameters like Oil Pressure within the damper, Shaft Speed, and Oil Blending Ratio that exist between optimized and experimental values further support the correctness and dependability of the optimization technique.

- The optimization process has yielded valuable insights and optimal input values, considering important factors such as maximizing speed and minimizing vibration amplitude. After analysis, it is concluded that the most effective combination of input parameters consists of a rotational speed of 10,000 rpm, a blend ratio of 13.08%, and an oil pressure of 99.82 bar. The adjustments have successfully decreased the response vibration amplitudes on the x and z axes to 3.285 and 3.268, respectively.
- To validate the obtained results, experiments were performed using the optimized input parameters. The experiments yielded response vibration amplitudes of 3.391 for the x-axis and 3.401 for the z-axis. The disparities between the experimental values and the predicted values are 3.125% for the x-axis and 3.91% for the z-axis. These results highlight the accuracy and reliability of the optimization process.
- Although the measured values for Vibration "X" and Vibration "Z" showed minor fluctuations, the percentage variations of 3.125% and 3.91%, respectively, nonetheless show a considerable increase in vibration control compared to the baseline. These variations are to be anticipated given the inherent ambiguity and variances involved with experimental measurements.

Overall, the successful experimental validation confirms the accuracy and reliability of the optimized values for controlling the vibration of the high-speed rotating shaft. This validation process in stills confidence in the effectiveness of the optimization approach and supports the practical implementation of the optimized values in vibration control systems.

Chapter 5; Comprehensive experimental and statistical examination of vibration amplitudes in a squeeze film damper-equipped high-speed rotating shaft was done. The experiments and analysis spans input and response parameters by examining vibration amplitudes along the X and Z axes. RSM, Box-Behnken design, and ANN was used for optimization. Critical

considerations include shaft rotational speed up to 8000 rpm, oil pressure up to 100 bar, and oil mix ratios from 10% to 50%. This study's main findings:

- Residual plot of experimental shaft vibration amplitude data at x and z axes showed the data was mostly linear with little divergence from a normal distribution. A successful vibration prediction model using this data. Graphs of VRFV are random. If residuals vary consistently across projected values, RVOP may assist. A FVRP without outliers indicates a homogenous distribution with many data points. A bar graph illustrates a preference for quantifying early observations' effect on outcomes.
- The ANN model outperforms the RSM in forecasting vibration amplitudes along the shaft's x and z axes per Mean Absolute Percentage Error (MAPE) values. ANN has a 50% lower MAPE than RSM, demonstrating its accuracy. ANN has 9.73% MAPE for x-axis and 9.38% for z-axis, whereas RSM has 18.18% and 20.50%. The findings demonstrate the ANN model's ability to improve vibration amplitude prediction, especially in systems with high rotating speeds.
- ANN outperforms RSM models in predicting vibration amplitudes along both x and z axes, as shown by comparing MAE and RMSE. ANN has a 1.88 MAE and 2.41 RMSE on the x-axis, compared to 3.50 and 4.50 for RSM. ANN's MAE of 1.70 and RMSE of 2.12 surpass RSM's 3.77 and 4.72 on the z-axis. These lower MAE and RMSE readings for ANN show that its forecasts are far more accurate than RSM. Its constantly excellent predictive skills make the ANN model the best option for exact vibration amplitude forecasts, particularly in high-speed rotating systems.
- A high R-squared (R^2) value of 0.94 and 0.95 indicates that the ANN model effectively explains and predicts vibration amplitudes for both the x and z axes. For exact vibration amplitude predictions, ANN is best due to its great explanatory power. Conversely, the RSM model has lower R^2 values (0.81 for x-axis, 0.79 for z-axis),

indicating less explanation. In situations where vibration amplitude forecasts are crucial, researchers choose the ANN model for its resilience in collecting data patterns.

The study found that the ANN predictive model outperforms the RSM-based regression model in technical terms. Designing and optimizing experiments using RSM is beneficial. In forecasting vibration amplitudes, the ANN model excels.

Chapter 6; *We* examined the amplitude of shaft vibrations in different point load scenarios. As part of this inquiry, we will analyze and differentiate circumstances where a squeeze film damper is absent from those where it is present. The experimental setting incorporates a methodical adjustment of load location. To be more precise, the load is positioned at different distances of 10, 20, 30, 40, and 50 centimetres from the terminal support of the shaft. Vibration amplitudes along the x and z axes are measured and recorded after each installation. These measurements are meticulously obtained. When the load is placed near the support, there is a noticeable increase in vibration amplitudes along both axes. This is shown by the results obtained from the diverse investigation of the vibrational signals.

- The loading state remained constant when subjected to varying point loading and a fixed oil supply pressure, indicating a stable situation comparable to when the SFD is not present. A comparative investigation of vibration amplitudes along the X and Z axes was conducted by systematically testing several oil samples with varied viscosities. The tests were performed at a constant oil supply pressure of 5 bar.
- The experimental study on the impact of oil viscosity on vibration amplitude revealed a significant pattern. When the viscosity of the oil reached its ideal level, there was a corresponding reduction in vibration amplitude along both the X and Z axes. This creates a direct and evident relationship between the viscosity of oil and the amplitudes of vibration that occur as a consequence.

- A thorough analysis was performed to compare the levels of vibration amplitudes in the presence and absence of a Squeeze Film Damper (SFD) for each oil sample. The findings demonstrated a persistent decrease in the amplitudes of rotor vibration with the application of the SFD. Moreover, the observed pattern indicated that there was a concomitant reduction in the magnitude of vibrations as the viscosity of the oil increased, reaching a certain threshold. This emphasizes the reciprocal influence of oil viscosity and the SFD in reducing vibrations in the rotor system.

7.2 Future scopes

In this work, an effort was made to find out the optimum selection of process parameters for the high-speed rotating shaft vibration control through squeeze film damper with development of single unit of squeeze film damper for shaft speed up to 10,000 rpm and oil pressure 100 bar. However, these processes were limited to the mild steel material of solid rotor shaft and single unit of squeeze film damper only. The future directions in the area of squeeze film damper are discussed below.

- Examine the effects of using different shaft materials, including both coarse and dense options, on vibration amplitudes, enabling the identification of optimal materials for specific applications and operating conditions.
- Explore the influence of introducing solid lubricant nanoparticles into the liquid oil on vibration amplitudes, potentially uncovering innovative approaches to enhancing lubrication and reducing vibrations with use of squeeze film damper.
- Investigate how altering the material composition of damper housing and damper journal impacts the vibration characteristics of high-speed rotating shafts, potentially leading to more efficient vibration control solutions.

- This research examined how a single squeeze film damper device controlled high-speed rotating shaft vibration amplitude. This study examined one damper's performance, while multiple dampers can be used to study the effectiveness with respect to single damper.

REFERENCES

1. Shigehiko Kaneko, Tomomichi Nakamura, Fumio Inada, Minoru Kato, Kunihiko Ishihara, Takashi Nishihara, Mikael A. Langthjem (2013) Chapter 7 - Vibrations in Rotary Machines. In: Flow-induced Vibrations (Second Edition). pp 311–358

2. Jaroslav Zapomel, Petr Ferfecki JK (2021) Effect of the controllable support elements lubricated by magnetically sensitive fluids on chaotic and regular vibration of flexible rotors during rubbing,. Mech Mach Theory 155:. https://doi.org/doi.org/10.1016/j.mechmachtheory.2020.104096.

3. Meeus H, Fiszer J, Van De Velde G, Verrelst B, Desmet W, Guillaume P, Lefeber D (2019) Dynamic performance of a squeeze film damper with a cylindrical roller bearing under a large static radial loading range. Machines 7:. https://doi.org/10.3390/machines7010014

4. Zhang Y, He L, Yang J, Zhu G, Jia X, Yan W (2021) Multi-objective optimization design of a novel integral squeeze film bearing damper. Machines 9:. https://doi.org/10.3390/machines9100206

5. Andrés LS (2013) Squeeze Film Dampers BT - Encyclopedia of Tribology. In: Wang QJ, Chung Y-W (eds). Springer US, Boston, MA, pp 3252–3263

6. Hamzehlouia S, Behdinan K (2016) Squeeze Film Dampers Executing Small Amplitude Circular-Centered Orbits in High-Speed Turbomachinery. Int J Aerosp Eng 2016:. https://doi.org/10.1155/2016/5127096

7. R. Holmes and iVl. Dogan (1982) Investigation of squeeze-film dampers. In: NASA. Lewis Research Center Rotordyn. Instability Probl. in High-Performance Turbomachinery

8. Zeidan FY, San Andrés L, Vance JM (1996) DESIGN AND APPLICATION OF SQUEEZE FILM DAMPERS IN ROTATING MACIDNERY. Proc TWENTY-FIFTH Turbomach Symp 169–188. https://doi.org/https://doi.og/10.21423/R1649R

9. Sane RWS and SK (1988) Squeeze Film Damping for Aircraft Gas Turbines. DEFSCI J 38:439–456

10. (2019) Application of gain-scheduled vibration control to nonlinear journal-bearing supported rotor. J Sound Vib 442:714–734. https://doi.org/doi.org/10.1016/j.jsv.2018.11.027.

11. Petr FerfeckiPetr FerfeckiJaroslav ZapomelJaroslav (2017) Analysis of the vibration attenuation of rotors supported by magnetorheological squeeze film dampers as a multiphysical finite element problem. Adv Eng Softw. https://doi.org/10.1016/j.advengsoft.2016.11.001

12. Gupta RK, Singh RC (2023) Development and Experimental Investigations of Squeeze Film Damper Setup for High Rotational Speeds and Oil Pressure. J Vib Eng Technol. https://doi.org/10.1007/s42417-023-01186-y

13. Perreault M, Student BAS, Hamzehlouia S, Behdinan K (2019) Application of Computational Fluid Dynamics for Thermohydrodynamic Analysis of High-Speed Squeeze-Film Dampers. Transantions Can Soc Mech Eng 43:1–49

14. Donald Margolis (2010) Bond Graph Modelling of Engineering Systems

15. Sivaraos, Milkey KR, Samsudin AR, Dubey AK, Kidd P (2014) Comparison between taguchi method and response surface methodology (RSM) in modelling CO2 laser machining. Jordan J Mech Ind Eng 8:35–42

16. Rezvani MA, Hahn EJ (2000) Floating ring squeeze film damper: Theoretical analysis. Tribol Int 33:249–258. https://doi.org/10.1016/S0301-679X(00)00038-4

17. Du QW, Zheng ZL, Xie YH (2016) Optimization on start-up process of high-pressure rotor for large power steam turbine. Therm Sci 20:815–822. https://doi.org/10.2298/TSCI160201204D

18. S.S Rao (2005) The finite Element Method in Engineering

19. Han Z, Ding Q, Zhang W (2019) Dynamical characteristic analysis of elastic ring squeeze film damper in rotor system. In: Mechanisms and Machine Science. Springer Science and Business Media B.V., pp 56–71

20. Arzt E, Quan H, McMeeking RM, Hensel R (2021) Functional surface microstructures inspired by nature – From adhesion and wetting principles to sustainable new devices. Prog Mater Sci 120:100823. https://doi.org/10.1016/j.pmatsci.2021.100823

21. Cardoso D, Ferreira L (2021) Application of predictive maintenance concepts using artificial intelligence tools. Appl Sci 11:1–18. https://doi.org/10.3390/app11010018

22. Zheng W, Pei S, Zhang Q, Hong J (2021) Experimental and theoretical results of the performance of controllable clearance squeeze film damper on reducing the critical amplitude. Tribiology Int 107155. https://doi.org/10.1016/j.triboint.2021.107155

23. Squeeze LR, System FD, Shi M, Yang Y, Deng W, Wang J, Fu C (2022) applied sciences Analysis of Dynamic Characteristics of Small-Scale and

24. Zhou H, Cao G, Chen X, Zhang Y, Cang Y (2023) A Study on the Thermal Properties of Oil-Film Viscosity in Squeeze Film Dampers. Lubricants 11:. https://doi.org/10.3390/lubricants11040163

25. Gehannin J, Arghir M, Bonneau O (2010) Complete squeeze-film damper analysis based on the "Bulk Flow" equations. Tribol Trans 53:84–96. https://doi.org/10.1080/10402000903226382

26. Agnew JS (2011) Rotordynamic Performance of a Flexure Pivot Pad Bearing

27. Wang H (2021) Passive vibration reduction of a squeeze film damper for a rotor system with fit looseness between outer ring and housing. J Low Freq Noise Vib Act Control 40:1473–1492. https://doi.org/10.1177/1461348420968692

28. Yao SM, Teo WK, Geng Z, Turner S, Ridgway K (2011) Squeeze film damping and application in shell machining. IOP Conf Ser Mater Sci Eng 26:. https://doi.org/10.1088/1757-899X/26/1/012012

29. Journal I (2017) Hazard Identification and Risk Assessment in Automotive Industry Hazard Identification and Risk Assessment in Automotive Industry. 13:7639–7667

30. Adiletta G (2017) An insight into the dynamics of a rigid rotor on two-lobe wave squeeze film damper. Tribol Int 116:69–83. https://doi.org/10.1016/j.triboint.2017.06.029

31. Engines GEA (2002) (12) Patent Application Publication (10) Pub. No.: US 2002/0136473 A1. 1:

32. Jareland MH (2001) The Use of Platform Dampers to Reduce Turbine Blade Vibrations. 1–28

33. Ashraf WM, Uddin GM, Tariq R, Ahmed A, Farhan M, Nazeer MA, Hassan RU, Naeem A, Jamil H, Krzywanski J, Sosnowski M D V. (2023) Artificial Intelligence Modeling-Based Optimization of an Industrial-Scale Steam Turbine for Moving toward Net-Zero in the Energy Sector. ACS Omega. https://doi.org/doi: 10.1021/acsomega.3c01227.

34. Lu K, He L, Zhang Y (2017) Experimental Study on Vibration Reduction Characteristics of Gear Shafts Based on ISFD Installation Position. Shock Vib 2017:. https://doi.org/10.1155/2017/7246356

35. Younan AA, Cao J, Dimond TW, Allaire PE (2011) Nonlinear analysis of squeeze film damper with entrained air in rotordynamic systems. Tribol Trans 54:132–144. https://doi.org/10.1080/10402004.2010.529543

36. Wang W, Chen Q, Yan D, Geng D (2019) A novel comprehensive evaluation method of the draft tube pressure pulsation of Francis turbine based on EEMD and information entropy. Mech Syst Signal Process 116:772–786. https://doi.org/10.1016/j.ymssp.2018.07.033

37. Ding H, Zhao L, Yan J, Feng HY (2023) Implementation of Digital Twin in Actual Production: Intelligent Assembly Paradigm for Large-Scale Industrial Equipment. Machines 11:1–19. https://doi.org/10.3390/machines11111031

38. Sedivy Dominik et al., , . 020034-1-020034-7. (1889) force effects on rotor of squeeze film damper using Newtonian and non-Newtonian fluid. In: AIP Conf. Proc. pp 020034-1-020034–7.

39. Bonneau O, Frêne J (1997) Non-linear behavior of a flexible shaft partly supported by a squeeze film damper. Wear 206:244–250. https://doi.org/10.1016/S0043-1648(97)00004-5

40. Chu F, Holmes R (1998) Efficient computation on nonlinear responses of a rotating assembly incorporating the squeeze-film damper. Comput Methods Appl Mech Eng 164:363–373. https://doi.org/10.1016/S0045-7825(98)00097-8

41. Inayat-Hussain JI, Kanki H, Mureithi NW (2003) On the bifurcations of a rigid rotor response in squeeze-film dampers. J Fluids Struct 17:433–459. https://doi.org/10.1016/S0889-9746(02)00146-9

42. Inayat-Hussain JI (2005) Bifurcations of a flexible rotor response in squeeze-film dampers without centering springs. Chaos, Solitons and Fractals 24:583–596. https://doi.org/10.1016/j.chaos.2004.09.047

43. Inayat-Hussain JI, Mureithi NW (2006) Transitions to chaos in squeeze-film dampers. Commun Nonlinear Sci Numer Simul 11:721–744. https://doi.org/10.1016/j.cnsns.2004.12.003

44. Susan-Resiga D (2009) A rheological model for magneto-rheological fluids. J Intell Mater Syst Struct 20:1001–1010. https://doi.org/10.1177/1045389X08100979

45. Chang-Jian CW, Yau HT, Chen JL (2010) Nonlinear dynamic analysis of a hybrid squeeze-film damper-mounted rigid rotor lubricated with couple stress fluid and active control. Appl Math Model 34:2493–2507. https://doi.org/10.1016/j.apm.2009.11.014

46. Hsu WC, Wang CR, Shiau TN, Liu DS, Young TH (2014) Nonlinear dynamic study on effects of flywheel eccentricity in a turbine generator with a squeeze film damper. Procedia Eng 79:397–406. https://doi.org/10.1016/j.proeng.2014.06.360

47. Zapoměl J, Ferfecki P, Forte P (2017) A new mathematical model of a short magnetorheological squeeze film damper for rotordynamic applications based on a bilinear oil representation – derivation of the governing equations. Appl Math Model 52:558–575. https://doi.org/10.1016/j.apm.2017.07.040

48. Inayat-Hussain JI (2009) Bifurcations in the response of a flexible rotor in squeeze-film dampers with retainer springs. Chaos, Solitons and Fractals 39:519–532. https://doi.org/10.1016/j.chaos.2007.01.086

49. Zhang J, Ellis J, Roberts JB (1993) Observations on the nonlinear fluid forces in short cylindrical squeeze film dampers. J Tribol 115:692–698. https://doi.org/10.1115/1.2921695

50. Inayat-Hussain JI, Kanki H, Mureithi NW (2001) Stability and bifurcation of a rigid rotor in cavitated squeeze-film dampers without centering springs. Tribol Int 34:689–

702. https://doi.org/10.1016/S0301-679X(01)00062-7

51. Altu Bak MM, Rao MD (2010) Analytical modeling of squeeze film damping for rectangular elastic plates using Green's functions. J Sound Vib 329:4617–4633. https://doi.org/10.1016/j.jsv.2010.05.008

52. Wang C, Au YHJ (2011) Study of design parameters for squeeze film air journal bearing-Excitation frequency and amplitude. Mech Sci 2:147–155. https://doi.org/10.5194/ms-2-147-2011

53. Bai C, Huang J (2014) Improving the validity of squeeze film air-damping model of MEMS devices with border effect. J Appl Math 2014:. https://doi.org/10.1155/2014/192891

54. Chen H, Chen Y, Hou L, Li Z (2014) Bifurcation analysis of rotor-squeeze film damper system with fluid inertia. Mech Mach Theory 81:129–139. https://doi.org/10.1016/j.mechmachtheory.2014.07.002

55. Adiletta G (2015) Bifurcating behaviour of a rotor on two-lobe wave squeeze film damper. Tribol Int 92:72–83. https://doi.org/10.1016/j.triboint.2015.05.026

56. Shah RC, Kataria RC (2016) On the squeeze film characteristics between a sphere and a flat porous plate using ferrofluid. Appl Math Model 40:2473–2484. https://doi.org/10.1016/j.apm.2015.09.042

57. Heidari HR, Safarpour P (2016) Design and modeling of a novel active squeeze film damper. Mech Mach Theory 105:235–243. https://doi.org/10.1016/j.mechmachtheory.2016.07.004

58. Zapoměl J, Ferfecki P, Kozánek J (2017) Modelling of magnetorheological squeeze film dampers for vibration suppression of rigid rotors. Int J Mech Sci 127:191–197. https://doi.org/10.1016/j.ijmecsci.2016.11.009

59. Heidari H, Ashkooh M (2016) The influence of asymmetry in centralizing spring of squeeze film damper on stability and bifurcation of rigid rotor response. Alexandria Eng J 55:3321–3330. https://doi.org/10.1016/j.aej.2016.08.013

60. Xing C, Braun MJ, Li H (2010) Damping and added mass coefficients for a squeeze film damper using the full 3-D Navier-Stokes equation. Tribol Int 43:654–666.

https://doi.org/10.1016/j.triboint.2009.10.005

61. Qingchang T, Wei L, Jun Z (1997) Fluid forces in short squeeze-film damper bearings. Tribol Int 30:733–738. https://doi.org/10.1016/S0301-679X(97)00041-8

62. Tan Q, Li X (1999) Analytical study on effect of a circumferential feeding groove on unbalance response of a flexible rotor in squeeze film damper. Tribol Int 32:559–566. https://doi.org/10.1016/S0301-679X(99)00086-9

63. Groves KH, Bonello P (2010) Improved identification of squeeze-film damper models for aeroengine vibration analysis. Tribol Int 43:1639–1649. https://doi.org/10.1016/j.triboint.2010.03.010

64. Veijola T, Lehtovuori A (2009) Numerical and analytical modelling of trapped gas in micromechanical squeeze-film dampers. J Sound Vib 319:606–621. https://doi.org/10.1016/j.jsv.2008.05.038

65. Fischer M, Giousouf M, Schaepperle J, Eichner D, Weinmann M, Von Münch W, Assmus F (1998) Electrostatically deflectable polysilicon micromirrors - Dynamic behaviour and comparison with the results from FEM modelling with ANSYS. Sensors Actuators, A Phys 67:89–95. https://doi.org/10.1016/S0924-4247(97)01770-6

66. Ku CP, Tichy JA (1990) An experimental and theoretical study of cavitation in a finite submerged squeeze film damper. J Tribol 112:725–733. https://doi.org/10.1115/1.2920321

67. Chen PYP, Hahn EJ (2000) Side clearance effects on squeeze film damper performance. Tribol Int 33:161–165. https://doi.org/10.1016/S0301-679X(00)00022-0

68. Qin W, Zhang J, Ren X (2009) Response and bifurcation of rotor with squeeze film damper on elastic support. Chaos, Solitons and Fractals 39:188–195. https://doi.org/10.1016/j.chaos.2007.01.115

69. Hajhashemi MS, Rasouli A, Bahreyni B (2014) Performance optimization of high order RF microresonators in the presence of squeezed film damping. Sensors Actuators, A Phys 216:266–276. https://doi.org/10.1016/j.sna.2014.05.014

70. Zhang X, Yin Z, Gao G, Li Z (2015) Determination of stiffness coefficients of hydrodynamic water-lubricated plain journal bearings. Tribol Int 85:37–47.

https://doi.org/10.1016/j.triboint.2014.12.019

71. Novikov DK, Diligensky DS (2015) Calculation Algorithm for Squeeze Film Damper. Procedia Eng 106:218–223. https://doi.org/10.1016/j.proeng.2015.06.027

72. Tichy JA (1985) Measurements of squeeze-film bearing forces and pressures, including the effect of fluid inertia. ASLE Trans 28:520–526. https://doi.org/10.1080/05698198508981650

73. Jose J. Granda (2002) The role of bond graph modeling and simulation in mechatronics systems an integrated software tool: CAMP-G, MATLAB–SIMULINK. In: Mechatronics. pp 1271–1295

74. Jose J. Granda and Jim Reus (1997) New developments in bond graph modeling software tools: the computer aided modeling program camp-g and Matla. ieee 97:7803–4053

75. Adiletta G (2008) Self-organizing maps for surveying lubrication within squeeze film dampers. Tribol Int 41:1255–1266. https://doi.org/10.1016/j.triboint.2008.04.006

76. Groves KH, Bonello P (2013) Empirical identification of squeeze-film damper bearings using neural networks. Mech Syst Signal Process 35:307–323. https://doi.org/10.1016/j.ymssp.2012.08.014

77. Amalendu Mukherjee and A.K. Samantaray (2000) System Modeling through Bond graph Objects on SYMBOLS 2000

78. Liming YU and Xiaoye Qi (2012) Bond-Graph Modeling in System Engineering. In: International Conference on Systems and Informatics ,ICSAI 2012

79. A. K. Samantaray et al (2010) Bond Graph Modeling of an Internally Damped Nonideal Flexible Spinning Shaft. J Dyn Syst Meas Control 132:

80. Walton JF, Walowit JA, Zorzi ES, Schrand J (1987) Experimental observation of cavitating squeeze-film dampers. J Tribol 109:290–294. https://doi.org/10.1115/1.3261353

81. Levesley MC, Holmes R (1996) The effect of oil supply and sealing arrangements on the performance of squeeze-film dampers : An experimental study. Proc Inst Mech

Eng Part J J Eng Tribol 210:221–232. https://doi.org/10.1243/PIME_PROC_1996_210_504_02

82. Dias RA, Wolffenbuttel RF, Cretu E, Rocha LA (2011) Squeeze-film damper design with air channels: Experimental verification. Procedia Eng 25:47–50. https://doi.org/10.1016/j.proeng.2011.12.012

83. Bonello P, Pham HM (2014) A theoretical and experimental investigation of the dynamic response of a squeeze-film damped twin-shaft test rig. Proc Inst Mech Eng Part C J Mech Eng Sci 228:218–229. https://doi.org/10.1177/0954406213484223

84. Kumar HNA, Shilpashree DJ, Adarsh MS, Amith D, Kulkarni S (2016) Development of Smart Squeeze Film Dampers for Small Rotors. Procedia Eng 144:790–800. https://doi.org/10.1016/j.proeng.2016.05.088

85. Adams MJ, Edmondson B, Caughey DG, Yahya R (1994) An experimental and theoretical study of the squeeze-film deformation and flow of elastoplastic fluids. J Nonnewton Fluid Mech 51:61–78. https://doi.org/10.1016/0377-0257(94)85003-8

86. Khalid AA, Albagul A, Faris W, Ismail GA (2006) An experimental study on steel and Teflon squeeze film dampers. Shock Vib 13:33–40. https://doi.org/10.1155/2006/387302

87. Andres LS (2014) Force coefficients for a large clearance open ends squeeze film damper with a central feed groove: Experiments and predictions. Tribol Int 71:17–25. https://doi.org/10.1016/j.triboint.2013.10.021

88. Chu F, Holmes R (2000) Damping capacity of the squeeze film damper in suppressing vibration of a rotating assembly. Tribol Int 33:81–97. https://doi.org/10.1016/S0301-679X(00)00030-X

89. Siew CC, Hill M, Holmes R (2002) Evaluation of various fluid-film models for use in the analysis of squeeze film dampers with a central groove. Tribol Int 35:533–547. https://doi.org/10.1016/S0301-679X(02)00048-8

90. Haider B, Mukherjee A, Karmaka R (1990) A. Mukherjee Theoretical and Experimental Studies on Squeeze Film Stabilizers for Flexible Rotor-Bearing Systems Using Newtonian and Visooelastio Lubricants

91. Grigory L. Arauz and Luis San Andres (1997) experimental force response of a grooved squeeze film damper. Tribol Int 30:77–86

92. Bai H, Liu X, Li H, Zhang W, Meng G, Li M, Wang X (2014) Nonlinear dynamic characteristics of a large-scale tilting pad journal bearing-rotor system. JVE Int Ltd J vibroengineering 16:4045–4064

93. Zhou W, Qiu N, Wang L, Gao B, Liu D (2018) Dynamic analysis of a planar multi-stage centrifugal pump rotor system based on a novel coupled model. In: Journal of Sound and Vibration. Academic Press, pp 237–260

94. Hamzehlouia S, Behdinan K (2016) First order perturbation technique for squeeze film dampers executing small amplitude circular centered orbits with aero-engine application. pp 1–9

95. Hamzehlouia S, Behdinan K (2018) Thermohydrodynamic modeling of squeeze film dampers in high-speed turbomachinery. SAE Interational J Fuels Lubr 11:129–146. https://doi.org/https://www.jstor.org/stable/26554702

96. PIETRA D, ADILETTA (2002) The squeeze Film Damper over four decades of investigations. Part I: Characteristics and operating features. In: The Shock and vibration digest. Sage, Thousands Oaks, CA, pp 3–26

97. D. M. Smith (1964) Journal Bearing Dynamic Characteristics—Effect of Inertia of Lubricantle. In: Proceedings of the Institution of Mechanical Engineers. SAGE Publications Inc., pp 37–44

98. Dousti S, Cao J, Younan A, Allaire P, Dimond T (2012) Temporal and convective inertia effects in plain journal bearings with eccentricity, velocity and acceleration. J Tribol 134:. https://doi.org/10.1115/1.4006928

99. Zhao JY, Linnett IW, McLean LJ (1994) Stability and bifurcation of unbalanced response of a squeeze film damped flexible rotor. In: Journal of Tribology. pp 361–376

100. McLean LJ, Hahn EJ (1984) Stability of squeeze film damped multi-mass flexible rotor bearing systems. Trans ASME 107:402–409

101. McLean LJ, Hahn EJ (1983) Unbalance behavior of squeeze film damped multi-mass flexible rotor bearing systems. J Tribol 105:22–28. https://doi.org/10.1115/1.3254538

102. Barrett LE, Gunter EJ (1975) Dyrobes Rotordynamics Software https://dyrobes.com STEADY-STATE AND TRANSIENT ANALYSIS OF A SQUEEZE May 1975 FILM DAMPER BEARING FOR ROTOR STABILITY 6. Performing Organization Code 7. Author(s) 8. Performing Organization Report No

103. Zhao JY, Linnett IW, Mclean LJ (1994) Stability and Bifurcation of Unbalanced Response of a Squeeze Film Damped Flexible Rotor

104. Zhao JY, Linnett IW, McLean LJ (1994) Subharmonic and Quasi-Periodic Motions of an Eccentric Squeeze Film Damper-Mounted Rigid Rotor. J Vib Acoust 116:357–353. https://doi.org/https://doi.org/10.1115/1.2930436

105. Oscar C, Santiago D, A. L, Andrés S (2014) Imbalance Response and Damping Force Coefficients of a Rotor Supported on End Sealed Integral Squeeze Film DampersNo Title. In: Turbo Expo: Turbomachinery Technical Conference and Exposition (GT). pp 99–103

106. Diaz SE, San Andrés LA (1999) A method for identification of bearing force coefficients and its application to a squeeze film damper with a bubbly lubricant. Tribol Trans 42:739–746. https://doi.org/10.1080/10402009908982277

107. Haldar B, Mukharjee A, Karmakar R (1990) Theoretical and Experimental Studies on Squeeze Film Stabilizers for Flexible Rotor-Bearing Systems Using Newtonian and Visooelastio Lubricants

108. Zhang W, Ding Q (2015) Elastic ring deformation and pedestal contact status analysis of elastic ring squeeze film damper. J Sound Vib 346:314–327. https://doi.org/10.1016/j.jsv.2015.02.015

109. Chen X, Gan X, Ren G (2020) Dynamic modeling and nonlinear analysis of a rotor system supported by squeeze film damper with variable static eccentricity under aircraft turning maneuver. J Sound Vib 485:. https://doi.org/10.1016/j.jsv.2020.115551

110. Rabinowitz MD, Hahn EJ (1977) Stability of squeeze-film-damper supported flexible rotors. J Eng power 10:545–551

111. Rabinowitz MD, Hahn EJ (1977) Steady-State Performance of Squeeze Film Damper Supported Flexible Rotors. Trans ASME 10:552–558

112. Bonello P, Brennan MJ, Holmes R (2002) Non-linear modelling of rotor dynamic systems with squeeze film dampers - An efficient integrated approach. J Sound Vib 249:743–773. https://doi.org/10.1006/jsvi.2001.3911

113. Sun G, Zhang H, Fang J, Li G, Li Q (2018) A new multi-objective discrete robust optimization algorithm for engineering design. Appl Math Model 53:602–621. https://doi.org/10.1016/j.apm.2017.08.016

114. He B, Ouyang H, Ren X, He S (2017) Dynamic response of a simplified turbine blade model with under-platform dry friction dampers considering normal load variation. Appl Sci 7:. https://doi.org/10.3390/app7030228

115. Xu X, Lei Y, Li Z (2020) An Incorrect Data Detection Method for Big Data Cleaning of Machinery Condition Monitoring. IEEE Trans Ind Electron 67:2326–2336. https://doi.org/10.1109/TIE.2019.2903774

116. Rizvi A, Smith CW, Rajasekaran R, Evans KE (2016) Dynamics of dry friction damping in gas turbines: Literature survey. JVC/Journal Vib. Control 22:296–305

117. San Andrés L, Koo B, Jeung S-H, Design Engineer Sean C Experimental Force Coefficients for Two Sealed Ends Squeeze Film Dampers (Piston Rings And O-Rings): An Assessment of Their Similarities and Differences Gt2018-76224

118. Jeung SH, Kim -Jong, Chen H-C, Kim Y-J (2017) EXPERIMENTAL PERFORMANCE OF AN OPEN ENDS SQUEEZE FILM DAMPER AND A SEALED ENDS SQUEEZE FILM DAMPER A Dissertation

119. Biçak MMA (2011) Analytical investigation of squeeze film dampers. Michigan Technological University

120. Jeung SH, San Andrés L, Den S, Koo B (2019) Effect of Oil Supply Pressure on the Force Coefficients of a Squeeze Film Damper Sealed with Piston Rings. J Tribol 141:. https://doi.org/10.1115/1.4043238

121. Meeus H, Fiszer J, Van De Velde G, Verrelst B, Lefeber D, Guillaume P, Desmet W (2019) Dynamic Performance of an Oil Starved Squeeze Film Damper Combined with a Cylindrical Roller Bearing. J Eng Gas Turbines Power 141:. https://doi.org/10.1115/1.4042418

122. Haider ST, Saleem MM, Ahmad M (2017) FEM Modeling of Squeeze Film Damping Effect in RF-MEMS Switches. Proceeding Electr Eng Comput Sci Informatics 4:. https://doi.org/10.11591/eecsi.v4.1102

123. Han B, Ding Q (2018) Forced responses analysis of a rotor system with squeeze film damper during flight maneuvers using finite element method. Mech Mach Theory 122:233–251. https://doi.org/10.1016/j.mechmachtheory.2018.01.004

124. Luo Z, Wang J, Tang R, Wang D (2019) Research on vibration performance of the nonlinear combined support-flexible rotor system. Nonlinear Dyn 98:113–128. https://doi.org/10.1007/s11071-019-05176-2

125. Hamzehlouia S, Behdinan K (2021) Squeeze film dampers supporting high-speed rotors: Rotordynamics. Proc Inst Mech Eng Part J J Eng Tribol 235:495–508. https://doi.org/10.1177/1350650120922082

126. Agrawal T, Gautam R, Agrawal S, Singh V, Kumar M, Kumar S (2020) Optimization of engine performance parameters and exhaust emissions in compression ignition engine fueled with biodiesel-alcohol blends using taguchi method, multiple regression and artificial neural network. Sustain Futur 2:. https://doi.org/10.1016/j.sftr.2020.100039

127. Ahmad S, Singari RM, Mishra RS (2020) Modelling and optimisation of magnetic abrasive finishing process based on a non-orthogonal array with ANN-GA approach. Trans Inst Met Finish 98:186–198. https://doi.org/10.1080/00202967.2020.1776966

128. Kumar P, Parkash R (2016) Experimental investigation and optimization of EDM process parameters for machining of aluminum boron carbide (Al–B4C) composite. Mach Sci Technol 20:330–348. https://doi.org/10.1080/10910344.2016.1168931

129. Antony J, Perry D, Wang C, Kumar M (2006) An application of Taguchi method of experimental design for new product design and development process. Assem Autom 26:18–24. https://doi.org/10.1108/01445150610645611

130. Dach J, Koszela K, Boniecki P, Zaborowicz M, Lewicki A, Czekała W, Skwarcz J, Qiao W, Piekarska-Boniecka H, Białobrzewski I (2016) The use of neural modelling to estimate the methane production from slurry fermentation processes. Renew Sustain Energy Rev 56:603–610. https://doi.org/10.1016/j.rser.2015.11.093

131. Krzywanski J (2019) A general approach in optimization of heat exchangers by bio-inspired artificial intelligence methods. Energies 12:. https://doi.org/10.3390/en12234441

132. Krzywanski J (2019) Heat transfer performance in a superheater of an industrial CFBC using fuzzy logic-based methods. Entropy 21:. https://doi.org/10.3390/e21100919

133. Zhu X, Wan Z, Tsang DCW, He M, Hou D, Su Z, Shang J (2021) Machine learning for the selection of carbon-based materials for tetracycline and sulfamethoxazole adsorption. Chem Eng J 406:126782. https://doi.org/10.1016/j.cej.2020.126782

134. Zhu X, Ho CH, Wang X (2020) Application of Life Cycle Assessment and Machine Learning for High-Throughput Screening of Green Chemical Substitutes. ACS Sustain Chem Eng 8:11141–11151. https://doi.org/10.1021/acssuschemeng.0c02211

135. Wang F, Sahana M, Pahlevanzadeh B, Chandra Pal S, Kumar Shit P, Piran MJ, Janizadeh S, Band SS, Mosavi A (2021) Applying different resampling strategies in machine learning models to predict head-cut gully erosion susceptibility. Alexandria Eng J 60:5813–5829. https://doi.org/10.1016/j.aej.2021.04.026

136. Ibrahim KSMH, Huang YF, Ahmed AN, Koo CH, El-Shafie A (2022) A review of the hybrid artificial intelligence and optimization modelling of hydrological streamflow forecasting. Alexandria Eng J 61:279–303. https://doi.org/10.1016/j.aej.2021.04.100

137. Li J, Zhu X, Li Y, Tong YW, Ok YS, Wang X (2021) Multi-task prediction and optimization of hydrochar properties from high-moisture municipal solid waste: Application of machine learning on waste-to-resource. J Clean Prod 278:123928. https://doi.org/10.1016/j.jclepro.2020.123928

138. Li J, Lim K, Yang H, Ren Z, Raghavan S, Chen PY, Buonassisi T, Wang X (2020) AI Applications through the Whole Life Cycle of Material Discovery. Matter 3:393–432. https://doi.org/10.1016/j.matt.2020.06.011

139. Dhini A, Kusumoputro B, Surjandari I (2017) Neural network based system for detecting and diagnosing faults in steam turbine of thermal power plant. Proc - 2017 IEEE 8th Int Conf Aware Sci Technol iCAST 2017 2018-Janua:149–154. https://doi.org/10.1109/ICAwST.2017.8256435

140. Yingyong Zou , Yongde Zhang HM (2021) Fault diagnosis on the bearing of traction motor in high-speed trains based on deep learning. Alexandria Eng J 60:1209–1219. https://doi.org/https://doi.org/10.1016/j.aej.2020.10.044

141. Teksin S, Azginoglu N, Akansu SO (2022) Structure estimation of vertical axis wind turbine using artificial neural network. Alexandria Eng J 61:305–314. https://doi.org/10.1016/j.aej.2021.05.002

142. Bai H, Liu C, Breaz E, Gao F (2020) Artificial neural network aided real-time simulation of electric traction system. Energy AI 1:100010. https://doi.org/10.1016/j.egyai.2020.100010

143. Paper H, Wavelet VD in G, Benrabeh Djaidir AH& AK (2016) Vibration Detection in Gas Turbine Rotor Using Artificial Neural Network Combined with Continuous Wavelet. In: Advances in Acoustics and Vibration Conference. pp 101–113

144. Castellani F, Garibaldi L, Daga AP, Astolfi D, Natili F (2020) Diagnosis of faulty wind turbine bearings using tower vibration measurements †. Energies 13:1–18. https://doi.org/10.3390/en13061474

145. Xu M, Feng G, He Q, Gu F, Ball A (2020) Vibration characteristics of rolling element bearings with different radial clearances for condition monitoring of wind turbine. Appl Sci 10:. https://doi.org/10.3390/app10144731

146. Karkalos NE, Efkolidis N, Kyratsis P, Markopoulos AP (2019) A comparative study between regression and neural networks for modeling Al6082-T6 alloy drilling. Machines 7:. https://doi.org/10.3390/machines7010013

147. Awodele O, Jegede O (2009) Neural Networks and Its Application in Engineering. In: Proceedings of Informing Science & IT Education Conference (InSITE) 2009. pp 1–13

148. Hassan EA, Hassan ML, Abou-zeid RE, El-Wakil NA (2016) Novel nanofibrillated cellulose/chitosan nanoparticles nanocomposites films and their use for paper coating. Ind Crops Prod 93:219–226. https://doi.org/10.1016/j.indcrop.2015.12.006

149. Dey S, Reang NM, Das PK, Deb M (2021) Comparative study using RSM and ANN modelling for performance-emission prediction of CI engine fuelled with bio-diesohol blends: A fuzzy optimization approach. Fuel 292:120356.

https://doi.org/10.1016/j.fuel.2021.120356

150. Youssefi S, Emam-Djomeh Z, Mousavi SM (2009) Comparison of artificial neural network (ANN) and response surface methodology (RSM) in the prediction of quality parameters of spray-dried pomegranate juice. Dry Technol 27:910–917. https://doi.org/10.1080/07373930902988247

151. Ofuyatan OM, Agbawhe OB, Omole DO, Igwegbe CA, Ighalo JO (2022) RSM and ANN modelling of the mechanical properties of self-compacting concrete with silica fume and plastic waste as partial constituent replacement. Clean Mater 4:100065. https://doi.org/10.1016/j.clema.2022.100065

152. Patel KA, Brahmbhatt PK (2016) A Comparative Study of the RSM and ANN Models for Predicting Surface Roughness in Roller Burnishing. Procedia Technol 23:391–397. https://doi.org/10.1016/j.protcy.2016.03.042

153. A. El-Shafei M. El-Hakim, Department (2000) Experimental Investigation of Adaptive Control Applied to HSFD Supported Rotors. J Eng Gas Turbines Power 122:685–692

154. Wang H, Zhao Y, Luo Z, Han Q (2022) Analysis on Influences of Squeeze Film Damper on Vibrations of Rotor System in Aeroengine. Appl Sci 12:. https://doi.org/10.3390/app12020615

155. Jinya Zhang, Jiaxiang Zhang, Qingping Li, Chang Gao ZC (2022) Effect of pressure fluctuation in oil-gas multiphase pump on cavitation and performance of sealing liquid film. J Pet Sci Eng 210:. https://doi.org/doi.org/10.1016/j.petrol.2021.110074

156. Mukherjee, A., and Rao Dasari AM (1988) Experimental Study of Rotor Bearing Systems Influenced by Dilute Viscoelastic Lubricants. Tribol Int Vol. 21:109–115

157. Humes B, Holmes R (1978) Role of Subatmospheric Film Pressures in the Vibration Performance of Squeeze-Film Bearings. J Mech Eng Sci 20:283–289. https://doi.org/10.1243/JMES_JOUR_1978_020_048_02

158. de Souza HJC, Silva MB, Moyses BC, Alberto FL PF, Ferreira FU, Duarte RN da SC (2013) Robust design and taguchi method application

159. Sarkar K RR (2010) A primer on the taguchi method a primer on the taguchi method, 2nd editio

160. Kumar P, Parkash R, Wicaksana A, Rachman T, Mishra HP, Jalan A, Ansari AK, Kumar P (2023) Vibration and Acoustics Analyses of Tapered Roller Bearing. J Vib Eng Technol 3:10–27. https://doi.org/10.1007/s42417-023-00991-9

161. Abdul Khaliq Ansari1 · Paras Kumar (2023) Vibration and Acoustics Analyses of Tapered Roller Bearing. J Vib Eng Technol. https://doi.org/https://doi.org/10.1007/s42417-023-00991-9

162. R. MEAD (1990) The Non-orthogonal Design of Experiments. R Stat Soc part2- 2:151–201

163. Judd CM, McClelland GH RC (2017) Data analysis: a model comparison approach to regression.

164. Mishra HP, Jalan A (2021) Analysis of faults in rotor-bearing system using three-level full factorial design and response surface methodology. Noise Vib Worldw 52:365–376. https://doi.org/10.1177/09574565211030711

165. Gao Y, Xu J, Luo X, Zhu J, Nie L, Mohamad Said KA, Mohamed Amin MA, Bezerra MA, Santelli RE, Oliveira EP, Villar LS, Escaleira LA (2016) Response surface methodology (RSM) as a tool for optimization in analytical chemistry. Talanta 76:965–977. https://doi.org/10.33736/jaspe.161.2015

166. Mohamad Said KA, Mohamed Amin MA (2016) Overview on the Response Surface Methodology (RSM) in Extraction Processes. J Appl Sci Process Eng 2:. https://doi.org/10.33736/jaspe.161.2015

167. Gao Y, Xu J, Luo X, Zhu J, Nie L (2016) Experiment research on mix design and early mechanical performance of alkali-activated slag using response surface methodology (RSM). Ceram Int 42:11666–11673. https://doi.org/10.1016/j.ceramint.2016.04.076

168. Ferreira SLC, Bruns RE, Ferreira HS, Matos GD, David JM, Brandão GC, da Silva EGP, Portugal LA, dos Reis PS, Souza AS, dos Santos WNL (2007) Box-Behnken design: An alternative for the optimization of analytical methods. Anal Chim Acta 597:179–186. https://doi.org/10.1016/j.aca.2007.07.011

169. Demirel C, Kabutey A, Herák D, Sedlaček A, Mizera Č, Dajbych O (2022) Using Box–Behnken Design Coupled with Response Surface Methodology for Optimizing

Rapeseed Oil Expression Parameters under Heating and Freezing Conditions. Processes 10:. https://doi.org/10.3390/pr10030490

170. Huang S, Hu Y, Li F, Jin W, Godara V, Wu B (2019) Optimization of mechanical oil extraction process from Camellia oleifera seeds regarding oil yield and energy consumption. J Food Process Eng 42:1–11. https://doi.org/10.1111/jfpe.13157

171. Tan D, Suvarna M, Shee Tan Y, Li J, Wang X (2021) A three-step machine learning framework for energy profiling, activity state prediction and production estimation in smart process manufacturing. Appl Energy 291:116808. https://doi.org/10.1016/j.apenergy.2021.116808

172. Uddin GM, Niazi SG, Arafat SM, Kamran MS, Farooq M, Hayat N, Malik SA, Zeid A, Kamarthi S, Saqib S, Chaudhry IA (2020) Neural networks assisted computational aero-acoustic analysis of an isolated tire. Proc Inst Mech Eng Part D J Automob Eng 234:2561–2577. https://doi.org/10.1177/0954407020915104

173. Oktem H, Erzurumlu T, Erzincanli F (2006) Prediction of minimum surface roughness in end milling mold parts using neural network and genetic algorithm. Mater Des 27:735–744. https://doi.org/10.1016/j.matdes.2005.01.010

174. Stojanovic B, Vencl A, Bobić I, Miladinović S, Skerlic J (2018) Experimental optimization of the tribological behavior of Al/SiC/Gr hybrid composites based on Taguchi's method and artificial neural network. J Brazilian Soc Mech Sci Eng 40:. https://doi.org/10.1007/s40430-018-1237-y

175. Wang K, Gelgele HL, Wang Y, Yuan Q, Fang M (2003) A hybrid intelligent method for modelling the EDM process. Int J Mach Tools Manuf 43:995–999. https://doi.org/10.1016/S0890-6955(03)00102-0

176. Awolusi TF, Oke OL, Akinkurolere OO, Atoyebi OD (2019) Comparison of response surface methodology and hybrid-training approach of artificial neural network in modelling the properties of concrete containing steel fibre extracted from waste tyres. Cogent Eng 6:1–17. https://doi.org/10.1080/23311916.2019.1649852

177. Talib NSR, Halmi MIE, Ghani SSA, Zaidan UH, Shukor MYA (2019) Artificial Neural Networks (ANNs) and Response Surface Methodology (RSM) Approach for Modelling the Optimization of Chromium (VI) Reduction by Newly Isolated

Acinetobacter radioresistens Strain NS-MIE from Agricultural Soil. Biomed Res Int 2019:. https://doi.org/10.1155/2019/5785387

178. Igwegbe CA, Mohmmadi L, Ahmadi S, Rahdar A, Khadkhodaiy D, Dehghani R, Rahdar S (2019) Modeling of adsorption of Methylene Blue dye on Ho-CaWO4 nanoparticles using Response Surface Methodology (RSM) and Artificial Neural Network (ANN) techniques. MethodsX 6:1779–1797. https://doi.org/10.1016/j.mex.2019.07.016

PUBLICATION FROM THE PRESENT WORK

Paper Published/Accepted /communicated (International Journals/Proceedings)

[1]. R. Gupta, R.C. Singh. (2023) Development and experimental investigations of squeeze film damper setup for high rotational speeds and oil pressure. Journal of Vibration Engineering & Technologies. (SCIE INDEXED***, Springer, IF=2.7).*** **Published, DOI: 10.1007/s42417-023-01186-y.**

[2]. R. Gupta, R.C. Singh. (2023) Comprehensive Experimental Analysis of a Squeeze Film Damper for Flexible Rotor Applications: Utilizing Box-Behnken Design with Desirability Optimization. Journal of Vibration Engineering & Technologies. (SCIE INDEXED, ***Springer, IF=2.7***). **Published, DOI:10.1007/s42417-023-01197-9.**

[3]. R. Gupta, R.C. Singh. (2023) Optimizing High-Speed Rotating Shaft Vibration Control: Experimental Investigation of Squeeze Film Dampers and a Comparative Analysis using Artificial Neural Networks (ANN) and Response Surface Methodology (RSM). Expert Systems with Applications. (SCIE INDEXED, ***Elsevier, IF=8.5***). **Published.**

[4]. R. Gupta, V. Rastogi, R. C. Singh and N. Tandon, (2019), Experimental investigation of ball bearing lubrication conditions by shock pulse method, Published by Tribologia - Finnish Journal of Tribology**, DOI: 10.30678/fjt.79897**.(SCOPUS INDEXED) **Published.**

[5]. R. Gupta, R.C. Singh. (2023), Experimental Analysis and Optimization of Squeeze Film Dampers for Vibration Control in flexible rotors. Journal of Vibration Engineering & Technologies. (SCIE INDEXED, ***Springer, IF=2.7***). **communicated.**

[6]. R. Gupta, R.C. Singh. (2023), Experimental Analysis and Optimization of Squeeze Film Dampers for Vibration Control in flexible rotors. Journal of Vibration Engineering & Technologies. (SCIE INDEXED, ***Springer, IF=2.7***). **communicated.**

[7]. R. Gupta, R.C. Singh. (2024), Modeling of vibration amplitude of high-speed rotating shaft through artificial intelligence and comparative investigation with Orthogonal Array. Expert Systems with Applications. (SCIE INDEXED**, Elsevier, IF=7.5**). **under review.**

Paper Published (International/National Conferences)

[1]. R. Gupta, V. Rastogi and R. C. Singh, (2019), studies of squeeze film damper for mechanical systems, international conference academic research in engineering, management and information technology, (ICAREMIT-2019). **Published**

[2]. R. Gupta, V. Rastogi and R. C. Singh, (2019), squeeze film damper for mechanical systems-A Review, international conference innovative research in agriculture, engineering, technology, applied sciences, humanities, and business management for sustainable development (ETAHBS-2019). **Published.**

[3]. R. Gupta, V. Rastogi and R. C. Singh, (2019), Experimental Investigation of Ball Bearing Lubricant Condition by Acoustic Emission Measurement, international conference on industrial and manufacturing systems, (CIMS-2021). **Published.**

[4]. R. Gupta, R. C. Singh, (2023), Computational Framework using Bond Graph and FEM to Model the Squeeze Film Damper supported on Rotors, International Conference on Innovative Research in Agriculture, Engineering, Technology, Applied Sciences, Humanities and Business Management for Sustainable Development" (ETAHBS-2023). **Published.**